Rapid Bridge Deck Joint Repair Investigation – Phase III

Final Report
December 2020

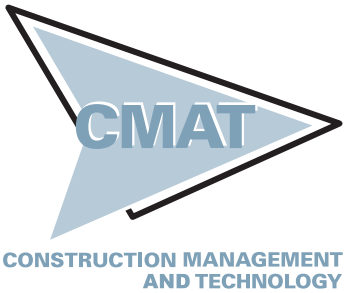

IOWA STATE UNIVERSITY
Institute for Transportation

Sponsored by
Federal Highway Administration
Iowa Department of Transportation
(InTrans Project 13-451)

About the Construction Management and Technology program

The mission of the Construction Management and Technology (CMAT) program is to improve the efficiency and cost-effectiveness of planning, designing, constructing, and operating transportation facilities through innovative construction processes and technologies.

About the Institute for Transportation

The mission of the Institute for Transportation (InTrans) at Iowa State University is to develop and implement innovative methods, materials, and technologies for improving transportation efficiency, safety, reliability, and sustainability while improving the learning environment of students, faculty, and staff in transportation-related fields.

Iowa State University Nondiscrimination Statement

Iowa State University does not discriminate on the basis of race, color, age, ethnicity, religion, national origin, pregnancy, sexual orientation, gender identity, genetic information, sex, marital status, disability, or status as a US veteran. Inquiries regarding nondiscrimination policies may be directed to the Office of Equal Opportunity, 3410 Beardshear Hall, 515 Morrill Road, Ames, Iowa 50011, telephone: 515–294–7612, hotline: 515–294–1222, email: eooffice@iastate.edu.

Disclaimer Notice

The contents of this document reflect the views of the authors, who are responsible for the facts and the accuracy of the information presented herein. The opinions, findings and conclusions expressed in this publication are those of the authors and not necessarily those of the sponsors.

The sponsors assume no liability for the contents or use of the information contained in this document. This report does not constitute a standard, specification, or regulation.

The sponsors do not endorse products or manufacturers. Any trademarks or manufacturers' names appear only because they are considered essential to the objective of the document.

Quality Assurance Statement

The Federal Highway Administration (FHWA) provides high-quality information to serve Government, industry, and the public in a manner that promotes public understanding. Standards and policies are used to ensure and maximize the quality, objectivity, utility, and integrity of its information. The FHWA periodically reviews quality issues and adjusts its programs and processes to ensure continuous quality improvement.

Iowa DOT Statements

Federal and state laws prohibit employment and/or public accommodation discrimination on the basis of age, color, creed, disability, gender identity, national origin, pregnancy, race, religion, sex, sexual orientation or veteran's status. If you believe you have been discriminated against, please contact the Iowa Civil Rights Commission at 800-457-4416 or the Iowa Department of Transportation affirmative action officer. If you need accommodations because of a disability to access the Iowa Department of Transportation's services, contact the agency's affirmative action officer at 800-262-0003.

The preparation of this report was financed in part through funds provided by the Iowa Department of Transportation through its "Second Revised Agreement for the Management of Research Conducted by Iowa State University for the Iowa Department of Transportation" and its amendments.

The opinions, findings, and conclusions expressed in this publication are those of the authors and not necessarily those of the Iowa Department of Transportation or the U.S. Department of Transportation Federal Highway Administration.

Technical Report Documentation Page

1. Report No.	2. Government Accession No.	3. Recipient's Catalog No.
InTrans Project 13-451		

4. Title and Subtitle	5. Report Date
Rapid Bridge Deck Joint Repair Investigation – Phase III	December 2020
	6. Performing Organization Code

7. Author(s)	8. Performing Organization Report No.
David Morandeira (orcid.org/0000-0002-1312-186X), Elizabeth Miller (orcid.org/0000-0001-8796-3595), and Charles T. Jahren (orcid.org/0000-0003-2828-8483)	InTrans Project 13-451

9. Performing Organization Name and Address	10. Work Unit No. (TRAIS)
Institute for Transportation Iowa State University 2711 South Loop Drive, Suite 4700 Ames, IA 50010-8664	11. Contract or Grant No.

12. Sponsoring Organization Name and Address		13. Type of Report and Period Covered
Iowa Department of Transportation 800 Lincoln Way Ames, IA 50010	Federal Highway Administration 1200 New Jersey Avenue, SE Washington, DC 20590	Final Report
		14. Sponsoring Agency Code SPR RB33-013

15. Supplementary Notes

Visit https://intrans.iastate.edu/ for color pdfs of this and other research reports.

16. Abstract

The Iowa Department of Transportation (DOT) funded a three-phase research project focusing on rapid bridge deck joint repair. Phase I focused on the documentation of current means and methods of bridge expansion joint maintenance and replacement. Under Phase II, a workshop with Iowa DOT personnel, engineers, and researchers identified possible improvements to traditional expansion joint options. From the workshop, a deck over backwall detail was developed that moved the expansion joint away from the bridge deck and instead placed it on the approach slab. This would not only minimize the concrete removal needed for a rehabilitation but would, in turn, prevent deicing chemicals from leaking through the deck joints and damaging the bridge's substructure. In Phase III, the research team was tasked with the further development of this deck over backwall concept.

Full-scale finite element (FE) models of two different bridges were developed to analyze the impact of the deck over backwall concept. Both models were validated using the original drawing plans and American Association of State Highway and Transportation Officials (AASHTO) specifications.

Through experimental testing and the development of FE models, two reinforcing options within the approach slab and diaphragm sections were considered. The results showed that, when both the top and bottom longitudinal reinforcing was kept continuous through the approach slab and diaphragm section, negative moment was transferred to the bridge deck. This transfer of stress through the top reinforcing caused cracking to occur on the top of the bridge deck, which could lead to harmful chemicals leaking onto the substructure. Conversely, experimental testing showed that these stresses could be eliminated if the top longitudinal reinforcing and concrete cover were saw cut.

A plan for construction observation and post-construction testing was developed that included an instrumentation plan and various real-world truck loading cases to be correlated with the FE models; an initial cost estimate was also developed. Implementation of the deck over backwall concept and the post-construction plan is expected to be conducted in a future Iowa DOT construction season.

17. Key Words	18. Distribution Statement
bridge joint repair—bridge maintenance—deck over backwall—design details—expansion joint design—expansion joint replacement	No restrictions.

19. Security Classification (of this report)	20. Security Classification (of this page)	21. No. of Pages	22. Price
Unclassified.	Unclassified.	207	NA

Form DOT F 1700.7 (8-72) **Reproduction of completed page authorized**

RAPID BRIDGE DECK JOINT REPAIR INVESTIGATION – PHASE III

Final Report
December 2020

Principal Investigator
Charles T. Jahren, Professor
Construction Management and Technology
Institute for Transportation, Iowa State University

Research Assistants
David Morandeira and Elizabeth Miller

Authors
David Morandeira, Elizabeth Miller, and Charles T. Jahren

Sponsored by
Iowa Department of Transportation

Preparation of this report was financed in part
through funds provided by the Iowa Department of Transportation
through its Research Management Agreement with the
Institute for Transportation
(InTrans Project 13-451)

A report from
Institute for Transportation
Iowa State University
2711 South Loop Drive, Suite 4700
Ames, IA 50010-8664
Phone: 515-294-8103 / Fax: 515-294-0467
https://intrans.iastate.edu/

TABLE OF CONTENTS

LIST OF FIGURES

LIST OF TABLES

ACKNOWLEDGMENTS

The authors would like to thank the Iowa Department of Transportation (DOT) for sponsoring this research as well as the Federal Highway Administration for state planning and research (Federal SPR Part II, CFDA 20.205) funds used for this project.

The authors would like to thank the technical advisory committee for this project, including Dean Bierwagen, Mark Carter, Dan Cramer, Matt Johnson, Linda Narigon, James Nelson, Steve Sandquist, Justin Sencer, and Wayne Sunday. A multitude of Iowa DOT personnel, too numerous to list, were engaged on this project, and the authors would like to thank each of them for their individual contributions.

EXECUTIVE SUMMARY

Bridge deck expansion joints are used to allow movement of the bridge deck due to thermal expansion, dynamic loading, and other factors. More recently, expansion joints have been sealed to prevent winter deicing chemicals and other corrosives applied to bridge decks from leaking through the deck joints and damaging the bridge's substructure. Expansion joints are often one of the first components of a bridge deck to fail, and repairing or replacing expansion joints is essential to extending the life of the bridge.

The Iowa Department of Transportation (DOT) funded a three-phase research project focusing on rapid bridge deck joint repair. In the Phase I study, the research team focused on documenting the current processes, means, and methods of bridge expansion joint deterioration, maintenance, and replacement and on identifying improvements to joint design, maintenance, and replacement based on the input gathered.

After maintenance and replacement strategies were identified, a workshop was held at the Institute for Transportation at Iowa State University to develop ideas to better maintain and replace expansion joints. Maintenance strategies were included in the discussion to explore ways to extend the useful life of joints and thereby decrease the number of joints replaced in a year and reduce traffic disruptions.

In the Phase II study, the research team focused on providing details about the types of failure exhibited by expansion joints in Iowa, measures taken to repair and prevent these types of failures, current construction methods used by contractors in Iowa, and hypothesized ways to improve methods of expansion joint repair and maintenance.

A second workshop was held with an emphasis solely on the replacement of expansion joints. Discussion topics included various methods of replacing joints, the possibility of using partial-depth deck removals for replacements, the removal of existing reinforcing steel from the end of the deck, and an alternative construction design that would eliminate the joint at the abutment and move it to a less problematic location. This alternative design was named the deck over backwall concept.

In this Phase III study, the deck over backwall concept was developed in detail. Full-scale finite element (FE) models of two different bridges were developed to analyze the impact of the deck over backwall concept. Both models were validated using the original drawing plans and American Association of State Highway and Transportation Officials (AASHTO) specifications. Further investigation using these full-scale models led to more design options within the deck over backwall concept. Experimental testing was conducted with two reinforcing options within the approach slab and diaphragm section. The results were then compared to smaller finite element models that matched the testing setup.

The results showed that when the both the top and bottom longitudinal reinforcing was kept continuous through the approach slab and diaphragm section, negative moment was transferred

to the bridge deck. This transfer of stress through the top reinforcing caused cracking to occur on the top of the bridge deck that could lead to harmful chemicals penetrating the substructure. Conversely, experimental testing showed that these stresses could be eliminated if the top longitudinal reinforcing and concrete cover were saw cut.

In summary, through a cooperative effort with the Iowa DOT Office of Bridges and Structures and Office of Construction and Materials, district bridge maintenance crews, and contractors, the researchers on this project developed the deck over backwall design concept. Implementation of the deck over backwall concept and the post-construction plan is expected to be conducted in a future Iowa DOT construction season.

CHAPTER 1. INTRODUCTION

1.1 Problem Statement

Accelerated bridge construction (ABC) techniques are changing the way that bridges are built across the US. Given the ever-increasing number of vehicles traveling over the nation's roadway infrastructure, reducing lane closure times has been identified as a key benefit of ABC techniques and practices. In recent years, extensive research has been conducted on ABC. However, less attention has been devoted to accelerated repair and replacement of bridge deck expansion joints. For bridges requiring expansion joints, there is a need for accelerated replacement techniques that would lengthen the life cycle of bridges in areas with high annual average daily traffic (AADT) levels and limited time for lane closures.

Many aging multiple-span bridges utilize some form of expansion joint to properly counteract thermal movement and other behaviors. These joints are also intended to prevent the passage of winter deicing chemicals and other corrosives applied to bridge decks so that they do not penetrate and damage the substructure components of the bridge. The majority of these expansion joints require frequent repair and multiple replacements during the normal service life of a bridge. Over the years, extensive research has been done to improve the longevity of these joints but has met with limited success. The elimination of deck joints instead of repair or replacement has been identified as a suitable and preferred option for bridges of moderate length, especially those with high traffic loads and where there are limited or no detour possibilities. Deck joints can be eliminated as part of an accelerated construction project that minimizes traffic disruptions. When deck joints are eliminated, the possible penetration of deicing chemical-laden water into the substructure components would be much less of a concern.

This three-phase project, Rapid Bridge Deck Joint Repair Investigation, was initiated to address the acute need for further research into accelerated options for the repair, replacement, and elimination of deteriorating bridge deck expansion joints in the state of Iowa and across the US.

1.2 Background

Phase I of this research project focused on documenting the current means and methods of bridge expansion joint maintenance and replacement and then conducting a workshop whose objective was to identify improvements to joint design, maintenance, and replacement. Phase II involved a literature review of topics related to bridge deck expansion joints, including the types of joints used or tested in other states, common and reported modes of failure in other states, integral abutments and differences in their use among states, and methods of eliminating deck joints from existing bridges, and surveys regarding the average life span of particular types of expansion joints. Two workshops were held that emphasized the replacement of expansion joints. Discussions during the workshops indicated that a desirable approach would be to develop a design that would (1) minimize the amount of required concrete removal and (2) move the joint away from the bridge deck at the abutment interface and instead place it on the approach slab. A schematic cross-section of both concepts can be seen in in Figure 1.1 and Figure 1.2.

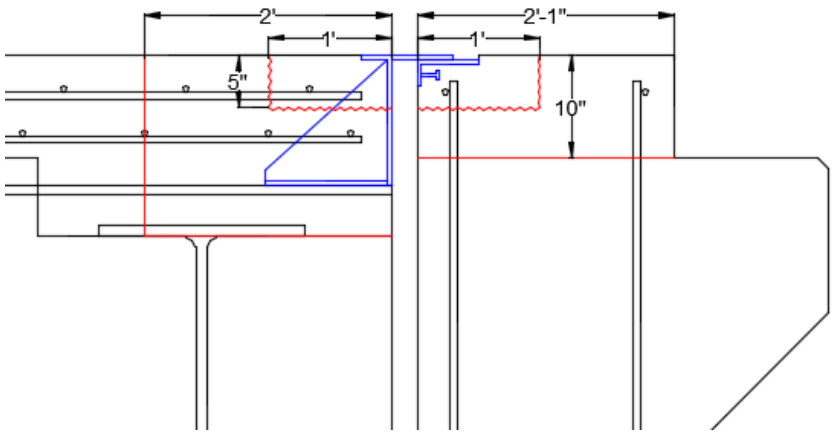

Miller and Jahren 2017

Figure 1.1. Minimum concrete removal concept

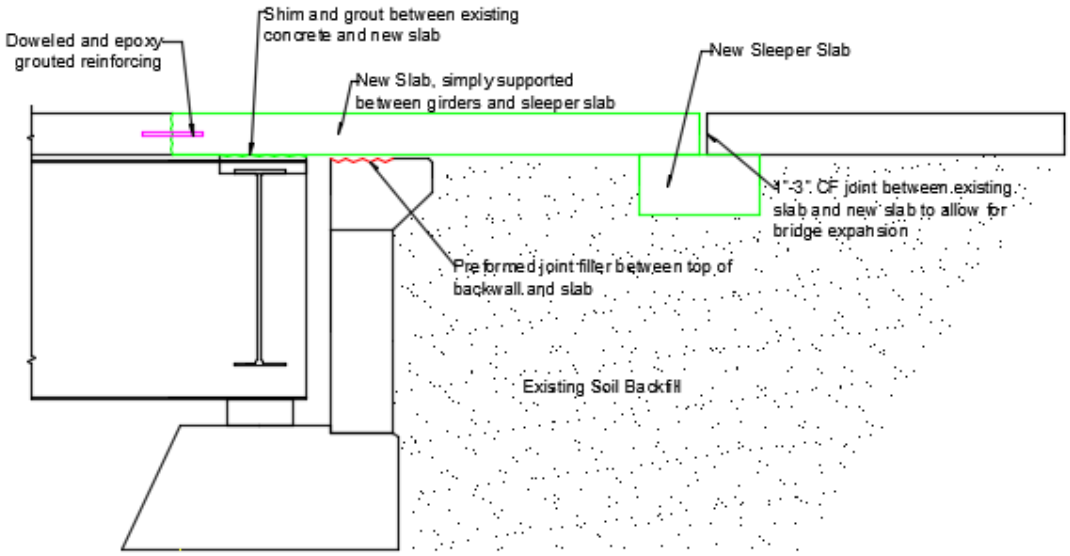

Miller and Jahren 2017

Figure 1.2. Deck over backwall concept

By minimizing the amount of concrete removed, as shown in the schematic cross-section in Figure 1.1, schedule times can also be minimized. Concrete removal has been recognized as one of the factors that most affects construction time during expansion joint replacement projects. The other schematic cross-section, Figure 1.2, shows a precast or cast-in-place (CIP) panel that is used to span the existing abutment backwall and relocate the joint onto the approach slab. By using this concept, the joint is moved to a location where the possible penetration of deicing chemical-laden water into the substructure components cannot occur and cause deterioration, and its construction time can be comparable to that required for traditional joint replacements.

1.3 Joint Detailing

In Phases I, II, and III of this project, the researchers worked with engineers from the Iowa Department of Transportation (DOT) to develop an appropriate detail for the deck over backwall concept that would perform well under Iowa DOT standards. The researchers presented various detailing options, including a cast-in-place approach slab, a precast slab, a sleeper slab, and micropiles. Using the various options presented, the detail described below was developed by Iowa DOT engineers in consideration of typical construction practices and preferences.

A section view of the preliminary detail developed is shown in Figure 1.3.

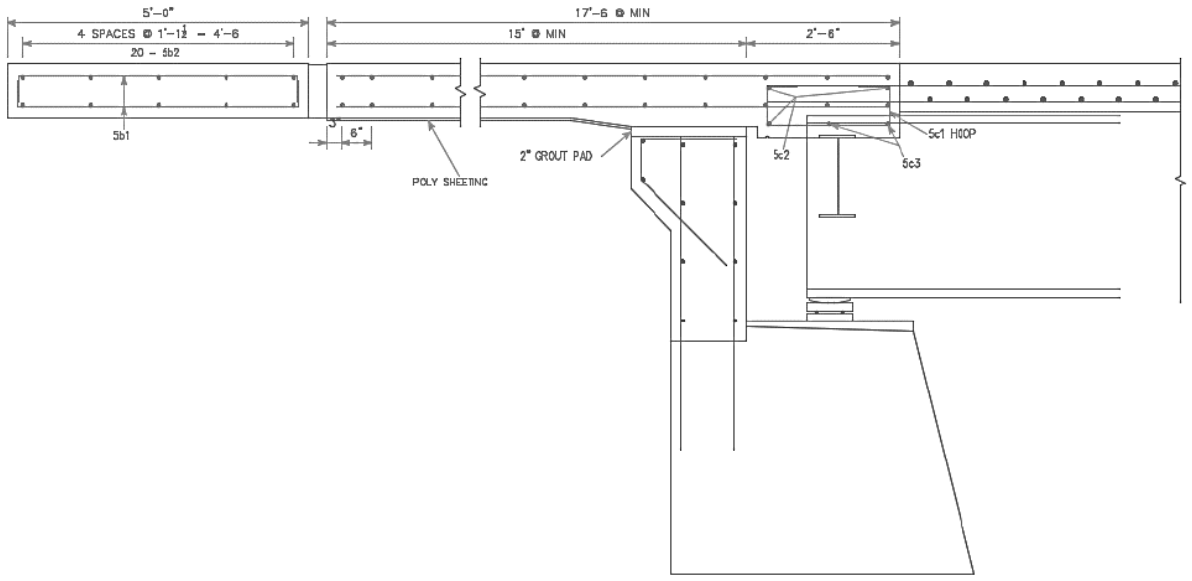

Iowa DOT

Figure 1.3. Preliminary approach slab detail developed by the Iowa DOT

As the figure shows, the initial detailing of the approach slab contains both top and bottom longitudinal reinforcing, continuous through the diaphragm and into the bridge deck. Additionally, reinforcing hoops are provided within the concrete diaphragm. The approach slab is not connected to the backwall and can freely slide over the element.

While both the top and bottom reinforcing are shown as continuous in Figure 1.3, the Iowa DOT provided the option of saw cutting either one or both of these longitudinal reinforcing elements. This is shown in Figure 1.4.

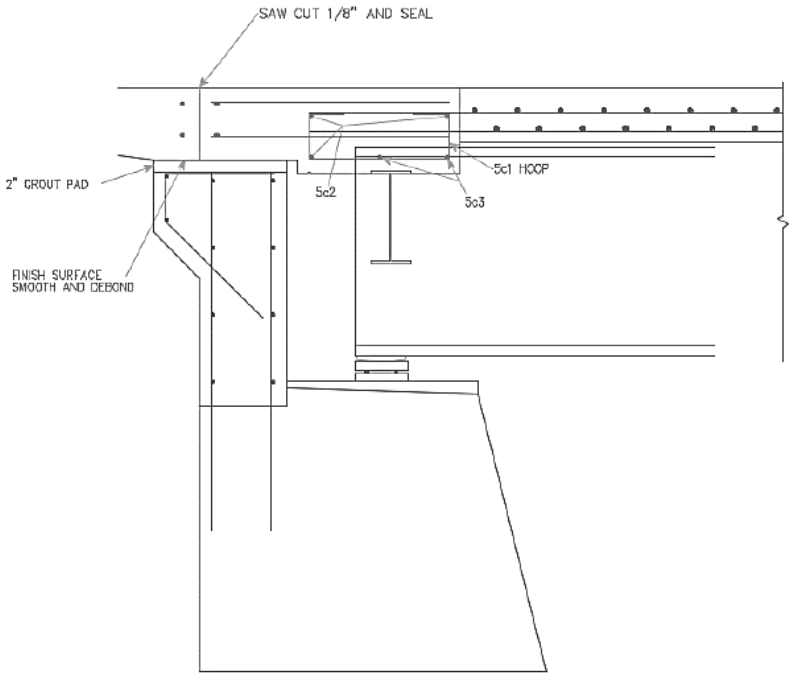

Iowa DOT

Figure 1.4. Preliminary approach slab detail with option of saw cut and seal

In this figure, both the top and the bottom reinforcing are shown as being cut. The detail identifies that after saw cutting, the joint should be sealed. This type of joint would aid the performance of the deck, should the approach slab deflect a considerable amount. With considerable deflection, the rotation of the approach slab would cause negative moment to be transferred into the existing bridge deck. The saw cut and sealed joint would prevent this moment and additional stresses from fully transferring to the existing bridge deck. This would mitigate any extra cracking that may occur while also preventing any rotation of the deck that might affect driver comfort.

Figure 1.3 also shows that a joint is to be provided a minimum of 17 ft 6 in. from the existing bridge deck in the approach slab. Possible options for this joint could include a sleeper slab, a subdrain, or the Iowa DOT's EF, CF, or CD joints. A combination of these could also be implemented.

Figure 1.5 details the concrete removal process that should occur to implement the detail outlined in the previous figures.

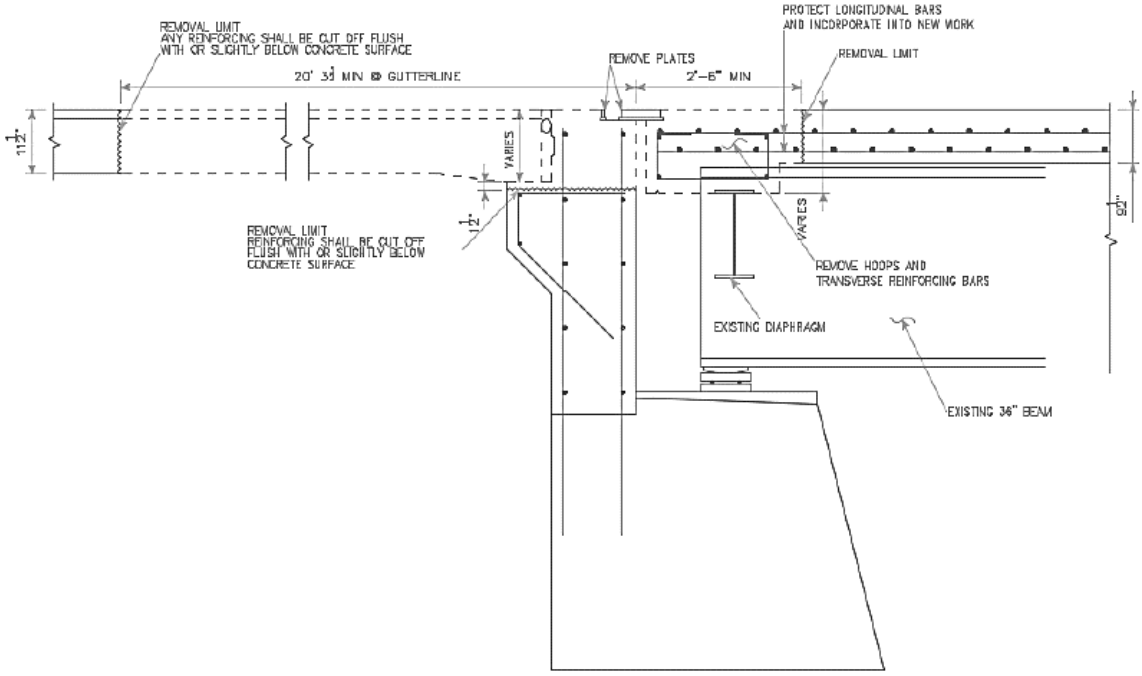

Iowa DOT

Figure 1.5. Concrete removal process for Iowa DOT joint

Several important aspects critical to the performance of the joint are detailed. First, the figure identifies that both the top and bottom longitudinal bars from the bridge deck should be protected during the removal process. Keeping these bars ensures that their strength can be fully developed in the new approach slab section. Second, the detail identifies that the minimum removal limit of the bridge deck can be no less than 2 ft 6 in. Finally, the removal limits for the approach slab should be approximately 20 ft, corresponding to the length of an Iowa DOT approach slab section. The depths of the previously existing bridge deck, the concrete above the steel diaphragm girders, and the new approach slab sections vary.

Figure 1.6 shows an example plan view of the joint developed by the Iowa DOT.

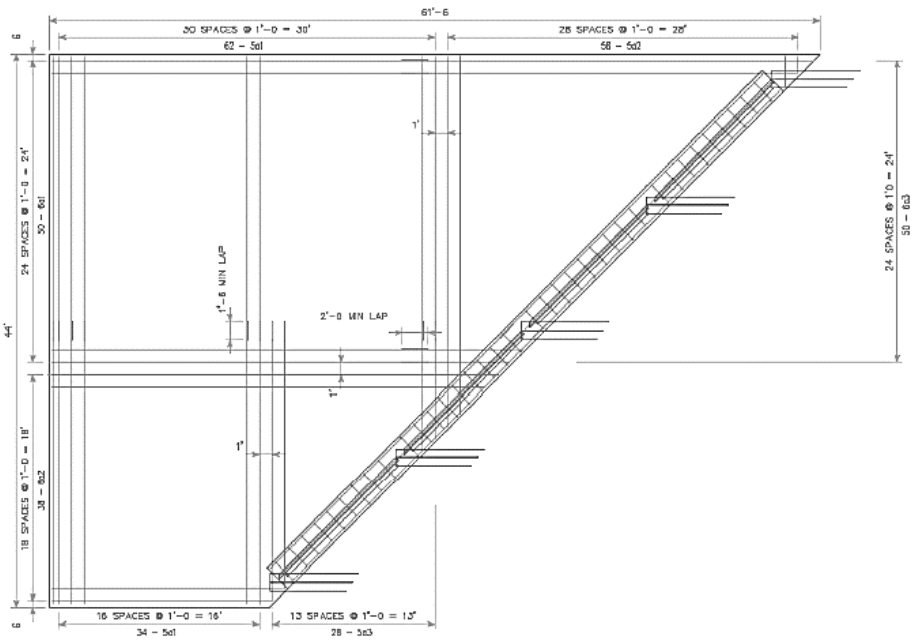

Iowa DOT

Figure 1.6. Plan view of Iowa DOT joint

The example plan view is provided for a skewed bridge. The reinforcing in both the longitudinal and transverse directions of the approach slab is shown. Spacing for these bars is 1 ft in all directions. Additionally, splice lengths for these bars are provided.

1.4 Objectives

The objectives of this research are as follows:

- Conduct a literature review on the repair, replacement, and elimination of bridge deck expansion joints
- Further develop the deck over backwall concept with plans that conform to the design concepts developed in previous phases of this project
- Create finite element (FE) models of selected bridges and study the impact of the concept on the existing bridge structures
- Conduct experimental testing to evaluate the performance of the deck over backwall concept
- Compare the cost of application of the concept to that of other types of joints
- Develop a plan for construction observation and post-construction testing where the concept can be further studied after implementation

By achieving these objectives, the deck over backwall concept will be furthered developed and the Iowa DOT can confidently design and implement the concept.

CHAPTER 2. LITERATURE REVIEW

The research team conducted a review of the published literature on three relevant topics. The first topic is the current practices and options for the accelerated repair and replacement of expansion joints. Related to the first topic, the use of ultra-high performance concrete (UHPC) in bridge joints and connections was reviewed. Finally, the various practices for modeling and analyzing bridge structures and soil properties using commercial software were studied.

2.1 Repair, Replacement, and Elimination of Expansion Joints

A thorough review of the literature on accelerated methods of repair, replacement, and elimination of expansion joints was conducted in Phases I and II of this research. In conjunction with the Iowa DOT, Miller and Jahren (2014) conducted an investigation focused on determining the best ways to rapidly repair and replace expansion joints in Iowa and other states. Their findings were synthesized by Phares and Cronin (2015). The findings are discussed and summarized in the following pages.

2.1.1 Joint Repair and Replacement

The literature review revealed that demolition and concrete cure times account for the longest segments of construction time in expansion joint replacement projects (Miller and Jahren 2017). Hydrodemolition was identified as an effective and quick way to remove concrete from the surrounding areas of the expansion joint; however, it is costly, and runoff containing small concrete particles is an issue that must be dealt with (Phares and Cronin 2015).

To repair or replace sliding plate expansion joints, Iowa DOT personnel stated that it would be best to remove the joint entirely. The open space would be filled with new concrete while leaving a flat gap between the abutment and deck for expansion and contraction of the bridge (Miller and Jahren 2014). This method of replacement avoids any unnecessary traffic delay (Phares and Cronin 2015) but allows the free flow of chemical-laden water into the substructure below. Therefore, this is recommended as a temporary solution.

There are various methods of repair and replacement for strip seal and compression seal expansion joints. These methods depend on the condition of the expansion joint mechanism in question. The use of compressed air or pressurized water to remove debris from the joint is acceptable as long as the seal or extrusion is not damaged. If the strip seal or compression seal is damaged, it may need to be removed and cleaned, or a new seal could be installed. The new section may be spliced in, or the entire length of the seal may be replaced (Miller and Jahren 2014). Miller and Jahren (2014) pointed out that a new section should not be spliced between two existing sections due to buckling concerns.

Various methods were recognized to replace the compression seal armoring. The armoring can be replaced by removing and replacing the existing concrete with new concrete for a flat riding surface. However, the process takes several hours to complete. Miller and Jahren (2014) found

an alternative system that can be installed in as little as 30 minutes per lane if no repair of the vertical face of the concrete is required. This system is an inverted strip seal called the Silicoflex joint sealing system from RJ Watson, Inc. It is installed using adhesives instead of extrusions. The system has to be installed against a clean, flat, vertical face below the damaged extrusion (Miller and Jahren 2014).

Other types of joints were also considered in the literature review. Finger and modular expansion joints were found to be repairable by replacing the damaged joint component. The effort required for replacement is variable and depends on the specific circumstances. In some cases, replacement is a straightforward process. If a torn neoprene gland is discovered, the entire joint does not have to be replaced. A new neoprene gland can be installed after the damaged one is removed (Miller and Jahren 2014).

Integral abutment joints were also investigated. Miller and Jahren (2014) found that possible locations of damage can usually be found on the tire buffing and silicon sealant. To repair these deteriorated items, missing pieces from the tire buffing are replaced and new silicon is poured into the joint (Miller and Jahren 2014).

2.1.2 Joint Elimination

In Phase II of this research, Miller and Jahren (2017) found that most bridge engineers would consider the best type of joint to be no joint. Through a survey distributed to all state highway agencies in the US, Palle et al. (2012) similarly found that most state highway agencies sought to eliminate joints wherever possible. Several noted that joint elimination was a goal for new bridge designs (Palle et al. 2012). In their investigation, Miller and Jahren (2017) conducted a thorough review of the literature for possible joint elimination options. Elimination options were found in integral abutments, semi-integral abutments, and link slabs.

2.1.2.1 Integral Abutments

The trend for accelerated methods of repair and replacement of expansion joints seems to be toward eliminating deck joints altogether by utilizing the integral abutment design. A few agencies are using this design as their sole option for new construction (Baker Engineering 2006). It is for this reason that integral abutment bridges are becoming increasingly popular in the US.

Integral abutments differ from the more traditional type of abutments, which are most commonly known as stud abutments, in that they embed the ends of the bridge girders into the backwall. An integral abutment moves along with the movement of the girders due to thermal loading, dynamic loading, and other factors. The pile supports of the abutment deflect as necessary to accommodate abutment movement. A cross-section of a typical integral abutment can be seen in Figure 2.1.

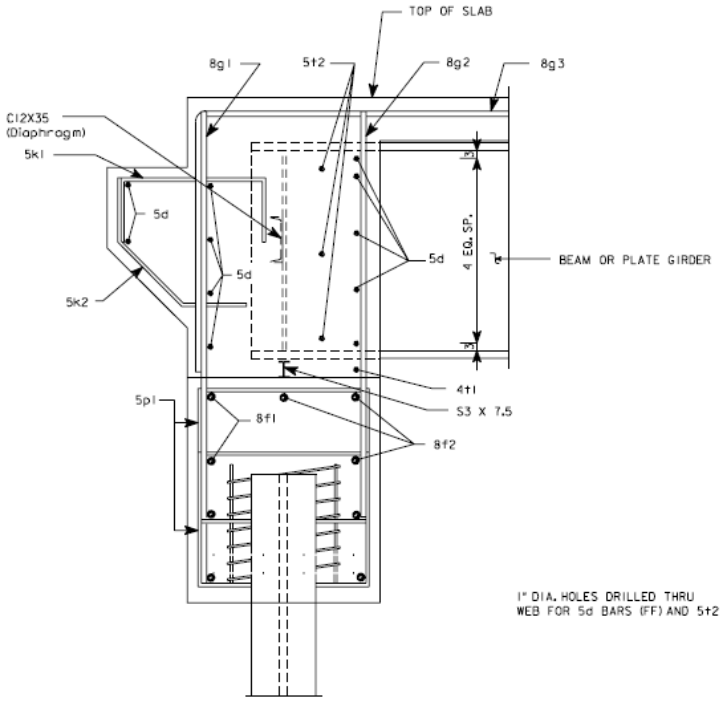

Dunker and Abu-Hawash 2005, Mid-Continent Transportation Research Symposium, Iowa State University Center for Transportation Research and Education

Figure 2.1. Integral abutment cross-section

Most states that employ the use of these abutments have reported that they are satisfied with their performance. Maruri and Petro (2005) surveyed all transportation agencies in the US regarding their use of integral abutment bridges. A large number of agencies responded to the survey, providing a 79% response rate. The survey results indicated that the estimated number of in-service integral abutment bridges increased by almost 200% from an estimated 4,000 integral abutment bridges in 1995 to an estimated 13,000 or more integral abutment bridges in 2004 (Miller and Jahren 2017).

Since deicing chemicals and snowplows are widely used in the northern states of the US versus the southern states, integral abutments are much more common in the former than the latter. The survey results showed that the use of integral abutments will continue in the future, as 77% of the respondents stated that they will continue to use integral abutments for bridges where it is possible to do so. While most states reported that they were satisfied with the performance of their integral abutment bridges, three states in particular deviated. Arizona encountered problems with the bridges' approach slabs, while Vermont encountered scour issues. These two states abandoned the use of integral abutments for future bridges. The third state, Washington, encountered seismic issues and decided to move forward with semi-integral abutments for bridges under circumstances where integral abutments might have been considered.

2.1.2.2 Semi-integral Abutments

Semi-integral abutments were created as an alternative to integral abutments. This option functions in many of the same ways as an integral abutment. These abutments have the ends of the bridge girders embedded in the backwall. The semi-integral abutment also moves with the movement of the girders due to thermal loading, dynamic loading, and other factors. The main difference between the two is that for semi-integral abutments the entire backwall and girder system is situated on bearings and allowed to slide over a fixed foundation (Miller and Jahren 2017). A typical cross-section for a semi-integral abutment can be seen in Figure 2.2.

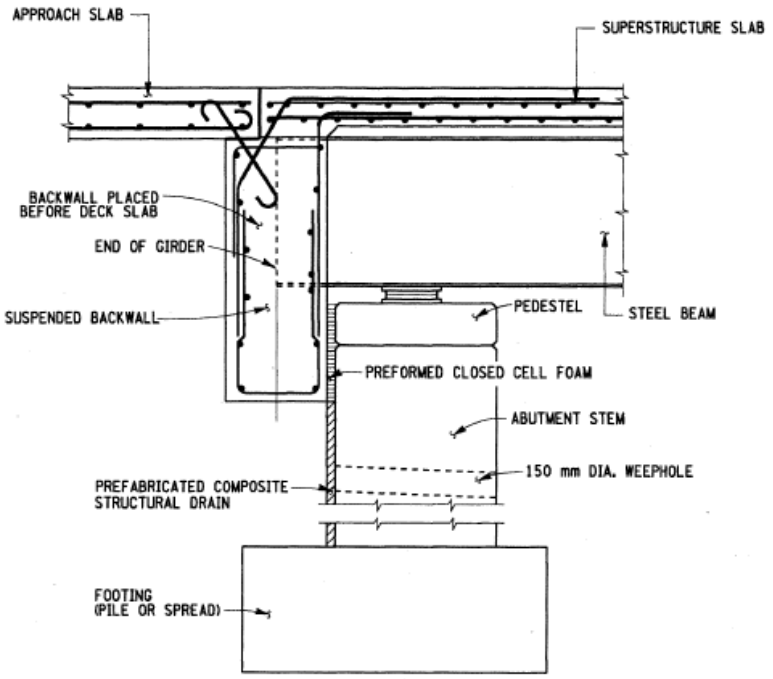

Yannotti et al. 2005, Integral Abutment and Jointless Bridges 2005 FHWA Conference. Constructed Facilities Center, College of Engineering and Mineral Resources

Figure 2.2. New York semi-integral abutment cross-section

In Iowa, semi-integral abutments are not often used for new bridge construction. Instead, semi-integral abutments are used for joint retrofits where an integral abutment is not compatible with the existing bridge design. Expansion joints across the states have been replaced with semi-integral abutments, mitigating the concern about possible deicing chemical-laden water penetrating the substructure components. While the use of semi-integral abutments has been increasing, semi-integral abutments have received much less attention than integral abutments. Semi-integral abutments have largely been used in unique situations where integral abutments do not work well, such as bridges with large skew angles or high backwalls or those built on difficult soil conditions (Miller and Jahren 2017). One common difficulty arises when bedrock is close to the surface and piles cannot develop sufficient horizontal resistance to provide fixity for the footing (Yanotti et al. 2005).

2.1.2.3 Link Slabs

While integral and semi-integral abutments are alternatives to eliminating expansion joints at the abutment interface, options for eliminating expansion joints above the piers are also available. Link slabs have been used in numerous projects across the US to replace expansion joints located over bridge piers. Link slabs do exactly what the name says: link the existing bridge deck between two girders over the pier supports.

Miller and Jahren (2017) explain that the stiffness of the continued deck is so small in comparison to that of the girders that continuity is assumed not to be provided. This means that the bridge will continue to act as a series of simply supported members, and thus the original bridge design will not be affected. The link slab acts as a beam with a moment caused by the rotation at the ends of the girders. To provide the necessary flexibility for the link slab, a portion of the deck is debonded at the ends of the girders (Aktan et al. 2008). A typical cross-section of a link slab can be seen in Figure 2.3, which shows the moment and rotation detailing.

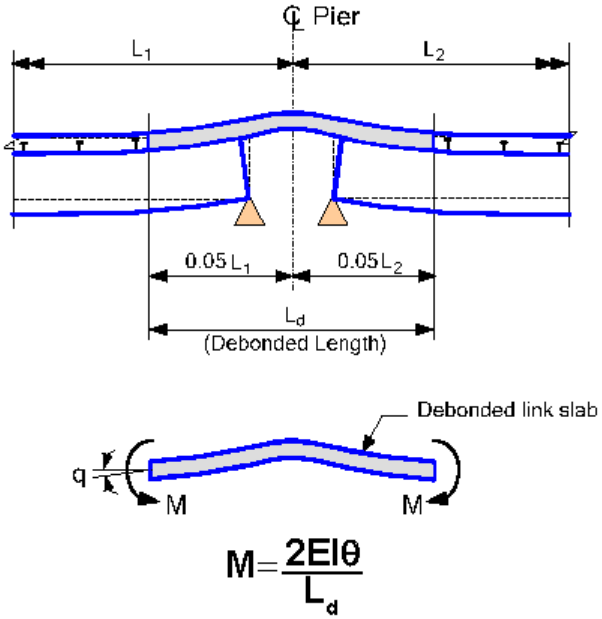

Lam et al. 2008, Ministry of Transportation of Ontario

Figure 2.3. Debonded link slab system

Since link slabs have not been implemented to the same extent as other methods of bridge deck joint repair, replacement, and elimination, there is a limited amount of knowledge in terms of their performance when implemented. Miller and Jahren (2017) describe a pilot link slab that was built in 1998 by the North Carolina DOT (NCDOT). The pilot link slab was instrumented, monitored, and tested after implementation. Beam end rotations of 0.02 radians were taken into account in the design of the link slab. The link slab was also meant to have fine cracks under service loads. The maximum width of these fine cracks was designed to be 0.013 in.

At no point over the next year of monitoring did the link slab exceed the 0.02 radians of beam end rotations. A crack wider than 0.013 in. was noticed in the middle of the link slab. This crack had a width of 0.063 in., was present before live load testing, and did not widen during the tests. It was ultimately believed that this crack was larger than designed due to localized debonding of the reinforcement (Wing and Kowalsky 2005).

Michigan installed numerous link slabs in the early 2000s as part of several deck rehabilitation projects across the state. Inspections of these bridges in 2006 yielded observations similar to those made by Wing and Kowalsky (2005) during the NCDOT study discussed above. In every link slab inspected, a full-depth crack was found approximately at the centerline of the pier, regardless of whether a saw cut had been made at these locations. However, other than the transverse cracking at the pier centerlines, little other cracking or damage was reported at the link slab locations (Aktan et al. 2008).

Aktan et al. (2008) completed a detailed FE analysis that was used to predict how certain parameters affect the performance of link slabs used in the state of Michigan. The investigated design parameters of the link slab were as follows: the link slab debonded length with respect to adjacent span lengths, girder height, adjacent span ratio, and support conditions. Several conclusions were drawn from the FE results:

- The top and bottom layer of steel should be continuous throughout the link slab.
- Additional moment and axial loads should be considered in the design of link slabs to account for thermal gradients.
- Saw cuts should be provided at the centerline of the pier and at each end of the link slab. These saw cuts concentrate cracking in areas where the performance of the link slab would not be diminished.

2.1.2.4 Deck over Backwall

Miller and Jahren (2017) held various workshops with the objective of identifying improvements to bridge deck joint maintenance and replacement. Workshop participants came up with a concept that eventually evolved into the deck over backwall concept shown in Chapter 1, Figure 1.2. Further review of the literature was conducted to study possible implementation of this concept in other states.

According to a 2004 survey, approximately 3,900 bridges with deck extensions are currently in use in the United States (Miller and Jahren 2017). This type of bridge is stated to be particularly prominent in the northeastern region of the US as opposed to the midwestern and northern regions, where full integral abutment designs are more common (Maruri and Petro 2005). The New York State DOT (NYSDOT) in particular has been building bridges with deck extensions since the 1980s or earlier (Alampalli and Yannotti 1998).

Alampalli and Yannotti (1998) detailed 105 deck extensions that were inspected by the NYSDOT, 72 with concrete superstructures and 33 with steel superstructures. These bridges

were found to be performing as anticipated, with minor deck cracking being the only significant problem. Miller and Jahren (2017) drew several conclusions regarding deck extensions, including the following two:

- Steel structures are usually less prone to deck cracking than prestressed-concrete superstructures.
- Performance typically worsens with increased skew or span length.

Miller and Jahren (2017) compared jointless bridges and other types of joints, mainly compression seals, utilizing NYSDOT bridge inspection and inventory data. The results of the analysis show that components of jointless bridges performed better than components of compression seal bridges.

Construction details for a typical NYSDOT deck extension are shown in Figure 2.4.

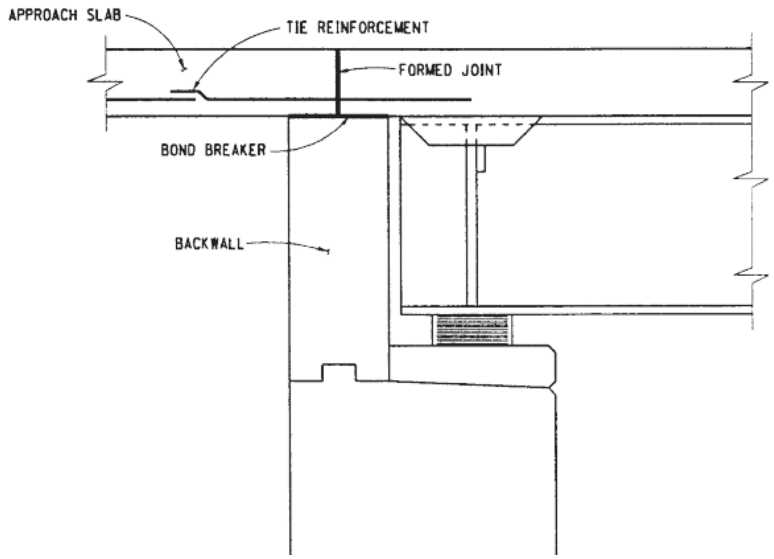

Alampalli and Yannotti 1998

Figure 2.4. NYSDOT deck extension detail

Discussing the detail, Alampalli and Yannotti (1998) mentioned that the deck and approach slab used to be included in a single placement, and the formed joint was merely a saw cut to promote full-depth cracking at the correct location. The design of NYSDOT deck extensions has since been changed. The approach slab and deck are placed separately now, eliminating the need for a saw cut. This joint is provided to allow superstructure rotation with the bottom layer of longitudinal deck steel continuous through the joint to keep the deck and approach slab from separating (Alampalli and Yannotti 1998).

Other DOTs have also developed jointless bridge decks with deck extension details similar to those of the NYSDOT joint and the concept introduced in the Phase II workshops for this study, which eventually evolved into the deck over backwall concept.

The Michigan DOT (MDOT) has worked on developing jointless bridge decks to combat deterioration of the leaking expansion joints. MDOT's detailing is shown in Figure 2.5.

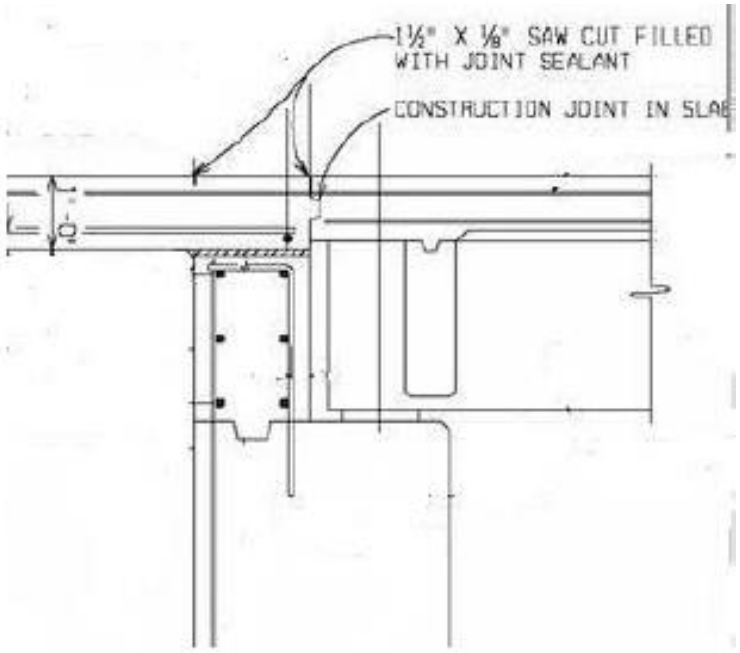

Aktan et al. 2008

Figure 2.5. MDOT deck extension detail

Various differences can be seen between the NYSDOT and MDOT joints:

- Location of the construction joint (in line with the center of the backwall for the NYDOT joint; in line with inside edge of the backwall for the MDOT joint)
- Location of the continuous longitudinal reinforcing (bottom reinforcement for the NYSDOT joint; top reinforcement for the MDOT joint)
- Incorporation of a sleeper slab in the MDOT joint

Miller and Jahren (2017) pointed out that continuing the top layer of reinforcing through the joint should allow negative moment transfer across the construction joint as opposed to allowing the joint to act as a hinge.

Approach slab standards differ between the Iowa DOT and MDOT. The Iowa DOT uses 20 ft approach slabs, while MDOT only uses 20 ft approach slabs for bridges with integral and semi-integral abutments. However, for deck extension details, MDOT extends the approach slab 5 ft from the near edge of the backwall to rest on a sleeper slab. This sleeper slab is intended to help

mitigate possible settlement issues between the existing pavement and the new approach slab. MDOT's sleeper slab detailing can be seen in Figure 2.6.

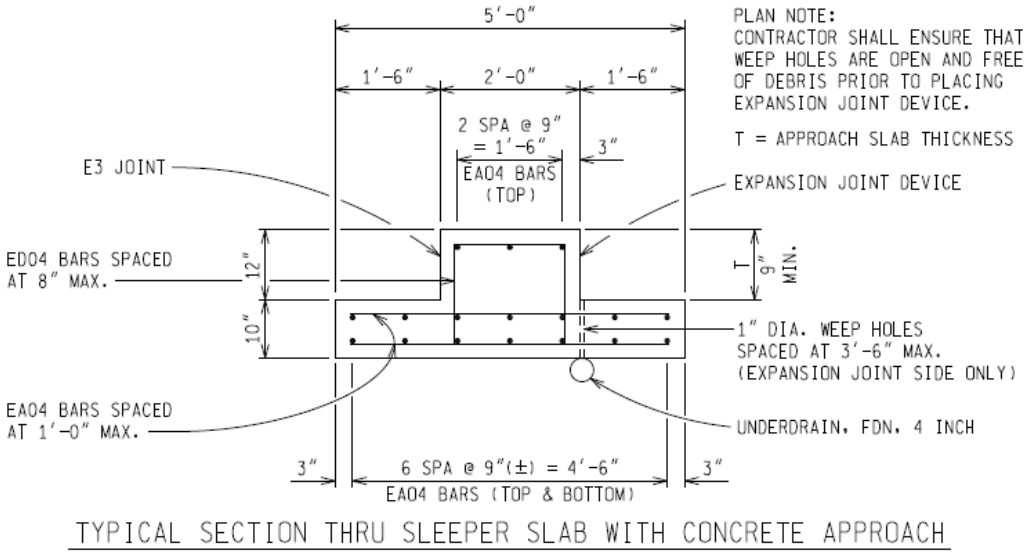

Michigan DOT

Figure 2.6. MDOT sleeper slab detail

Western Michigan University (WMU) developed FE models to help MDOT to analyze its deck extension details and further improve its designs. The difference between continuing the top layer of steel reinforcement versus the bottom layer of steel reinforcement was of particular interest. FE results showed that continuing the top layer of reinforcing caused the construction joint to transfer negative moment, i.e., tensile stresses, at the top of the approach slab around the construction joint. Continuing the bottom layer of longitudinal reinforcing caused the joint to act as a hinge, eliminating the stresses at the construction joint but increasing the nominal positive moment at the midpoint of the approach slab. Given the later situation, continuity of the bottom layer of steel was preferred (Aktan et al. 2008).

Miller and Jahren (2017) agreed with this conclusion because cracking can be allowed on the bottom side of the slab. Designing for the additional midspan moment is more achievable than designing for negative moment capacity at the top of the deck, where cracking should be prevented. A waterstop could be included in the construction joint to prevent the passage of water and mitigate additional cracking (Miller and Jahren 2017).

The research team contacted MDOT staff to obtain more information about their experiences with bridge extension. The following summarizes the key takeaways:

- The implemented deck extensions for MDOT achieved the objectives that the Iowa DOT is seeking to accomplish.
- Future detailing will provide continuous bottom reinforcement.

- An approach slab will be poured after the deck to provide a cold joint in the abutment interface.
- Settlements issues at the sleeper slab can cause a bump at the transition from the approach slab to the highway pavement.

2.2 Use of Ultra-High Performance Concrete for Bridge Joints

Thirty years ago, a new technology called UHPC started being researched for use in bridge design and construction. This new material offered very durable solutions but required new shapes, new design codes and standards, and new precast fabrication methods and formworks (Perry and Corvez 2016). The lack of design codes and standards increased the risk of implementation for owners and designers. These limitations held the material back from growing in use at a faster pace. Nonetheless, as a very young material, 30 years into research and 20 years into development, acceptance has been growing as more research has been conducted. The industry has been noticing the advantageous properties that the material possesses (Perry and Corvez 2016).

2.2.1 Mechanical Properties

According to American Concrete Institute (ACI) Committee 239 – Ultra-High Performance Concrete (2012), UHPC is "a cementitious, concrete material that has a minimum specified compressive strength of 150 MPa (21.6 ksi) with specified durability, tensile ductility and toughness requirements; fibers are generally included to achieve specified requirements." UHPC exhibits very high compression strength, improved tensile behavior, and sustained post cracking strength (Ronanki et al. 2016). This high compression strength and improved tensile behavior facilitate high bond strength and, as a result, a short development length for steel reinforcement. This is fully explained in the Federal Highway Administration (FHWA) Technical Note *Design and Construction of Field-Cast UHPC Connections* (Graybeal 2014).

Additionally, Fehling et al. (2015) explain that "compared with conventional normal- and high-strength concretes with their capillary porosity, UHPC exhibits a much denser microstructure. It has virtually no capillary pores and is therefore so impervious to liquids and gases that its corrosion [potential for embedded reinforcing] is practically zero; it can serve as the wearing course of a bridge deck without any additional protection against chlorides, alkalis, or deicing salts." The low permeability is attributed to the fine powders and chemical reactivity, which create an extremely compact matrix and a small, discontinuous pore structure (Perry and Royce 2010). UHPC formulations often consist of a combination of portland cement, fine sand, silica fume, high-range water-reducing admixture (HRWR), fibers (usually steel), and water. Small aggregates are sometimes used, as well as a variety of chemical admixtures (Russell and Graybeal 2013). The improved properties of UHPC provide such benefits as simplified construction techniques, increased speed of construction, improved durability, reduced maintenance, reduced service outages, minimum interruption of traffic, reduced element size and complexity, extended usage life, and improved resiliency (Perry and Corvez 2016).

2.2.2 Implementation of UHPC in Bridges

The first use of UHPC in a North American bridge was in 1997 for construction of the Sherbrooke Pedestrian Bridge in Quebec, Canada (Perry and Seibert 2013). This 197 ft clear span bridge, shown in Figure 2.7, was constructed from six precast 3D space truss UHPC elements, post-tensioned together on site.

Lafarge

Figure 2.7. Sherbrooke Pedestrian Bridge, Quebec, Canada (1997)

Russell and Graybeal (2013) explain that "[t]he structural concept consists of a space truss with a top UHPC chord that serves as the riding surface, two UHPC bottom chords, and truss diagonals that slope in two directions."

In 2001, the FHWA initiated a research program to evaluate and introduce UHPC into the US highway program (Graybeal 2008). The first UHPC highway bridge completed in North America was the Mars Hill Bridge in Wapello County, Iowa (Bierwagen et al. 2006). The simple single-span bridge, shown in Figure 2.8, comprises three 110 ft long, 45 in. deep, precast, prestressed concrete modified Iowa bulb-tee beams topped with a CIP concrete bridge deck.

Bridge Engineering Center 2008

Figure 2.8. Mars Hill Bridge, Wapello County, Iowa (2006)

Each beam containes 47 0.6 in. diameter, low-relaxation prestressing strands and no shear reinforcement (Russell and Graybeal 2013). The most significant aspect of this first UHPC highway bridge was the use of the three UHPC I-girders without any stirrups for shear reinforcing. This was a major milestone and a significant step toward the introduction of UHPC into the North American highway system (Perry and Corvez 2016).

During this same period, the FHWA was working on an optimized precast bridge profile called the pi-girder (π). The first generation of this girder was prototyped and installed at a test track at the FHWA's Turner-Fairbank Research Center near Washington, DC (Perry et al. 2010). In 2008, Buchanan County, Iowa, completed the Jakway Park Bridge, shown in Figure 2.9, using the second generation precast UHPC pi-girder (Graybeal 2004).

Bridge Engineering Center 2011

Figure 2.9. Jakway Park Bridge, Buchanan County, Iowa (2008)

The cross-section, shown in Figure 2.10, is similar to that of a double-tee section but with bottom flanges on the outside of each web (Russell and Graybeal 2013).

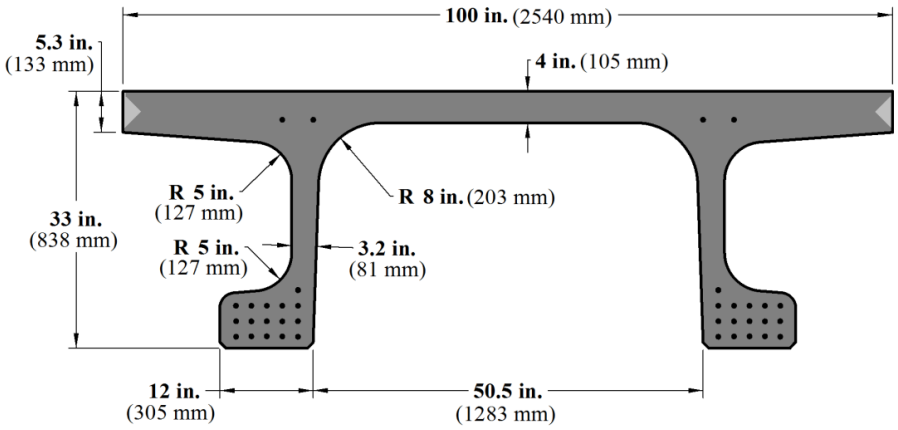

Russell and Graybeal 2013

Figure 2.10. Cross-section of pi-shaped girder

By the end of 2016, more than 200 bridges with UHPC elements had been completed in North America. These bridges included precast bridge elements, field-cast connections (for precast bridge elements), or, in some cases, both precast and field-cast UHPC solutions (Perry and Corvez 2016).

While it is recognized that precast bridge components can provide high durability, conventional joints are often the weakest link in a bridge deck system. During the period from 2006 through 2016, more than 200 precast bridges were completed using UHPC field-cast connections in North America (Perry and Corvez 2016). The UHPC joints are filled with UHPC, and reinforcing steel is lapped across the joint. The lap length of the reinforcing steel is based on the recommendations found in *Design and Construction of Field-Cast UHPC Connections* (Graybeal 2014). UHPC field-cast connections have been used to connect precast bridge elements such as full-depth precast deck panels (shown in Figure 2.11), side-by-side box girders, and side-by-side deck bulb-tees; provide live-load continuity connections; connect precast approach slabs to abutments, curbs to decks, and piles to abutments; and provide connections in the haunches (to provide horizontal shear for composite construction) (Perry and Seibert 2013).

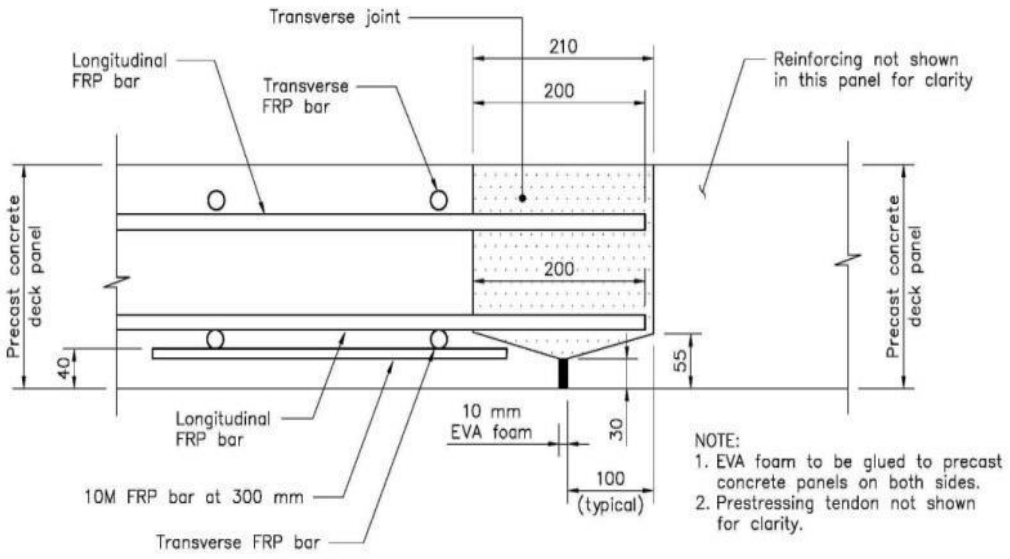

Perry and Seibert 2013

Figure 2.11. Typical section through a transverse, full-depth precast panel joint

In 2009, the first highway bridge using UHPC joints between full-depth deck panels was constructed in the US. Since then, 17 bridges of its kind have been built in the US. As of 2013, six states had built precast deck panel bridges with UHPC joints (Liu and Schiff 2016). In 2012, 13 bridges were completed using this technology, and in 2013 more than 30 bridges with UHPC elements were completed in multiple state and provincial jurisdictions in the US and Canada (Perry and Corvez 2016).

The following three sections describe the use of UHPC joints in three states: New York, Illinois, and New Jersey. For New York, four case studies are presented, one of which describes the first use of UHPC joints for a highway bridge in the US in 2009. One project each is presented for Illinois and New Jersey.

2.2.2.1 UHPC in New York

New York's extensive state and local highway network, which annually handles over 130 billion vehicle miles driven, is often in need of repair or replacement of bridge decks and bridge superstructures. New York has a long history of using prefabricated bridge elements and systems (PBES) for accelerating bridge construction to maintain acceptable levels of mobility. Since 2008, NYSDOT has been deeply involved in the development, testing, trial application, and utilization of field-cast UHPC joints between prefabricated elements for ABC (Royce 2016). As of 2016, NYSDOT has successfully completed the construction of 30 bridges utilizing UHPC connections between prefabricated elements. Royce (2016) presents the NYSDOT's experience with ABC using PBES and field-cast UHPC joints.

This section presents four case studies describing projects in New York that involved UHPC elements and describes the development of an innovative link slab design utilizing UHPC.

Case Study 1 involves the first field application of UHPC joints in bridge construction in the US: the superstructure replacement of Route 31 over Canandaigua Outlet in 2009. The bridge is an 85 ft single-span bridge with limited available beam depth (Figure 2.12).

Royce 2016, NYSDOT Office of Structures

Figure 2.12. Route 31 over Canandaigua Outlet - deck bulb-tee in place before UHPC placement

Longitudinal UHPC connections joints were used with deck bulb-tees. Royce (2016) explains that this was implemented to shorten construction times and make the system more durable than CIP systems. The material supplier educated the contractor about the importance of leak-proof forms before placing UHPC. The top ¼ in. of the UHPC joint fill has a tendency to have a low-quality material that needs to be removed; therefore, joints were overfilled to ensure that the entire finished joint was filled with high-quality material. The success of this experience led to the design and construction of several bridge superstructures with prefabricated deck beam elements with UHPC joints.

Case Study 2 details the second application of UHPC in the US, which was the construction in 2009 of a 127 ft single-span steel girder bridge with a precast concrete deck with UHPC joints near Oneonta, New York (Figure 2.13).

Royce 2016, NYSDOT Office of Structures

Figure 2.13. Route 23 over Otego Creek in Oneonta - precast deck placement in progress

The UHPC placement operation was completed in two days without any major problems. Royce (2016) says it could have been completed in a day if the contractor had sufficient labor and had larger UHPC mixers. Careful storage of the UHPC premix through the storage period was observed because any moisture penetration into the premix powder results in the formation of silica balls in the UHPC mix (Royce 2016). To reduce or eliminate this problem, the supplier improved the packaging and storage of the material as well as the mixing process. During the placement of UHPC in the joints, a few areas of leakage were noticed and corrected during construction. NYSDOT contract documents now alert contractors about the need for water-tight forms (Royce 2016).

Case Studies 1 and 2 both utilized prefabricated components and achieved a considerable reduction in construction time compared to conventional methods. After these projects were completed, further improvements to this technology that would help accelerate construction were identified. Among them were, first, to avoid the use of overlays over the precast components. The use of concrete overlays was problematic due to the needed cure times, and avoiding their use was a desirable improvement. As a solution, NYSDOT developed precast deck systems that have a sacrificial thickness of ½ in. for diamond grinding after the completion of the deck to obtain a smooth riding surface. Two types of composite connections were developed to avoid the use of overlays: (1) UHPC haunches with open stud pockets in addition to the joints and (2) hidden haunches with two types of fill material, cementitious grout or UHPC. The cementitious grout fill material needed to have 6 in. studs penetrating above the bottom layer of the deck reinforcement, while the UHPC-filled haunches were designed with 3 in. studs. The shorter studs are allowable with the UHPC due to its high sustained tensile strength. The use of UHPC-filled haunches with 3 in. studs was found to be the most efficient construction method, though the material cost is bit higher. Second, accelerating the compressive strength gain of the UHPC joints was identified as another desirable improvement. A compressive strength of 14 ksi was determined to be adequate for the performance of UHPC joints under live traffic. To complete a

deck removal and replacement during one weekend closure, the available cure time for UHPC was determined to be 12 to 14 hours.

Case Study 3 details the construction of two bridges on Route 42 over West Kill in Lexington, New York. A 120 ft single-span precast deck over a new multi-girder steel superstructure with UHPC joints over the steel girders is shown in Figure 2.14.

Royce 2016, NYSDOT Office of Structures

Figure 2.14. Route 42 over West Kill - panel joint placement in progress

These bridges were constructed during the winter of 2011 under an emergency contract. In August of 2011, the original bridges were washed out during Hurricane Irene. Stud sheer connectors were installed through openings in the deck panel with UHPC-filled haunches and stud pockets. A diamond-ground deck surface with no overlay was used for these bridges. The UHPC was cured under artificial heating because the ambient temperature during the curing time was mostly below freezing. The NYSDOT is now confident that construction during wintertime is feasible with the use of precast elements with UHPC. Even though UHPC joints need artificial heating to cure, the heating setup is significantly less complex and the duration is shorter compared to what would be needed for a CIP operation. In addition, based on the NYSDOT's past experience, artificial heating of CIP decks often results in deck cracking. That problem was obviously avoided with these bridges (Royce 2016).

Case Study 4 involves many bridges constructed under various contracts in different parts of the state. This group of bridges includes a number of single-span bridges, a two-span steel curve girder bridge, and four three-span bridges. Ten of these bridges are located in urban areas carrying Interstate traffic, while seven are on state highways in rural settings. The degree of construction acceleration required was determined based on the needs of the specific location. About half of these bridges required deck replacement within a window of 72 hours: from a Friday night closure to an early Monday morning opening to traffic. Many of the bridges used 5

to 10 days of closure time. The cost of deck replacement increased with the degree of acceleration. The NYSDOT allowed the longest window feasible to keep the cost as low as possible. A typical example of one of these bridges can be observed in Figure 2.15.

Royce 2016, NYSDOT Office of Structures

Figure 2.15. I-81 over East Castle St. - precast deck placement in progress

This bridge is a 120 ft single-span precast deck without an overlay over an existing multi-girder steel superstructure. Construction involved UHPC joints placed over the steel girders, hidden haunches with non-shrink grout, and studs penetrating above the bottoms of the precast panels (Royce 2016).

In addition to constructing the bridges described above in the four case studies, the NYSDOT Office of Structures also developed an innovative link slab design utilizing UHPC to eliminate transverse deck joints wherever feasible. The link slab design assumes that the UHPC section is subject to bending. The link slab also acts as a semi-rigid link between spans, transferring compressive, tensile, and shear stresses due to various loads (Royce 2016). The design of the link slab is influenced by variables such as span arrangement, bearing type and arrangement, girder end rotation due to live load, and bridge skew. A conceptual design of this link slab is shown in Figure 2.16.

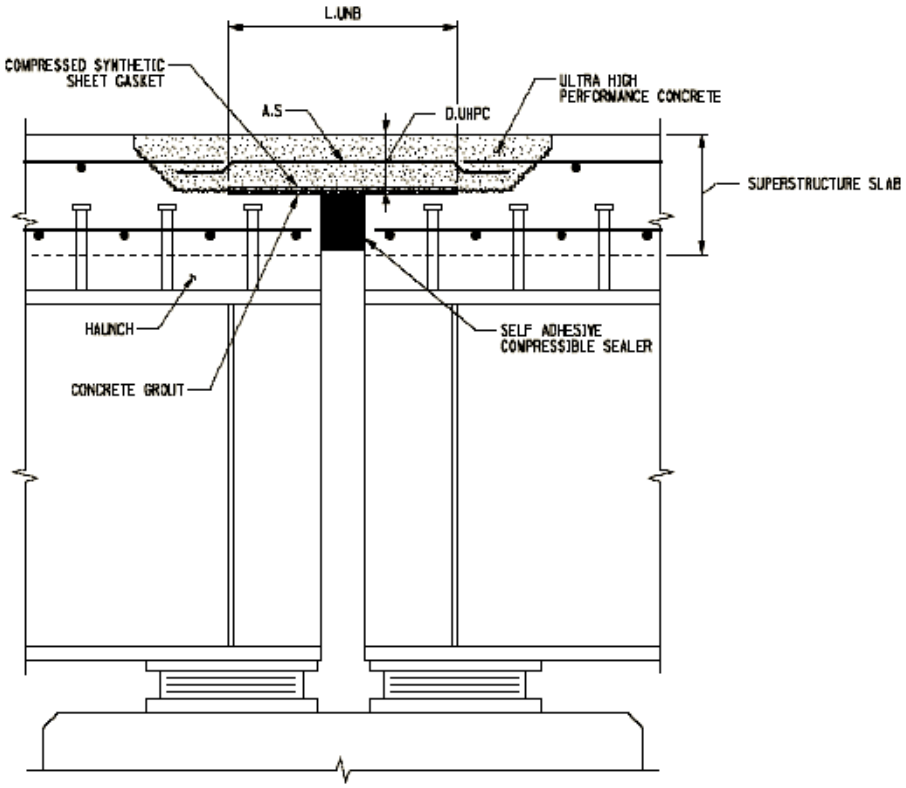

Royce 2016, NYSDOT Office of Structures

Figure 2.16. NYSDOT link slab cross-section

Several rehabilitation projects utilizing UHPC link slabs to eliminate joints are in progress at the NYSDOT. Based on the NYSDOT's experience as of 2016, the link slabs are performing well, with no visible cracks within the UHPC slabs (Royce 2016). Figure 2.17 shows a finished link slab.

Royce 2016, NYSDOT Office of Structures

Figure 2.17. Finished NYSDOT link slab

2.2.2.2 UHPC in Illinois

Liu and Schiff (2016) present the design and construction of Illinois's first precast deck panel bridge with UHPC joints, the $450 million Circle Interchange Project in Chicago. This project involved the replacement of the Peoria Street Bridge over I-290 and a Chicago Transit Authority (CTA) train station with a three-span continuous steel plate girder bridge with a total length of 273 ft 0 in. and a width of 56 ft 4 in. Three alternatives were proposed to the Illinois DOT (IDOT) for consideration: (1) precast deck panels with internal post-tensioning, (2) an AccelBridge system, and (3) precast deck panels with UHPC joints. IDOT decided to select the new-generation deck system: precast deck panels with UHPC joints.

The bridge has 52 deck panels in total, and a longitudinal UHPC joint is provided to accommodate the 56 ft wide bridge. Twenty different deck panels are required due to the complex bridge layout, which accommodates a CTA train station entrance to the west, a CTA staircase to the east, and light poles and drainage scuppers. All of the transverse and longitudinal joints are filled with UHPC. The design of the UHPC joints is based on pull-out research. The UHPC transverse joint and longitudinal joint details are shown in Figure 2.18 and Figure 2.19, respectively.

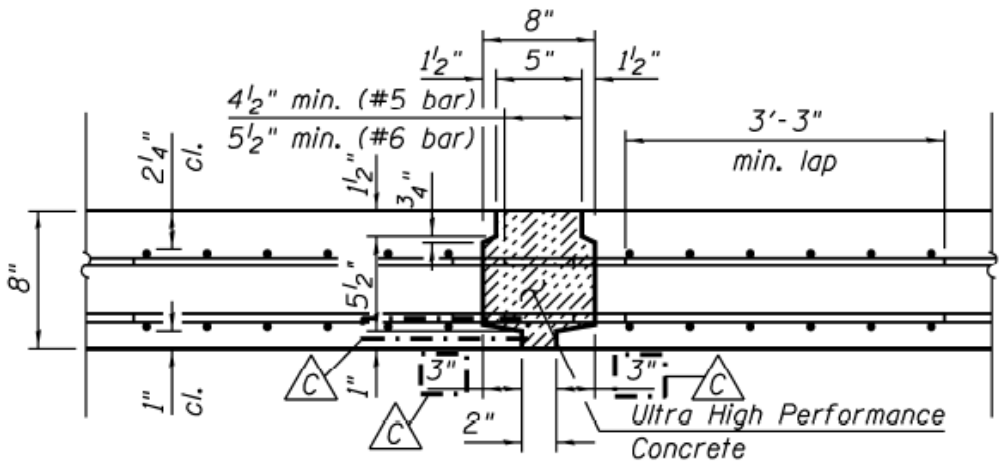

Liu and Schiff 2016, IDOT

Figure 2.18. Circle Interchange Project - UHPC transverse joint

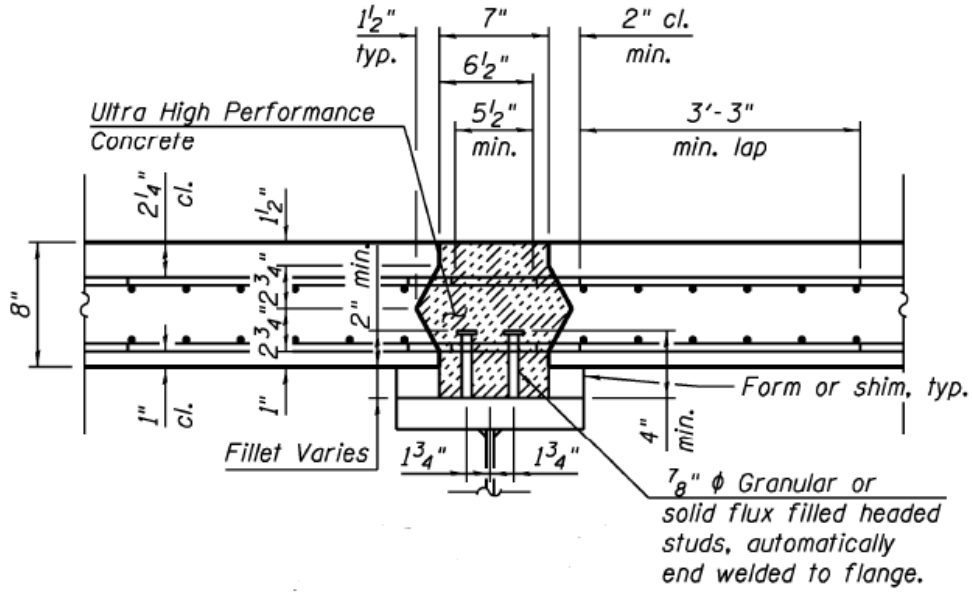

Liu and Schiff 2016, IDOT

Figure 2.19. Circle Interchange Project - UHPC longitudinal joint

The shear stud pockets are filled with non-shrink grout. The shear stud pocket detail is presented in Figure 2.20. (Shear stud pockets utilizing UHPC are described below for the New Jersey project.)

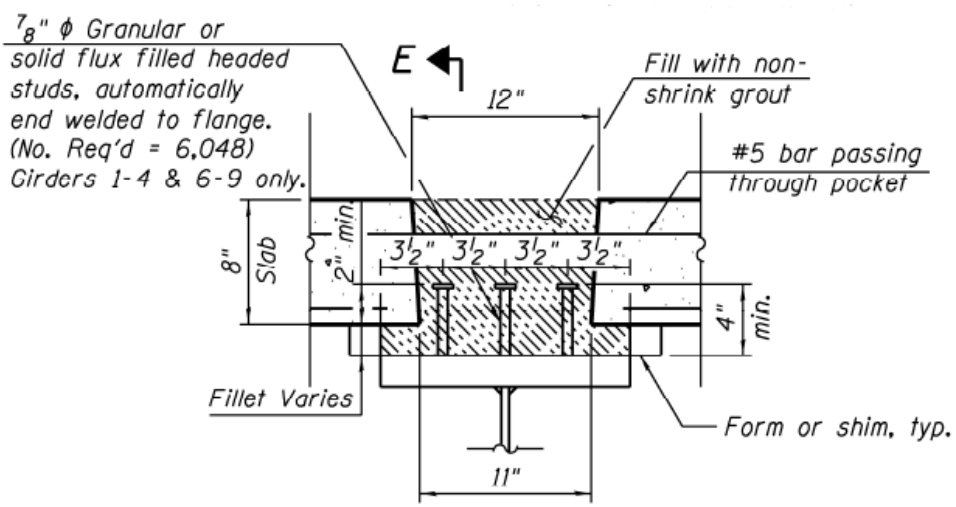

Liu and Schiff 2016, IDOT

Figure 2.20. Circle Interchange Project - shear stud pocket

Deck construction started in May 2015, and deck panel construction took about 10 days to complete.

2.2.2.3 UHPC in New Jersey

McDonagh and Foden (2016) detail the benefits of using UHPC for the rehabilitation of the Pulaski Skyway, a four-lane, 3.5-mile-long viaduct located in northern New Jersey that serves as a direct link to New York City via the Holland Tunnel. Because of the critical nature of the Skyway to the region's transportation system and the narrowness of the structure, which makes it difficult to perform maintenance without impacting traffic, the New Jersey DOT (NJDOT) desired that the new bridge deck would have a service life of 75 years, with little maintenance required during that time. Consequently, plant-cast concrete deck panels with stainless steel reinforcing bars and field-cast UHPC panel closure joints were selected as the re-decking system.

UHPC is used in three specific situations on the Pulaski Skyway: for the transverse panel-to-panel joints throughout the project, to fill the shear connections and haunches between the panels and the steel framing, and to fill the longitudinal joint at the median of the bridge. Each of these uses and their benefits are described below.

The majority of the transverse panel-to-panel joints on the project are 8 in. wide, as shown in Figure 2.21.

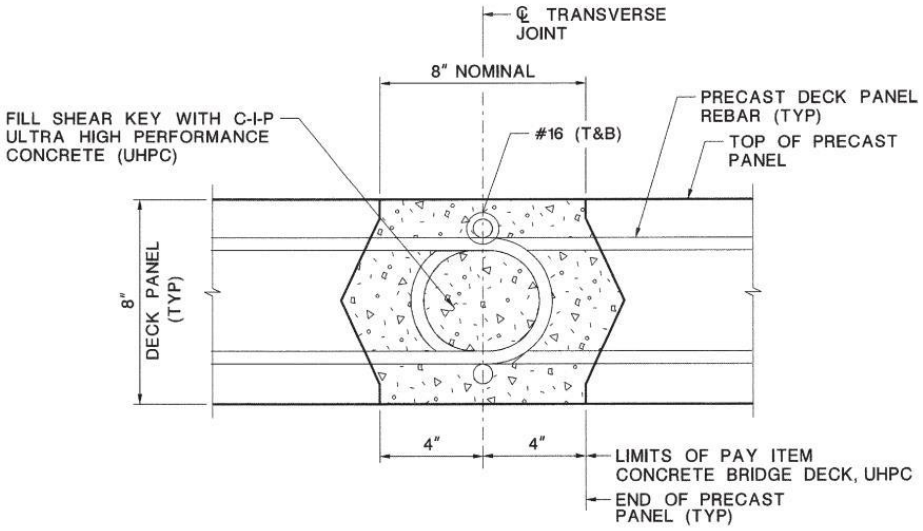

New Jersey DOT, McDonagh and Foden 2016

Figure 2.21. Pulaski Skyway - typical transverse joint

The high strength of UHPC allows for the use of short reinforcing bars and lap splice lengths, which enables the use of very narrow panel joints. This maximizes the amount of precast concrete deck and minimizes the amount of CIP material, which results in time savings. The fast cure time means that in as little as 24 hours after pouring the joints, the panels can be put into service, either for construction or service loads. The high flowability of UHPC means that there is a very low risk of unconsolidated material or air pockets in the joints. Finally, the deck panels are more likely to crack and see reinforcing bar corrosion than the joints because of the high durability and strength of the UHPC. This ensures that all of the durability measures incorporated into the precast panels themselves will be fully realized and not compromised by the panel joints.

A typical full-depth precast concrete panel used for the new Pulaski Skyway deck has rectangular shear pockets to facilitate the connection between the panels and the shear studs so that the panels will act compositely with the underlying steel framing. The panels are also connected to the stringers and floor beams, although rather than using rectangular block-outs, the entire length of the underlying stringers and floor beams is blocked out. The haunches are beneath the panel between the pockets for the typical precast panel but integral with the continuous block-outs for the panels.

These haunches and shear pockets were not originally designed to be UHPC, as can be seen in Figure 2.22, which indicates two different grouts, Type A and Type B.

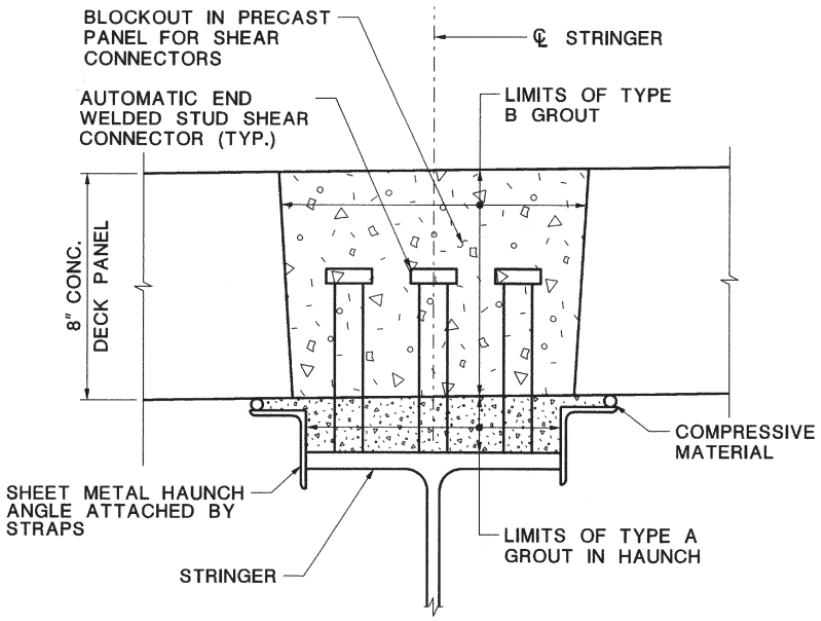

New Jersey DOT, McDonagh and Foden 2016

Figure 2.22. Pulaski Skyway - typical shear pocket detail

However, the contractor elected to use UHPC in order to combine the pockets with the haunches as well as the pockets with the transverse joints into a single pour. The high strength of the UHPC in the pockets gave the designers and contractor some added flexibility over shear stud placement. Since minimum shear stud spacing criteria are typically based on local failure of the concrete around the stud, the extremely high strength of the UHPC meant that the designers could accept tighter spacing of the shear studs when conditions required it.

As with the transverse joints, the fast curing time of UHPC means that the panels can be put into service in as little as 24 hours. The high flowability of UHPC is critical for the haunches, which are as thin as 5/8 in. The high durability and low permeability of UHPC ensures that the shear pockets and block-outs, such as those used for the transverse joints, will never become weak points in the precast deck system (McDonagh and Foden 2016).

In order to maintain partial traffic during the re-decking operation, only half of the Skyway was permitted to be closed at any time. Therefore, the presence of the existing southbound roadway carrying two lanes of traffic was a restriction for construction of the new northbound deck, which also had to be configured to carry two lanes of traffic when completed so that traffic on the existing southbound deck could be routed to the northbound side. This arrangement meant that very little open space was available between the existing southbound deck and the new northbound deck for the extension of rebar necessary to make the two halves continuous in the final condition. This open space was typically only 10 to 12 in. wide.

As a result, the high strength of UHPC was critical for this application. The designers detailed 6 in. long rebar hooks extending out of the edge of the northbound precast panels along the median. This provided more than enough extension to ensure that these bars would be fully

developed in the UHPC median concrete. The subsequently placed southbound precast panels, which had the advantage of a 3 ft typical open median, had straight rebar extending out of the panels along the median with a typical 12 in. extension. Lastly, a set of straight reinforcing bars 2 ft 8 in. long were placed in the median, lapping the rebar extending from both the northbound and southbound panels, as shown in Figure 2.23.

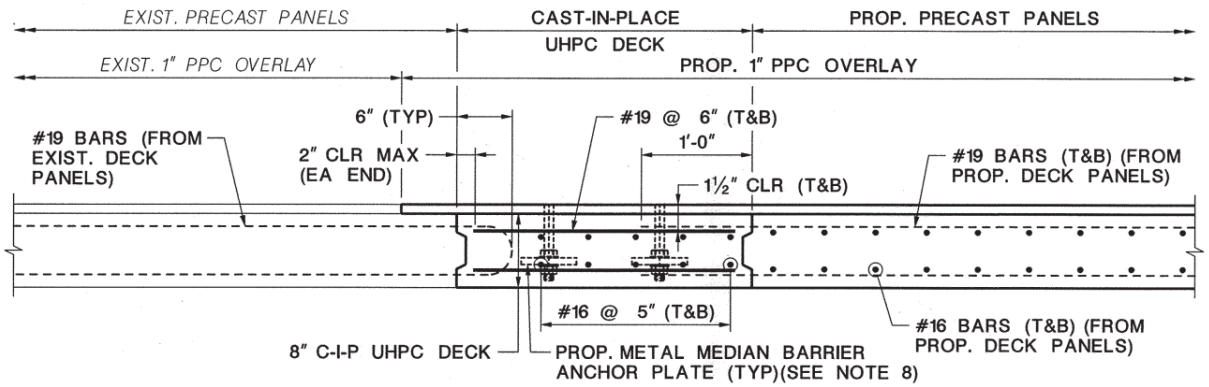

New Jersey DOT, McDonagh and Foden 2016

Figure 2.23. Pulaski Skyway - typical median detail

Thanks to the high strength of the UHPC, this rebar had fully developed lap splices to the rebar extending from each panel, thereby ensuring that the rebar that extends transversely across the bridge is continuous between both edges of the bridge and across the median.

Once again, with UHPC curing in as little as 24 hours, construction can proceed quickly, and the median can be loaded rather rapidly. Furthermore, the fluidity of UHPC eliminates any concern for air pockets or unconsolidated concrete that could be caused by the anchors for the metal median barrier that are cast in the median. Finally, as with the transverse panel joints, this continuous longitudinal panel joint is stronger and more durable than the panels it is connecting, thereby ensuring the long-term durability of the entire deck system.

Overall, with UHPC employed for nearly all precast panel connections, the connections are no longer the weak points that they traditionally have been, both in terms of strength and durability. Instead, the connections are the strongest and most durable points of the deck system, stronger and more durable than the precast deck panels with shop-cast concrete and corrosion-resistant rebar. All of these features of the deck system are expected to eliminate the need for major deck maintenance over the next 75 years (McDonagh and Foden 2016).

2.2.4 UHPC Summary

Several examples of UHPC joints have been presented in this report, and many more can be found in the literature and in the field. The documentation for these completed projects shows that the technology is working and has met the needs of users and owners on a number of projects in demanding situations. Given these positive experiences, designers could consider the

use of UHPC at critical locations, such as concrete units in which joint hardware is embedded or deck or approach slab components that are subjected to higher stresses due to soil settlement or impact loads.

2.3 Modeling and Analysis of Bridges

The present research required various bridge components to be modeled and analyzed using FE models. A review of the literature was conducted to provide the research team with the necessary background to use FE modeling to analyze various bridge components.

2.3.1 Modeling of Bridge Components

Various modeling practices for concrete decks and steel girders were reviewed in the literature. With this variety of information comes different ways of considering boundary conditions and constraints between the concrete deck and steel girders. These factors have to be included in FE models to properly analyze the structures.

Four papers in particular were compared in terms of their modeling practices. The similarities and differences among the four papers are highlighted in the following discussion.

2.3.1.1 Concrete and Steel Elements

Biggs et al. (2000) detailed the development of FE models used to analyze the composite action and global response of a reinforced concrete deck and steel girders. In these models, the concrete deck elements were modeled as shell element S4R, a four-node, doubly curved, thin or thick shell element with reduced integration, hourglass control, and finite membrane strains. The steel girder elements were modeled as three-dimensional, first-order beam element B31OS, a two-node, linear, open-section beam in space. Similarly, Klein (2006) developed separate FE models for composite bridge deck bridges with reinforced concrete slabs and longitudinal steel girders. The models were varied in terms of girder spacing to identify the optimum case from among the responses obtained from the FE results. For both the concrete deck and the steel girders, shell element S4R was utilized. The results stage of the modeling is shown in Figure 2.24.

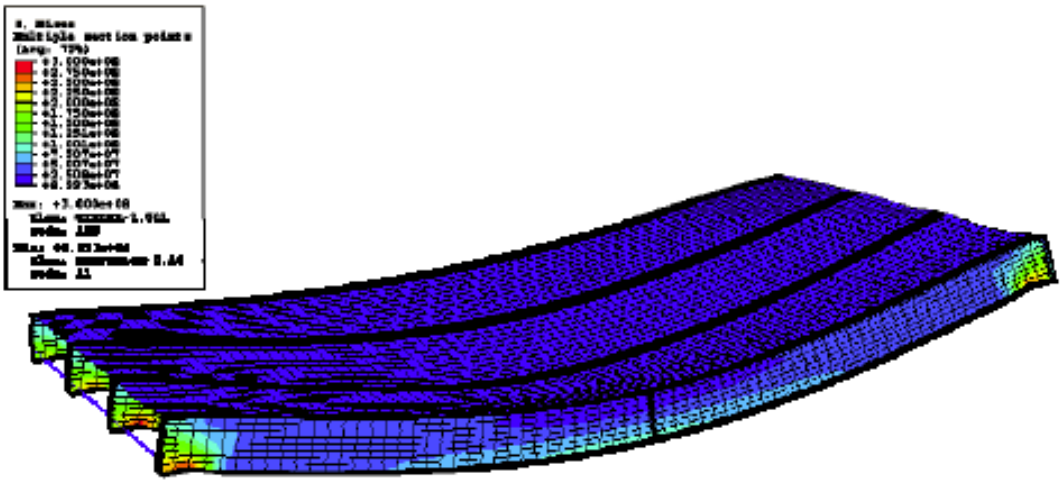

Klein 2006

Figure 2.24. Full 3D finite element model

Bengtsson and Widén (2010) discussed the development of FE models to investigate fatigue cracks observed in the Vårby Bridge near Stockholm, Sweden. The Vårby Bridge was modeled with 3D deformable shell elements for all elements, including both the concrete deck and the steel girders. The composite bridge model was built up from four different parts for the steel details and one part representing the concrete deck. The deck was divided into a number of different strips along the bridge to simulate the different thicknesses of the concrete deck (Bengtsson and Widén 2010). The components of the model can be seen in Figure 2.25 and Figure 2.26. A full view of the model can be seen in Figure 2.27.

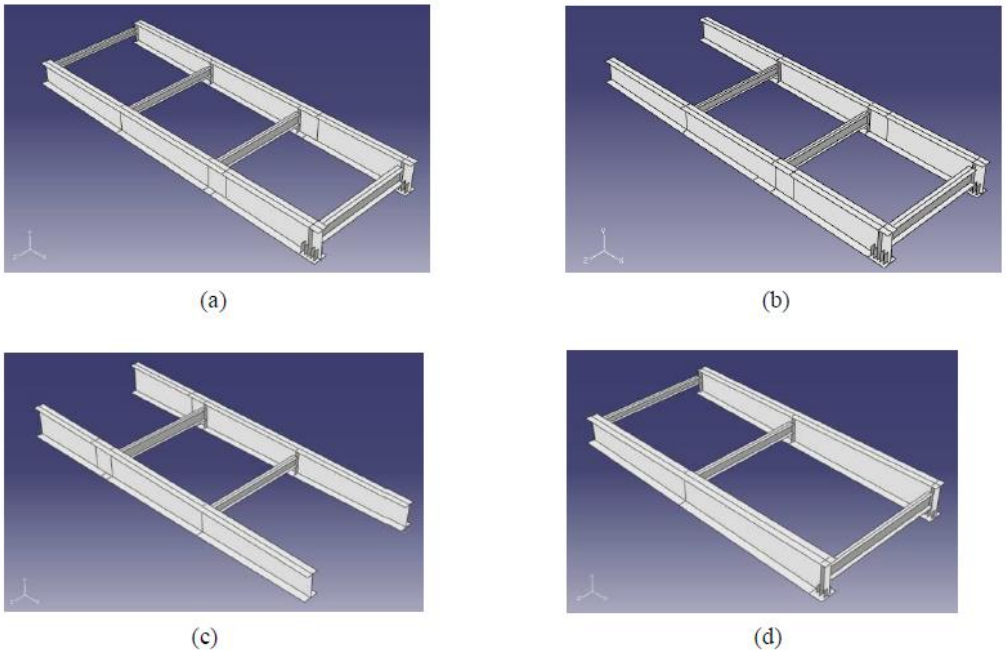

Bengtsson and Widén 2010

Figure 2.25. Vårby Bridge 2010 - steel girders

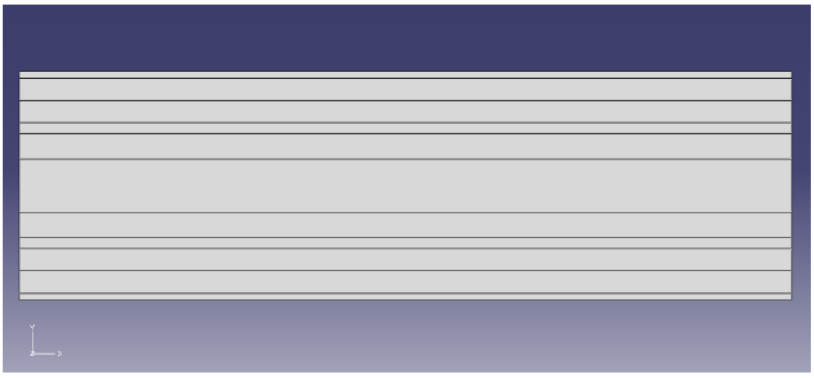

Bengtsson and Widén 2010

Figure 2.26. Vårby Bridge 2010 - concrete deck

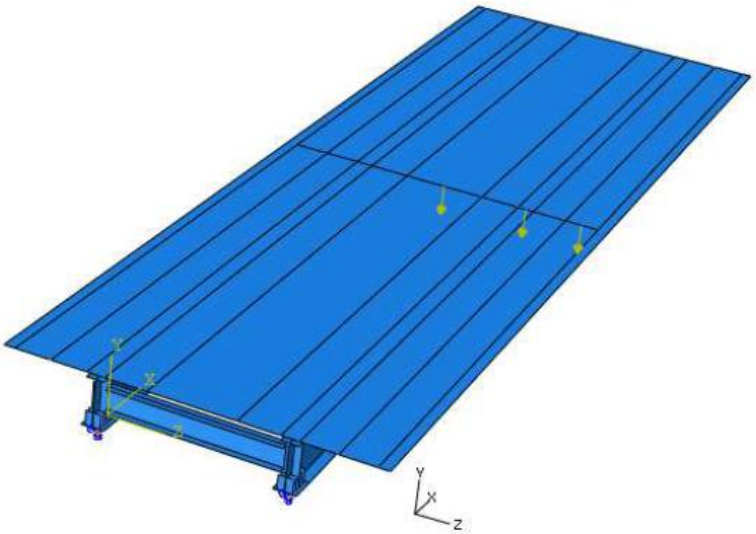

Bengtsson and Widén 2010

Figure 2.27. Vårby Bridge 2010 - full 3D FE model

A subsequent paper on the Vårby Bridge investigation undertook a numerical analysis and updated the model. Abdulrahman and Portus (2015) developed FE models with a wide range of parameter combinations. In these models, the concrete deck was modeled as shell elements while beam elements were used in most of the steel girders and crossbeams. Shell elements were used in the main girders. The main girders were identified as the girders that were monitored with strain gages during previous phases of the investigation. The beam elements can be seen in Figure 2.28, while the main girders can be seen in Figure 2.29.

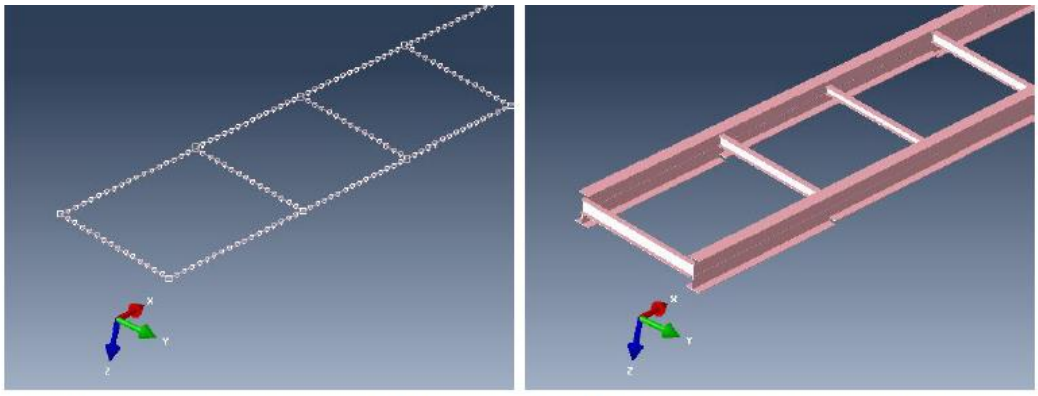

(a) *The longitudinal beams and the cross-beams modeled with beam elements with a mesh size of 500mm*

(b) *The longitudinal beams and the cross-beams modeled with beam elements and with rendered profiles.*

Abdulrahman and Portus 2015

Figure 2.28. Vårby Bridge 2015 - beam elements

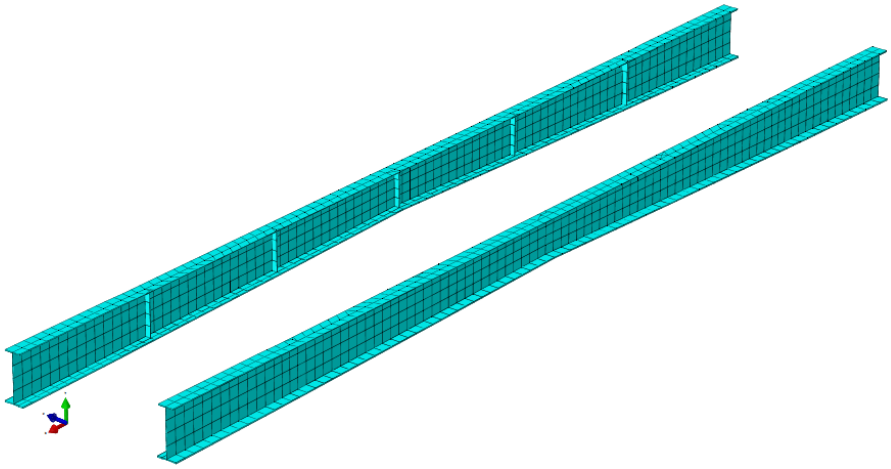

Abdulrahman and Portus 2015

Figure 2.29. Vårby Bridge 2015 - main girders

2.3.1.2 Boundary Conditions

Both Biggs et al. (2000) and Klein (2006) modeled the steel girders in their FE models as simply supported structures. One end of the structure was pinned while the opposite end was a pinned/sliding restraint. The nodes chosen for the boundary condition allocation were located at each end of the bottom side of the girders. One end was restrained for the three displacement directions, while the opposite end was restrained in only two directions. The nodes were not supported in the longitudinal direction of the bridge. This condition resulted in a sliding behavior for the simply supported condition being modeled (Klein 2006).

In the Vårby Bridge investigation, Bengtsson and Widén (2010) detailed the boundary conditions for the two main girders. There were seven supports for the two main girders, C and D. The bridge was free to move along the longitudinal axis (x-axis) for both girders, but only girder C could move in the transverse direction (z-axis). This applied for all supports but the mid supports, where the bearings were fixed for main girder D and partially fixed for main girder C (Bengtsson and Widén 2010). The boundary conditions are summarized in Table 2.1.

Table 2.1. Vårby Bridge 2010 - boundary conditions

	-x	-z	-y	Rotations		
C	Free	Free	Fixed	Free	Free	Free
C;mid support	Fixed	Free	Fixed	Free	Free	Free
D	Free	Fixed	Fixed	Free	Free	Free
D; mid support	Fixed	Fixed	Fixed	Free	Free	Free

Bengtsson and Widén (2010)

Just like in Klein (2006), the boundary conditions in Bengtsson and Widén (2010) were attached to one node located directly under the web in the main girders and in line with the vertical web stiffeners. To represent the bearings in a reasonable way, the horizontal plates under the vertical support stiffeners in the bottom flange were free to rotate around the node using a multi-point constraint (MPC) (Bengtsson and Widén 2010). This is shown in Figure 2.30.

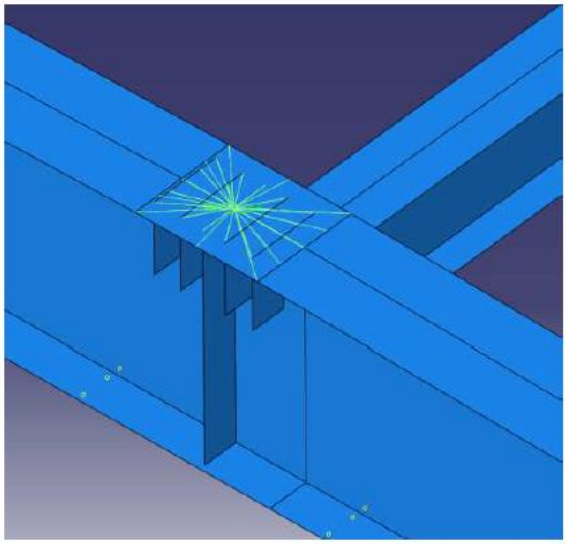

Bengtsson and Widén 2010

Figure 2.30. Vårby Bridge 2010 - boundary condition MPC

Abdulrahman and Portus (2015) detailed the boundary conditions in a subsequent paper on the Vårby Bridge investigation. It is noteworthy that the boundary conditions from the Bengtsson and Widén (2010) paper were kept intact. The boundary conditions depend mostly on the bearing pads used in a particular bridge. Since the same bridge was under investigation in both studies, the bearing pads remained constant and the boundary conditions therefore stayed the same.

2.3.1.3 Constraints

Different constraints between the concrete deck and steel girders were used across the four papers discussed in this literature review. Even the two papers on the Vårby Bridge investigation implemented different constraints. Shear studs are present in most, if not all, steel girder bridges. These studs may elongate during uplift loads on the bridge deck since the shear studs are embedded into the concrete. The studs would prevent the deck from lifting off the top flange of the girders. Different ways of modeling this constraint are evident across the papers.

Biggs et al. (2000) modeled the constraints between the concrete deck and steel girders by employing MPCs similar to the one shown in Figure 2.30. On the other hand, Klein (2006) used tie constraints assuming full interaction between the two elements and transference of all degrees of freedom.

Similarly to Klein (2006), Bengtsson and Widén (2010) also used tie constraints between the concrete deck and the steel girders in the FE models developed for the Vårby Bridge investigation. In a subsequent paper, Abdulrahman and Portus (2015) employed very different constraints on multiple elements of the FE model. Since the main girders were modeled as a combination of beam elements and shell elements, these different elements had to be connected to model continuous beam behavior. MPCs were employed to connect the beam and shell elements. MPCs were also used to connect the crossbeams to the main girders. Web stiffeners were modeled in the main girders and were used as the source of the MPCs. Both applications of MPCs can be seen in Figure 2.31 and Figure 2.32.

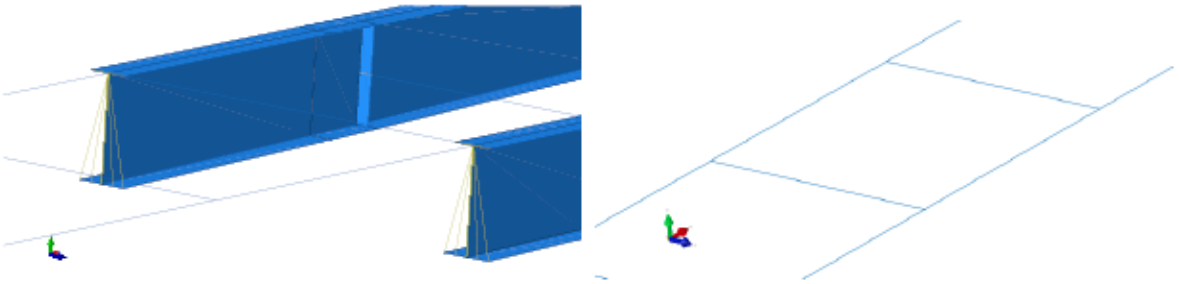

(a) *Showing the multiple point constraint connecting the beam elements to the shell elements of the longitudinal beams.*

(b) *Beam elements where main girders and crossbeams are modelled in the same part, ensuring full constraint.*

Abdulrahman and Portus 2015

Figure 2.31. Vårby Bridge 2015 - main girder constraints

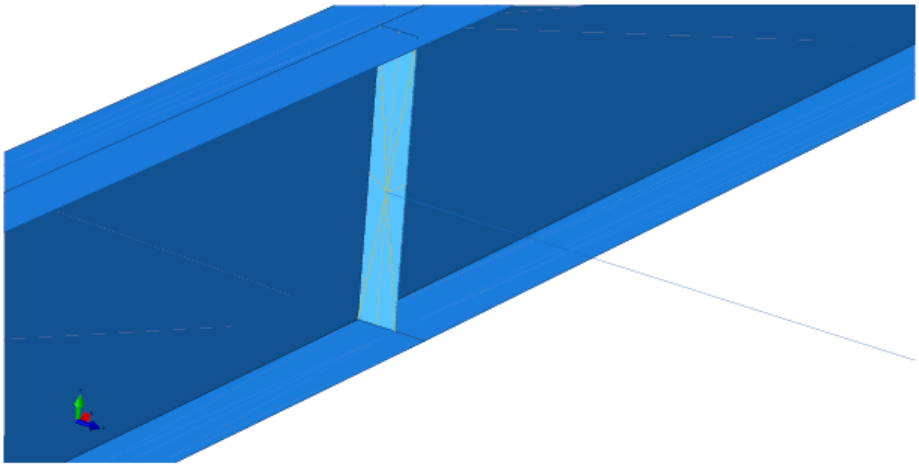

Abdulrahman and Portus 2015

Figure 2.32. Vårby Bridge 2015 - crossbeam constraints

In Abdulrahman and Portus (2015), the interaction between the concrete deck and the steel girders was modified from the previous paper on the Vårby Bridge investigation. In Bengtsson and Widén (2010), these two elements were connected with a tie constraint between the bottom

surface of the concrete deck and the top face of the top flanges of the main steel girders. In Abdulrahman and Portus (2015), the connection was modeled with linear axial springs. These linear axial springs connected the main steel girder and the concrete deck. The springs were modeled using two different approaches: engineering springs (SPRING2) and connectors (CONN3D2); both approaches are illustrated in Figure 2.33.

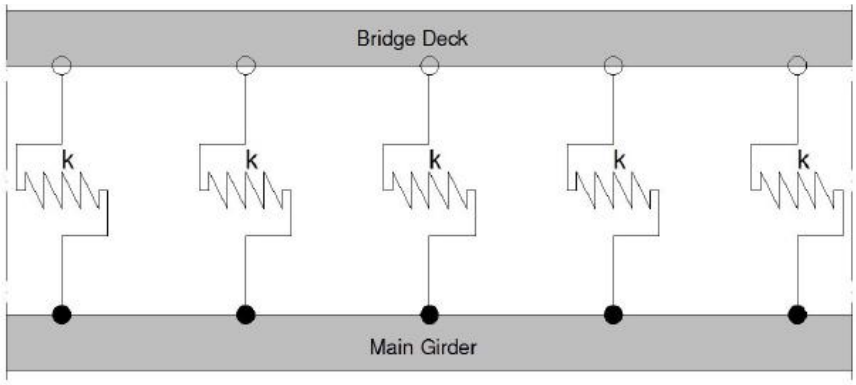

(a) *Axial springs in theory.*

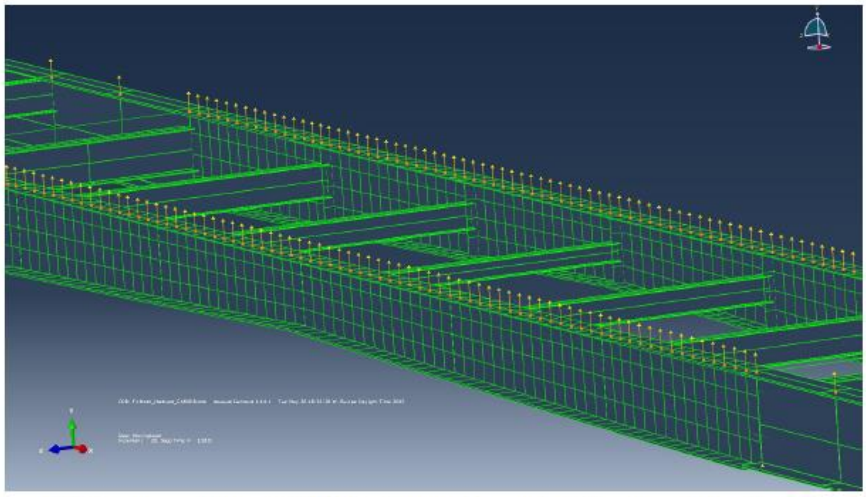

(b) *Spring connectors (CONN3D2) assigned to mesh nodes along the bridge deck.*

Abdulrahman and Portus 2015

Figure 2.33. Vårby Bridge 2015 - deck and main girder constraints

Abdulrahman and Portus (2015) provide the following overview of both approaches:

> When using the SPRING2 approach in Abaqus, the springs are modeled in such a way that they are very stiff in the y and z directions so that the only action that is active is the slip action between the steel and concrete, i.e., the stiffness of the spring in the x direction.
>
> The other approach is to use connector elements, CONN3D2, where wires are created between the mesh-nodes of the bridge deck and the longitudinal beams. The wires are

then assigned different properties, having rigid connections in the y and z directions and a defined stiffness in the x direction. (Abdulrahman and Portus 2015)

2.3.2 Modeling of Approach Slab and Soil Support

To further develop the deck over backwall concept, FE models of full-scale bridges had to be modified to factor in the possible effects of the concept on the existing structures. The concept includes an approach slab extending from the existing bridge deck on one end to the roadway pavement on the other. To help model this feature, a review of the literature on approach slab modeling was conducted.

Rajek (2010) used FE models to analyze the possible causes of approach slab deterioration. The models included the bridge roadway, approach slab, abutment, and fill because all of these elements relate to approach slab deterioration. Parametric studies were performed to determine the influential parameters that contribute to the deterioration of the approach slab. Rajek (2010) lists the parameters as void geometry, abutment height, approach slab length, soil stiffness, concrete stiffness, and joint restrictions (i.e., for the joint between the roadway and approach slab).

The approach slab incorporated in the model was made to conform to Wisconsin DOT (WisDOT) standard specifications. WisDOT specifies a length of 15 ft 8 in. and a thickness of 1 ft for its standard approach slabs (Rajek 2010). The width of the approach slab was the minimum lane width (12 ft) as defined by the 2007 American Association of State Highway and Transportation Officials (AASHTO) specifications. Rajek (2010) explains that friction was the primary constraint utilized in the model to control all concrete-to-concrete and soil-to-concrete interactions. The coefficient of friction used to define all concrete-to-concrete interactions was taken from section 11.6.4.3 of ACI 318-08.

Plane strain and plane stress elements were used in the model. Plane strain quadrilateral quadratic elements with reduced integration were used for the soil region (Helwany 2007). Plane stress quadrilateral quadratic elements with reduced integration were used for all concrete parts.

A section view of the model is shown in Figure 2.34 with all the pertinent elements labeled.

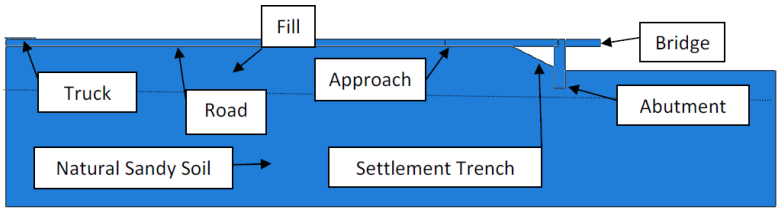

Rajek 2010

Figure 2.34. Section view of approach slab modeling

A vertical displacement restraint was implemented at the bottom of the soil to simulate very stiff natural soils or bedrock at depth. Horizontal displacement restraints were placed at the sides of the soil. The bottom of the abutment was fixed to simulate a rigid pile and pile connection (Rajek 2010). These can be seen in Figure 2.35.

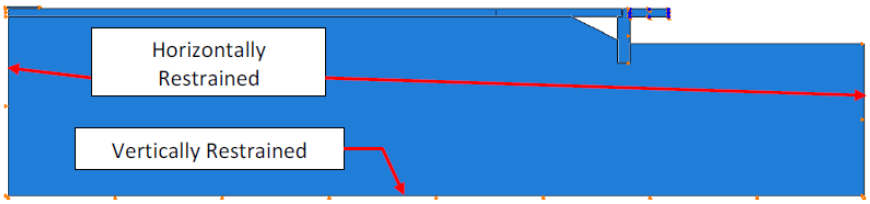

Rajek 2010

Figure 2.35. Boundary conditions for approach slab modeling

The soil was modeled as a compacted sandy soil using the elastoplastic Mohr-Coulomb material model within Abaqus. The sand emulated in the model was modeled after portage sand, as discussed by Schuettpelz et al. (2010). The soil properties are shown in Table 2.2.

Table 2.2. Soil properties for approach slab modeling

Classification	Mass Density (lbm/ft^3)	Young's Modulus (psi)	Poisson's Ratio	Friction Angle (deg)	Dilation Angle (deg)	ϕ'_{cv} (deg)	Meridional Eccentricity	Cohesion (psi)
Stiff	129	14500	0.3	45	12	35	0.1	0.145
Moderately Stiff	124	8700	0.3	37	5.6	32.5	0.1	0.145
Loose	121	1450	0.3	30	0	30	0.1	0.145

Rajek 2010

The geometry of the settlement trench formed under the approach slab was varied in the parametric study. The settlement trench geometries used in the parametric study are shown in Figure 2.36. These are in general agreement with the observations of Cosgrove and Lehane (2003).

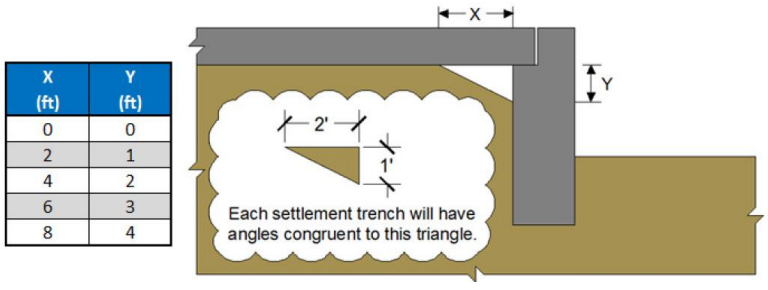

Rajek 2010

Figure 2.36. Trench geometry for approach slab modeling

Rajek (2010) explains this approach to trench geometry as follows:

[W]hile standard practice dictates that the angle of the settlement trench be equal to the constant volume friction angle (32.5°), the model utilized for this study set the angle of the settlement trench at approximately 26.5°. This was assumed accurate as the saturation of the soil and water pressure buildup within the soil would cause an increase in pore pressures. The effective stress of the soil would decrease as a result of the increase in pore pressure. (Rajek 2010)

CHAPTER 3. FINITE ELEMENT MODELING AND ANALYSIS

Two case study bridges were considered throughout the course of the research. The first bridge is located on I-35 (Northbound, 049310; Southbound, 049320) 3.3 miles south of SR E-18 over Bear Creek in Story County. The second bridge is located on IA-330/Marshalltown Blvd. 2.5 miles southwest of Melbourne over the North Skunk River in Marshall County. These bridges will be referred to as the Story County bridge and the Marshall County bridge.

The selected bridges were analyzed using FE models that were developed to model the conditions of the bridges presented in the original drawing plans. The information for the FE analyses was obtained from as-built drawings, design documents, and expansion joint specifications for the Story County bridge and the Marshall County bridge. For the analysis, AASHTO specifications were followed to evaluate the behavior of the bridges.

The analysis results will eventually be used to identify critical conditions to guide the development of a plan for post-construction testing of the structures and to correlate field responses with the predictions from the models. Subsequently, the models may be calibrated using the future field test results in order to increase the models' accuracy. The verification of the models will permit their confident use for designing expansion joints in the future.

3.1 Story County Bridge

A full 3D model was developed in Abaqus FEA for the Story County bridge. This model includes a concrete bridge deck supported by welded plate steel girders and diaphragms that rest on abutments at the ends and piers. A full 3D model can be seen in Figure 3.1, with a sectional view in Figure 3.2.

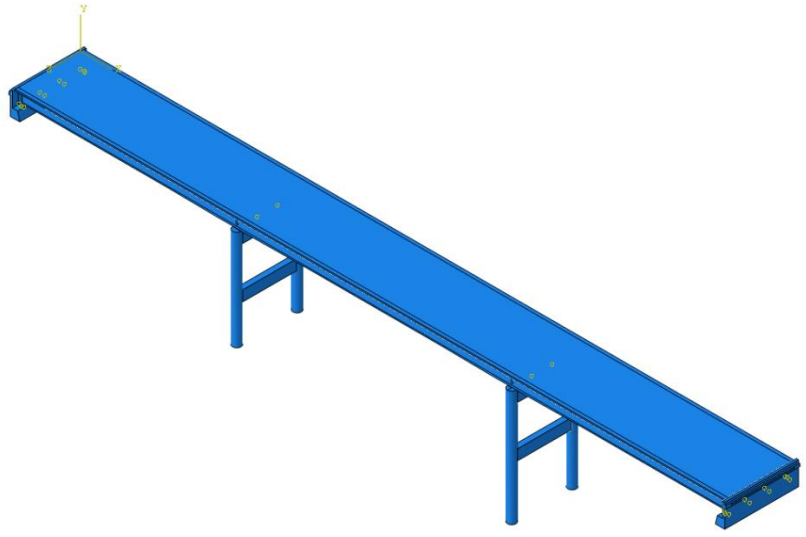

Figure 3.1. Story County bridge - full 3D FE model

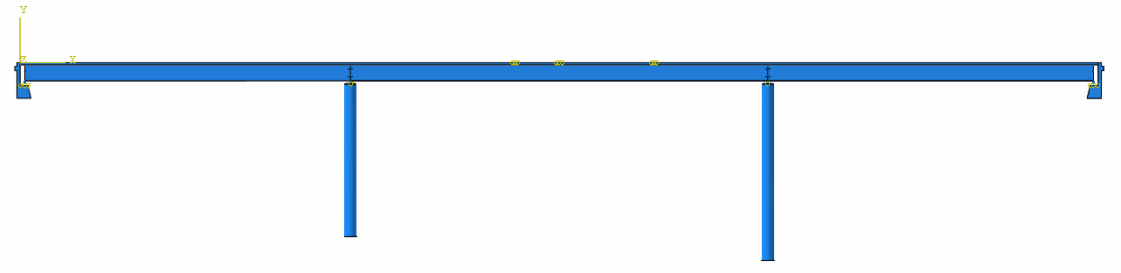

Figure 3.2. Story County bridge - section view

Constraints, boundary conditions, and other elements were assigned in the model. Loading conditions due to self-weight, surface weathering, and truck loading were also incorporated into the model.

An 8 in. by 338 ft bridge deck was modeled as a C3D8R element, which is an eight-node linear brick element with reduced integration and hourglass control. In addition, C3D8R was utilized for all concrete parts in the model, including the abutments and piers with their corresponding column and beam dimensions. The steel superstructure is composed of welded plate steel girders and transverse diaphragms at the ends and over the piers. The web and flanges of the welded plate girders as well as the diaphragms were modeled as S4R elements, which are four-node, doubly curved, thin or thick shell elements with reduced integration, hourglass control, and finite membrane strains. For the flanges of the welded plate girders, width and thickness were modeled per the drawing plans. All of the steel superstructure elements were merged together (Figure 3.3).

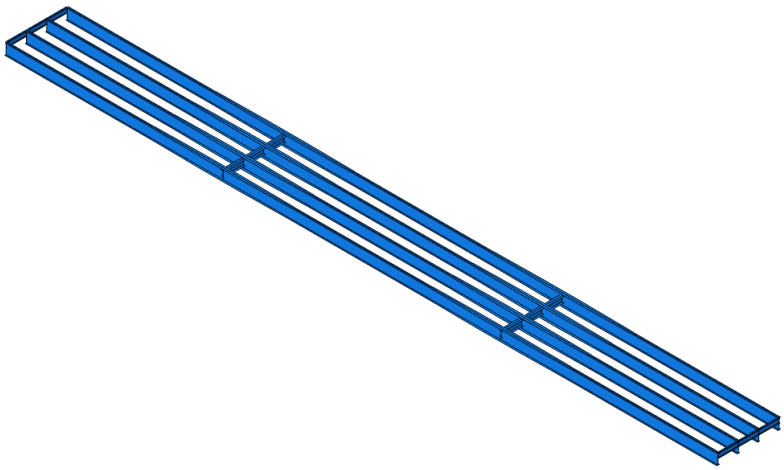

Figure 3.3. Story County bridge - steel superstructure

This model underwent an elastic analysis. Only mass density and elastic properties like Young's modulus and Poisson's ratio were needed for a successful analysis. The mass densities utilized for the concrete and steel were assigned as their specific weights: 150 lb/ft^3 and 490 lb/ft^3, respectively. As for the Young's modulus and Poisson's ratio, 3,718 ksi and 0.15 was utilized for the concrete and 29,000 ksi and 0.3 for the steel, respectively. In addition, the coefficients of

thermal expansion for both concrete and steel were selected as 5.5E-6 1/°F and 6.5E-6 1/°F, respectively.

Boundary conditions were assigned to the abutment's vertical and horizontal faces that are in the direction of the supporting soil. Vertical faces have horizontal constraints and horizontal faces have vertical constraints. A fixed boundary condition was assigned to the bottom face of the pier columns, simulating the foundations that rest under the topsoil. Boundary conditions can be seen in Figure 3.4 as red lines at the abutment and on the bottom face of the pier.

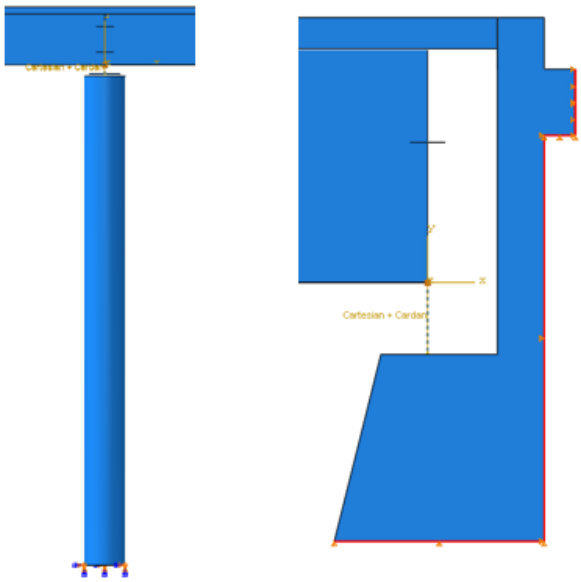

Figure 3.4. Story County bridge - boundary conditions

Tie constraints were assigned between the beams and columns of the piers. Tie constraints were also assigned between the top flanges of all the welded plate girders and the bottom surface of the bridge deck. Connection wires were utilized between the steel girders and the abutments and piers to simulate the rocker and fixed bearings at their locations. All reaction values presented in the following pages correspond to these connection wires.

3.1.1 Convergence Study

The model was trialed on numerous occasions with various meshing sizes. The results stabilized at an approximate meshing size of 5 in. A meshing size of 4 in. was determined to be the most effective for the model at this point. The time elapsed to complete the analysis for a meshing size of 3 in. was almost five times as long as the time elapsed for a meshing size of 4 in. (Table 3.1).

Table 3.1. Story County bridge - mesh convergence study

Mesh Size (in.)	Max Deflection at Midspan (in.)	Time Elapsed (s)
8	1.242	108.4
6	1.248	178.6
5	1.035	416.1
4.5	1.031	552
4	1.032	785.2
3.5	1.031	1056.6
3	1.031	4641

The time elapsed for each trial is shown for all mesh sizes along with their deflection values.

A graph of the different values that were trialed with their results is shown in Figure 3.5.

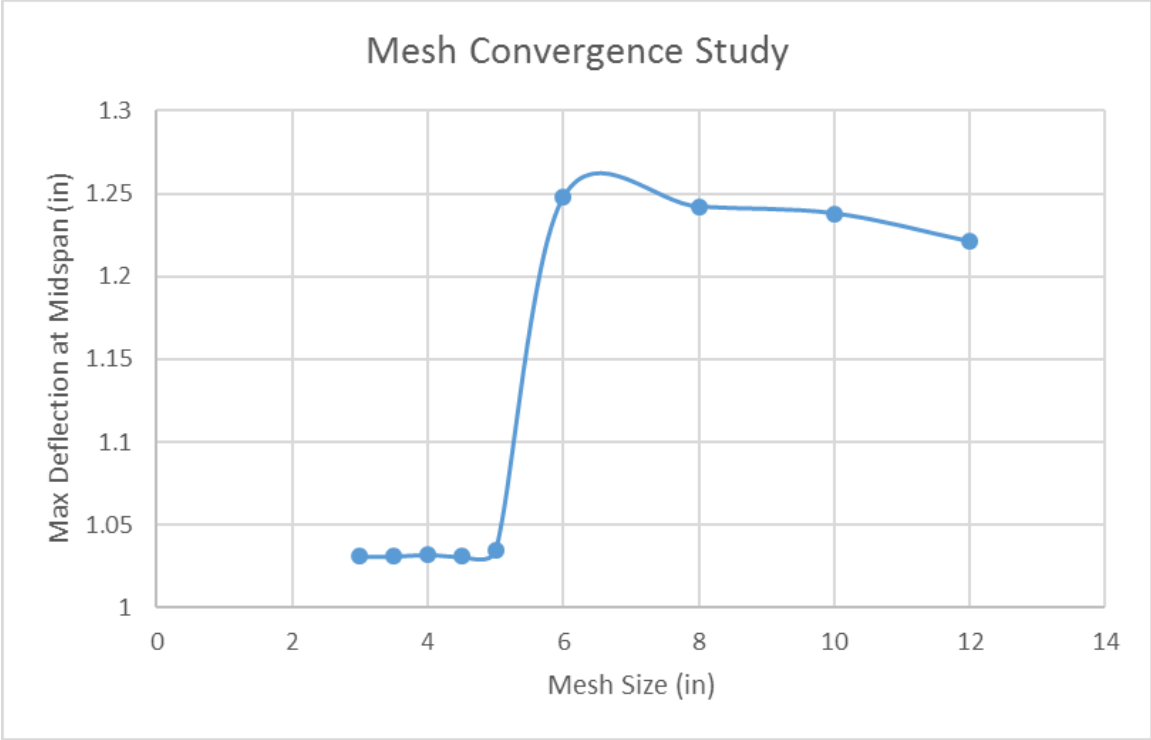

Figure 3.5. Story County bridge - mesh convergence study

With a mesh size of 4 in., the structure was modeled using 332,627 elements, 437,973 nodes, and 1,663,341 variables.

3.1.2 Validation with Original Plans

The information needed to create the FE model and conduct the analysis for the Story County bridge was obtained from its original drawing plans. The abutment and pier reactions can be observed in these plans and in Table 3.2.

Table 3.2. Story County bridge - abutment and pier reactions from the drawing plans

	Abutment Reactions (kips)		Pier Reactions (kips)	
	Exterior	**Interior**	**Exterior**	**Interior**
DL #1	31	47.1	113.4	172.1
DL #2	21.5	4.5	74.5	15.5
ULL	-	-	67	78
CLL	-	-	19.6	22.8
HS20-16	48.2	56.3	-	-
Impact	10.6	12.3	17.9	20.8
Total	111.3	120.2	292.4	309.2

Source: Story County Bridge Plans
Dead load #1 includes weight of slab, girders, and diaphragms.
Dead Load #2 includes weight of curbs, rail, and future wearing surface.

These reactions were the source of comparison for the results obtained from the FE analysis shown in the following section. It is important to mention that the FE model does not fully incorporate all of the elements shown in the plans but includes the most pertinent ones.

Note that an HS20-16 truck load is shown in Table 3.2. References to this truck load were not found in the literature. Therefore, this truck load was assumed to be an HS20-44 truck loading condition and was allocated in the same manner as the other loads in the FE model. Even though this truck load was assumed to be HS20-44, it is referred to as HS20-16 in the discussion.

3.1.2.1 Dead Load Reactions and Deflection

Self-weight was included in the whole model. A surface weathering loading condition of 19 lb/ft^2 over the roadway was also added. Curb loading on 1.5 ft of the edges was added as a surface area simulating a 2 ft 8 in. by 1 ft area of concrete along the entire length of the bridge deck. The results for dead load deflection and a comparative loading conditions table are shown in Figure 3.6, Figure 3.7, and Table 3.3.

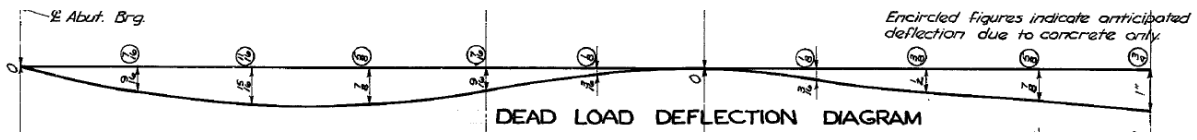

Story County Bridge Plans

Figure 3.6. Story County bridge - anticipated dead load deflection

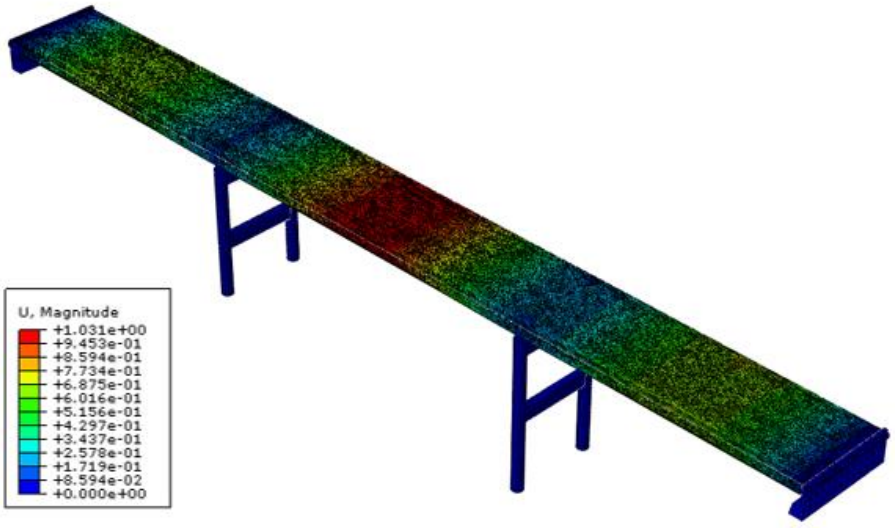

Figure 3.7. Story County bridge - deformation contour plot for dead load

Table 3.3. Story County bridge - dead load abutment and pier reactions

	Abutment Reactions (kips)				Pier Reactions (kips)			
	Ext	% diff	Int	% diff	Ext	% diff	Int	% diff
DL #1	33.08	6.71	44.54	5.44	124.87	10.11	154.39	10.29
DL #2	18.01	16.24	6.95	54.47	58.43	21.57	22.94	48.00
Total	51.09	2.69	51.49	0.22	183.30	2.45	177.33	5.48

The maximum deflection obtained was approximately 1 in. at the center of the bridge. This value correlates with the value obtained from the original drawing plans. The resulting abutment and pier reactions were tabulated and compared with the values obtained from the drawing plans. Two dead load loading conditions were considered for the pier and abutment reactions. Lower percentages of difference were achieved for the exterior reactions than for the interior reactions, mainly due to the oversimplification in the original drawings regarding the curb and railing load. Both pier reactions show low percentages of difference from the total reaction, 2.45% for the exterior support and 5.48% for the interior support. The abutment reactions also show low percentages of difference from the total reaction, 2.69% and 0.22% for the exterior and interior reactions, respectively.

3.1.2.2 Temperature Loading

Temperature loading was also modeled. The rocker and expansion plate settings from the original drawing plans are shown in Table 3.4.

Table 3.4. Story County bridge - expansion plate settings

ROCKER & EXPANSION PLATE SETTINGS						
	S. Abut.		Pier #1	Pier #2	N. Abut.	
Temp. at time of setting	"D"					D
10°	3"	½	0	0	½	3"
50°	2½	0	0	0	0	2½
90°	2"	½	0	0	½	2"

Story County Bridge Plans

A shrinkage and expansion of 0.5 in. can be seen at 10°F and 90°F, respectively, with a base temperature of 50°F.

The results from the FE modeling for temperature can be seen in Figure 3.8.

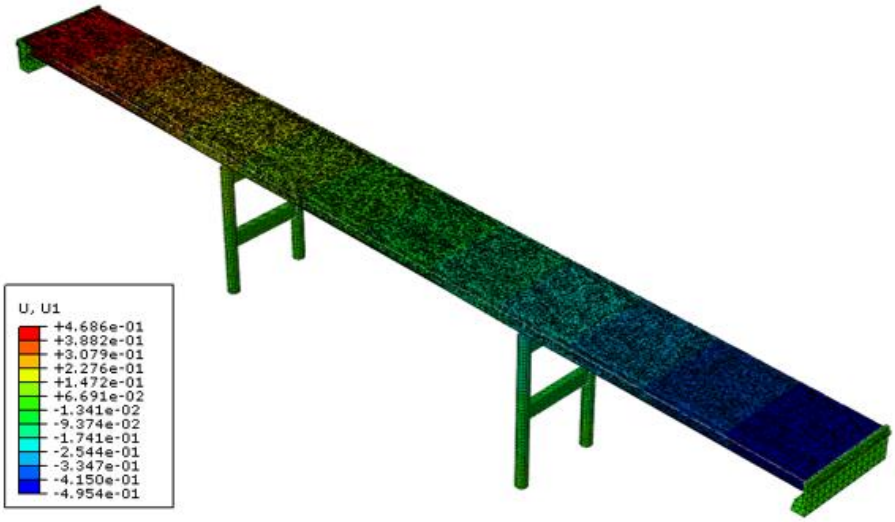

Figure 3.8. Story County bridge - deformation contour plot for temperature loading

A maximum deformation of approximately 0.5 in. was obtained from the FE modeling. This value matches the original plan value noted above. The results obtained from the FE modeling were also compared to the values obtained using equation (1).

$$\Delta L = \alpha \Delta T L \quad \textbf{(1)}$$

where ΔL is the change in length, α is the coefficient of thermal expansion of the material, ΔT is the change in temperature, and L is the original length.

For the Story County bridge, the original length was taken as half of the total length of the bridge deck, 169 ft or 2,028 in., resulting in a change in length of approximately 0.45 in. when the

change in temperature equals 40°F and the coefficient of thermal expansion of concrete is used, 5.5E-6 1/°F. The value obtained results in a percentage of difference of 10% from the original plan value and the FE results.

3.1.2.3 Live Load Reactions and Deflection

HS20-44 truck loading conditions per AASHTO specifications were modeled and placed on top of the bridge deck. Based on the AASHTO specifications, the wheel loads were assumed to be uniformly distributed over an area of 20 in. by 10 in. The wheel spacing and loading is shown in Figure 3.9.

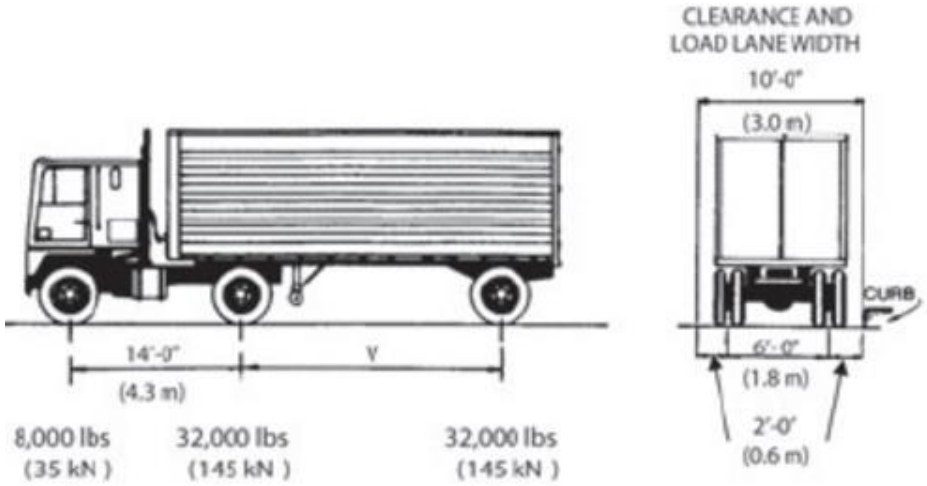

Ghosn and Fiorillo 2013

Figure 3.9. HS20-44 loading conditions and tire spacing

A linear load of 0.640 kips per linear foot of lane over a 10 ft width was also included in the truck loading conditions. This was modeled as a surface area over the length of the bridge. The concentrated loads and linear load can be seen in Figure 3.10.

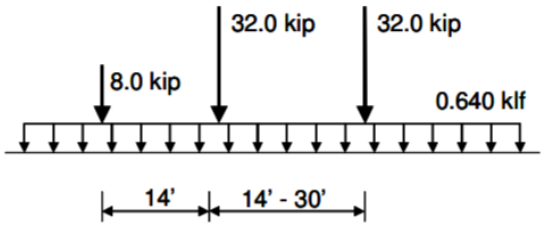

Original source unknown

Figure 3.10. HS20-44 loading conditions and uniform live load

Impact loads were also considered. A 20% impact load based on the concentrated load from the tires was modeled. This impact load was calculated according to equation (2).

$$I = \frac{50}{L+125} \leq 0.3 \quad \textbf{(2)}$$

where L is the longest span of the bridge in feet.

For the Story County bridge, the longest span is equal to 132 ft, which results in an impact load of approximately 19.46%. Because of this result, a 20% impact load was used.

3.1.2.3.1 Controlling Truck Loading Conditions

A 3D model was created in VBridge. This program was used to verify the controlling truck loading conditions to maximize the desired results (deflection, pier reactions, abutment reactions). The 3D model can be seen in Figure 3.11.

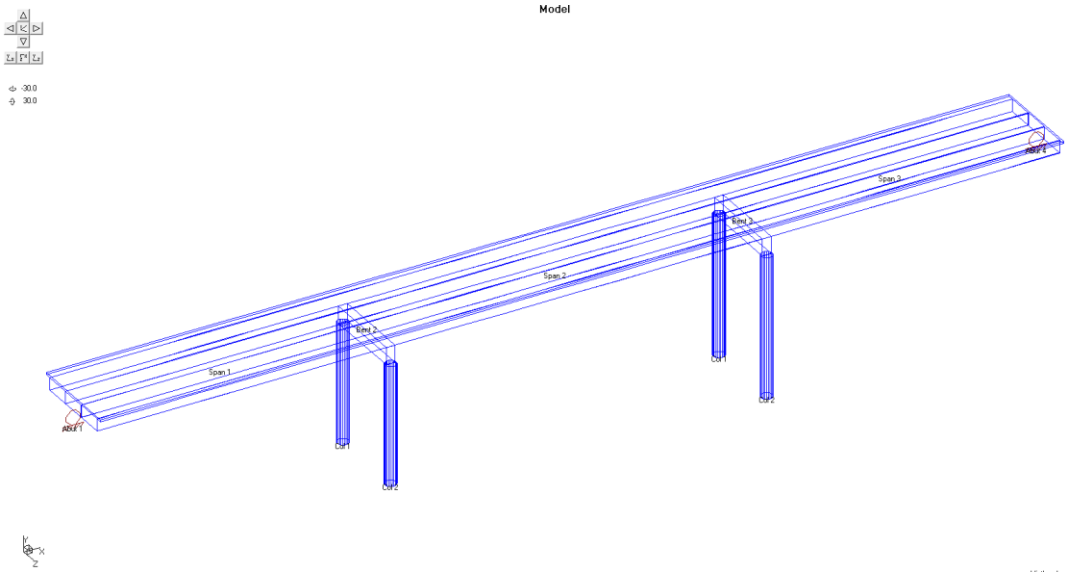

Figure 3.11. Story County bridge - full 3D VBridge model

HS20-44 truck loading conditions per AASHTO specifications were modeled and placed on top of the bridge deck. The controlling truck loading conditions for the abutment reactions, pier reactions, and deflection can be seen in Figure 3.12, Figure 3.13, and Figure 3.14, respectively.

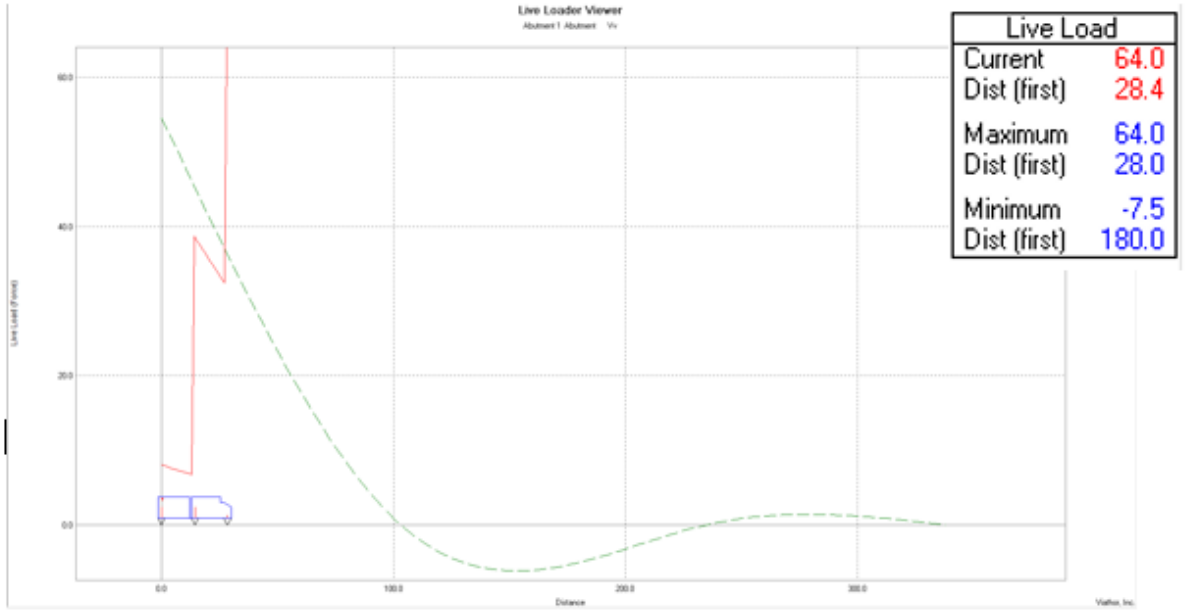

Figure 3.12. Story County bridge - controlling truck loading conditions for abutment reactions

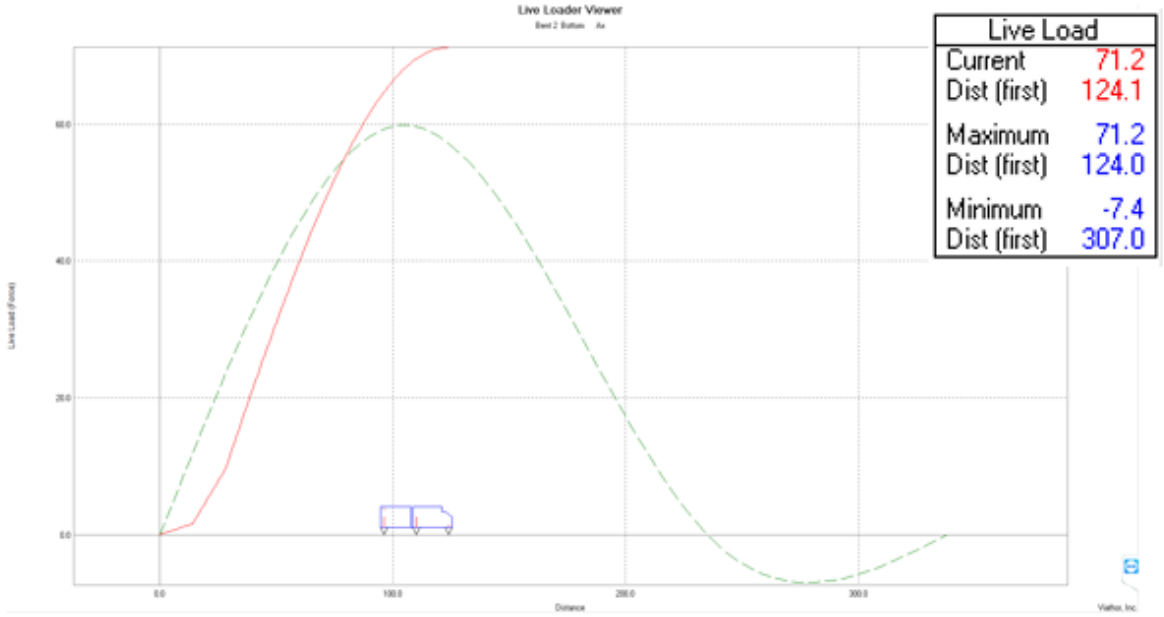

Figure 3.13. Story County bridge - controlling truck loading conditions for pier reactions

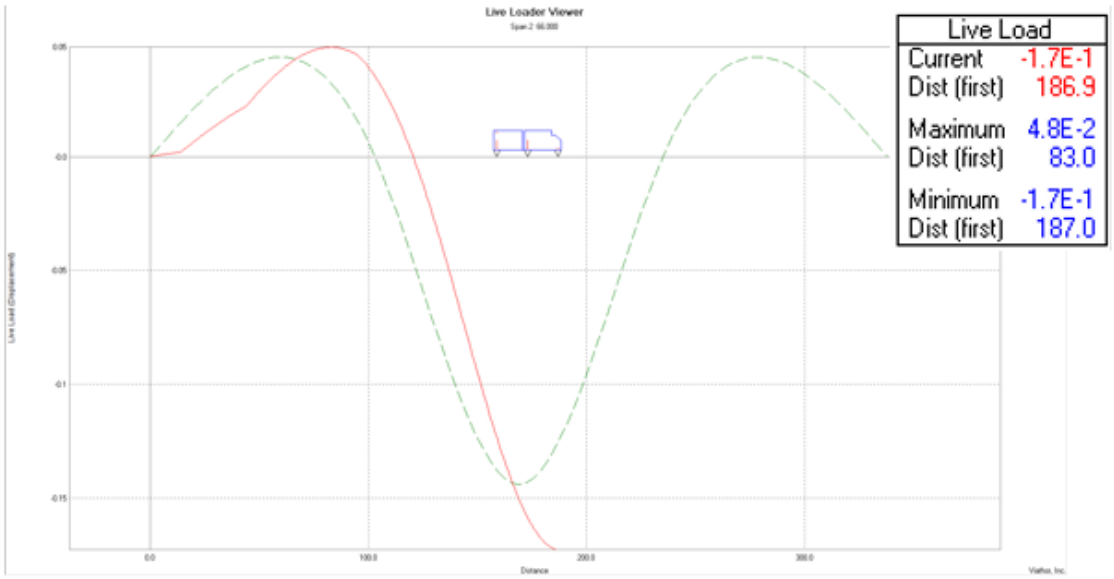

Figure 3.14. Story County bridge - controlling truck loading conditions for deflection

The lane load allocations can be seen in Figure 3.15, Figure 3.16, and Figure 3.17.

Figure 3.15. Controlling lane load for abutment reactions

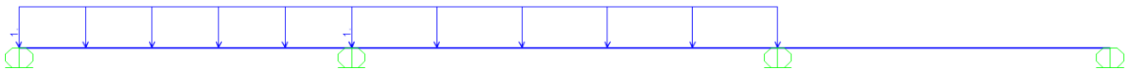

Figure 3.16. Controlling lane load for pier reactions

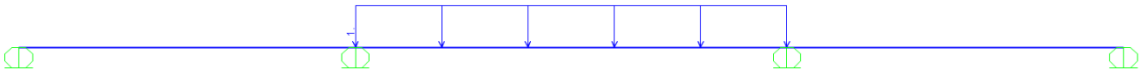

Figure 3.17. Controlling lane load for deflection

3.1.2.3.2 Truck Loading Deflection

The Story County bridge model was loaded with the truck loading conditions discussed above. The load allocation that corresponds with the maximum deflection at the midspan of the bridge

can be seen in Figure 3.14 for the truck load and Figure 3.17 for the lane load. The load in the model can be seen in Figure 3.18.

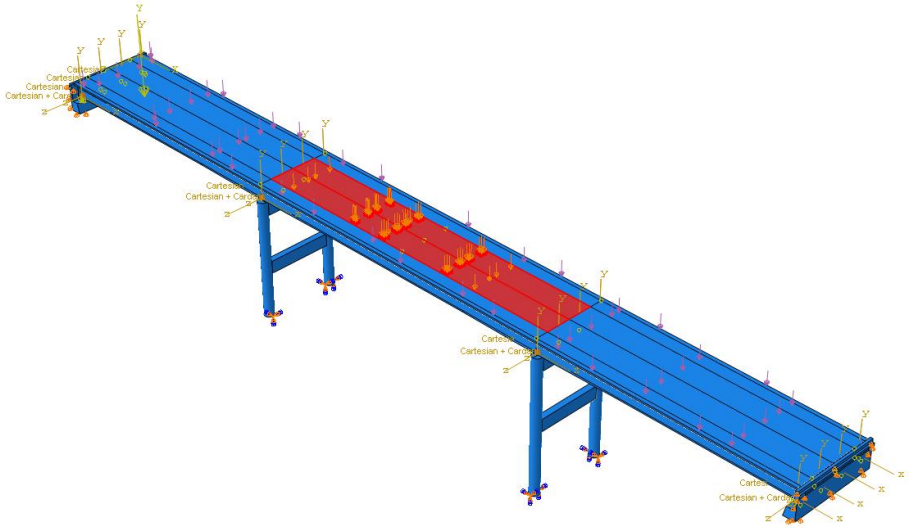

Figure 3.18. Story County bridge - load allocation for deflection

Lane load is marked in red in the interior span. Two concurrent 10 ft wide pressure loads were modeled in the center of the roadway. The truck load is shown with orange arrows indicating the location and direction.

Two HS20-44 trucks were modeled acting over each lane load location. The results for these loading conditions can be seen in Figure 3.19.

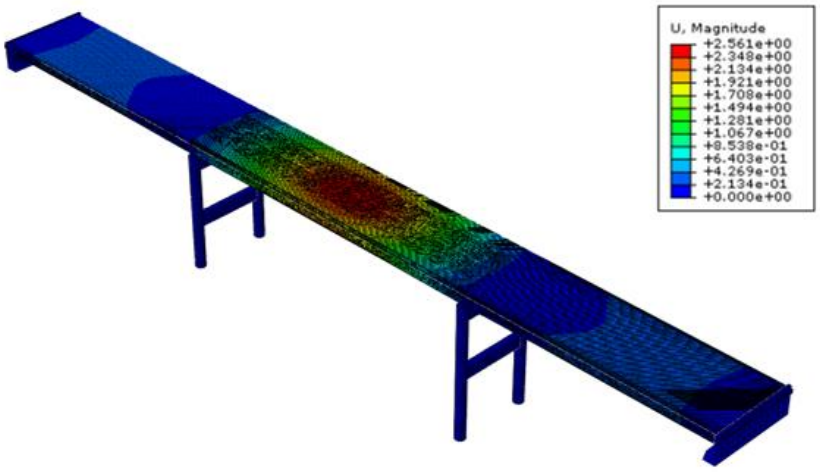

Figure 3.19. Story County bridge - deformation contour plot for deflection truck load

From the results of the FE model, a maximum deflection at midspan of approximately 2.5 in. was obtained. AASHTO specifications provide certain deflection limits for vehicular bridges in the absence of other criteria. These limits are set as L/800 for general vehicular loads and L/1000 for vehicular and pedestrian loads, where L is the span where the deflection is being questioned. Since the Story County bridge does not have pedestrian loads, L/800 is applicable. Using the center span of the Story County bridge, for which L is 132 ft or 1,584 in., the L/800 design limit is approximately 1.98 in. Accounting for the dead load deflection shown previously, the live load resulted in a deflection of approximately 1.53 in., which is lower than the L/800 deflection limit.

3.1.2.3.3 Truck Loading Reactions

To maximize the abutment and pier reactions, different truck loading allocations were needed. The load allocation that corresponds with the maximum abutment reactions can be seen in Figure 3.12 for the truck load and Figure 3.15 for the lane load. The load allocation that corresponds with the maximum pier reactions can be seen in Figure 3.13 for the truck load and Figure 3.16 for the lane load.

The abutment reactions results will be discussed first. The load in the model is shown in Figure 3.20 marked in red.

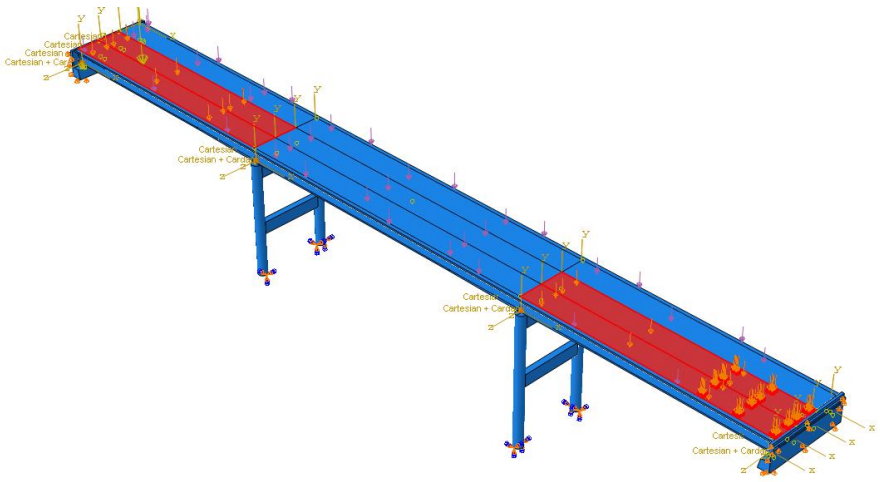

Figure 3.20. Story County bridge - load allocation for abutment reactions

The lane load can be clearly seen in the exterior spans with the rear axle of the concentrated truck load at the edge of the bridge deck. Two HS20-44 trucks were modeled side by side, with one side of the truck axle 2 ft from the curb. The lane loads were modeled as two concurrent 10 ft wide pressure loads starting from the curb.

A deformation contour plot is provided in Figure 3.21.

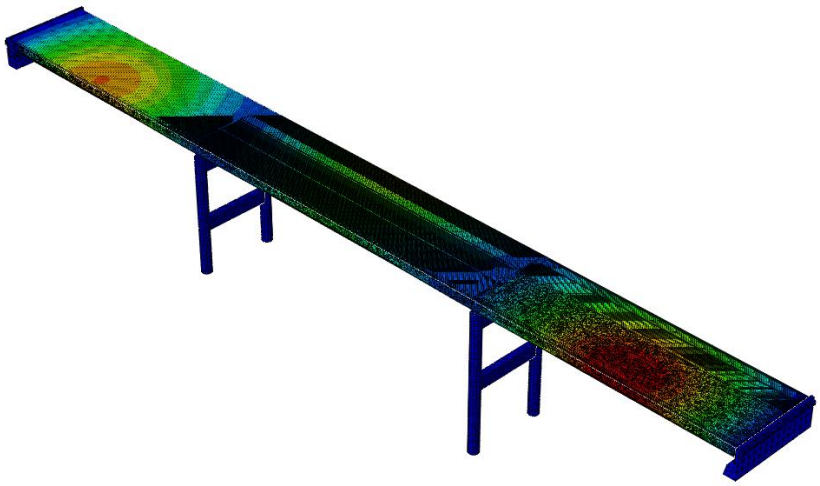

Figure 3.21. Story County bridge - deformation contour plot for abutment reactions truck load

Maximum deformation can be clearly seen in the exterior span where the concentrated truck load is applied.

The results for dead load and abutment reactions can be seen in Table 3.5.

Table 3.5. Story County bridge - dead load and live load abutment reactions

	Abutment Reactions (kips)			
	Ext	% diff	Int	% diff
DL #1	33.11	6.80	44.50	5.52
DL #2	18.03	16.14	6.95	54.35
ULL	-	-	-	-
CLL	-	-	-	-
HS-20-16	55.03	14.17	83.30	47.96
Impact	7.07	33.27	11.68	5.04
Total	113.24	1.74	146.43	21.82

A comparison between the results obtained from the FE model and the original plans is shown.

High percentages of difference were obtained for the truck loading values. The highest percentage of difference was almost 48% for the interior support for the HS20-16 load. This difference contributes to the percentage of difference of 21.82% that was obtained for the total load for the interior support. The exterior support also showed high percentages of difference, with 14.17% for the HS20-16 load and 33.27% for the impact load. The total load, however, only amounted to a percentage of difference of 1.74%.

After careful inspection of the original plan values, it was decided that it was necessary to alter the truck loading conditions in the FE model to try to improve its accuracy compared to the original plan values. The truck loading conditions for the model needed to be altered because the loads in the plans are calculated based on a one-dimensional bridge analysis.

From the literature (Ryan et al. 2012), it was discovered that a 26 kip load was used instead of the current HS20-44 truck loading conditions for the drawing plan values. This loading condition is shown in Figure 3.22.

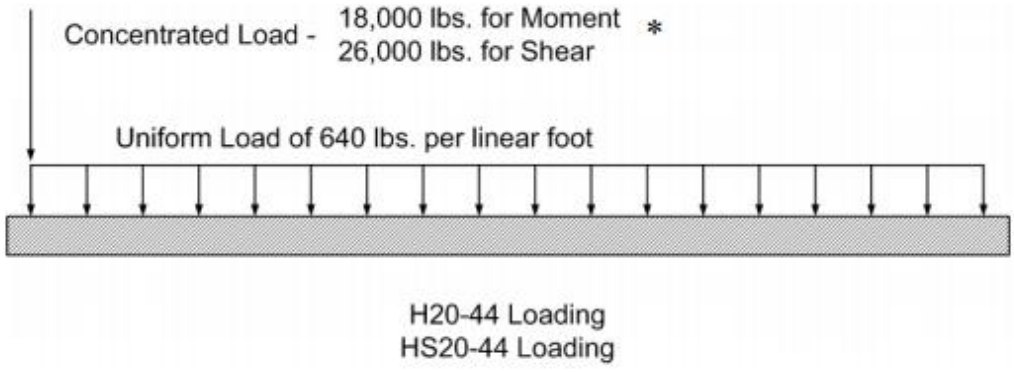

* Use two concentrated loads for negative moment in continuous spans (Refer to *AASHTO LRFD Bridge Design Specifications 5th edition*, 2010 Interim; Article 3.6.1.2)

MnDOT 2012

Figure 3.22. Truck loading conditions from the drawing plans

To obtain the drawing plan values, the 26 kip load is divided into the two axles of the truck and multiplied by various factors. For the interior girders, the load is multiplied by the load distribution factor (LDF) obtained using equation (3).

$$LDF = \frac{S}{5.5} \quad \textbf{(3)}$$

where LDF is the load distribution factor and S is the girder spacing in feet.

For the exterior girders, equation (4) is used with the factor calculated in equation (5).

$$g = e g_{interior} \quad \textbf{(4)}$$

$$e = 0.6 + \frac{d_e}{10} \quad \textbf{(5)}$$

where g is the LDF for the exterior girders, $g_{interior}$ is the LDF for the interior girders, e is a conversion factor from interior girder to exterior girder, and d_e is the distance between the exterior girders to the center of the curb in feet.

An additional factor for skewed bridges can also be added. This factor is relevant for the Marshall County bridge and will be discussed in the following section.

In addition, judging by the magnitudes of the original plan values, it was determined that an impact load was applied on the lane load in addition to the concentrated live load from the tire loads. This is contrary to the current AASHTO specifications.

The truck loading conditions in the FE model were altered to attempt to match the drawing plan values. One truck was modeled instead of two, with an impact load applied on the lane load as well. This new load allocation can be seen in Figure 3.23, with one truck instead of two in one of the exterior spans.

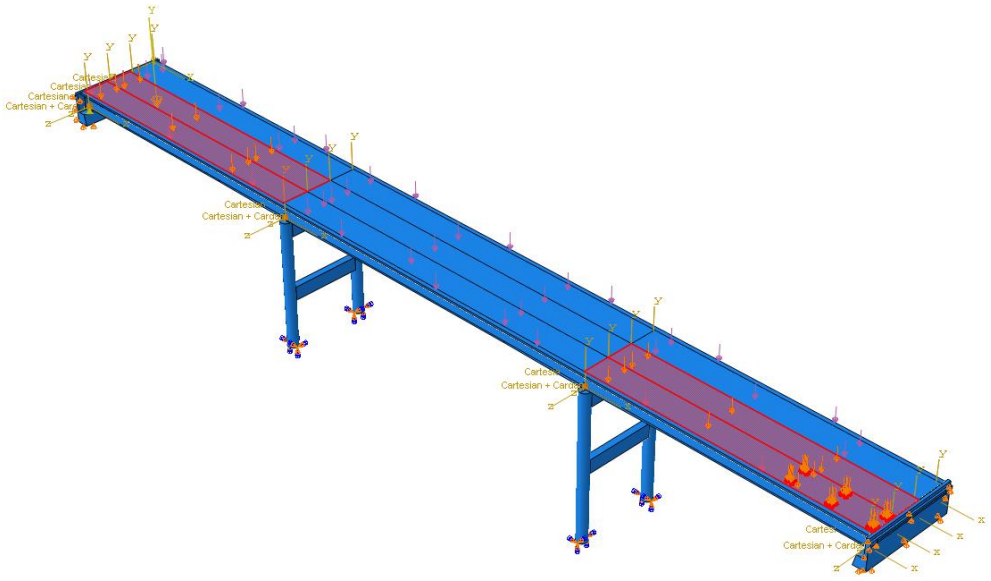

Figure 3.23. Story County bridge - updated load allocation for abutment reactions

The results for dead load and abutment reactions can be seen in Table 3.6.

Table 3.6. Story County bridge - dead load and updated live load abutment reactions

	Abutment Reactions (kips)			
	Ext	% diff	Int	% diff
DL #1	33.12	6.84	44.53	5.45
DL #2	18.08	15.93	6.96	54.56
ULL	-	-	-	-
CLL	-	-	-	-
HS-20-16	53.34	10.66	53.13	5.64
Impact	10.67	0.64	10.63	13.61
Total	115.20	3.50	115.24	4.12

A comparison between the results obtained from the updated FE model and the original plans is shown.

The percentages of difference decreased in the interior support after the truck loading conditions were altered. The HS20-16 load, which had a percentage of difference of 47.96% under the previous loading conditions, now resulted in a percentage of difference of 5.64%. The total load on the interior support decreased from 146.43 kips to 115.24 kips. The percentage of difference decreased from 21.82% to 4.12%. The total load decreased because the interior support is now taking only one side of the axle from the truck. Previously, the interior support took the same axle plus another axle.

The exterior support did not exhibit major differences from the previous loading conditions. The HS20-16 load went from 55.03 kips to 53.34 kips, and the impact load went from 7.07 kips to 10.67 kips. The percentage of difference for the total load on the exterior support went from 1.74% to 3.50%. This small change in the exterior support may be due to the fact that the exterior support was already taking the same axle of the truck nearest to the curb. The HS20-16 load decreased because there was no truck load in the adjoining lane.

The pier reactions will be discussed in the remainder of this section. The load in the model is shown in Figure 3.24 marked in red.

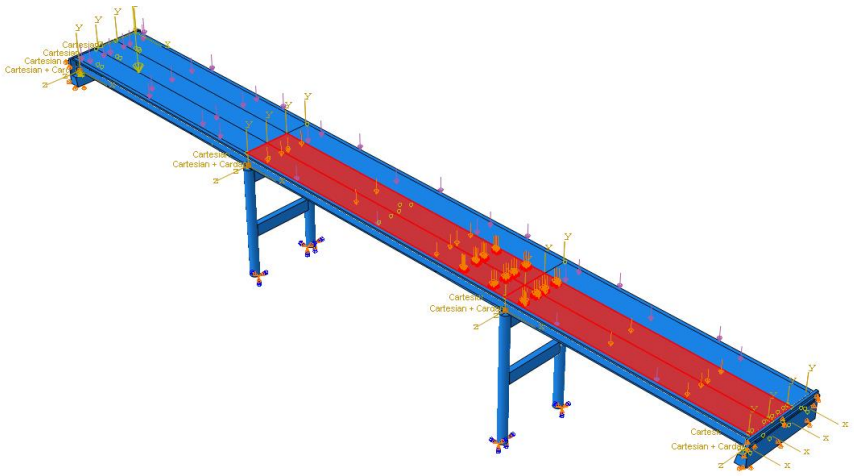

Figure 3.24. Story County bridge - load allocation for pier reactions

The lane load can be clearly seen in the spans on either side of the loaded pier, with the rear axle of the concentrated truck load located over the pier. Two HS20-44 trucks were modeled side by side, with one side of the truck axle 2 ft from the curb. The lane loads were modeled as two concurrent 10 ft wide pressure loads starting from the curb.

A deformation contour plot is provided in Figure 3.25.

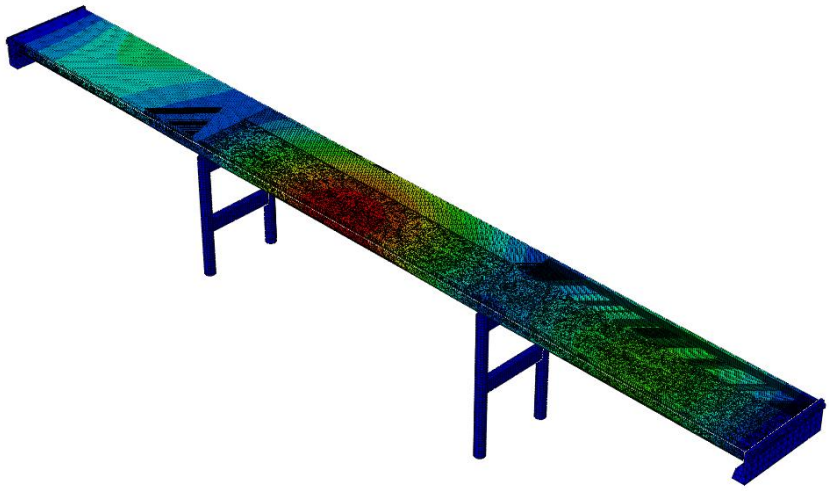

Figure 3.25. Story County bridge - deformation contour plot for pier reactions truck load

The maximum deformation is not prominent because much of the load is applied over a support.

The results for dead load and pier reactions can be seen in Table 3.7.

Table 3.7. Story County bridge - dead load and live load pier reactions

	Pier Reactions (kips)			
	Ext	% diff	Int	% diff
DL #1	126.23	11.31	150.29	12.68
DL #2	58.95	20.88	22.40	44.48
ULL	58.05	13.36	71.52	8.31
CLL	40.05	104.36	64.55	183.09
HS-20-16	-	-	-	-
Impact	8.01	55.25	12.91	37.94
Total	291.29	0.38	321.66	4.03

A comparison between the results obtained from the FE model and the original plans is shown.

High percentages of difference were obtained for the truck loading values. The highest percentage of difference was almost 183.09% for the interior support for the concentrated live load. This difference contributes to the percentage of difference of 4.03% that was obtained for the total load for the interior support. The exterior support also showed high percentages of difference, with 104.36% for the concentrated live load and 55.25% for the impact load. The total load, however, only amounted to a percentage of difference of 0.38%.

For the reasons explained above for the abutment reactions, the truck loading conditions in the FE model were altered to attempt to match the drawing plan values. One truck was modeled instead of two, with an impact load applied on the lane load as well. This new load allocation can be seen in Figure 3.26, with one truck instead of two in one of the exterior spans.

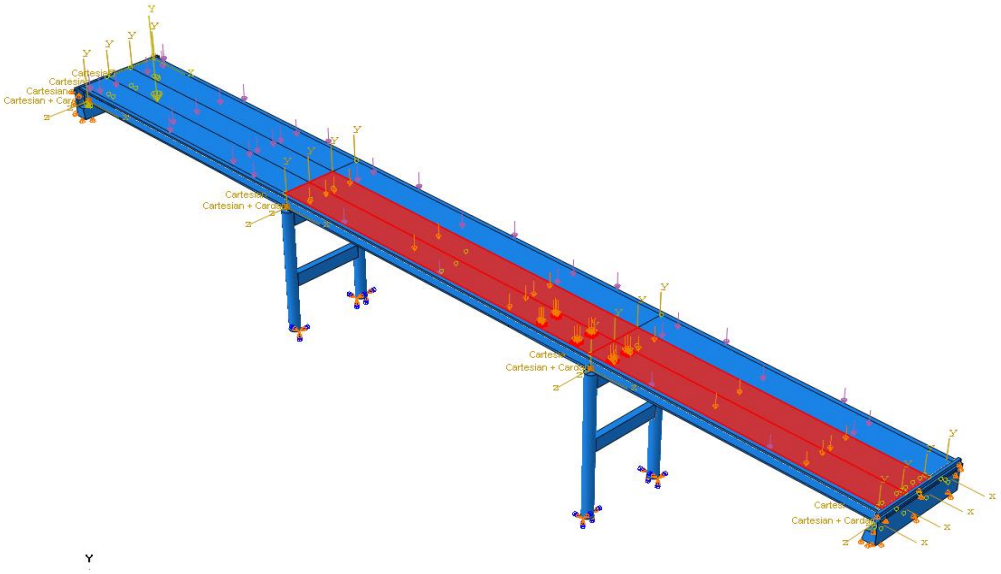

Figure 3.26. Story County bridge - updated load allocation for pier reactions

The results for dead load and pier reactions can be seen in Table 3.8.

Table 3.8. Story County bridge - dead load and updated live load pier reactions

	Pier Reactions (kips)			
	Ext	% diff	Int	% diff
DL #1	126.24	11.32	150.29	12.68
DL #2	58.95	20.88	22.40	44.48
ULL	58.05	13.35	71.51	8.32
CLL	37.03	88.91	32.51	42.60
HS-20-16	-	-	-	-
Impact	19.02	6.24	20.81	0.03
Total	299.28	2.35	297.51	3.78

A comparison between the results obtained from the updated FE model and the original plans is shown.

The percentages of difference decreased in the interior support after the truck loading conditions were altered. The concentrated live load, which had a percentage of difference of 183.09% under the previous loading conditions, now resulted in a percentage of difference of 42.60%. The percentage of difference for the impact load decreased from 37.94% to 0.03%. The total load on the interior support decreased from 321.66 kips to 297.51 kips. The percentage of difference decreased from 4.03% to 3.78%. The total load decreased because the interior support is now taking only one side of the axle from the truck. Previously, the interior support took the same axle plus another axle.

The exterior support did not exhibit major differences from the previous loading conditions. The concentrated live load went from 40.05 kips to 37.03 kips, and the impact load went from 8.01 kips to 19.02 kips. The percentage of difference for the total load on the exterior support went from 0.38% to 2.35%. This small change in the exterior support may be due to the fact that the exterior support was already taking the same axle of the truck nearest to the curb. The concentrated live load decreased because there was no truck load in the adjoining lane.

3.2 Marshall County Bridge

A full 3D model was developed in Abaqus FEA for the Marshal County bridge. This model includes a concrete bridge deck supported by welded plate steel girders and diaphragms that rest on abutments at the ends and piers. A skew of 45° is also modeled. A full 3D model can be seen in Figure 3.27, with a plan view in Figure 3.28, in which the skew is noticeable.

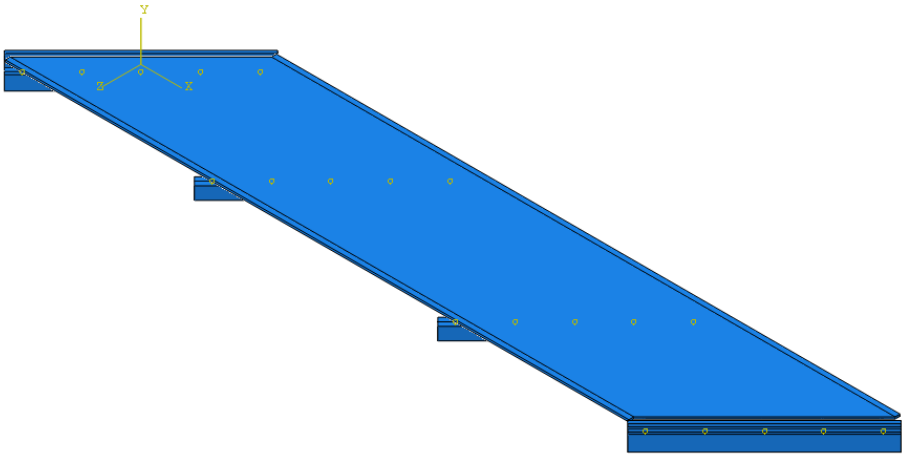

Figure 3.27. Marshall County bridge - gull 3D FE model

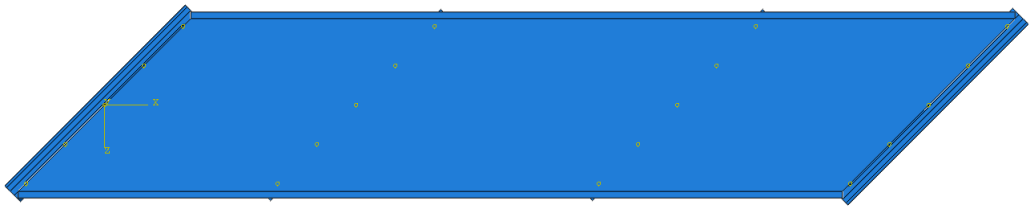

Figure 3.28. Marshall County bridge - plan view

Constraints, boundary conditions, and other elements were assigned in the model. Loading conditions due to self-weight, surface weathering, and truck loading were also incorporated into the model.

An 8 in. by 210 ft bridge deck was modeled as a C3D8R element, which is an eight-node linear brick element with reduced integration and hourglass control. In addition, C3D8R was utilized for all concrete parts in the model, including the abutments and the pier caps. The steel superstructure was composed of welded plate steel girders and transverse diaphragms at the ends and over the piers. The web and flanges of the welded plate girders as well as the diaphragms were modeled as S4R elements, which are four-node, doubly curved, thin or thick shell elements with reduced integration, hourglass control, and finite membrane strains. For the flanges of the welded plate girders, width and thickness were modeled per the drawing plans. All of the steel superstructure elements were merged together (Figure 3.29).

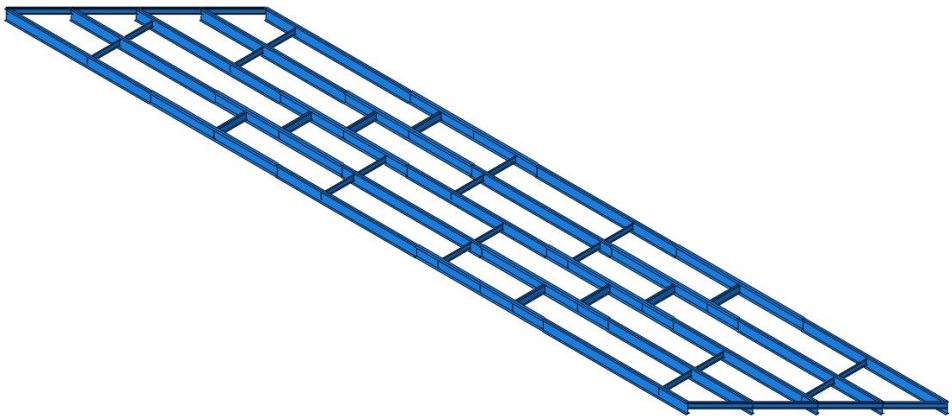

Figure 3.29. Marshall County bridge - steel superstructure

This model underwent an elastic analysis. Only mass density and elastic properties such as Young's modulus and Poisson's ratio were needed to execute the analysis successfully. The mass densities utilized for the concrete and steel were assigned as their specific weights: 150 lb/ft^3 and 490 lb/ft^3, respectively. As for the Young's modulus and Poisson's ratio, 3,718 ksi and 0.15 were utilized for concrete and 29,000 ksi and 0.3 were utilized for the steel, respectively. In addition, the coefficients of thermal expansion for both concrete and steel were selected as 5.5E-6 1/°F and 6.5E-6 1/°F, respectively.

Boundary conditions were assigned to the abutment's vertical and horizontal faces that are in the direction of the supporting soil. Vertical faces have horizontal constraints and horizontal faces have vertical constraints. A fixed boundary condition was assigned to the bottom face of the pier caps simulating the foundations that rest under the topsoil. Boundary conditions can be seen in Figure 3.30 as red lines at the abutment and on the bottom face of the pier cap.

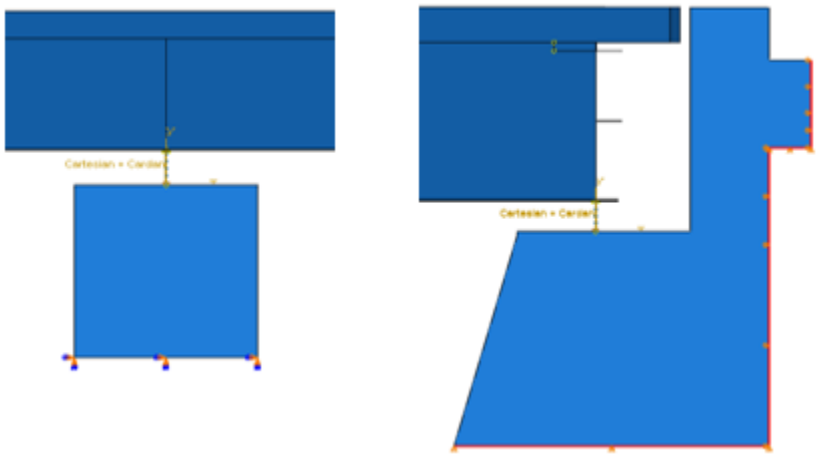

Figure 3.30. Marshall County bridge - boundary conditions

Tie constraints were assigned between the top flanges of all the welded plate girders with the bottom surface of the bridge deck. Connection wires were utilized between the steel girders and the abutments and piers to simulate the rocker bearings at their locations. All reaction values presented in the following pages correspond to these connection wires.

3.2.1 Convergence Study

The model was trialed on numerous occasions with various meshing sizes. The results stabilized at an approximate meshing size of 5 in. A meshing of 4 in. was determined to be the most effective for the model at this point. Just for reference, the time elapsed to complete the analysis for a meshing size of 3 in. was almost six times as long as the time elapsed for a meshing size of 4 in. (Table 3.9).

Table 3.9. Marshall County bridge - mesh convergence study

Mesh Size (in.)	Max Deflection at Midspan (in.)	Time Elapsed (s)
12	0.7187	77.7
10	0.7103	100.9
8	0.7513	144.5
6	0.7381	243.7
5	0.5261	654.7
4.5	0.5247	835
4	0.5272	1125.9
3.5	0.5375	1777.9
3	0.5213	11924.8

The time elapsed for each trial is shown for all mesh sizes along with their deflection values.

A graph of the different values that were trialed with their results is shown in Figure 3.31.

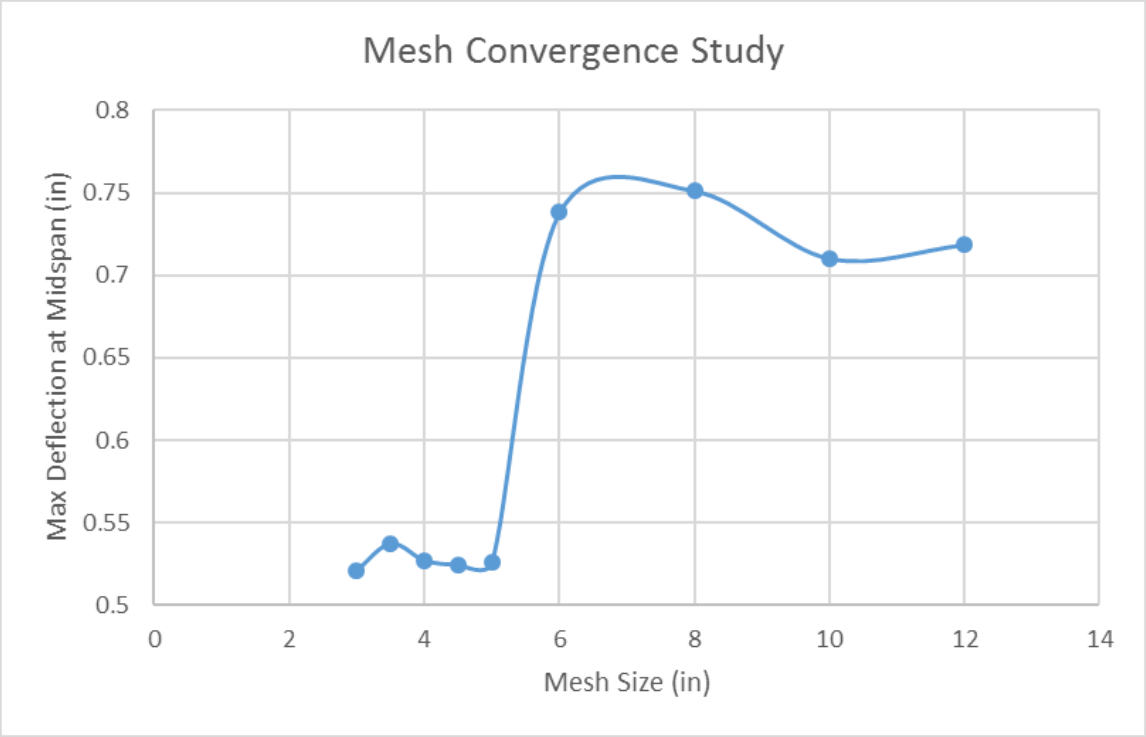

Figure 3.31. Marshall County bridge - mesh convergence study

With a mesh size of 4 in., the structure was modeled using 318,380 elements, 450,396 nodes, and 1,562,961 variables.

3.2.2 Validation with Original Plans

The information needed to develop the FE model and analysis for the Marshall County bridge was obtained from its original drawing plans. Abutment and pier reactions can be observed in these plans and in Table 3.10.

Table 3.10. Marshall County bridge - abutment and pier reactions from the drawing plans

	Abutment Reactions (kips)		Pier Reactions (kips)	
	Exterior	**Interior**	**Exterior**	**Interior**
DL #1	24.5	27.8	90.1	102.0
DL #2	10.0	4.7	34.6	16.3
ULL	-	-	42.5	50.3
CLL	-	-	20.0	23.7
HS20-44	45.6	53.9	-	-
Impact	12.0	14.2	15.8	18.7
Total	92.1	100.6	203.0	211.0

Source: Marshall County Bridge Plans
Dead load #1 includes weight of slab, girders, and diaphragms.
Dead Load #2 includes weight of curbs, rail, and future wearing surface.

These reactions were the source of comparison for the results obtained from the FE analysis shown in the following section. It is important to mention that the FE model does not fully incorporate all of the elements shown in the plans but includes the most pertinent ones.

3.2.2.1 Dead Load Reactions and Deflection

Self-weight was included in the whole model. A surface weathering loading condition of 20 lb/ft^2 over the roadway was also added. Curb loading on 1 ft 8 in. of the edges was added as a surface area simulating a 1 ft 8 in. by 1 ft area of concrete along the entire length of the bridge deck. The results for dead load deflection and a comparative loading conditions table can be seen in Figure 3.32, Figure 3.33, and Table 3.11.

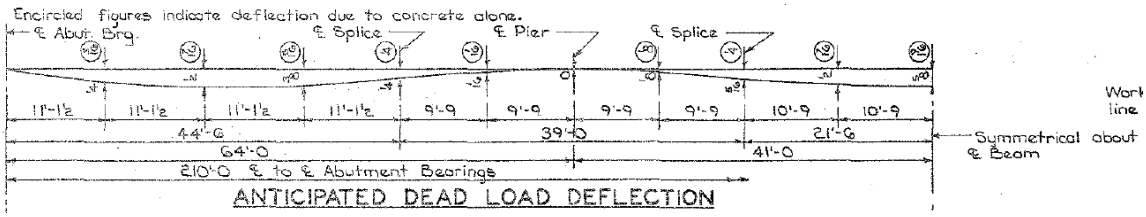

Marshall County Bridge Plans

Figure 3.32. Marshall County bridge - anticipated dead load deflection

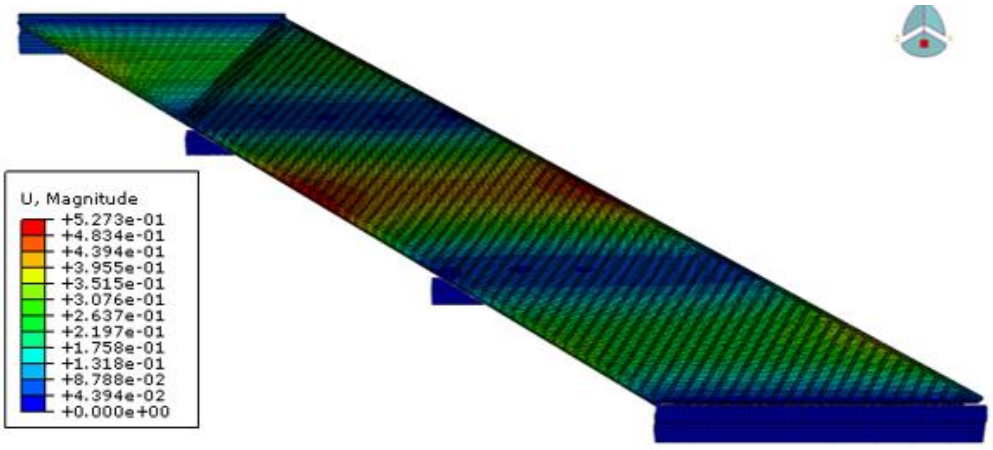

Figure 3.33. Marshall County bridge - deformation contour plot for dead load

Table 3.11. Marshall County bridge - dead load abutment and pier reactions

	Abutment Reactions (kips)				Pier Reactions (kips)			
	Ext	% diff	Int	% diff	Ext	% diff	Int	% diff
DL #1	25.01	2.07	28.13	1.19	86.36	4.15	100.35	1.61
DL #2	10.17	1.67	4.75	1.10	33.99	1.76	16.68	2.35

The maximum deflection obtained was approximately 0.53 in. at the center of the bridge. This value presents a percentage of difference of approximately 15% from the value obtained from the original drawing plans (5/8 in.).

The resulting abutment and pier reactions were tabulated and compared with the values obtained from the drawing plans. Two dead load loading conditions were considered for the pier and abutment reactions. Both the pier and abutment reactions show low percentages of difference ranging from a maximum of 4.15% to a minimum of 1.10%.

3.2.2.2 Temperature Loading

Temperature loading was also modeled. Expansion plate settings from the original drawing plans are shown in Table 3.12.

Table 3.12. Marshall County bridge - expansion plate settings

EXPANSION PLATE SETTINGS

Temp. at time of setting	South Abut.		Pier 1	Pier 2	North Abut.	
	D					D
10°	2¼	− 5/16	—	—	−5/16	2¼
50°	2	0	—	—	0	2
90°	1¾	+5/16	—	—	+5/16	1¾

NOTE: Settings for other temperatures are proportional

Marshall County Bridge Plans

A shrinkage and expansion of 0.25 in. can be seen at 10°F and 90°F, respectively, with a base temperature of 50°F.

The results from the FE modeling can be seen in Figure 3.34.

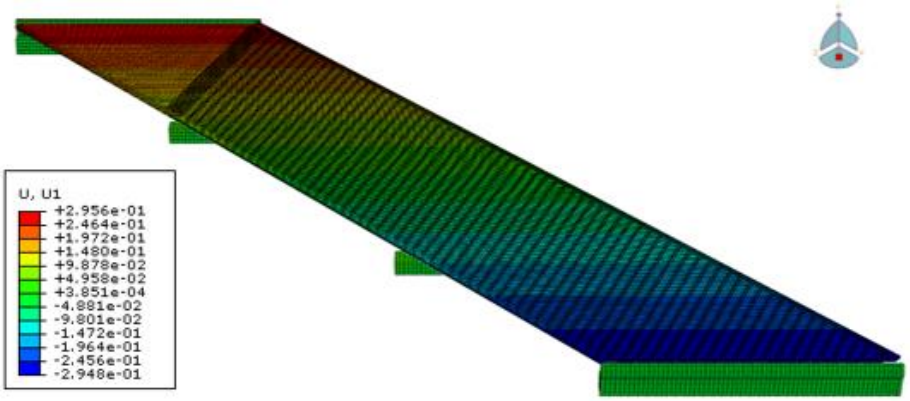

Figure 3.34. Marshall County bridge - deformation contour plot for temperature loading

A maximum deformation of approximately 0.3 in. was obtained from the FE modeling. This value is 20% different than the original plan value. The result obtained from the FE modeling was also compared to the value obtained using equation (1).

For the Marshall County bridge, the original length was taken as half of the total length of the bridge deck, 105 ft or 1,260 in., resulting in a change in length of approximately 0.28 in. when the change of temperature was 40°F and the coefficient of thermal expansion of concrete was used, 5.5E-6 1/°F. The value obtained results in a percentage of difference of 6.22% from the result obtained from the FE modeling.

3.2.2.3 Live Load Reactions and Deflection

The same loading conditions described in Section 3.1.2.3, Figure 3.9 and Figure 3.10, were applied. Impact loads were also considered. A 25% impact load based on the concentrated load from the tires was modeled. This impact load was calculated according to equation (2). For the Marshall County bridge, the longest span is equal to 82 ft, which results in an impact load of approximately 24.15%. Because of this result, a 25% impact load was used.

3.2.2.3.1 Controlling Truck Loading Conditions

A 3D model was created in VBridge. This program was used to verify the controlling truck loading conditions to maximize the desired results (deflection, pier reaction, abutment reaction). The 3D model can be seen in Figure 3.35, with a top view in Figure 3.36.

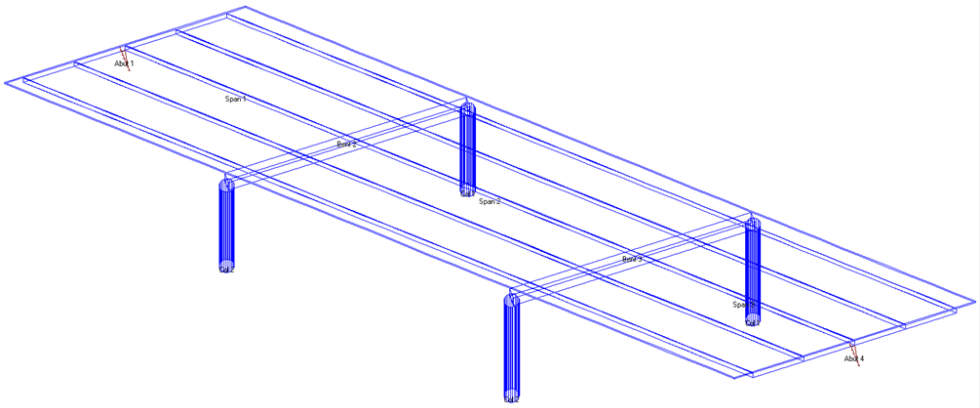

Figure 3.35. Marshall County bridge - full 3D VBridge model

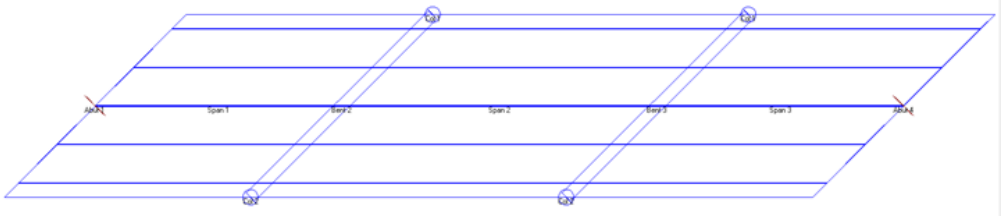

Figure 3.36. Marshall County bridge - plan view of VBridge model

HS20-44 truck loading conditions per AASHTO specifications were modeled and placed on top of the bridge deck.

The controlling truck loading conditions for the abutment reactions, pier reactions, and deflection can be seen in Figure 3.37, Figure 3.38, and Figure 3.39, respectively.

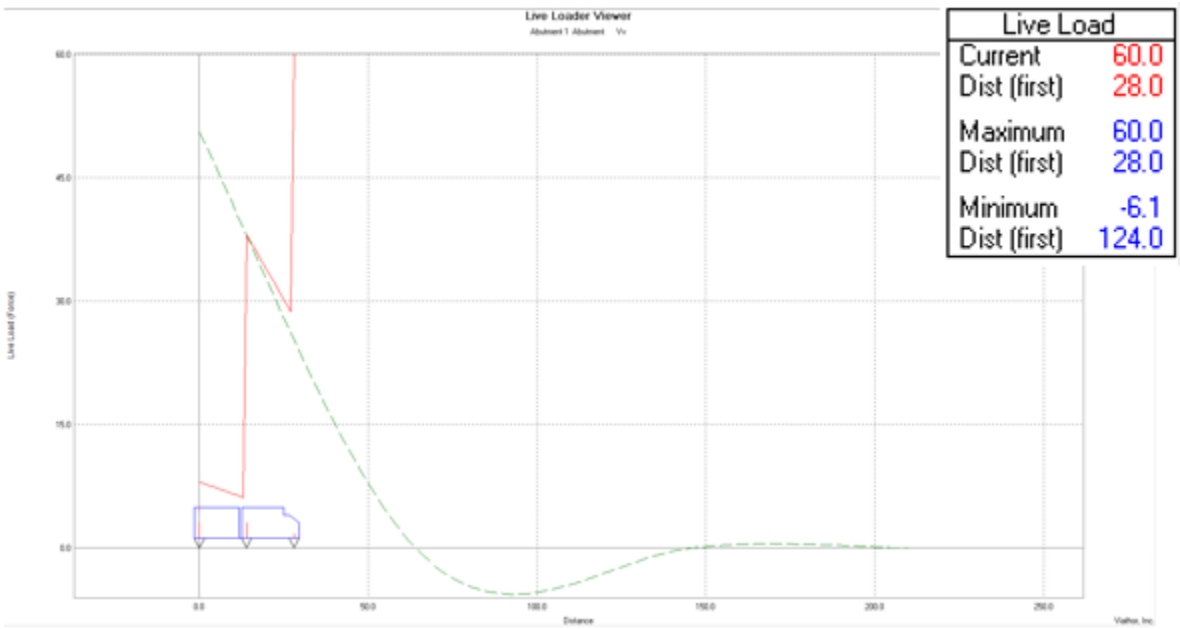

Figure 3.37. Marshall County bridge - controlling truck loading conditions for abutment reactions

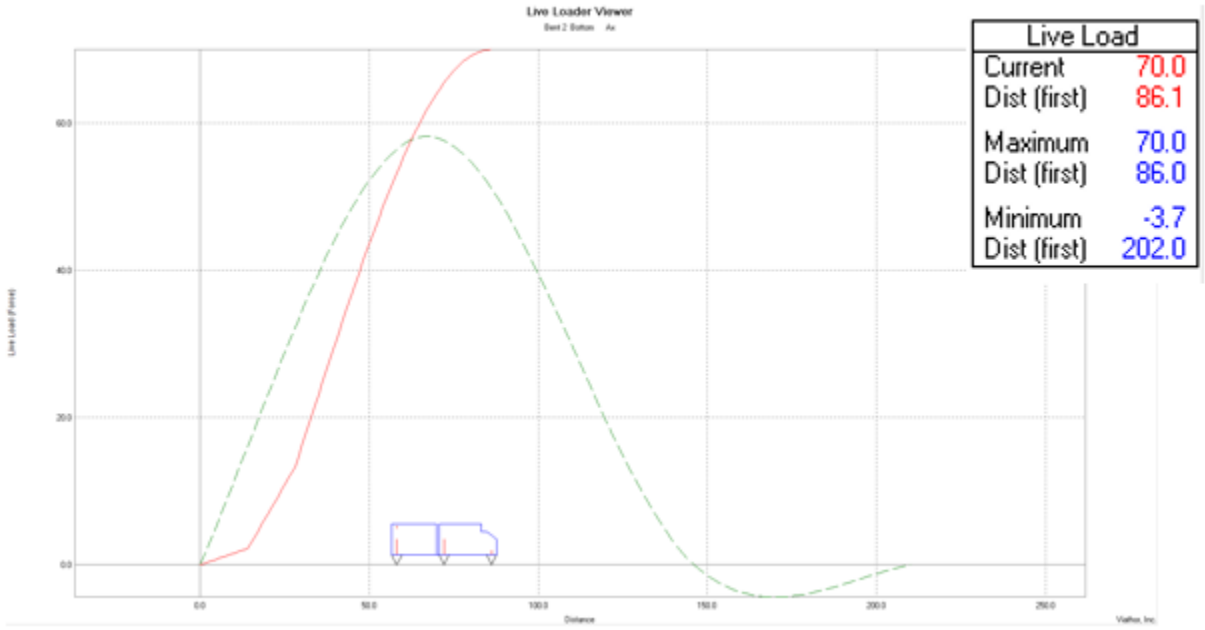

Figure 3.38. Marshall County bridge - controlling truck loading conditions for pier reactions

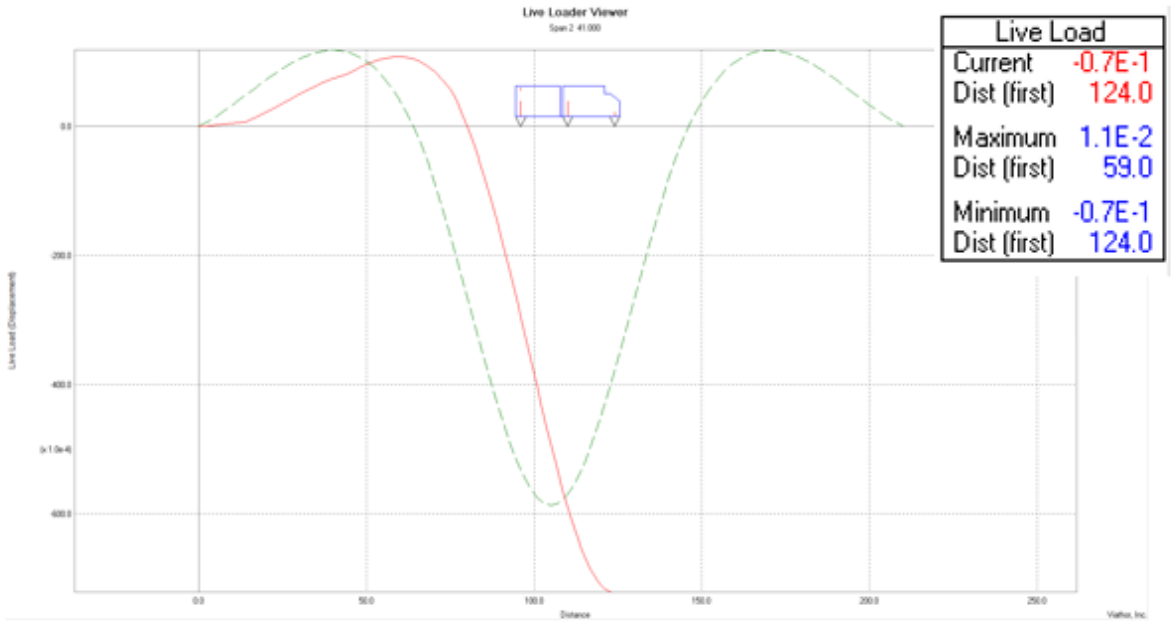

Figure 3.39. Marshall County bridge - controlling truck loading conditions for deflection

The controlling lane loads are the same as those shown in Section 3.1.2.3.1, Figure 3.16, Figure 3.17, and Figure 3.18. These conditions can be summarized as the lane load being applied on the exterior spans to maximize abutment reactions, on the continuous spans to observe the reactions of the piers in between, and on the center span to observe deflection at midspan.

3.2.2.3.2 Truck Loading Deflection

The Marshall County bridge model was loaded with the truck loading conditions discussed above. The load allocation that corresponds with the maximum deflection at the midspan of the bridge can be seen in Figure 3.39 for the truck load and Figure 3.17 for the lane load. The load in the model can be seen in Figure 3.40.

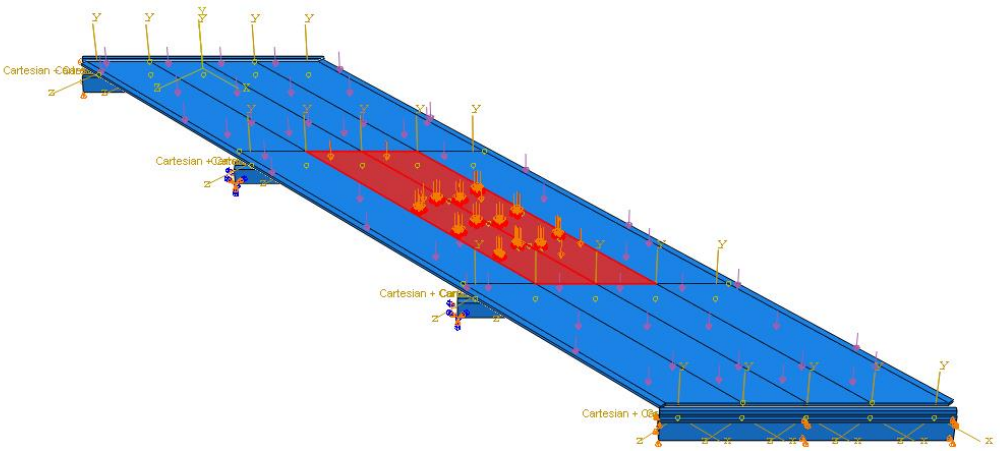

Figure 3.40. Marshall County bridge - load allocation for deflection

Lane load is marked in red in the interior span. Two concurrent 10 ft wide pressure loads were modeled in the center of the roadway. The truck load is shown with orange arrows indicating the location and direction.

Two HS20-44 trucks were modeled acting over each lane load location. The deflection results for these loading conditions can be seen in Figure 3.41.

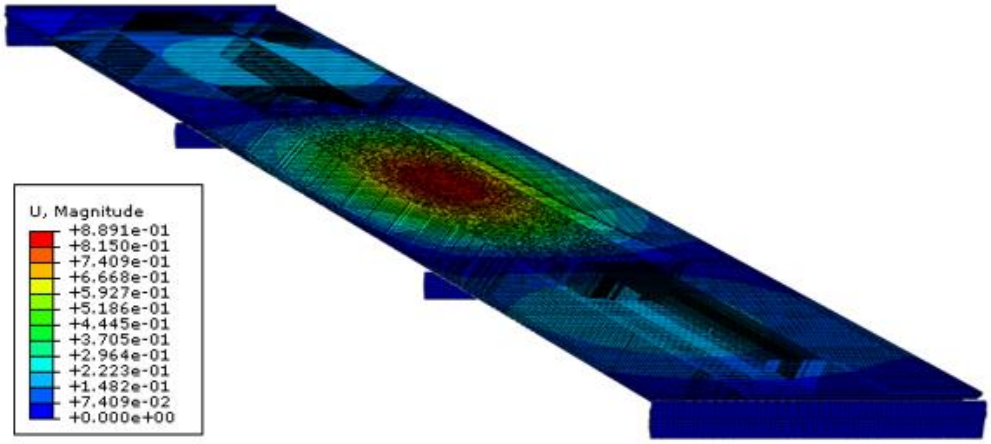

Figure 3.41. Marshall County bridge - deformation contour plot for deflection truck load

From the results of the FE model, a maximum deflection at midspan of approximately 1.3 in. was obtained. AASHTO specifications provide certain deflection limits for vehicular bridges in the absence of other criteria. These limits are set as L/800 for general vehicular loads and L/1000 for vehicular and pedestrian loads, where L is the span where the deflection is being questioned. Since the Marshall County bridge does not have pedestrian loads, L/800 is applicable. Using the center span of the Marshall County bridge, for which L is 82 ft or 984 in., the L/800 design limit is approximately 1.23 in. Accounting for the dead load deflection shown previously, the live load resulted in a deflection of approximately 0.89 in. which is lower than the L/800 deflection limit.

3.2.2.3.3 Truck Loading Reactions

To maximize abutment and pier reactions, different truck loading allocation were needed. The load allocation that corresponds with the maximum abutment reactions can be seen in Figure 3.37 for the truck load and Figure 3.15 for the lane load. The load allocation that corresponds with the maximum pier reactions can be seen in Figure 3.38 for the truck load and Figure 3.16 for the lane load.

The abutment reactions results will be discussed first. The load in the model is shown in Figure 3.42 marked in red.

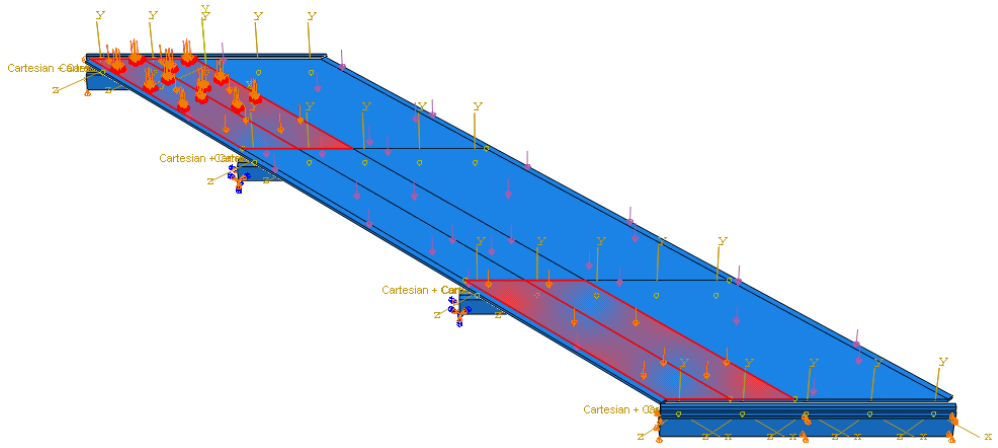

Figure 3.42. Marshall County bridge - load allocation for abutment reactions

The lane load can be clearly seen in the exterior spans with the rear axle of the concentrated truck load at the edge of the bridge deck. Two HS20-44 trucks were modeled side by side, with one side of the truck axle 2 ft from the curb. The lane loads were modeled as two concurrent 10 ft wide pressure loads starting from the curb.

A deformation contour plot is provided in Figure 3.43.

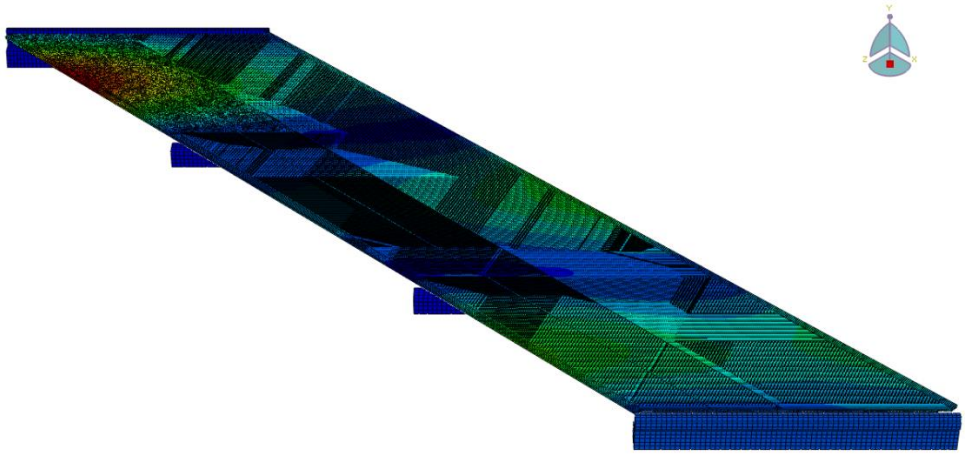

Figure 3.43. Marshall County bridge - deformation contour plot for abutment reactions truck load

Maximum deformation can be clearly seen in the exterior span where the concentrated truck load is applied.

The results for dead load and abutment reactions can be seen in Table 3.13.

Table 3.13. Marshall County bridge - dead load and live load abutment reactions

	Abutment Reactions (kips)			
	Ext	% diff	Int	% diff
DL #1	24.10	1.65	27.90	0.36
DL #2	10.30	3.00	4.60	2.23
ULL	-	-	-	-
CLL	-	-	-	-
HS-20-44	44.50	2.41	68.49	27.07
Impact	8.12	32.32	12.98	8.62
Total	87.02	5.52	113.96	13.28

A comparison between the results obtained from the FE model and the original plans is shown.

High percentages of difference were obtained for the truck loading values. The highest percentages of difference were 32.32% for the exterior support for the impact load and 27.07% for the interior support for the HS20-44 load. These differences contribute to the percentages of difference of 5.52% and 13.28% obtained for the total load for the exterior and interior support, respectively.

For the same reasons explained under the discussion of the Story County bridge analysis, truck loading conditions were altered to attempt to match the drawing plan values. One truck was

modeled instead of two, with an impact load applied on the lane load as well. This new load allocation can be seen in Figure 3.44, with only one truck instead of two in one of the exterior spans.

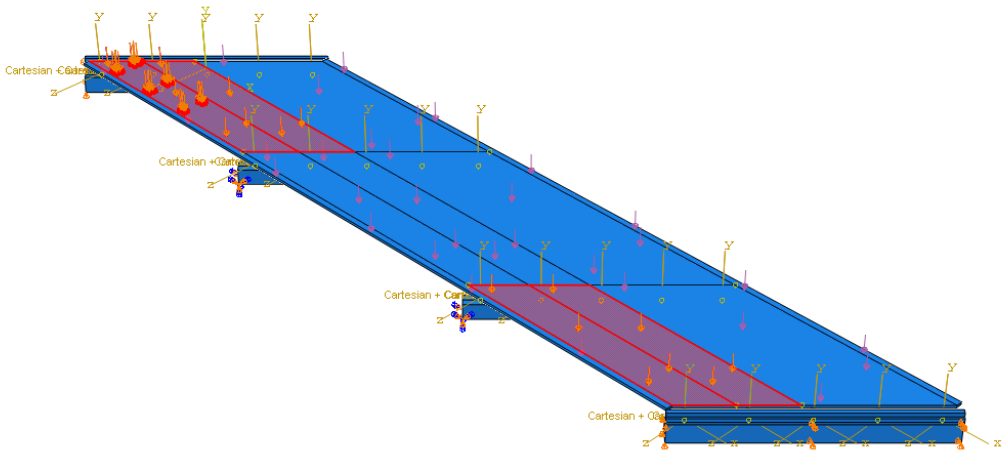

Figure 3.44. Marshall County bridge - updated load allocation for abutment reactions

The results for dead load and abutment reactions can be seen in Table 3.14.

Table 3.14. Marshall County bridge - dead load and updated live load abutment reactions

	Abutment Reactions (kips)			
	Ext	% diff	Int	% diff
DL #1	24.10	1.65	27.90	0.36
DL #2	10.30	3.01	4.60	2.22
ULL	-	-	-	-
CLL	-	-	-	-
HS-20-44	42.33	7.17	43.54	19.21
Impact	10.58	11.81	10.89	23.34
Total	87.31	5.20	86.93	13.59

A comparison between the results obtained from the updated FE model and the original plans is shown.

After the truck loading conditions were altered, the percentages of difference remained almost constant for the total abutment reaction of both the interior and exterior supports. The total load on the interior support decreased from 113.96 kips to 86.93 kips, yet the percentage of difference increased from 13.28 % to 13.59%. Under the previous loading conditions, the load was 13.28% higher than that of the original plan values, while under the altered truck loading conditions the load was 13.59% lower. The total load of the exterior support remained almost constant as well:

87.02 kips in the previous model and 87.31 kips in the altered truck loading model. The percentage of difference decreased from 5.52% to 5.20%.

The pier reactions will be discussed in the remainder of this section. The load in the model is shown in Figure 3.45 marked in red.

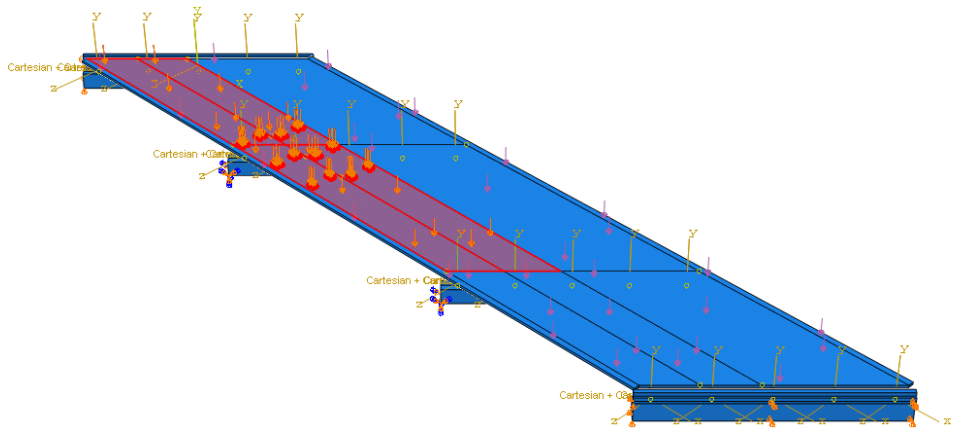

Figure 3.45. Marshall County bridge - load allocation for pier reactions

The lane load can be clearly seen in an exterior and middle span, with the rear axle of the concentrated truck load loaded over the pier. Two HS20-44 trucks were modeled side by side, with the one side of the truck axle 2 ft from the curb. The lane loads were modeled as two concurrent 10 ft wide pressure loads starting from the curb.

A deformation contour plot is provided in Figure 3.46.

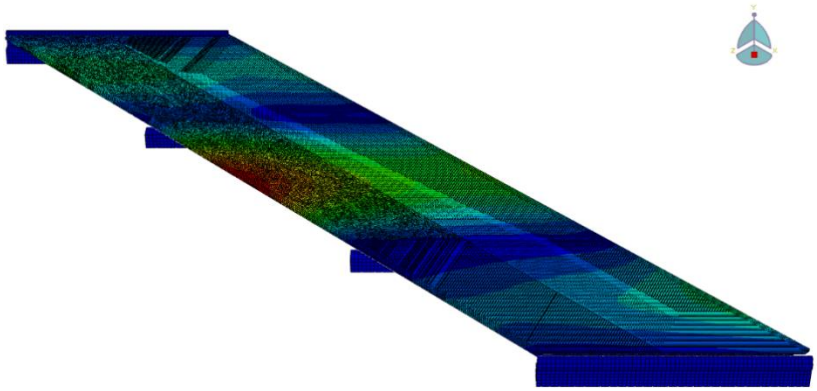

Figure 3.46. Marshall County bridge - deformation contour plot for pier reactions truck load

Maximum deformation is not prominent because much of the load is applied over a support.

The results for dead load and pier reactions can be seen in Table 3.15.

Table 3.15. Marshall County bridge - dead load and live load pier reactions

	Pier Reactions (kips)			
	Ext	% diff	Int	% diff
DL #1	86.96	3.48	101.42	0.56
DL #2	33.96	1.85	16.65	2.17
ULL	39.20	7.77	49.46	1.67
CLL	43.33	116.64	76.17	221.37
HS-20-44	-	-	-	-
Impact	10.83	31.45	19.04	1.82
Total	214.28	5.56	262.74	24.52

A comparison between the results obtained from the FE model and the original plans is shown.

High percentages of difference were obtained for the truck loading values. The highest percentage of difference was 221.37% for the interior support for the concentrated live load. This difference contributes to the percentage of difference of 24.52% obtained for the total load for the interior support. The exterior support also showed high percentages of difference, with 116.64% for the concentrated live load and 31.45% for the impact load. The total load, however, only amounted to a percentage of difference of 5.56%.

For the reasons explained above for the abutment reactions, the truck loading conditions in the FE model were altered to attempt to match the drawing plan values. One truck was modeled instead of two, with an impact load applied on the lane load as well. This new load allocation can be seen in Figure 3.47, with one truck instead of two in one of the exterior spans.

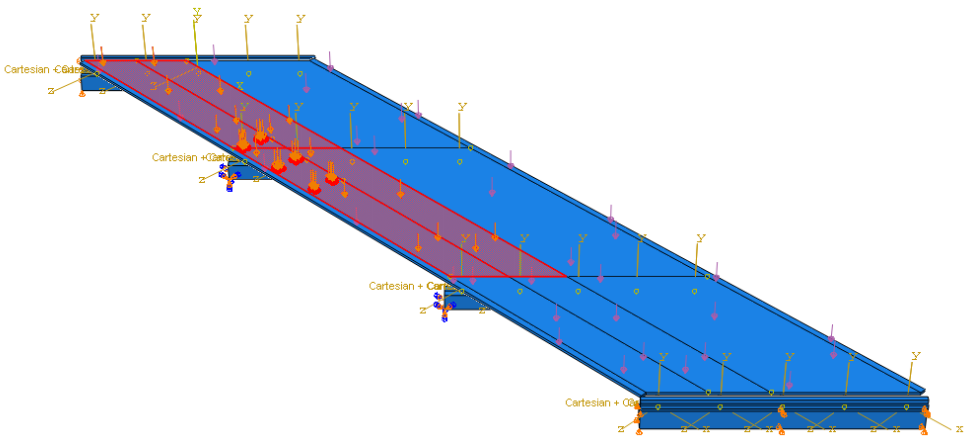

Figure 3.47. Marshall County bridge - updated load allocation for pier reactions

The results for dead load and pier reactions can be seen in Table 3.16.

Table 3.16. Marshall County bridge - Dead load and updated live load pier reactions

	Pier Reactions (kips)			
	Ext	% diff	Int	% diff
DL #1	87.04	3.39	101.22	0.76
DL #2	33.98	1.79	16.62	1.95
ULL	39.24	7.68	49.38	1.83
CLL	42.68	113.39	31.18	31.57
HS-20-44	-	-	-	-
Impact	20.48	29.61	20.14	7.70
Total	223.41	10.06	218.54	3.57

A comparison between the results obtained from the updated FE model and the original plans is shown.

The percentages of difference decreased in the interior support after the truck loading conditions were altered. The concentrated live load, which had a percentage of difference of 221.37% under the previous loading conditions, now resulted in a percentage of difference of 31.57%. The total load on the interior support decreased from 262.74 kips to 218.54 kips. The percentage of difference decreased from 24.52% to 3.57%. The total load decreased because the interior support is now taking only one side of the axle from the truck. Previously, the interior support took the same axle plus another axle.

The exterior support did not exhibit major differences from the previous loading conditions. The concentrated live load decreased from 43.33 kips to 42.68 kips, and the impact load increased from 10.83 kips to 20.48 kips. The percentage of difference for the total load on the exterior support actually increased from 5.56% to 10.06%. Less change would be expected for the exterior support because the exterior support was already taking the load of the same axle of the truck nearest to the curb.

3.2.3 Joint and Approach Slab Modeling

The Marshall County bridge model was updated with the deck over backwall concept described in Chapter 2. A 20 ft section was taken from the farthest abutment end in the longitudinal direction. Since the bridge is skewed 45°, the other end would span a total of 64 ft. The bridge deck was extended over the abutment interface while the top of the abutment was cut off.

Soil support was added as a C3D8R element, an eight-node linear brick element with reduced integration and hourglass control. Three soil support compositions were taken into consideration: loose, moderately stiff, and stiff. Soil properties for each one are shown in Chapter 2, Table 2.2. Pertinent results are shown for all three compositions in the following pages. A 12 ft void was modeled to be present in the direction away from the abutment backwall according to practices

suggested by the Iowa DOT Office of Bridges and Structures (2018a). A 2:1 slope was used for the horizontal to vertical distance of this void, as shown in Chapter 2, Figure 2.36.

A full-scale view of this model can be seen in Figure 3.48.

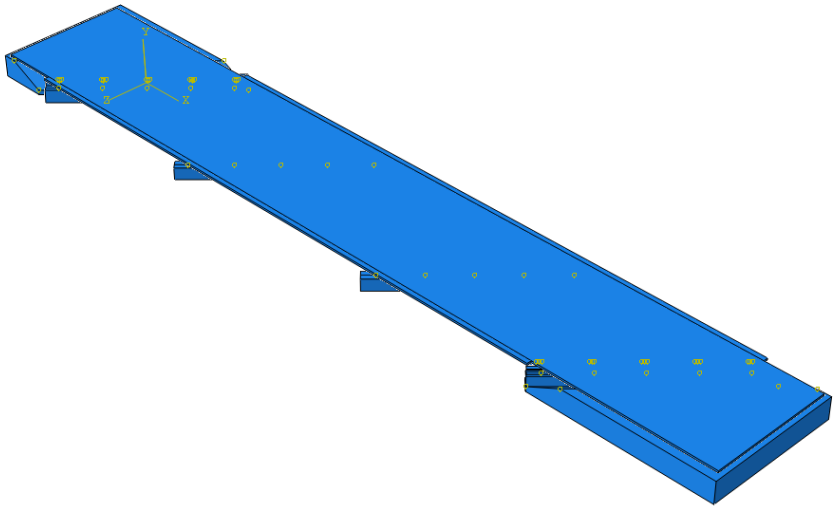

Figure 3.48. Full 3D FE model with approach slab

A section view of the abutment interface can be seen in Figure 3.49 and Figure 3.50.

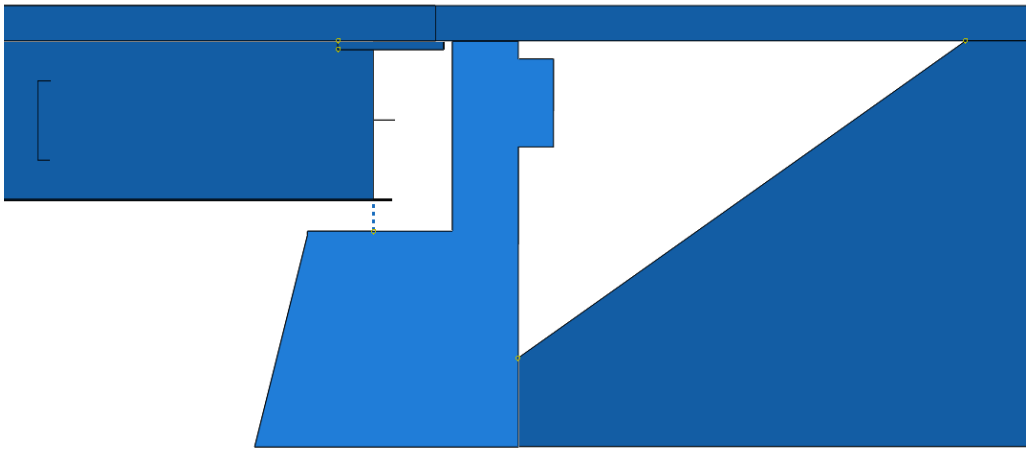

Figure 3.49. Section view without end span beam

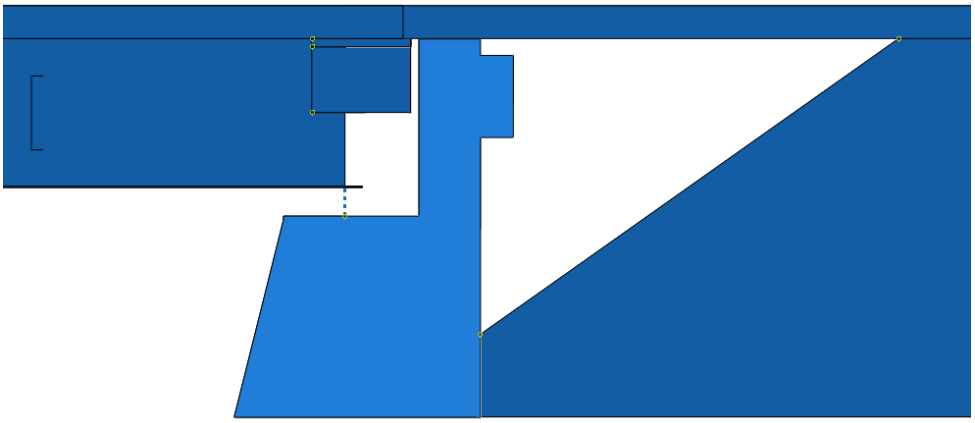

Figure 3.50. Section view with end span beam

In early developments of the detailing shown in Chapter 2, options included an end span beam that encased the diaphragms. While the Marshall County bridge does not have this end span beam, the effect of it on the various points of interest across the joint and approach slab can be demonstrated by its inclusion.

The webs of the girders were embedded into the curb and end span beam. The top flanges of the girders were also embedded into the curb. The end diaphragms were embedded into the end span beam. The tie constraints between the top flanges of all of the welded plate girders and the bottom face of the bridge deck were retained from the previous model. The top flanges of the end diaphragms were constrained with the bottom face of the curb. Tie constraints were also used between the bottom face of the bridge deck and the top face of the curb and between the bottom face of the curb and the top face of the end span beam.

Boundary conditions remained identical to those of the model detailed previously for the abutment and piers. New boundary conditions were assigned to the approach slab and soil. A vertical constraint was assigned at the far edge of the approach slab. Horizontal constraints were assigned to the vertical faces of the soil mass. Vertical constraints were assigned to the bottom face of the soil mass. An additional constraint in a third direction was assigned to the skewed face of the soil mass. These boundary conditions are shown in Figure 3.51 and Figure 3.52 marked in red.

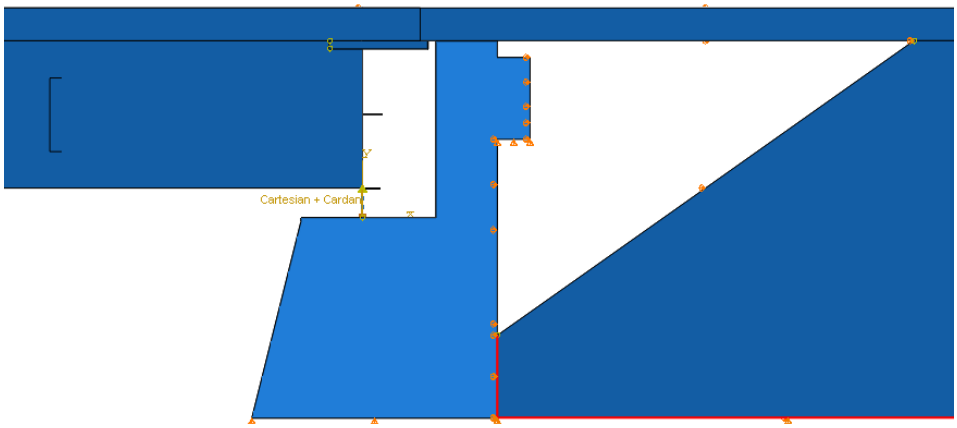

Figure 3.51. Boundary conditions section view

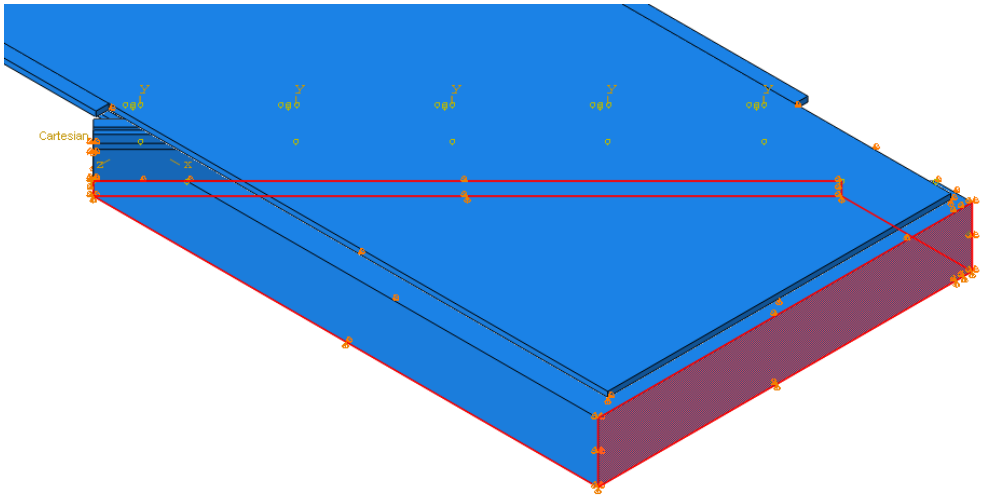

Figure 3.52. Boundary conditions 3D view

A contact interaction was provided between the bottom face of the bridge deck (approach slab) and the top face of the soil mass. This interaction is shown in Figure 3.53.

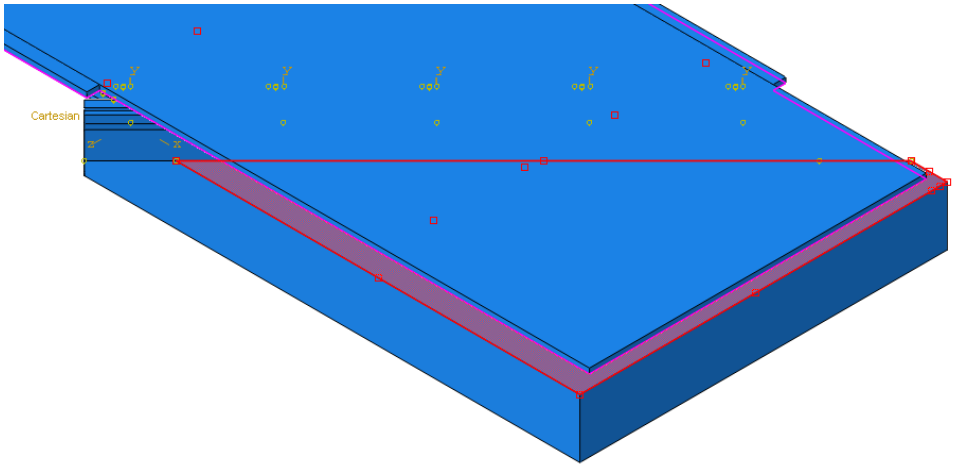

Figure 3.53. Contact interaction

In addition, connection wires were kept between the steel girders and the abutments/piers. All reaction values presented in the following pages correspond to these connection wires.

With this model, the impact of the deck over backwall concept on the existing structure can be predicted. Certain points of interest were identified as locations where the results of the model would be reported. First and foremost, the increase in bearing loads due to the new dead load of the bridge deck and support slab would be considered. Additional load would also be taken by the bearings due to live loads on the approach slab, which was previously not considered. Abutment reactions from the connection wires would be reported under various dead load and live load conditions in order to provide an analysis of the bearing loads. Additionally, deformation due to temperature loading, with the additional 20 ft of approach slab on one side and 64 ft on the other side, would also be considered. Deflection values at the abutment interface and at the midspan of the approach slab would also be reported. As reported here, midspan does not refer to exactly the midspan of the approach slab, but mainly the region between the abutment interface and the approach slab end support. Stress levels at the abutment interface and the midspan were also identified as points of interest. Both the top and bottom faces of the bridge deck (including the approach slab) would be considered.

The dead load reaction results from the FE model will be discussed first. Table 3.17 shows abutment reactions in kips for the two dead loads.

Table 3.17. Dead load abutment reactions (kips)

Support	No Beam		Beam	Approach Slab							
				No Soil		Soil					
						Loose		Moderately Stiff		Stiff	
	DL#1	DL#2	DL#1	DL#1	DL#2	DL#1	DL#2	DL#1	DL#2	DL#1	DL#2
Exterior	26.03	11.09	3.53	10.15	1.17	10.51	0.69	5.72	0.41	5.19	0.38
Interior	30.73	5.00	6.06	40.59	7.88	19.65	2.68	14.89	2.42	14.40	2.37
Interior	31.16	5.32	5.93	48.51	9.69	18.22	2.57	13.26	2.31	12.73	2.27
Interior	30.83	5.17	6.33	37.07	7.46	18.20	2.61	12.76	2.18	12.11	2.13
Exterior	27.82	10.70	3.33	7.53	1.04	8.30	1.13	7.80	1.06	7.71	1.06

The first two columns, corresponding to the dead loads with no end span beam, show the original dead loads that are being transferred to the bearings on each support. The columns show the values for DL#1 and DL#2 obtained previously. The remaining columns show the increase in dead load for each specific element. For example, when the bridge was modeled with the end span beam, 3.53 kips, 6.06 kips, 5.93 kips, 6.33 kips, and 3.33 kips were added to the DL#1 abutment reactions for the first exterior, first interior, second interior, third interior, and second exterior supports, respectively. Notice that only DL#1 is shown for the column with the end span beam section because adding this element does not affect DL#2. However, DL#2 is shown in all other columns because a larger area for the future wearing surface is provided by the top face of the approach slab.

When the approach slab was modeled with no soil support, the reactions showed the largest increase in dead load, which was expected since the bearings are taking most of the self-weight of the approach slab with only an edge support at the other end. The largest increase was seen at the middle interior support, with 48.51 kips and 9.69 kips for DL#1 and DL#2, respectively. As expected, when the soil support was modeled, these values decreased considerably. With each increase in the soil stiffness, the load taken by the bearings decreased, although the difference is minimal in some cases between a moderately stiff and a stiff soil. This relationship between the moderately stiff and stiff soil is consistent throughout the results presented in the following pages. This suggests that the truck load might not be large enough to deflect the slab and compress a moderately stiff or stiff soil to the degree that it would affect the support that the soil provides for the approach slab.

From top to bottom in Table 3.17, the first exterior reaction refers to the reaction closest to the 20 ft long section of the approach slab. Each subsequent reaction follows in the transverse direction until the remaining exterior reaction, which corresponds to the 64 ft long section of the approach slab.

Reactions for all possible combinations of dead load scenarios can be seen in Figure 3.54.

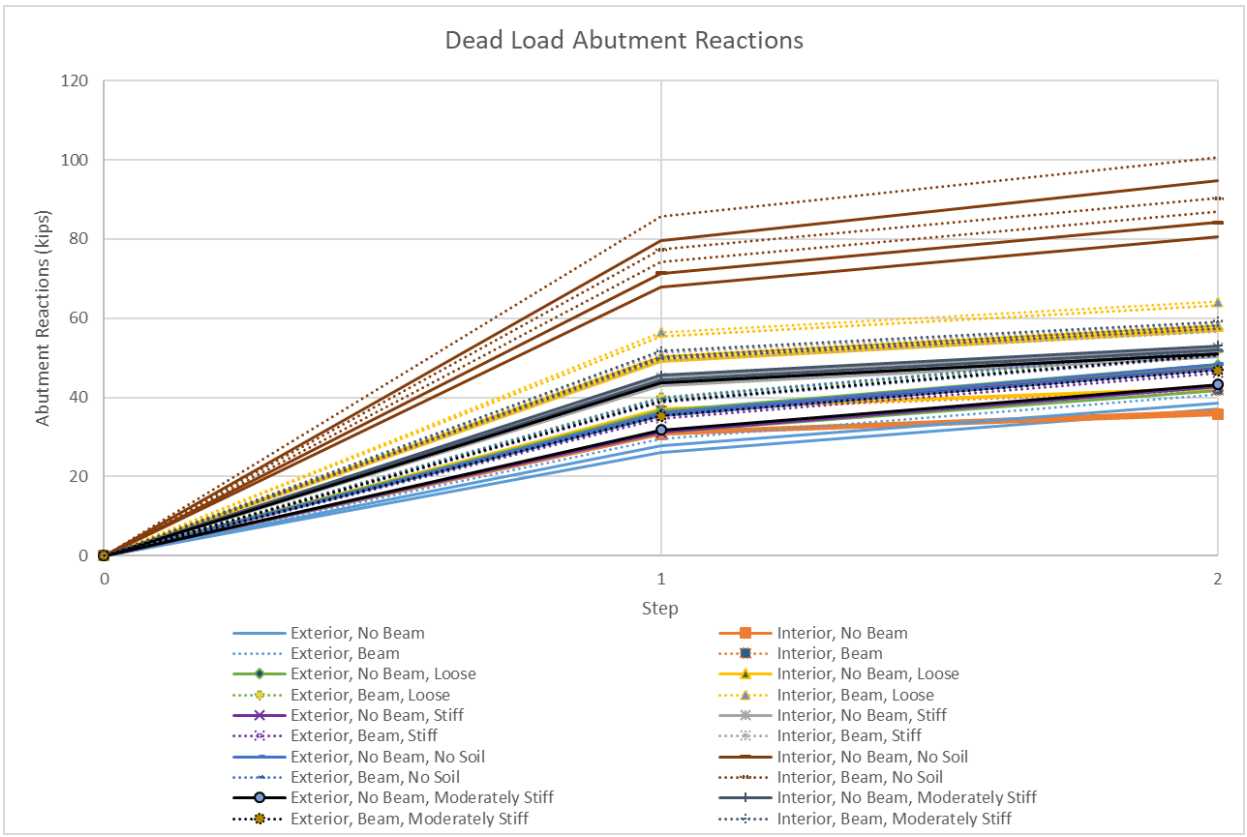

Figure 3.54. Dead load abutment reactions

The figure shows that most combinations would fall in a range of approximately 40 to 60 kips. Most of the lower values would correspond to exterior reactions while the higher values would correspond to interior reactions. The highest values, over 80 kips, correspond to scenarios with no support soil. The realistic values would fall within the 40- to 60-kip range mentioned above. Two steps can be seen in the horizontal axis, where each step corresponds to a different loading case. The first step corresponds to the combinations of DL#1, and the second step corresponds to the additional load from the combinations of DL#2.

Temperature loading was also included in this FE model. The results from the previous FE model can be seen in Figure 3.34. A maximum deformation of approximately 0.3 in. was obtained from that model. The results for the model with the approach slab are shown in Figure 3.55; a maximum deformation of approximately 0.46 in. was obtained.

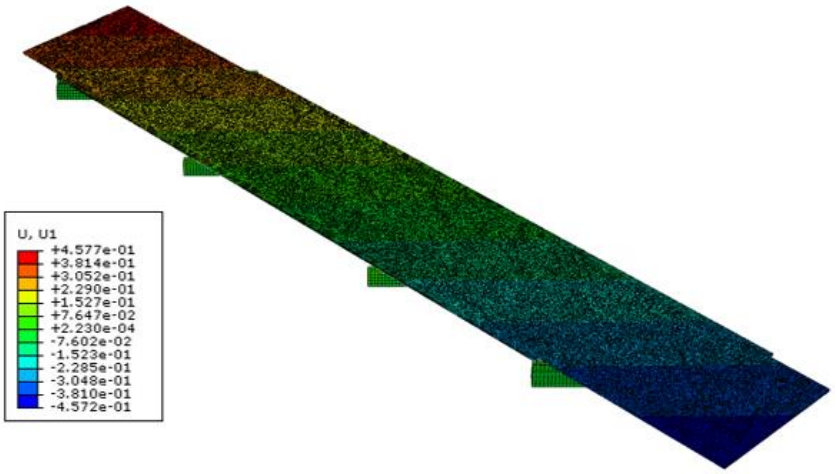

Figure 3.55. Deformation contour plot for temperature loading

This represents an increment of approximately 0.16 in. Comparing this value of 0.16 in. to the value obtained from equation (1), approximately 0.17 in., the FE result closely matches the one obtained from the equation. A percentage of difference of approximately 4% from the exact value is obtained using the result from the equation as the base value.

To study the additional bearing loads due to live loads in the approach slab, various live load configurations were modeled acting on the top face of the approach slab. Various live load configurations were modeled as various truck loading allocations. The different truck cases are detailed in Chapter 6, Figure 6.5, Figure 6.6, Figure 6.7, and Figure 6.8. In total, four cases were considered. Figure 3.56, Figure 3.57, Figure 3.58, and Figure 3.59 show the truck load allocations in the FE model for Case 1, Case 2, Case 3, and Case 4, respectively.

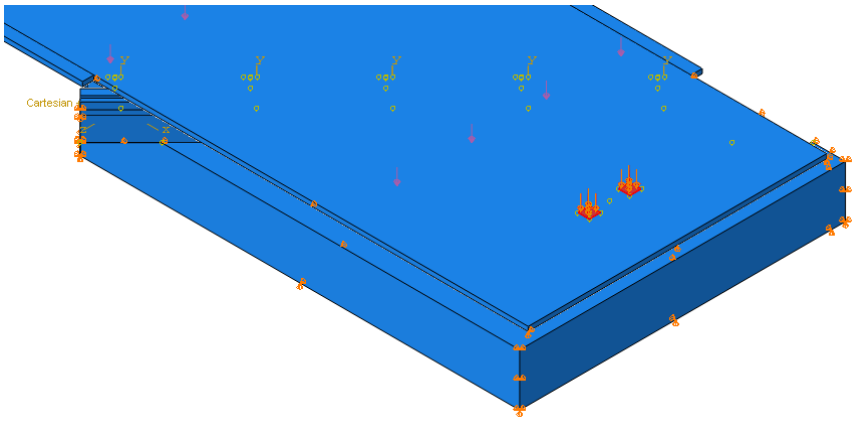

Figure 3.56. Case 1 - truck load allocation

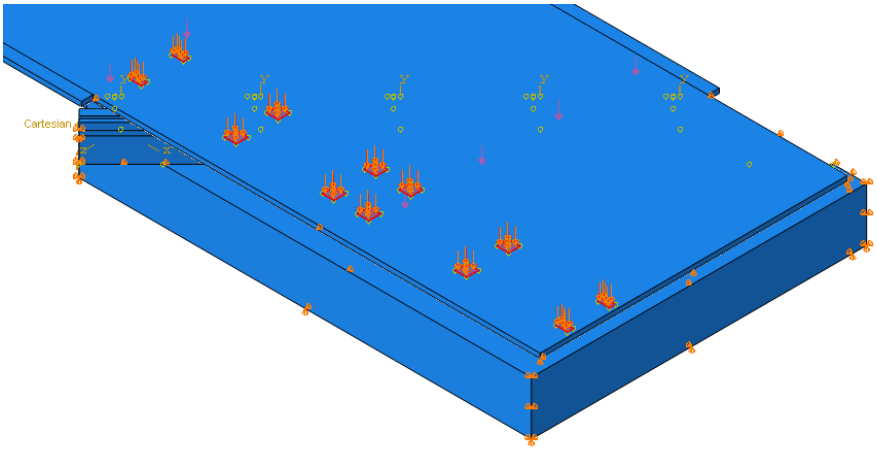

Figure 3.57. Case 2 - truck load allocation

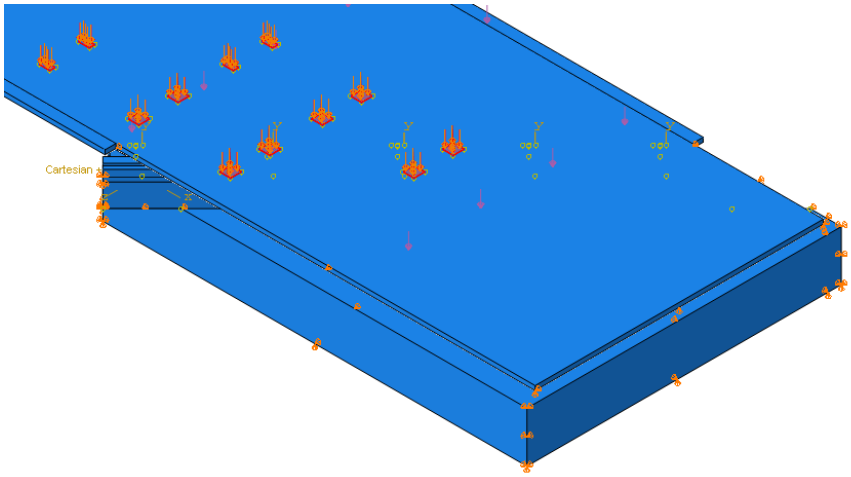

Figure 3.58. Case 3 - truck load allocation

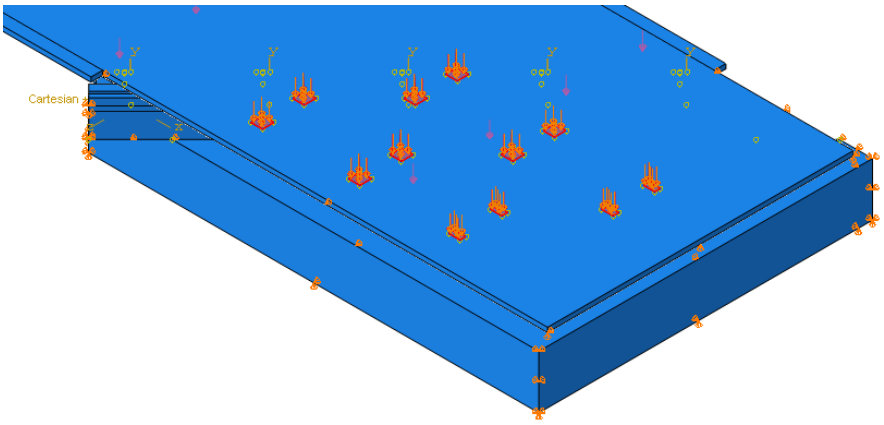

Figure 3.59. Case 4 - truck load allocation

The truck load allocations are marked in red in the four figures. Truck loading conditions were modeled as they were in Section 3.1.2.3, Figure 3.9 and Figure 3.10. Only the concentrated live load from the tires was considered in this investigation. However, the impact values can be calculated based on a fraction of the results obtained. This would apply not only for the live load reactions but also for the deflection and stress values.

The results for the live load abutment reactions in kips are shown in Table 3.18, Table 3.19, Table 3.20, and Table 3.21 for Case 1, Case 2, Case 3, and Case 4, respectively.

Table 3.18. Case 1 - live load abutment reactions (kips)

Support	No Beam				Beam			
	Soil			No Soil	Soil			No Soil
	Loose	Moderately Stiff	Stiff		Loose	Moderately Stiff	Stiff	
Exterior	-0.25	-0.13	-0.07	3.08	-0.26	-0.16	-0.09	4.33
Interior	-0.31	-0.12	-0.07	8.41	-0.30	-0.12	-0.07	7.45
Interior	-0.19	-0.01	-0.01	4.71	-0.20	-0.02	-0.01	4.74
Interior	-0.01	-0.01	0.00	1.41	-0.03	0.00	0.00	1.54
Exterior	0.00	0.00	0.00	-0.11	0.00	0.00	0.00	0.14

Table 3.19. Case 2 - live load abutment reactions (kips)

Support	No Beam				Beam			
	Soil			No Soil	Soil			No Soil
	Loose	Moderately Stiff	Stiff		Loose	Moderately Stiff	Stiff	
Exterior	-0.34	-0.01	0.00	-8.08	-0.80	-0.24	-0.20	-7.89
Interior	-2.07	-1.03	-0.87	15.03	-1.92	-1.22	-1.10	17.10
Interior	4.02	1.69	1.48	54.56	5.73	3.24	2.98	53.76
Interior	24.15	20.38	19.76	69.65	23.23	19.46	18.90	63.70
Exterior	7.02	6.41	6.24	8.30	8.97	7.93	7.72	14.32

Table 3.20. Case 3 - live load abutment reactions (kips)

Support	No Beam				Beam			
	Soil			No Soil	Soil			No Soil
	Loose	Moderately Stiff	Stiff		Loose	Moderately Stiff	Stiff	
Exterior	-1.55	-1.36	-1.31	-2.11	-1.82	-1.60	-1.56	-2.30
Interior	10.33	10.08	10.02	11.27	11.46	11.35	11.31	12.11
Interior	41.56	40.61	40.36	44.88	41.58	40.82	40.62	43.91
Interior	47.44	45.78	45.46	51.62	47.84	46.31	46.05	50.25
Exterior	24.20	23.65	23.53	24.67	26.41	25.72	25.59	26.84

Table 3.21. Case 4 - live load abutment reactions (kips)

Support	No Beam				Beam			
	Soil			No Soil	Soil			No Soil
	Loose	Moderately Stiff	Stiff		Loose	Moderately Stiff	Stiff	
Exterior	-2.28	-1.49	-1.36	-5.73	-2.51	-1.79	-1.67	-4.46
Interior	11.31	8.27	7.74	33.82	12.45	9.31	8.76	34.73
Interior	26.44	22.38	21.76	67.83	26.84	22.62	21.97	65.72
Interior	17.00	12.96	12.25	51.72	18.28	14.05	13.36	48.91
Exterior	1.17	0.47	0.33	2.58	2.54	1.30	1.09	6.97

Figure 3.60 shows a bar graph with all of the values compared.

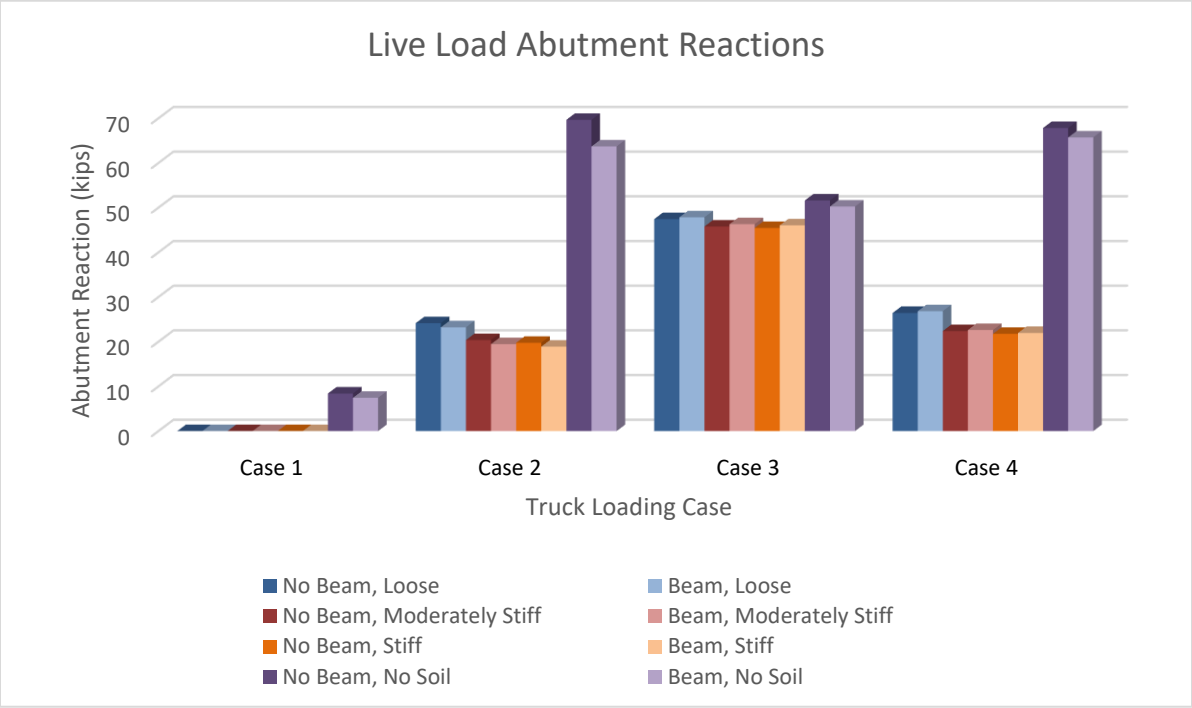

Figure 3.60. Live load abutment reactions

When modeled with soil support, Case 1 did not result in an increase in the live load abutment reaction of any support. This was because the load was being supported by the soil directly. In all other cases modeled with soil support, the live load abutment reaction increased noticeably for some of the supports. Case 3 showed the highest live load abutment reactions, with 47.84 kips and 26.41 kips for the third interior support and second exterior support, respectively. This was expected, since this truck allocation is the closest to the abutment interface. This case is similar to that of the controlling load case for the abutment reactions described in Section 3.2.2.3.1, Figure 3.37. It can clearly be seen how the live load reactions decrease as the soil stiffness increases. Additionally, no major difference is evident between the models with and without an end span beam. The largest difference was seen for Case 3 on the third interior support with no soil support, approximately 6 kips of difference. For the most part, values changed by less than 2 kips for cases with stiffer soil composition in comparison to those without soil support.

The results for the deflection values in inches are shown in Table 3.22, Table 3.23, Table 3.24, and Table 3.25 for Case 1, Case 2, Case 3, and Case 4, respectively.

Table 3.22. Case 1 - deflection values (in.)

Location	No Beam				Beam			
	Soil			No Soil	Soil			No Soil
	Loose	Moderately Stiff	Stiff		Loose	Moderately Stiff	Stiff	
Midspan	-0.28	-0.06	-0.04	-3.46	-0.28	-0.06	-0.04	-3.19
Abutment	-0.09	-0.03	-0.03	-0.27	-0.05	-0.02	-0.02	-0.17

Table 3.23. Case 2 - deflection values (in.)

Location	No Beam				Beam			
	Soil			No Soil	Soil			No Soil
	Loose	Moderately Stiff	Stiff		Loose	Moderately Stiff	Stiff	
Midspan	-0.32	-0.07	-0.06	-6.50	-0.32	-0.06	-0.04	-6.01
Abutment	-0.09	-0.04	-0.04	-0.51	-0.05	-0.03	-0.02	-0.31

Table 3.24. Case 3 - deflection values (in.)

Location	No Beam				Beam			
	Soil			No Soil	Soil			No Soil
	Loose	Moderately Stiff	Stiff		Loose	Moderately Stiff	Stiff	
Midspan	-0.21	-0.04	-0.03	-3.15	-0.21	-0.04	-0.03	-2.87
Abutment	-0.09	-0.05	-0.05	-0.28	-0.05	-0.03	-0.03	-0.17

Table 3.25. Case 4 - deflection values (in.)

Location	No Beam				Beam			
	Soil			No Soil	Soil			No Soil
	Loose	Moderately Stiff	Stiff		Loose	Moderately Stiff	Stiff	
Midspan	-0.28	-0.07	-0.06	-5.32	-0.28	-0.06	-0.05	-4.85
Abutment	-0.09	-0.05	-0.05	-0.51	-0.06	-0.03	-0.03	-0.31

Figure 3.61, Figure 3.62, Figure 3.63, and Figure 3.64 show bar graphs with all of the values compared.

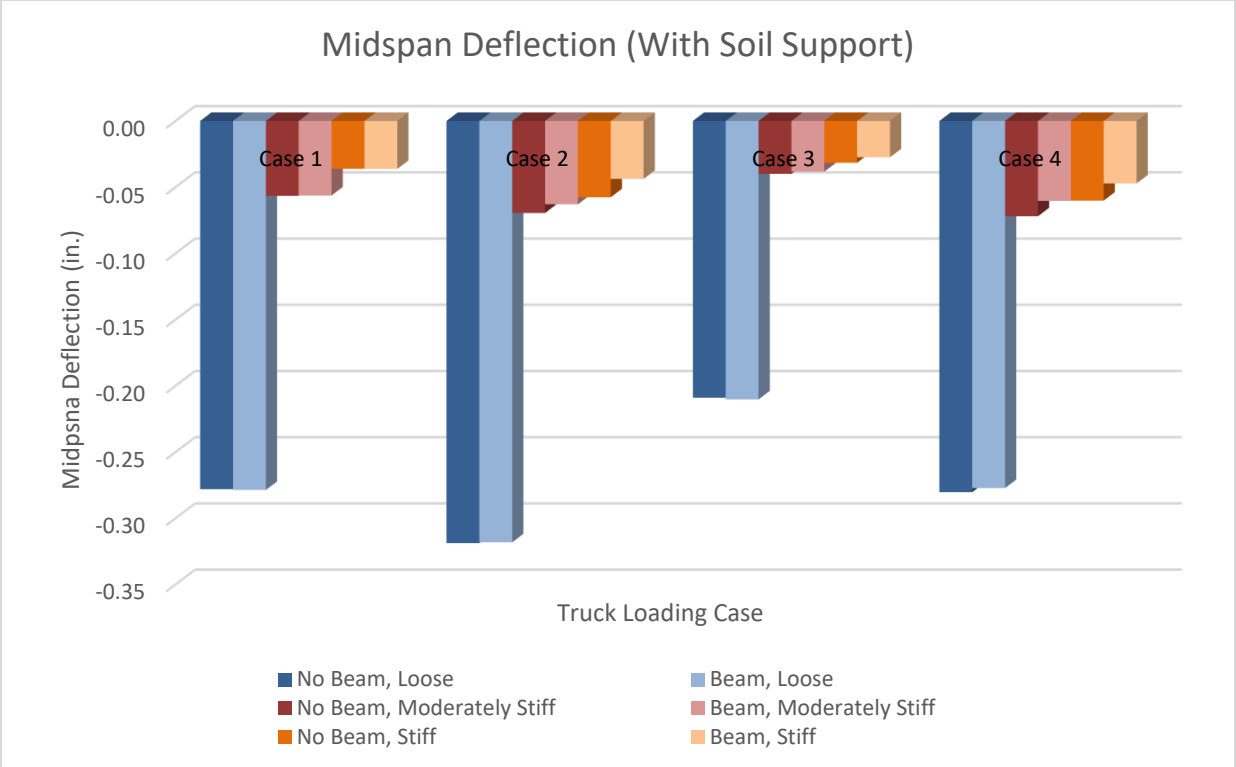

Figure 3.61. Midspan deflection values with soil support

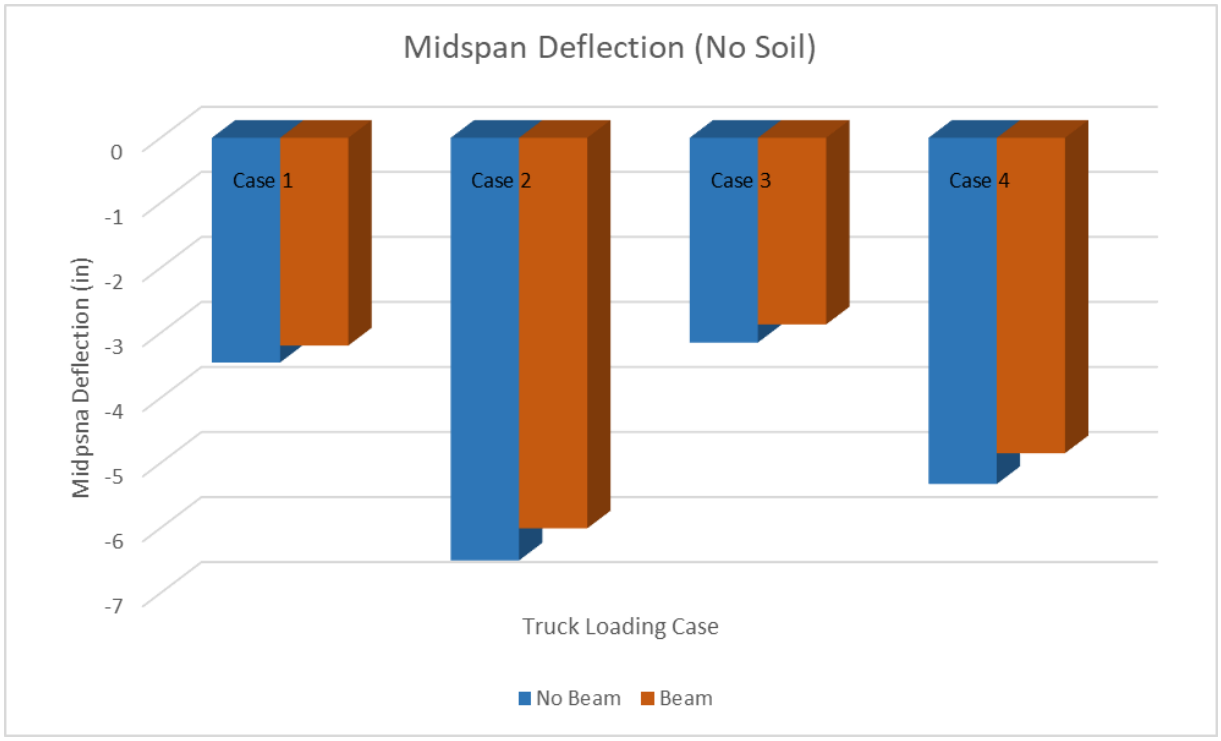

Figure 3.62. Midspan deflection values without soil support

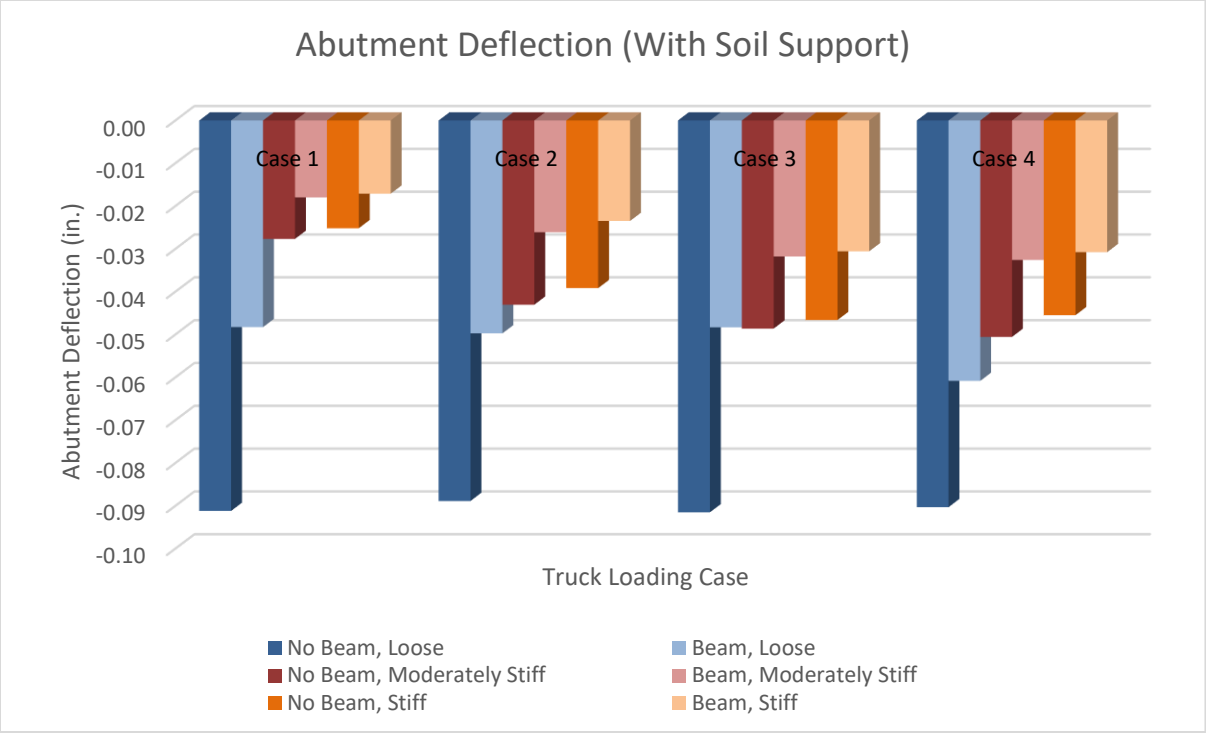

Figure 3.63. Abutment deflection values with soil support

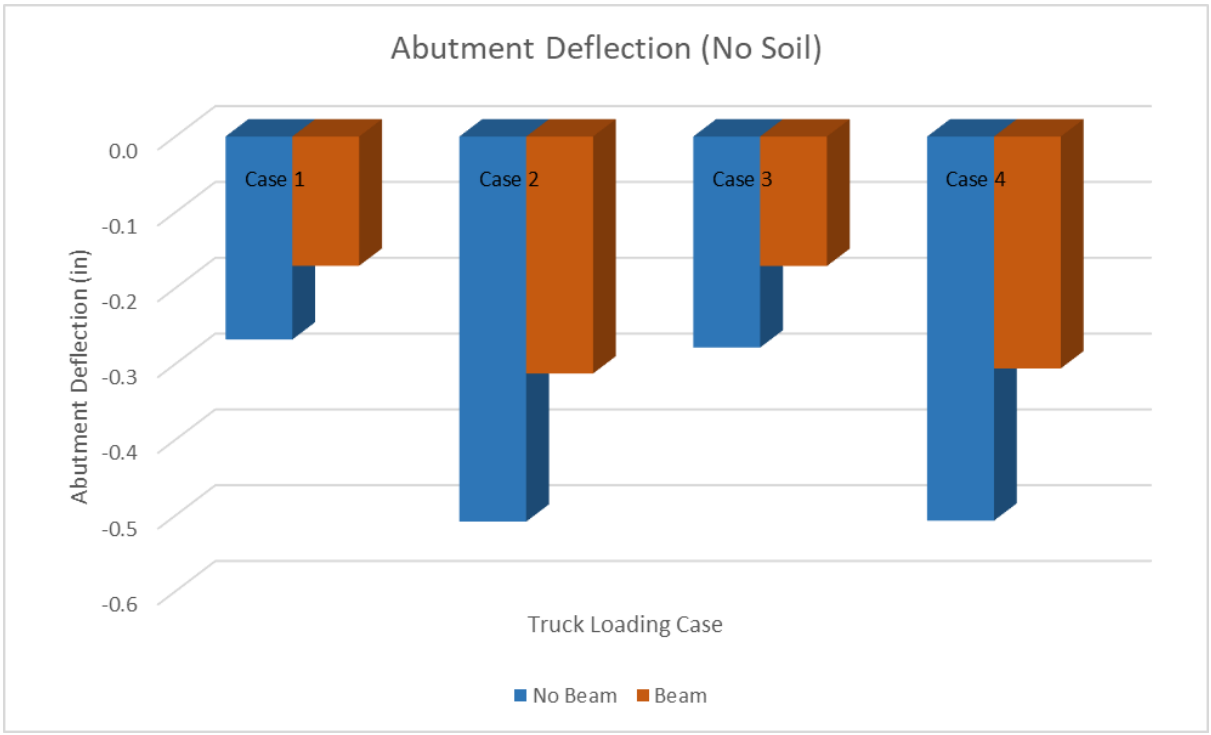

Figure 3.64. Abutment deflection values without soil support

Similar behavior was observed across all values obtained for deflection at the abutment interface and at the midspan of the approach slab. The highest midspan deflection for loose soil was obtained for Case 2, with a value of 0.32 in. For moderately stiff and stiff soil, the highest values decreased to 0.07 in. and 0.06 in., respectively. As for the abutment interface deflection, the highest value for loose soil was 0.09 in. across all truck loading cases. Values differed by anywhere from 0.03 in. to 0.05 in. when the abutment interface deflection was modeled with moderately stiff and stiff soil.

Models with no soil support resulted in values 10 and 20 times greater than the values from the loose soil models and in some cases 100 times greater than the values from the moderately stiff and stiff soil models. Models with an end span beam resulted in equal or lower deflection values at both the abutment interface and midspan of the approach slab in comparison to models without an end span beam. However, the difference between having an end span beam and not is minimal for values obtained at the midspan of the approach slab, where only 4 of the 24 results for midspan deflections changed when various soil compositions were modeled. The end span beam was found to have an effect on the deflection values in the abutment interface, however. Some values decreased by 40% when the end span beam was modeled. For example, the deflection at the abutment interface for all truck loading cases with the exception of Case 4 decreased from 0.09 in. to 0.05 in.

Given these values, the 2 in. grout pad in the Iowa DOT joint discussed in Chapter 1, Figures 1.3 and 1.4, between the approach slab and the top face of the abutment is more than enough to confidently implement the deck over backwall concept. The abutment was not designed to support the excess dead load and live load that comes with this design. Ideally, a 2 in. grout pad would prevent most of the dead and live load and stress levels to be transferred from the deck/approach slab to the backwall.

The results for stress levels in psi are shown in Table 3.26, Table 3.27, Table 3.28, and Table 3.29 for Case 1, Case 2, Case 3, and Case 4, respectively.

Table 3.26. Case 1 - stress values (psi)

Location		No Beam				Beam			
		Soil			No Soil	Soil			No Soil
		Loose	Moderately Stiff	Stiff		Loose	Moderately Stiff	Stiff	
Midspan	Top	285.4	132.7	132.5	1125.0	289.9	157.4	158.8	1047.0
	Bottom	332.5	176.7	176.6	1125.0	361.5	157.4	158.8	1047.0
Abutment	Top	568.1	396.7	397.0	1499.0	433.0	392.9	317.3	1569.0
	Bottom	473.8	308.7	308.8	1499.0	433.0	314.4	317.3	1569.0

Table 3.27. Case 2 - stress values (psi)

Location		No Beam				Beam			
		Soil			No Soil	Soil			No Soil
		Loose	Moderately Stiff	Stiff		Loose	Moderately Stiff	Stiff	
Midspan	Top	245.9	132.7	132.5	1706.0	227.5	169.6	172.1	1507.0
	Bottom	245.9	176.6	132.5	1706.0	302.1	169.6	172.1	1507.0
Abutment	Top	586.4	484.5	440.9	2680.0	600.7	423.4	429.8	3013.0
	Bottom	586.4	440.5	440.9	2923.0	675.4	423.4	429.8	3013.0

Table 3.28. Case 3 - stress values (psi)

Location		No Beam				Beam			
		Soil			No Soil	Soil			No Soil
		Loose	Moderately Stiff	Stiff		Loose	Moderately Stiff	Stiff	
Midspan	Top	222.4	78.5	79.0	810.1	236.9	126.5	127.4	704.2
	Bottom	222.4	78.5	79.0	810.1	236.9	126.5	127.4	704.2
Abutment	Top	589.9	469.8	473.2	1617.0	588.7	504.7	508.8	1687.0
	Bottom	589.9	469.8	473.2	1617.0	588.7	504.7	508.8	1687.0

Table 3.29. Case 4 - stress values (psi)

Location		No Beam				Beam			
		Soil			No Soil	Soil			No Soil
		Loose	Moderately Stiff	Stiff		Loose	Moderately Stiff	Stiff	
Midspan	Top	254.9	176.9	176.8	1301.0	292.2	238.5	240.7	1129.0
	Bottom	305.3	176.9	176.8	1301.0	292.2	238.5	240.7	1129.0
Abutment	Top	607.8	441.1	397.3	2382.0	652.9	397.2	401.0	2481.0
	Bottom	607.8	397.0	397.3	2599.0	652.9	476.5	401.0	2706.0

Figure 3.65, Figure 3.66, Figure 3.67, Figure 3.68, Figure 3.69, Figure 3.70, Figure 3.71, and Figure 3.72 show bar graphs with all of the values compared. The values shown correspond to the von Mises stress levels on the various points of interest across the joint and approach slab.

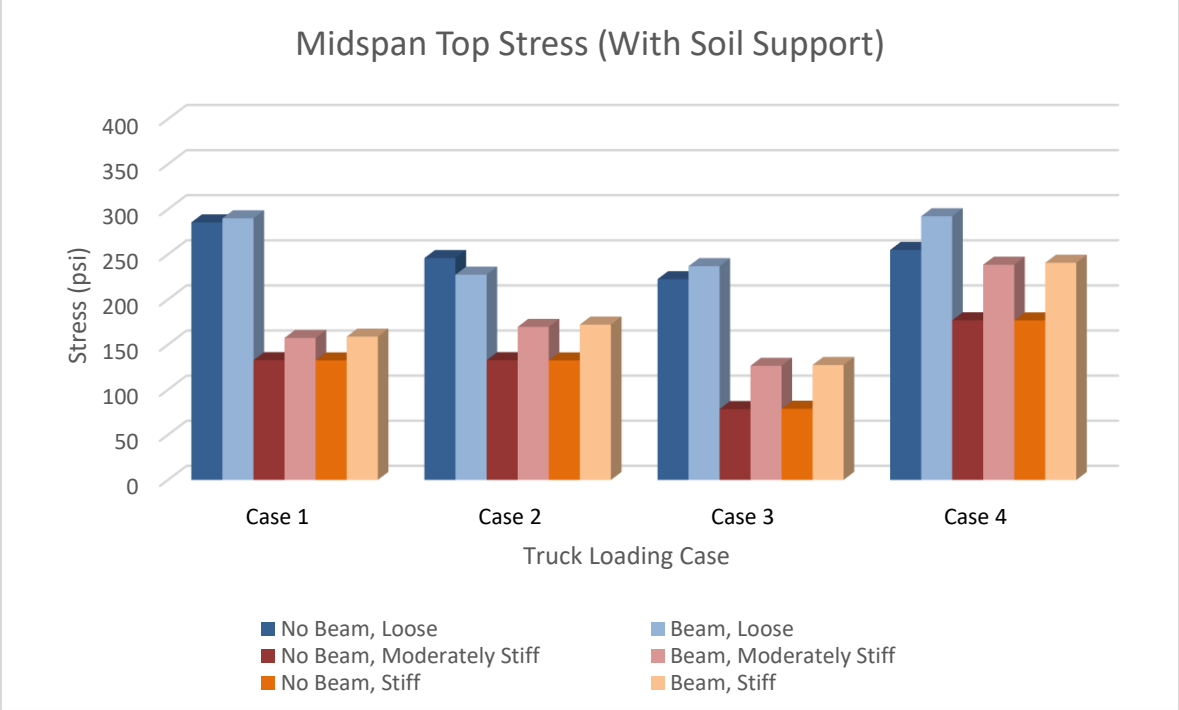

Figure 3.65. Midspan top stress values with soil support

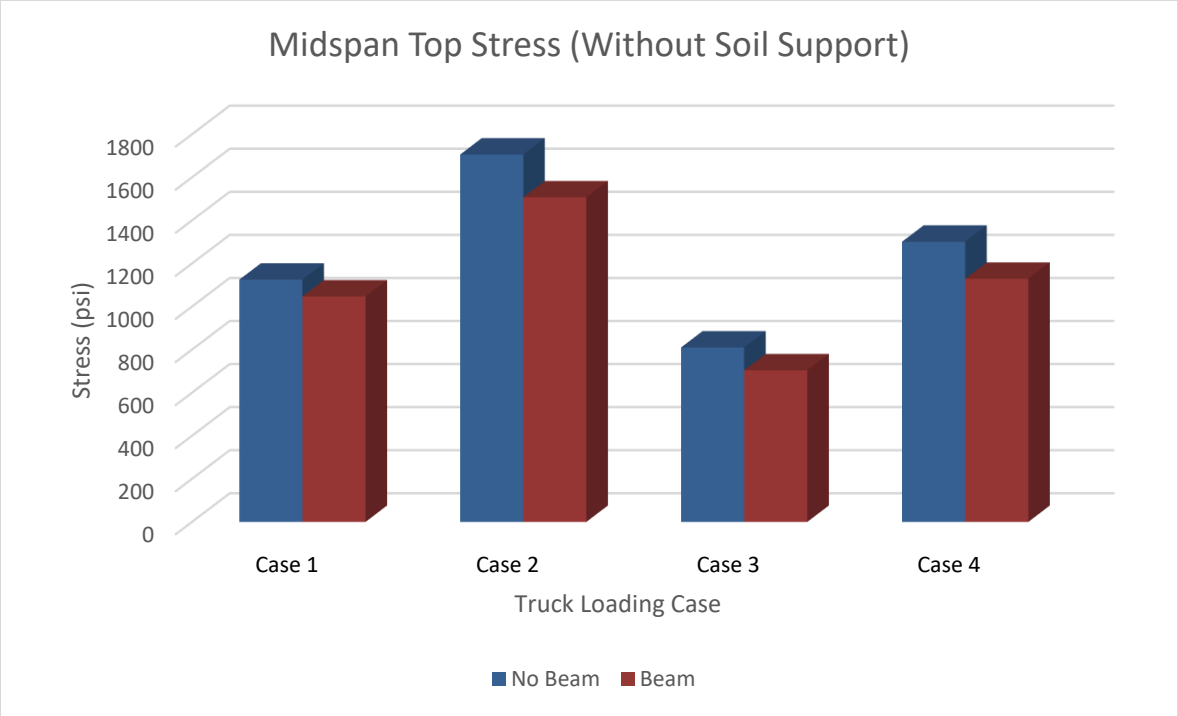

Figure 3.66. Midspan top stress values without soil support

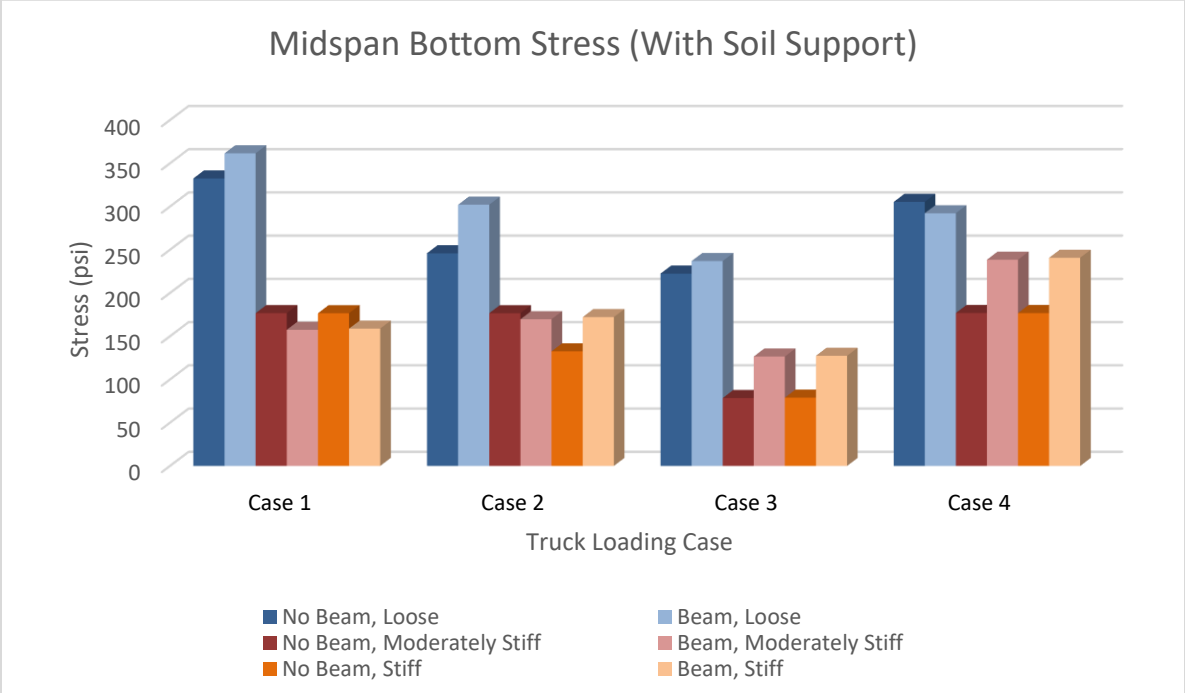

Figure 3.67. Midspan bottom stress values with soil support

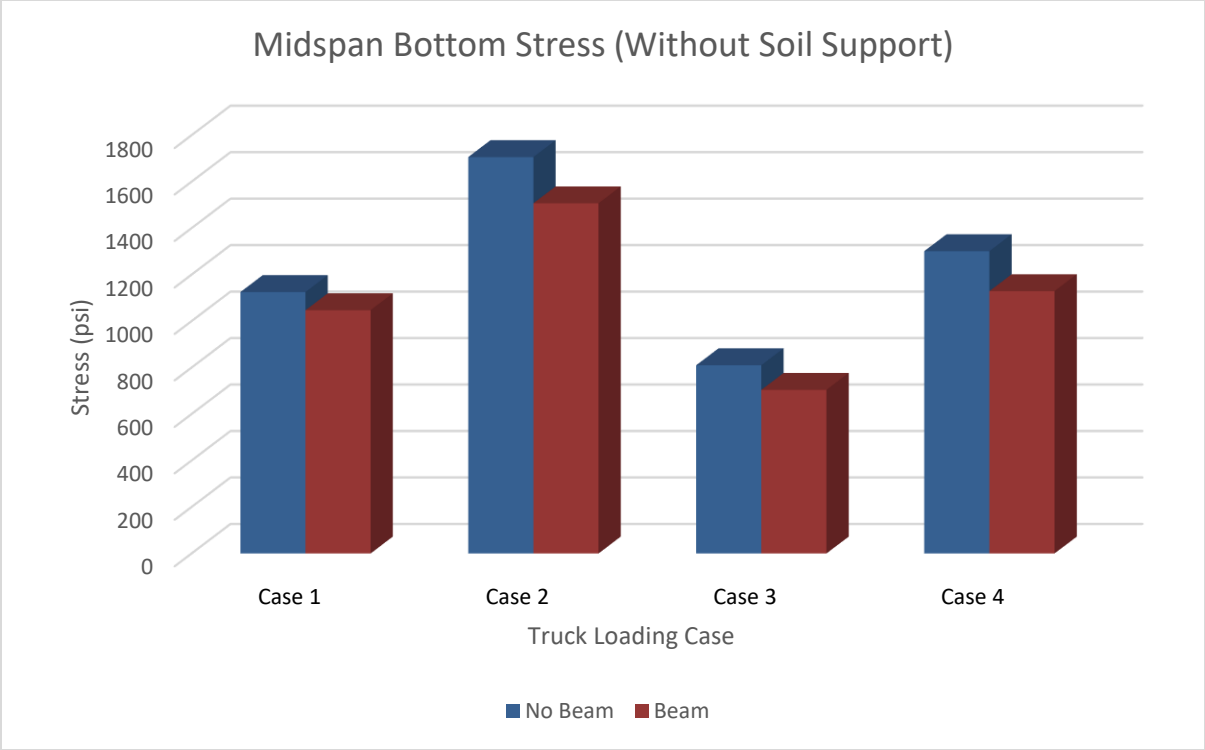

Figure 3.68. Midspan bottom stress values without soil support

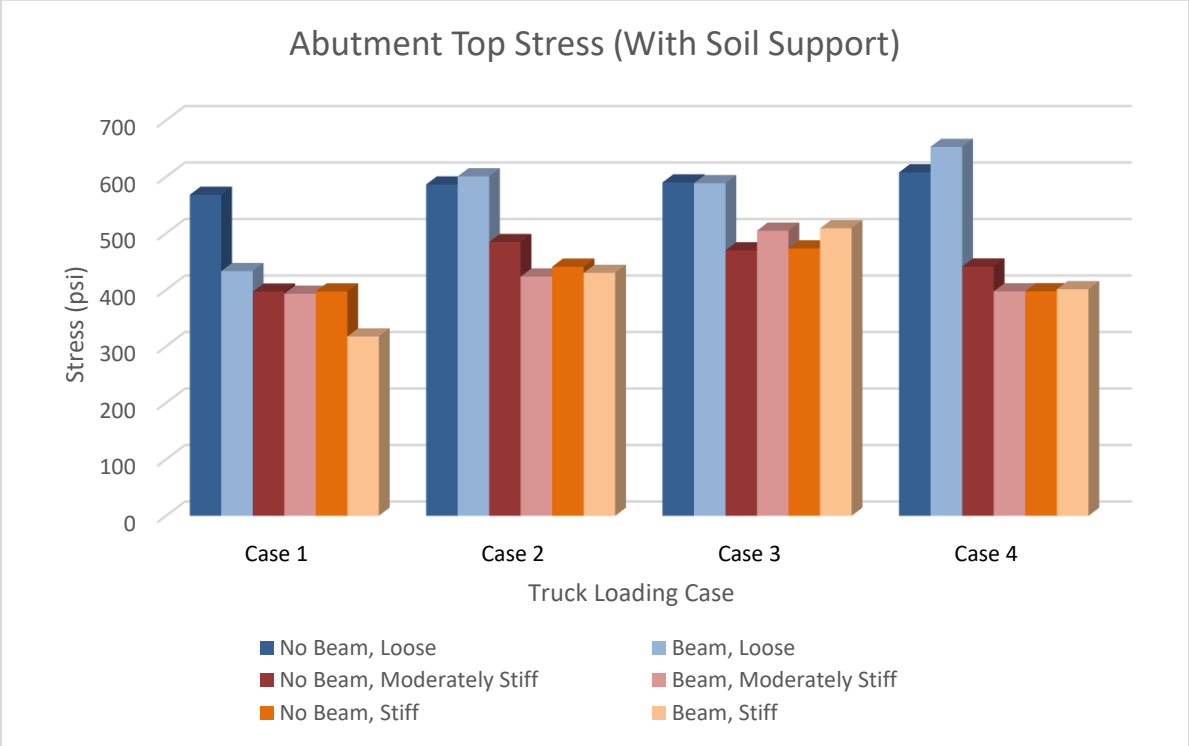

Figure 3.69. Abutment top stress values with soil support

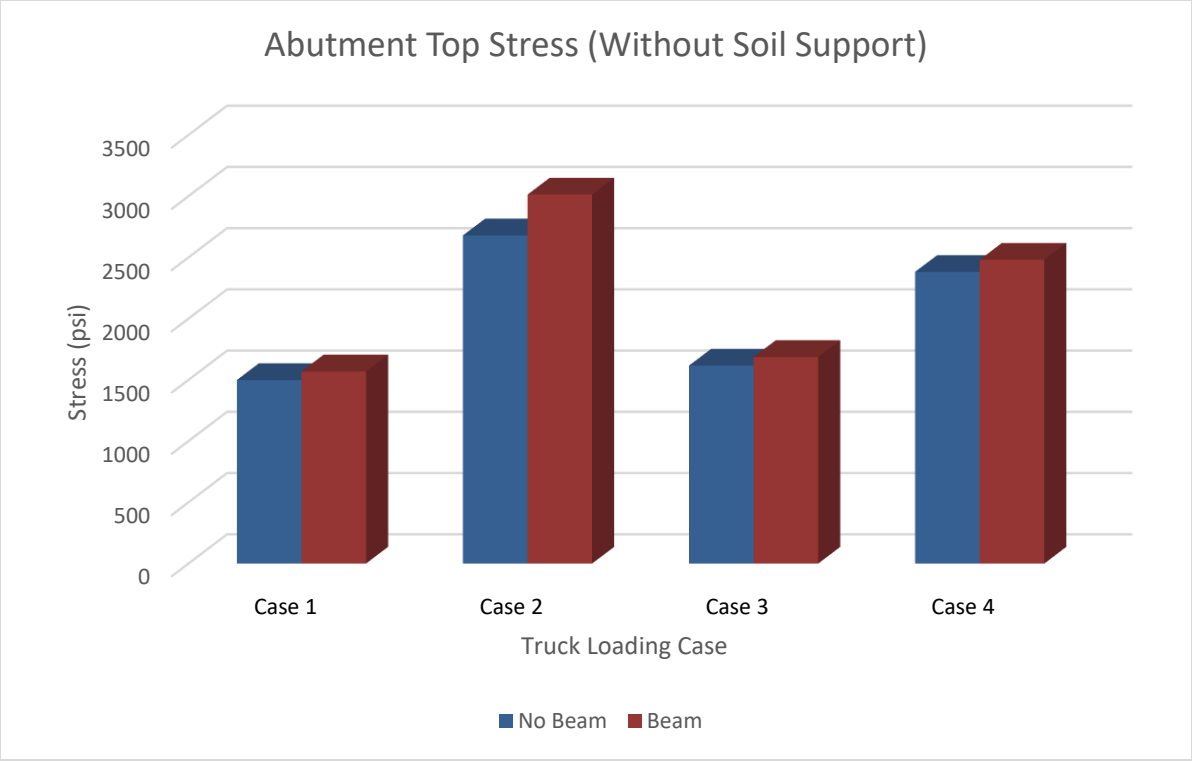

Figure 3.70. Abutment top stress values without soil support

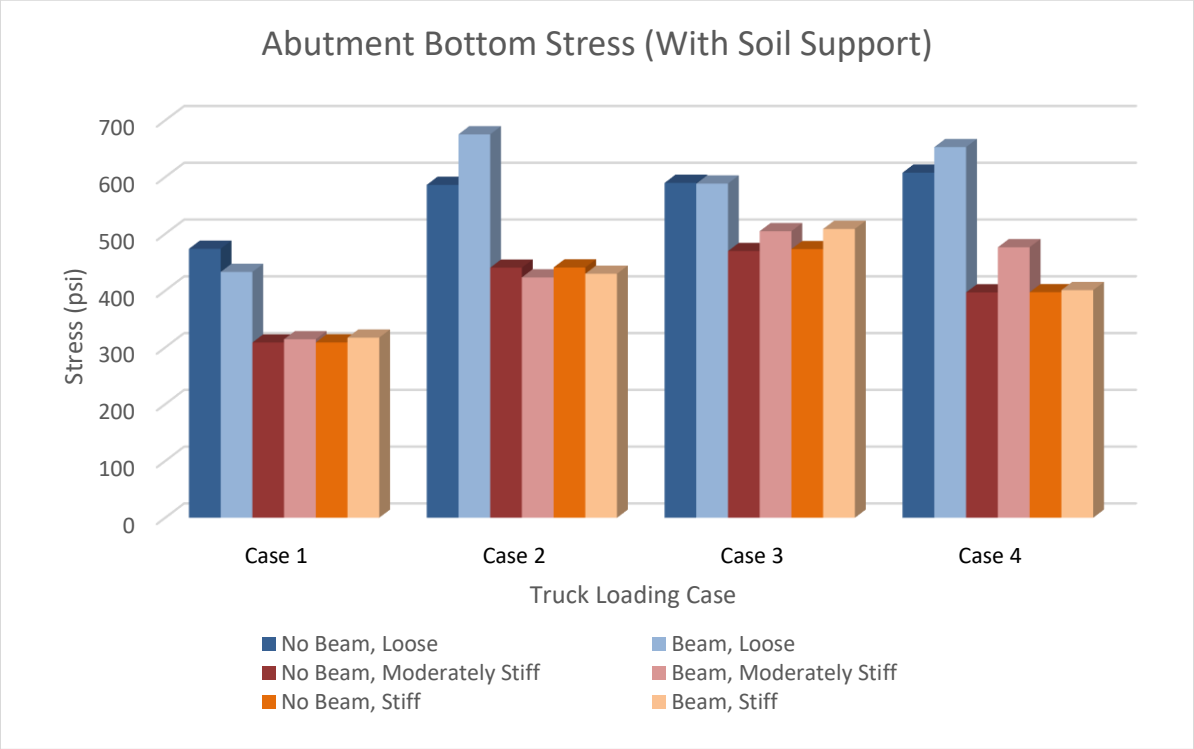

Figure 3.71. Abutment bottom stress values with soil support

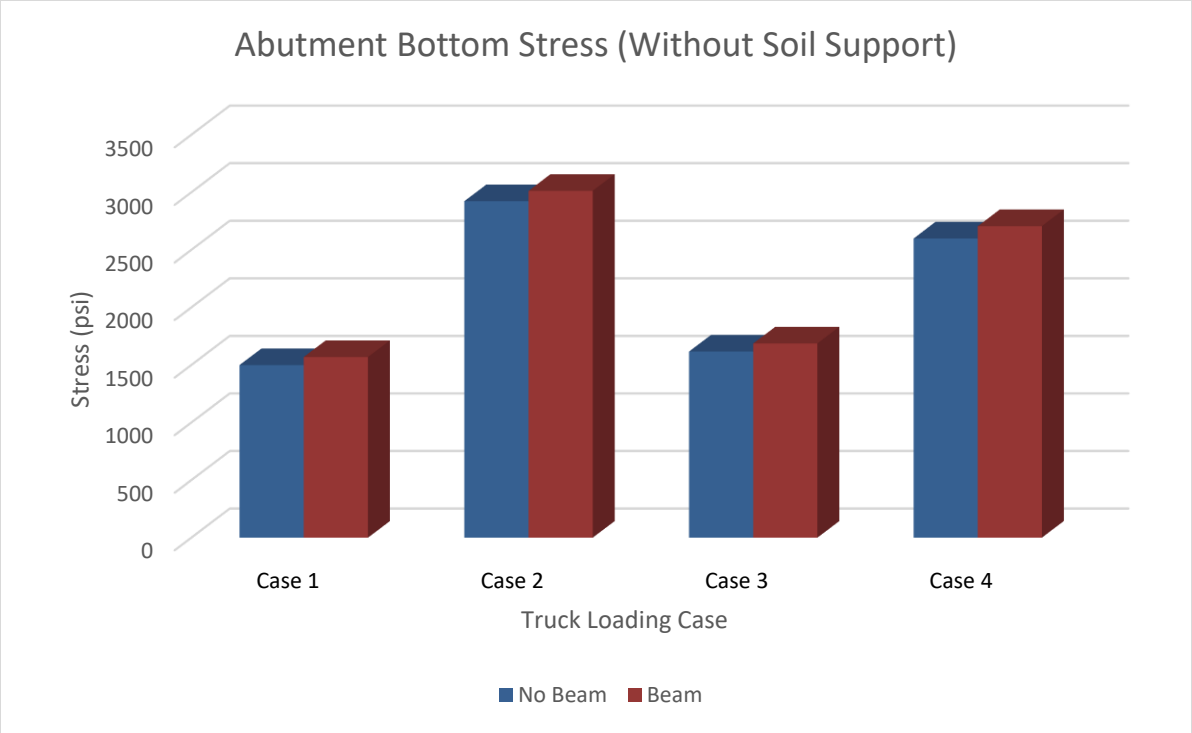

Figure 3.72. Abutment bottom stress values without soil support

Additional differences can be seen in the results for the stress levels in comparison to the deflection results detailed above. The stress values are rounded to the nearest 10 psi throughout the discussion.

The highest midspan stress at the top face of the approach slab for models with loose soil was obtained for Case 4; a value of 290 psi was obtained for models with an end span beam. For models without an end span beam, Case 1 controlled with 290 psi as well. With moderately stiff and stiff soils, the values decreased to 240 psi and 130 psi, respectively. However, Case 1 no longer controlled for models without an end span beam with moderately stiff soils. Instead, Case 4 controlled with a stress value of 180 psi.

The highest midspan stress at the bottom face of the approach slab for models with loose soil was obtained for Case 1; a value of 360 psi was obtained for models with an end span beam. For models without an end span beam, Case 1 also controlled with 330 psi. Moderately stiff and stiff soils had lower values of 160 psi and 180 psi, respectively. Again, Case 4 controlled for models without an end span beam with moderately stiff soil; a stress value of 180 psi was obtained as well.

A similar analysis was conducted for the abutment interface stress levels. The highest stress at the top face of the approach slab for models with loose soil was obtained for Case 4; a value of 650 psi was obtained for models with an end span beam. For models without an end span beam, Case 4 also controlled with 600 psi. As the soil changed from moderately stiff to stiff, the values decreased to 400 psi and 440 psi, respectively. However, Case 4 no longer controlled for both

models with moderately stiff soils. Instead, Case 3 controlled for models with an end span beam and Case 2 controlled for models without that element. The stress values were 500 psi and 480 psi, respectively.

The highest abutment interface stress at the bottom face of the approach slab for models with loose soil was obtained for Case 2; a value of 680 psi was obtained for models with an end span beam. For models without an end span beam, Case 4 controlled as well with 610 psi. As the soil changed from moderately stiff to stiff, the values decreased to 420 psi and 400 psi, respectively. However, Case 3 controlled for models with and without an end span beam with moderately stiff soil. The stress values were 500 psi and 470 psi, respectively, for moderately stiff and stiff soils.

Models with no soil support resulted in values five or six times greater than those for the loose, moderately stiff, and stiff soil models. The midspan stresses did not change from the top face to the bottom face of the approach slab for models without soil support. This can be seen in the fact that Figure 3.66 and Figure 3.68 are exactly the same bar graph. However, the abutment interface stresses showed more variance than the midspan stresses from the top face to the bottom face of the approach slab for models without soil support. As can be seen, Figure 3.70 and Figure 3.72 are not exactly the same, though they are very similar, only differing for Case 2 and Case 4.

While in most cases models with an end span beam resulted in slightly higher values in comparison to models without an end span beam, a direct correlation could not be established in a manner similar to that for the deflection values presented above. The increase or decrease in stress levels was not a constant value and varied over the different truck loading cases and the different soil compositions.

3.2.4 Parametric Study of Skew Angle

The Marshall County bridge model was used to study the effects of various bridge skew angles on various points of interest across the joint and approach slab. To supplement the values obtained above for the Marshall County bridge model with a skew angle of 45°, the model was altered to match skew angles of 30° and 60°; additionally, a non-skewed version of the model was developed. The previously discussed modeling procedures were followed in terms of material properties, element types, constraints, and boundary conditions. In discussions with the Iowa DOT, the decision was made that models with a loose soil composition produced results that were too conservative, while models with moderately stiff and stiff soils produced results that were similar to each other. For these reasons, one soil composition was used throughout this parametric study: moderately stiff. A plan view of each model is shown in Figure 3.73, Figure 3.74, and Figure 3.75 for the non-skewed, 30°, and 60° models, respectively. The plan view for the 45° skew model, the original Marshall County bridge model, is shown above in Figure 3.28.

Figure 3.73. Parametric study - non-skewed model

Figure 3.74. Parametric study - 30° skew model

Figure 3.75. Parametric study - 60° skew model

In this parametric study, certain points of interest were compared between the models. These were identified as the dead load abutment reactions and temperature deformation of the bridges with and without the approach slab, the live load abutment reactions due to various truck loading cases, and the deflection values and stress levels at the abutment interface and in the midspan of the approach slab. Both the top and bottom faces of the bridge deck (approach slab) were examined.

The dead load reaction results from the FE models will be discussed first. Table 3.30 shows the dead load abutment reactions in kips for the various skew angles.

Table 3.30. Parametric study - dead load abutment reactions (kips)

Support	No Skew		30		45		60	
	DL#1	DL#2	DL#1	DL#2	DL#1	DL#2	DL#1	DL#2
Exterior	25.65	10.57	26.12	10.64	27.82	10.70	28.06	10.13
Interior	30.13	5.06	30.22	5.11	30.83	5.17	30.86	5.08
Interior	30.31	5.16	30.46	5.18	31.16	5.32	29.77	5.08
Interior	30.13	5.06	30.24	5.03	30.73	5.00	29.98	5.01
Exterior	25.65	10.57	25.39	10.87	26.03	11.09	25.22	11.45

The columns show the values for DL#1 and DL#2 obtained previously.

Table 3.31 and Table 3.32 show the increase in dead load in the corresponding support due to the addition of the approach slab for models with and without soil support, respectively.

Table 3.31. Parametric study - dead load abutment reactions without soil support (kips)

Support	No Skew		30		45		60	
	DL#1	DL#2	DL#1	DL#2	DL#1	DL#2	DL#1	DL#2
Exterior	8.57	1.77	13.84	2.75	7.53	1.04	9.96	1.83
Interior	14.40	2.81	30.06	5.98	37.07	7.46	57.61	11.53
Interior	13.92	2.72	28.00	5.57	48.51	9.69	86.70	17.32
Interior	14.38	2.80	25.82	5.04	40.59	7.88	100.60	19.81
Exterior	8.58	1.77	8.83	1.75	10.15	1.17	-0.62	-0.58

Table 3.32. Parametric study - dead load abutment reactions with soil support (kips)

Support	No Skew		30		45		60	
	DL#1	DL#2	DL#1	DL#2	DL#1	DL#2	DL#1	DL#2
Exterior	6.70	1.30	6.87	1.19	7.80	1.06	8.50	1.27
Interior	11.41	1.93	11.18	2.00	12.76	2.18	16.66	2.75
Interior	11.02	1.88	11.36	2.07	13.26	2.31	17.37	2.94
Interior	11.40	1.93	12.14	2.09	14.89	2.42	19.57	2.95
Exterior	6.71	1.30	6.70	1.15	5.72	0.41	6.11	0.84

From top to bottom in the two tables, the first exterior reaction refers to the reaction associated with the long side of the approach slab. Each subsequent reaction follows in the transverse direction until the remaining exterior reaction, which corresponds to the short side of the approach slab. This explanation is not applicable to the non-skewed model since both sections of the approach slab are 20 ft long.

A general trend can be seen in these two tables, with the additional dead load from the approach slab being added on the long side of the approach slab as the skew increases. This trend can be seen more clearly in the approach slab models without soil support. The additional DL#1 from the approach slab to the most heavily loaded interior reaction increased by a maximum of 14.4 kips for the non-skewed model, 30.06 kips for the 30° skew model, 48.51 kips for the 45° skew model, and 100.6 kips for the 60° skew model. Similar increases in terms of proportion can be seen for DL#2. For models with soil support, the maximum dead load interior abutment reactions still increased as the bridge skew angle increased. However, the increase was lower in magnitude from model to model in comparison to models without soil support, with values of 11.41 kips for the non-skewed model, 12.14 kips for the 30° skew model, 14.89 kips for the 45° skew model, and 19.57 kips for the 60° skew model. This is expected because the additional support that the soil provides to the approach slab diverts some of the load to the soil instead of the abutment reactions.

Temperature loading was also included in the FE models. Table 3.33 shows the temperature deformation results for the various skew angles with and without the deck extending over the backwall to the approach slab.

Table 3.33. Parametric study - temperature deformation

Temperature Deformation (in)							
No Skew	Approach	30	Approach	45	Approach	60	Approach
0.30	0.35	0.33	0.38	0.30	0.46	0.39	0.45

The table shows a general increase in temperature deformation as the bridge skew angle increases. However, the 45° model presents some interesting results. It shows the lowest deformation for models without the approach slab yet the highest deformation for models with the approach slab. This may be due to the symmetry that exists between both bridge ends in the 45° skew model versus the 30° skew model and the 60° skew model.

To compare the live load abutment reactions for the various bridge skew models, two live load configurations were modeled acting in the top face of the approach slab. These live load configurations correspond to the two truck loading cases considered for this parametric study, Case 1 and Case 2. Case 2 presented some difficulties in modeling. For the non-skewed model, the middle and front axles of one of the trucks were not considered because they were located beyond the approach slab. Similarly, for the 30° skew model, the front axle of one of the trucks was not considered. These situations can be seen in Figure 3.76 and Figure 3.77 for the non-skewed model and the 30° skew model, respectively.

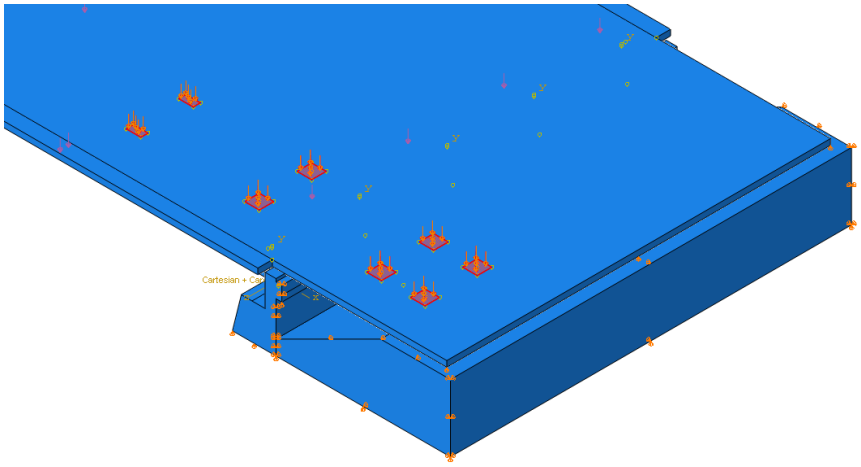

Figure 3.76. Case 2 - non-skewed model

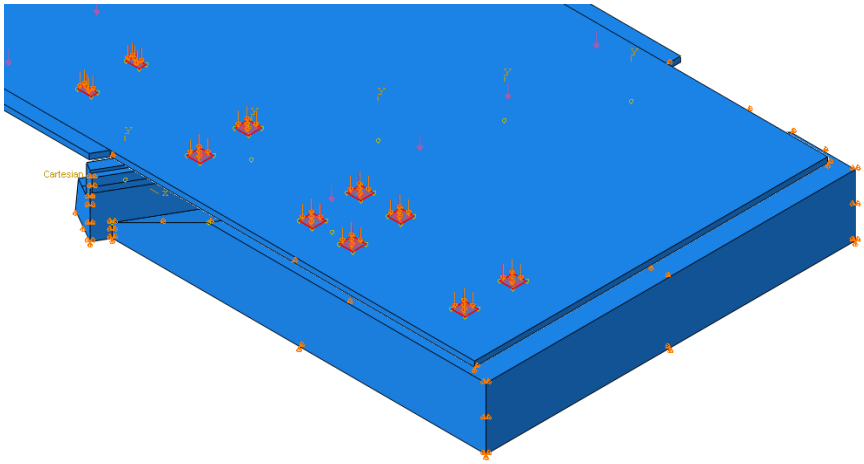

Figure 3.77. Case 2 - 30° skew model

Figure 3.78 shows the Case 2 truck loading allocation for the 60° skew model.

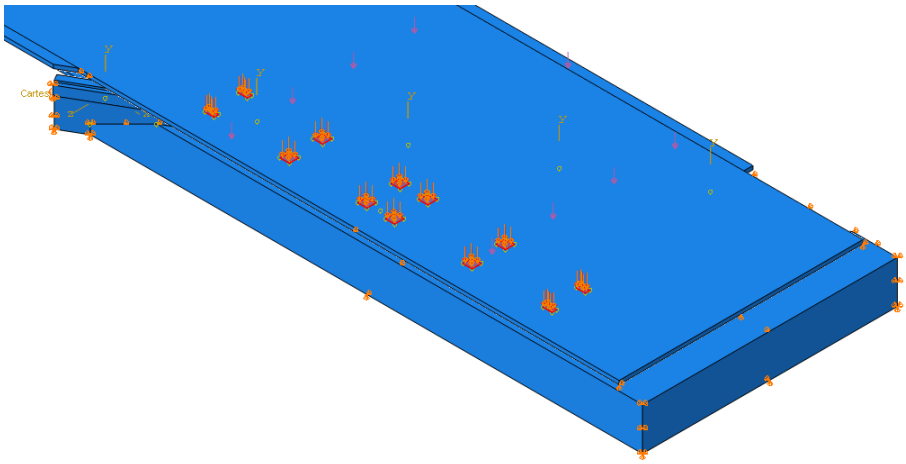

Figure 3.78. Case 2 - 60° skew model

The truck load is marked in red in Figures 3.76 through 3.78. Truck loading conditions were modeled as described previously in this chapter. Only the concentrated live load from the tires was considered in this study.

The results for the live load abutment reactions in kips are shown in Table 3.34 and Table 3.35 for Case 1 and Case 2, respectively.

Table 3.34. Parametric study - Case 1 - live load abutment reactions (kips)

Support	Soil				No Soil			
	No Skew	30	45	60	No Skew	30	45	60
Exterior	-0.56	0.00	0.00	0.00	-0.48	0.30	-0.11	0.15
Interior	2.36	-0.02	-0.01	-0.01	5.97	2.53	1.41	0.58
Interior	6.06	-0.12	-0.01	-0.01	11.50	5.98	4.71	2.63
Interior	2.35	-0.19	-0.12	-0.01	5.96	8.64	8.41	10.64
Exterior	-0.56	-0.10	-0.13	-0.06	-0.48	0.19	3.08	2.58

Table 3.35. Parametric study - Case 2 - live load abutment reactions (kips)

Support	Soil				No Soil			
	No Skew	30	45	60	No Skew	30	45	60
Exterior	22.47	12.21	6.41	0.36	31.84	28.40	8.30	6.68
Interior	31.61	23.87	20.38	7.03	42.02	60.89	69.65	68.74
Interior	3.17	1.64	1.69	1.71	6.68	24.43	54.56	98.32
Interior	-1.17	-0.96	-1.03	-0.81	-1.06	3.86	15.03	46.85
Exterior	-0.36	-0.07	-0.01	0.04	-0.60	-5.09	-8.08	-26.56

Figure 3.79 and Figure 3.80 show bar graphs with all of the values compared for models with soil and without soil support, respectively.

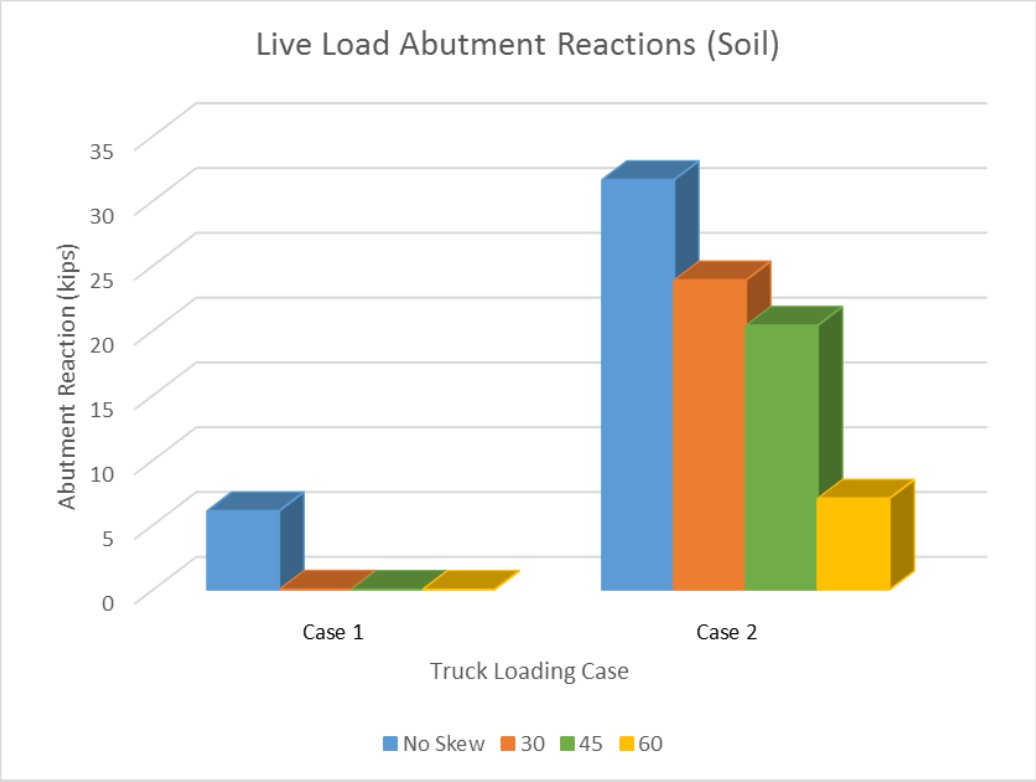

Figure 3.79. Parametric study - live load abutment reactions with soil support

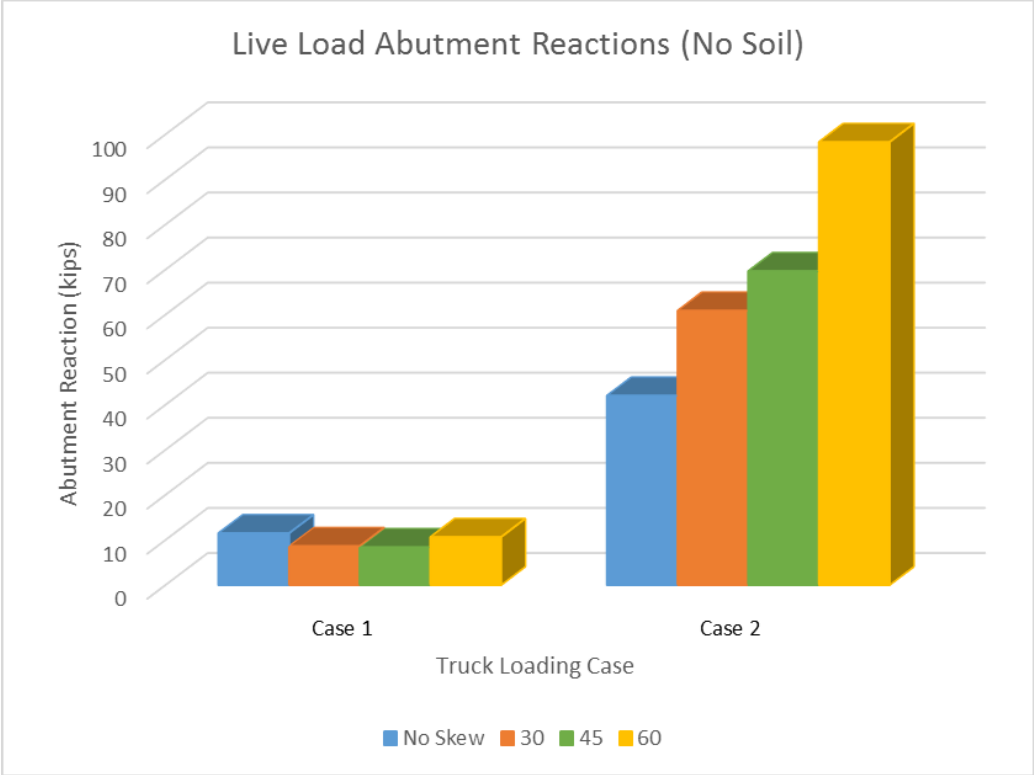

Figure 3.80. Parametric study - live load abutment reactions without soil support

A general trend can be seen in Table 3.34 and Table 3.35. For models without soil support, the live load abutment reactions for Case 2 increase as the bridge skew angle increases. This is expected since, without soil support, the applied load are transferred to the abutment supports and the edge support at the opposite end of the abutment interface. For models with soil support, the live load abutment reactions decrease as the bridge skew angle increases. This difference is due to the 12 ft void incorporated into the soil. In models with a lower skew angle, the applied load is applied closer to or on top of the void. In models with a higher skew angle, the load is applied farther from the void. For these reasons, the live load abutment reactions for Case 2 for models with soil support decrease as the bridge skew angle increases.

No clear trend could be recognized for Case 1 since the live load abutment reactions varied as the bridge skew angle changed. For skewed models with soil support, the abutment reaction was 0 kips, or uplift, as expected. The soil and the edge support at the opposite end of the abutment interface supported all of the truck load in these models. For the non-skewed model, some live load abutment reaction can be seen because the load is applied on top of the 12 ft void, in contrast with the skewed models.

The results for the deflection values in inches are shown in Table 3.36 and Table 3.37 for Case 1 and Case 2, respectively.

Table 3.36. Parametric study - Case 1 - deflection values (in.)

Location	Soil				No Soil			
	No Skew	30	45	60	No Skew	30	45	60
Midspan	-0.12	-0.06	-0.06	-0.06	-0.31	-2.32	-3.46	-12.32
Abutment	-0.03	-0.02	-0.03	-0.05	-0.07	-0.17	-0.27	-0.74

Table 3.37. Parametric Study - Case 2 - deflection values (in.)

Location	Soil				No Soil			
	No Skew	30	45	60	No Skew	30	45	60
Midspan	-0.17	-0.07	-0.07	-0.06	-0.53	-5.02	-6.50	-20.92
Abutment	-0.06	-0.05	-0.04	-0.05	-0.12	-0.34	-0.51	-1.22

Figure 3.81, Figure 3.82, Figure 3.83, and Figure 3.84 show bar graphs with all of the values compared for the midspan deflections and abutment interface deflections.

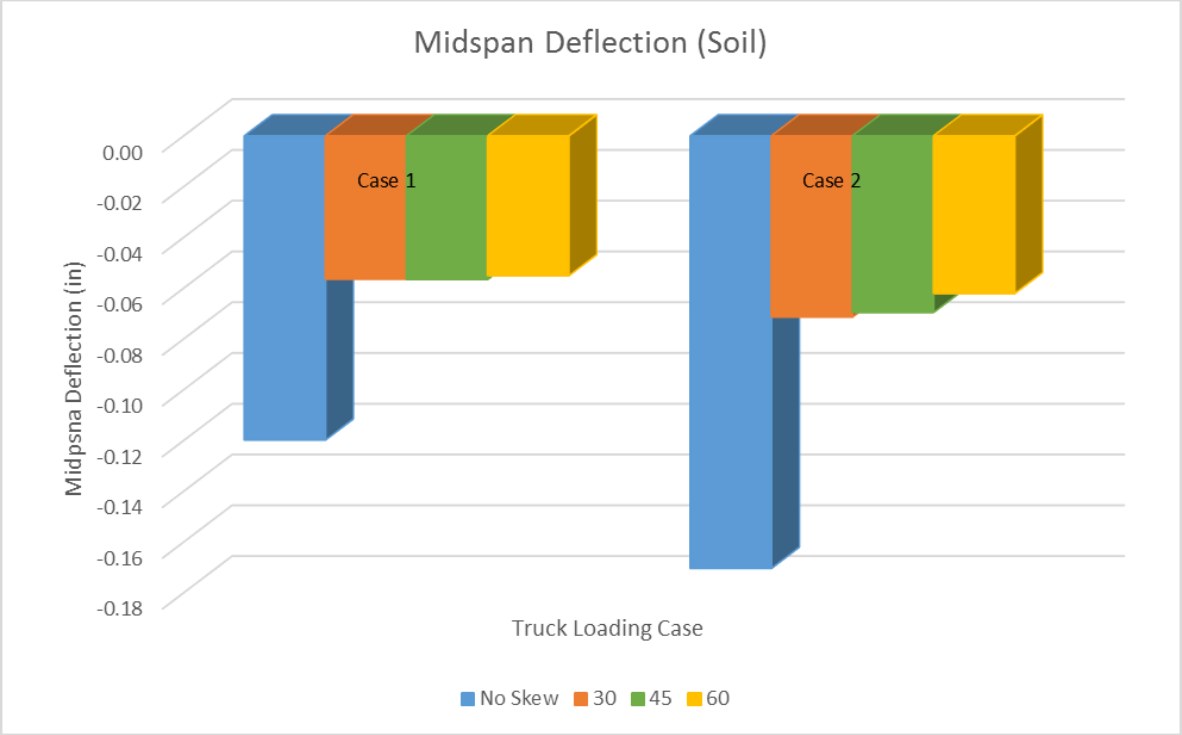

Figure 3.81. Parametric study - midspan deflection values with soil support

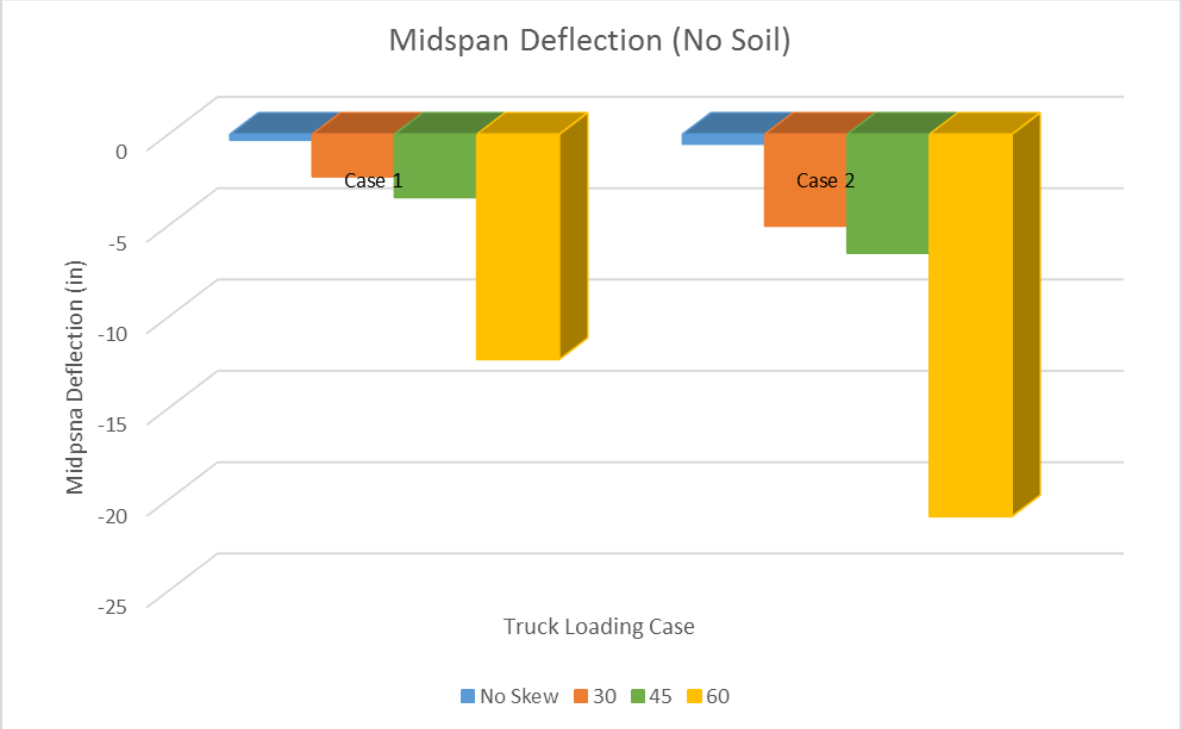

Figure 3.82. Parametric study - midspan deflection values without soil support

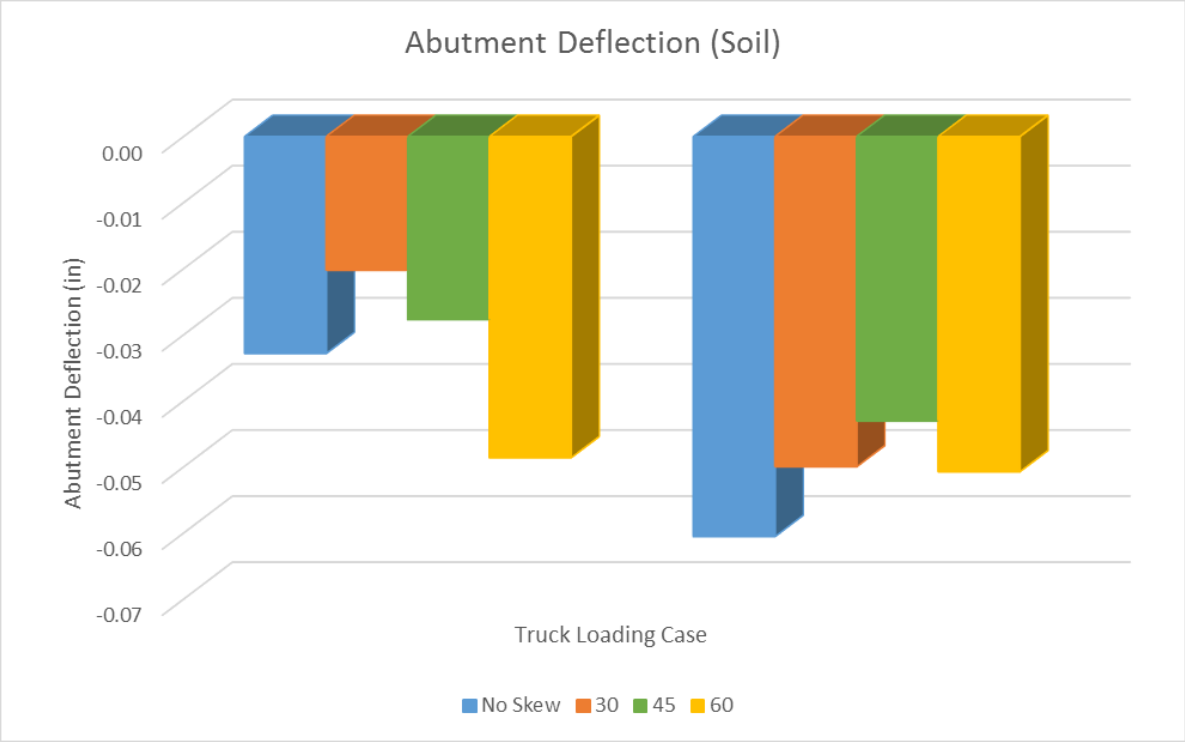

Figure 3.83. Parametric study - abutment deflection values with soil support

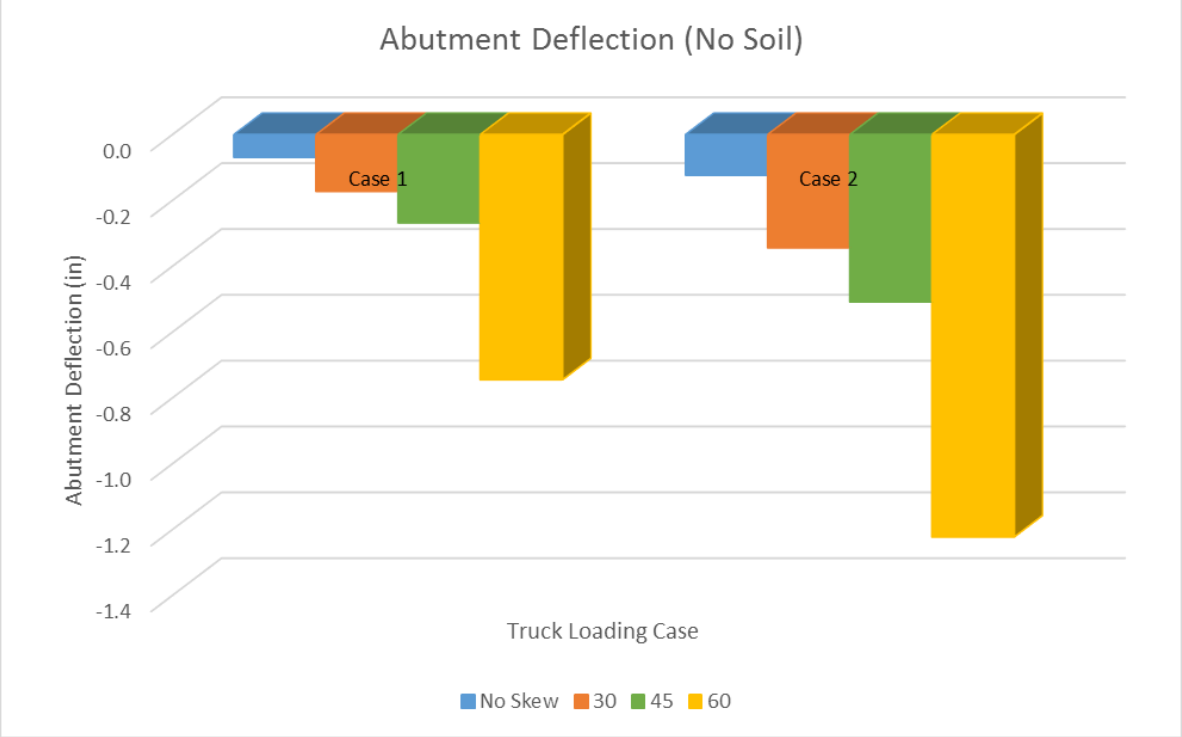

Figure 3.84. Parametric study - abutment deflection values without soil support

It is noted that the midspan deflection values without soil support are excessive and are provided as theoretical values only. The FE model assumes a linear elastic relationship and does not model deformations that might occur in the plastic range of materials.

A general trend can be seen in Table 3.36 and Table 3.37. As expected, for models without soil support, the deflection at the midspan of the approach slab and at the abutment interface increase as the bridge skew angle increases. This can be seen for both the Case 1 and Case 2 truck loading conditions. For models with soil support, the midspan deflection values decrease as the bridge skew angle increases. As explained above, this difference is due to the 12 ft void incorporated into the soil support aspects of the model. No clear trend could be recognized for the abutment deflection values in the models with soil support. The results vary without a pattern as the bridge skew angle changes.

The results for stress levels in psi are shown in Table 3.38 and Table 3.39 for Case 1 and Case 2 respectively.

Table 3.38. Parametric study - Case 1 - stress values (psi)

Location		Soil				No Soil			
		No Skew	30	45	60	No Skew	30	45	60
Midspan	Top	299.0	129.6	132.7	117.7	528.0	940.2	1125.0	1125.0
	Bottom	341.0	172.8	176.7	156.8	528.0	940.2	1125.0	1125.0
Abutment	Top	425.1	388.5	396.7	391.4	632.2	1252.0	1499.0	2801.0
	Bottom	383.1	302.2	308.7	430.5	632.2	1252.0	1499.0	3055.0

Table 3.39. Parametric study - Case 2 - stress values (psi)

Location		Soil				No Soil			
		No Skew	30	45	60	No Skew	30	45	60
Midspan	Top	355.0	175.5	132.7	156.6	818.0	1829.0	1706.0	2620.0
	Bottom	405.4	219.3	176.6	195.6	818.0	1829.0	1706.0	2620.0
Abutment	Top	607.0	482.2	484.5	468.6	1224.0	2438.0	2680.0	4799.0
	Bottom	506.2	394.6	440.5	468.6	1021.0	2438.0	2923.0	5235.0

Figure 3.85, Figure 3.86, Figure 3.87, and Figure 3.88 show bar graphs with all of the values compared.

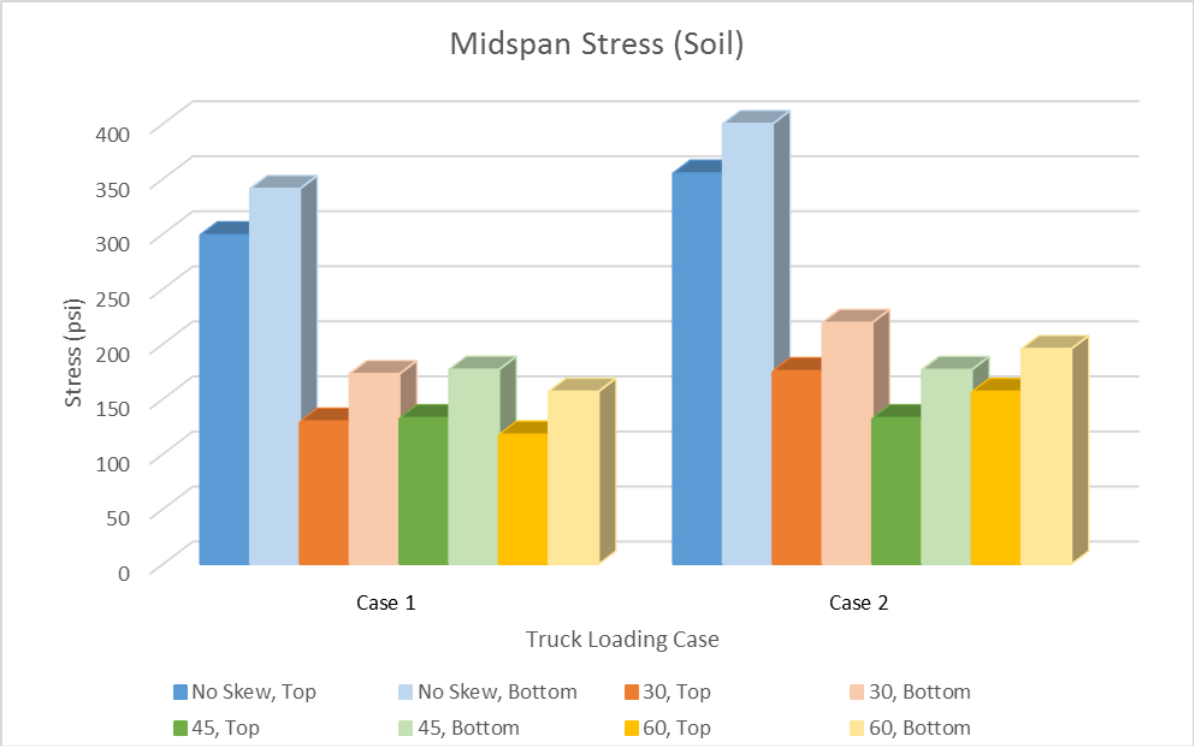

Figure 3.85. Parametric study - midspan stress values with soil support

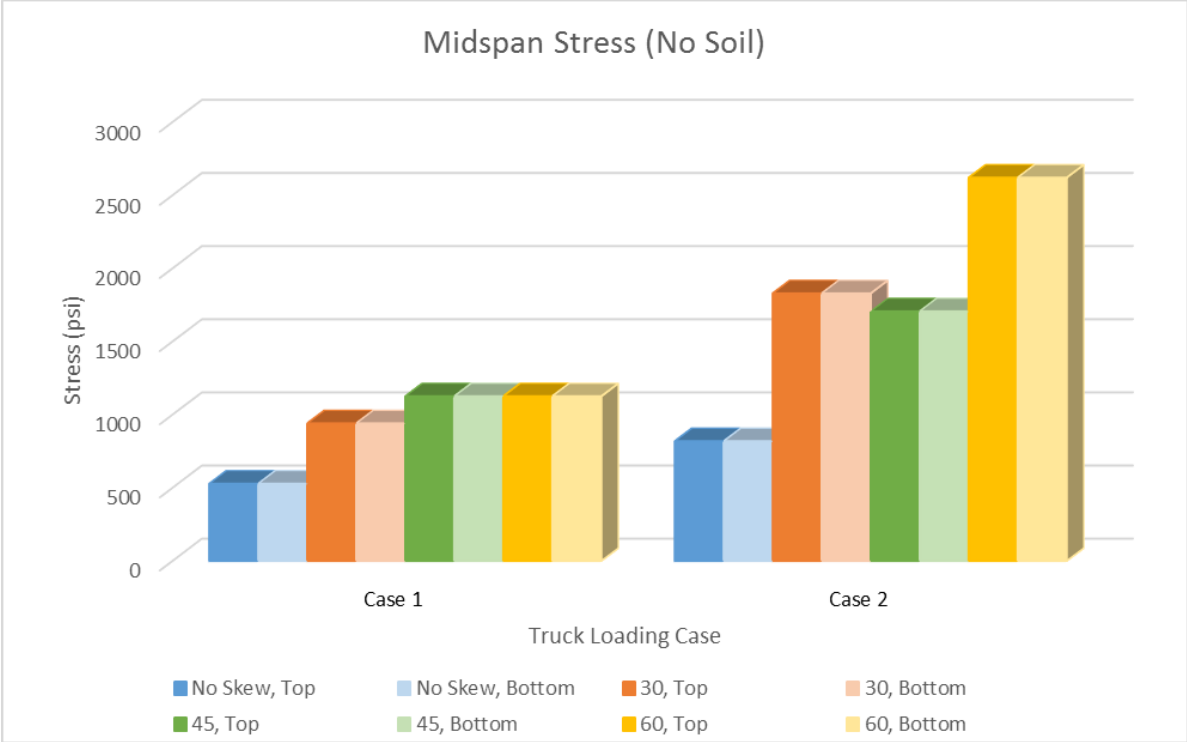

Figure 3.86. Parametric study - midspan stress values without soil support

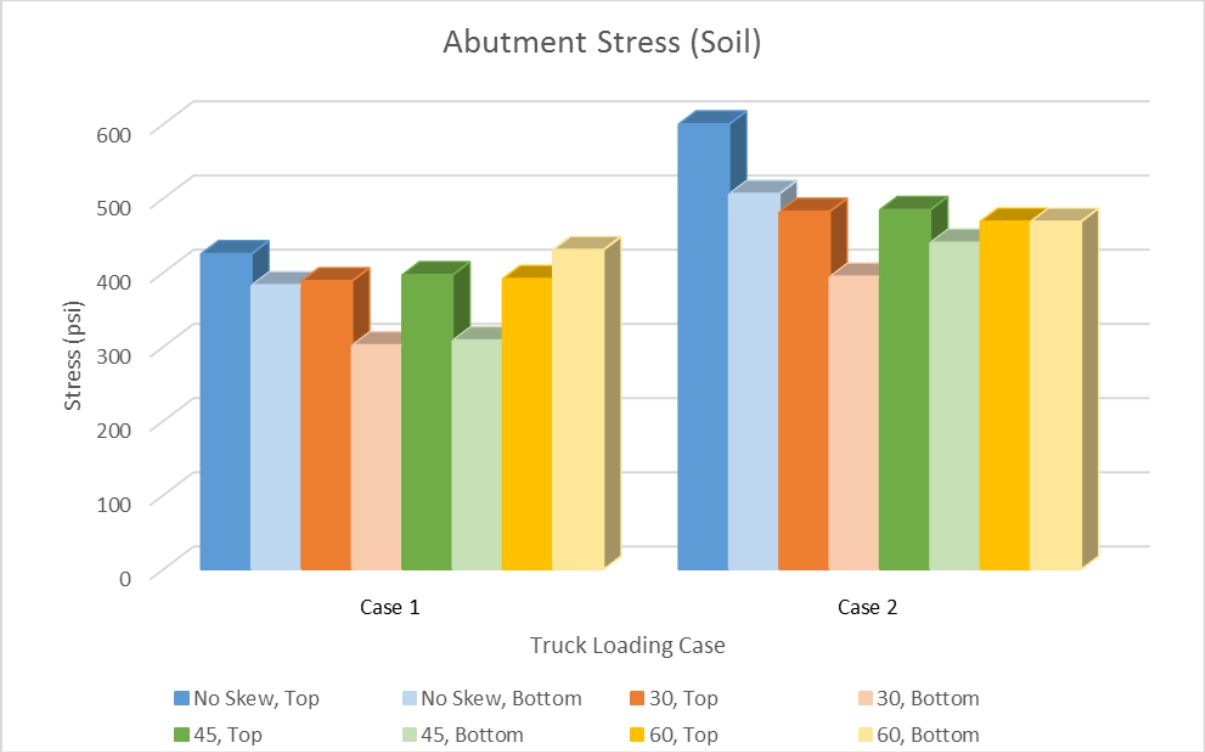

Figure 3.87. Parametric Study - abutment stress values with soil support

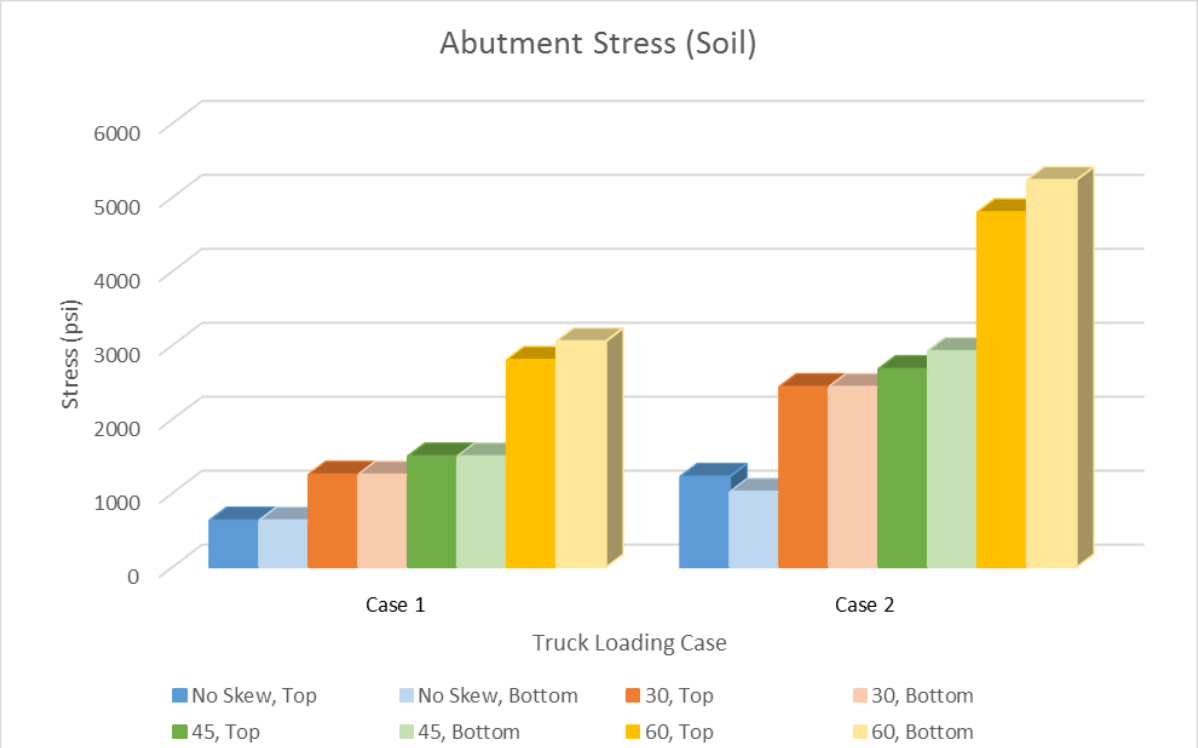

Figure 3.88. Parametric study - abutment stress values without soil support

The values shown correspond to the von Mises stress levels on the various points of interest across the joint and approach slab.

As expected, for models without soil support, the stress values at the midspan of the approach slab and at the abutment interface increase as the bridge skew angle increases. This is true for both the top face and the bottom face of the approach slab and for both Case 1 and Case 2. For models with soil support, the stress values for all of the skewed models were lower in comparison to those for the non-skewed models. As explained above, this difference is due to the 12 ft void that was included in the soil support aspects of the model. However, no clear trend could be recognized when comparing the values among the skewed models. The results vary without a pattern as the bridge skew angle changes. This inconsistency might be due to the difference in modeling the Case 2 truck loading conditions, with axles that were loaded beyond the end of the slab for two of the models: the non-skewed model and the 30° skew model. The 12 ft void incorporated into the soil support aspects of the models also impact these results.

3.3 Summary and Discussion

Full-scale FE models were developed to represent the selected candidate bridges as part of this investigation. Two bridges were modeled: the Story County bridge and the Marshall County bridge.

While both bridges are welded plate steel girder bridges with three spans and stud abutments, the two bridges differ in several respects. The Story County bridge is 338 ft long, or 343 ft from face to face of paving notches, with a roadway width of 30 ft. This bridge is a non-skewed bridge with four girders supporting the bridge deck. The interior span is 132 ft long while the exterior spans are 103 ft long. The Marshall County bridge is a 210 ft long bridge, or 217 ft 9 3/8 in. from face to face of paving notches, with a roadway width of 44 ft. This bridge is skewed 45° with five girders supporting the bridge deck. The interior span is 82 ft long while the exterior spans are 64 ft long. The detailing of the welded plate steel girders in terms of the height, width, and thickness of the flanges and webs is also different for each bridge. The differences can be seen in more detail in the original plans for each bridge presented in Appendix A and Appendix B for the Story County bridge and for the Marshall County bridge, respectively.

To properly model the bridges, various types of elements were used. All concrete members were modeled as C3D8R elements, which are eight-node linear brick elements with reduced integration and hourglass control. All steel elements were modeled as S4R elements, which are four-node, doubly curved, thin or thick shell elements with reduced integration, hourglass control, and finite membrane strains. These elements are commonly used for members where one dimensions is much smaller than the other two. For all flanges and webs, the thickness of the member is much smaller than the corresponding height or width. The concrete bridge deck could have been modeled as an S4R element as well, since two of the dimensions are much larger than the other (i.e., the length and width are much larger than the thickness). In early developments of the model, the concrete deck was modeled as a C3D8R element, and since this did not add recognizable computation time, the concrete deck was modeled in this way throughout the research.

All steel members of the welded plate steel girders and diaphragms were merged together and assigned a uniform mesh size. Boundary conditions were assigned to all faces that had soil support. These faces are at the bottom of the piers and in the bottom of the abutments and their accompanying backwall. Tie constraints were modeled between the top flanges of the steel girders and the bottom face of the concrete deck. These tie constraints assume full interaction between the two elements and transference of all degrees of freedom. Connecting wires between the bottom of the welded plate steel girders and the piers and abutments were also modeled. These wires were used to model the bearings at these locations. Dead load and live load reaction values were taken from these wires. as documented earlier in this chapter.

Both bridges were compared with the original plans to verify the values for dead load deflection and reactions, temperature expansion, and live load reactions. An additional verification was made with live load deflection values corresponding to AASHTO specification limits. The results for both bridges are discussed below.

For the Story County bridge, the dead load deflection results from the FE model matched the original plan value of 1 in. at midspan of the interior span. The dead load analysis was split between the DL#1 slab, girders, and diaphragm and the DL#2 curbs, rails, and future wearing structure. The dead load reactions showed high percentages of difference for DL#2, yet differences for the total load ranged only from 0.22% to 5.48%. The relatively large differences for DL#2 may be due to differing assumptions with regards to what that load included by the designers of the original plan and the current research team. For temperature loading, the FE results matched those of the original plans within 0.5 in. These values also show a 10% difference from the value obtained using equation (1) in Section 3.1.2.2.

For the live load results, the deflection values were verified with the AASHTO specification limit of L/800. The value obtained from the FE results indicated less deflection than this limit. For the live load reactions, various cases were analyzed depending on what value was being maximized. Additionally, the reaction values showed a very high percentage of difference when analyzed because of differences between the current loading conditions that were initially used in the model and those that were used by the designers. The loading conditions used in the model were altered because of this to match the ones used by the original designers. The discussion that follows corresponds to the values resulting from the altered loading conditions. For the abutment reactions, low percentages of difference were obtained in the total load, where the percentages ranged from 3.5% for the exterior supports to 4.12% for the interior supports. For the pier reactions, low percentages of difference were obtained in the total load, where the percentages ranged from 2.35% for the exterior supports to 3.78% for the interior supports.

With low percentages of difference across all loading conditions (dead load, temperature loading, and live loads), this model can be confidently used to compare and correlate with the experimental investigation results detailed in Chapter 6.

For the Marshall County bridge, the dead load deflection results from the FE model resulted in a percentage of difference of 15% from the original plan value. This may be due to additional dead load elements being taken into consideration by the original designers. The dead load reactions

showed low percentages of difference for all values, with values ranging from 1.1% to 4.15%. For temperature loading, the FE results showed percentages of difference of 20% from the original plan value and 6.22% from the value obtained using equation (1). The original plan value might be calculated based on a different coefficient of thermal expansion than the one used across all models.

For the live load results, the deflection values were verified with the AASHTO specification limit of L/800. The value obtained from the FE results was lower than this limit. For the live load reactions, various cases were analyzed depending on what value was being maximized. Additionally, the reaction values showed a very high percentage of difference when analyzed with current loading conditions. The loading conditions were revised to match the ones that apparently had been used in the original plans. The discussion that follows refers to the results from the analysis based on the revised loading conditions. For the total load abutment reactions, the percentages of difference ranged from 5.2% for the exterior supports to 13.59% for the interior supports. For the pier reactions, the percentages of difference ranged from 10.06% for the exterior supports to 3.57% for the interior supports.

With low percentages of difference between the results of the model and the original plan values across all loading conditions (dead load, temperature loading, and live loads), this model can be confidently used to assess the feasibility of the deck over backwall concept, as discussed below. This model can also be used to compare and correlate with the post-construction testing results that would be obtained according to the recommended testing plan detailed in Chapter 6.

The results of modeling for the deck over backwall concept are detailed in Section 3.2.3. Additional elements had to be included in the FE model for the deck over backwall concept and the approach slab. The soil was modeled as a C3D8R element just like the concrete members. Tie constraints were added in the abutment interface between the curb and the end span beam with the concrete deck. Diaphragms were embedded into this curb and end span beam. Additionally, a contact interaction was imposed between the soil and the bottom face of the approach slab.

This model was analyzed under dead load, temperature loading, and various configurations of live loads. The abutment reactions were examined under the dead loads and live loads described above. Deflection and stress levels were taken at various points of interest across the reactions of the abutment interface and the midpsan of the approach slab.

The results show an increase in bearing loads due to the additional dead loads from the approach slab and the live loads corresponding to the various truck loading conditions. The deck over backwall dead loads corresponded to approximately an additional 15 to 28 kips for the interior supports and 5 to 11 kips for the exterior supports. These values assume nominal soil support and the presence of an end span beam. For models without soil support, the dead load added approximately 60 kips to the interior supports and 11 kips to the exterior supports.

The additional 64 ft section on one end of the approach slab accounted for an additional temperature deformation of 0.16 in. This value showed a percentage of difference of 4% from the value calculated using equation (1) in Section 3.1.2.2.

The live load imposed an approximate maximum of 48 kips to the interior supports and 26 kips to the exterior supports. These values assume nominal soil support. For models without soil support, the live load imposed an approximate maximum of 70 kips for the interior supports and 27 kips for the exterior supports.

Deflection values were obtained at the abutment interface and the midspan of the approach slab. For the deflection values across the abutment interface, the maximum deflection for models with soil support was 0.09 in. For models without soil support, the value increased, as expected, to 0.51 in. For the midspan of the approach slab, the maximum for models with soil support was 0.32 in. For models without soil support, the value increased to a theoretical 6.5 in. Most midspan deflection values for situations without soil support were excessive and indicate that this concept is not feasible under such circumstances.

Stress values were obtained from the abutment interface and the midspan of the approach slab. For the stress values across the abutment interface, the maximum stress for models with soil support was 675.4 psi. For models without soil support, the value increased to 3,013 psi. For the stress in the approach slab, the maximum stress for models with soil support was 361.5 psi. For models without soil support, the value increased to 1,706 psi.

A parametric study of various bridge skew angles was also conducted for the Marshall County bridge. The model was altered to match skew angles of 30° and 60°, and a non-skewed version of the model was created. These models and the original 45° model were compared. The results for the models without soil support show that generally an increase in the bridge skew angle leads to an increase in all parameters of interest. These include the dead load abutment reactions and temperature deformation of the bridges with and without the approach slab, the live load abutment reactions, and the deflection values and stress levels at the abutment interface and in the midspan of the approach slab. The results for models with soil support were quite variable due to the inclusion of a 12 ft soil void in the model and difficulties with the Case 2 truck loading conditions.

The findings summarized above can be useful in developing the joint and approach slab configuration using the deck over backwall concept. Reinforcing and concrete design requirements can be selected using the stress levels provided by the FE model for the abutment interface and the midspan of the approach slab.

CHAPTER 4. EXPERIMENTAL TESTING PLAN

Experimental testing was completed to not only assess the performance of the deck over backwall concept but also understand the performance of that concept when various design decisions are made. The displacement of various sections of an experimental specimen, along with cracking patterns and stress concentrations, were analyzed.

4.1 Testing Objectives

Testing was completed to satisfy several objectives pertaining to the performance of the deck over backwall concept. The objectives were to investigate the following:

- The interaction between an existing concrete bridge deck and a newly placed approach slab section using typical Iowa DOT construction practices
- Cracking underneath the bottom of the approach slab
- How the detailing of the longitudinal reinforcing in the approach slab affects the performance of the joint
- How the presence of a backwall support could affect the performance of the joint

To achieve the objectives outlined above, it was decided that two tests would be performed on a single laboratory specimen. Two distinct differences existed between these two tests. First, the continuity of the top reinforcing was altered. In Test 1, both the top and bottom longitudinal reinforcing in the approach slab would be continuous, while in Test 2 the top reinforcing would be cut (see the detail in Figure 4.1).

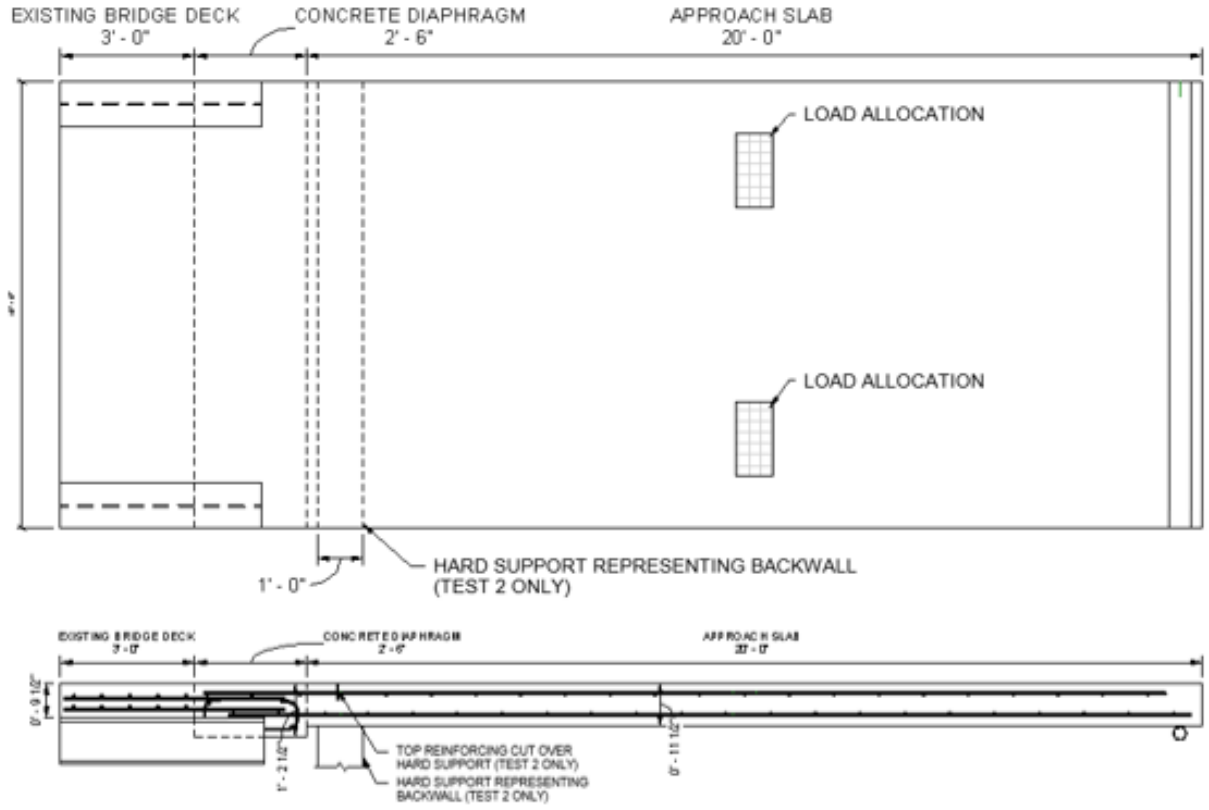

Figure 4.1. Laboratory test setup for Test 1 and Test 2

Second, the existence of a hard support, representative of an abutment stud wall and backwall, would change from Test 1 to Test 2. In Test 1, no support would exist. Because the deck slides over the backwall, it is possible that a full reaction force is not provided by this support. For this reason, a support that would represent a backwall was not included in Test 1. This was an extremely conservative approach because in an actual field installation, the backwall would likely provide some support. In Test 2, a hard support was provided to simulate the presence of a backwall. The top reinforcing would be cut at the center of the backwall location, as shown in Figure 4.1. Details surrounding the testing setup, specimen geometry, loading, and instrumentation are discussed in the following sections.

4.2 Testing Plan

4.2.1 Geometry

Simplifications regarding the joint detail that was developed by the Iowa DOT were made in order to facilitate the construction of the test specimen. These simplifications were not intended to impact the pertinent results that the experimental investigation would produce.

The overall dimensions of the cast-in-place specimen can be seen in Figure 4.1. The laboratory specimen consisted of three main sections, corresponding to the main structural components of

the Iowa DOT detail. The sections are referred to as the existing bridge deck, the concrete diaphragm, and the approach slab throughout this chapter. The existing bridge deck section was 3 ft in length and 9.5 in. thick, corresponding to the thickness provided by the Iowa DOT for a typical bridge deck. Next, the concrete diaphragm served as the main structural diaphragm for the specimen. The diaphragm was 14.5 in. thick and contained the reinforcing hoops, as seen in Figure 4.1. Finally, the approach slab section was 20 ft 0 in. in length and 11.5 in. thick. The entire specimen was 10 ft wide, corresponding to the spacing of typical girders on an Iowa DOT bridge as well as lane loads corresponding to AASHTO specifications (AASHTO 2014).

In both the plan and profile view in Figure 4.1, the location of the hard support utilized for Test 2 is shown. Above the hard support, the top reinforcing was cut for Test 2, as noted in both the plan and profile view in Figure 4.1.

Similar to field conditions for a removal and rehabilitation project, the existing bridge deck was placed at a separate time than the concrete diaphragm and approach slab. Because the bridge deck would not be demolished during the concrete removal process, its concrete was placed first and allowed to fully cure before the concrete for remainder of the specimen was placed monolithically (Figure 4.2).

Figure 4.2. Laboratory specimen after concrete for approach slab and diaphragm sections was placed, with steel girders visible

Because the different concrete components of the specimen were poured separately, a cold joint (also referred to as a construction joint) existed between the existing bridge deck and the concrete diaphragm sections (Figure 4.3).

Figure 4.3. Construction joint at interface of existing bridge deck and concrete diaphragm sections

4.2.2 Boundary Conditions

The bridge deck section specimen was supported on each side by a steel beam, simulating the girders in a full bridge. The two steel beams extended under the bridge deck section and into the concrete diaphragm. As noted previously, the spacing of the two beams was similar to that of the typical spacing of girders on an Iowa DOT bridge. The beams were 4 ft 6 in. long and had shear studs on the top flanges that were embedded into the concrete of the bridge deck. The end of the existing bridge deck section was tied down to the strong floor of the laboratory.

A steel pipe filled with concrete acted as a roller on the other end of the specimen. The roller was located 6 in. in from the edge of the specimen, allowing the slab to move horizontally during loading. The roller was supported by steel sections in order to support the approach slab specimen so that it was level with the remainder of the specimen.

Normally, soil would be present under a portion of the approach slab. However, soil was not included in the laboratory test plan. This was a conservative approach, but it was considered to be warranted because soil could compact over time, moving away from the bottom of the approach slab and no longer providing support.

4.2.3 Reinforcing

The reinforcing for the laboratory specimen followed that of a typical Iowa DOT bridge project. The reinforcing bars in the existing bridge deck were not epoxy coated, while the reinforcing

bars throughout the rest of the specimen were epoxy coated. The details of the reinforcing, sorted by the section of the specimen, are as follows:

- Existing Bridge Deck:
  - Top longitudinal bars: #6 bars at varied spacing, extending into the concrete diaphragm section 2 ft 0 in.
  - Bottom longitudinal bars: #6 bars at varied spacing, extending into the concrete diaphragm section 2 ft 0 in.; 2 in. cover
  - Transverse top bars: #7 bars at 7.5 in. spacing; 3.5 in. cover
  - Transverse bottom bars: #7 bars at 7.5 in. spacing
- Concrete Diaphragm:
  - Hoop: #5 hoop with four #5 bars at the corners and one #5 bar at the bottom middle; 2 in. cover on bottom; hoops tied to top bars of the approach slab
- Approach Slab:
  - Top longitudinal bars: #5 bars spaced every 12 in. on center; 2.5 in. cover
  - Bottom longitudinal bars: #6 bars spaced every 12 in. on center; 2.5 in. cover
  - Top transverse bars: #5 bars spaced every 12 in. on center
  - Bottom transverse bars: #5 bars spaced every 12 in. on center

Table 4.1 summarizes the details for all reinforcing bars.

Table 4.1. Reinforcing bar list

Part	Bar	Location/Type	Number	Length	Spacing	Epoxy
Existing Bridge Deck	#6	Top, Long	15	4 ft 11 in.	Varied, see plan view	No
	#6	Bottom, Long	14	4 ft 11 in.	Varied, see plan view	
	#7	Top, Transverse	5	9 ft 6 in.	7.5 in.	
	#7	Bottom, Transverse	5	9 ft 6 in.	7.5 in.	
Concrete Diaphragm	#5	Hoop	9	4 ft 4 in.	1 ft, with approach slab top bars	Yes
Approach Slab	#5	Transverse	5	6 ft 6 in.	Around hoop	Yes
	#5	Top, Long	9	21 ft 6 in.	12 in.	
	#6	Bottom, Long	9	21 ft 6 in.	12 in.	
	#5	Top, Transverse	24	9 ft 6 in.	12 in.	
	#5	Bottom, Transverse	24	9 ft 6 in.	12 in.	

4.2.4 Concrete

Typical concrete strengths were utilized, with all concrete specified as C4 mix. Two distinct placements were completed. The first placement, used for the existing bridge deck section of the specimen, had an average 28-day compressive strength of 6,505 psi. The second placement, used

for the remainder of the laboratory specimen, had an average 28-day compressive strength of 5,116 psi at the time of testing. These results of compressive strength tests are shown in Table 4.2.

Table 4.2. Compressive strength of concrete cylinders

Cylinder #	Existing Bridge Deck Section	Concrete Diaphragm/ Approach Slab Sections
1	6,531	5,205
2	6,372	4,830
3	6,612	5,313
Average	**6,505**	**5,116**
St. Deviation	**122**	**254**

Per typical Iowa DOT construction practices, the lateral surface of the existing concrete deck was roughened using a jack hammer. This promoted additional bonding between the two placements. This can be seen in Figure 4.4.

Figure 4.4. Jack hammering performed on construction joint to increase bond strength

4.2.5 Loading

Loading conditions were the same for Test 1 and Test 2. Loading corresponded to that of the rear axles of an HS20-44 model load. To simulate this load, 10 in. x 20 in. loading areas were spaced 6 ft apart. Load was applied to the specimen via actuators pushing onto loading pads anchored to

the specimen. The specimen was loaded to 16 kips per loading area, corresponding to the rear wheels of the HS20-44 loading condition. Test 2 was initially loaded up to 16 kips per loading area, and then the load was increased to failure. During Test 2, load control was used up to 20 kips per load area, then deflection control was used until failure.

4.2.6 Instrumentation

4.2.6.1 Strain Gages

Strain gages were one of two main instruments utilized to collect data during testing. A total of 23 strain gages were installed on the reinforcing of the laboratory specimen. The strain gage locations on the reinforcing can be seen in Figure 4.5.

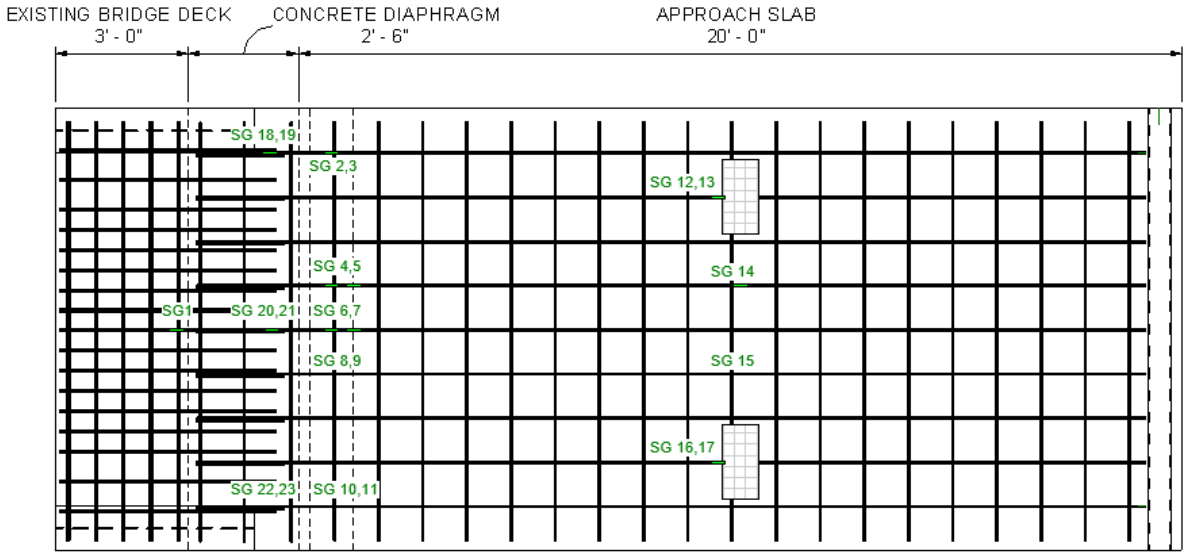

Figure 4.5. Reinforcing strain gage layout

Strain gages were placed on the reinforcing near the location of the hard support in Test 2. All strain gages in this area were placed past the development length of the reinforcing to ensure that a full bond existed between the reinforcing and the concrete. Additionally, strain gages were placed near the loading areas. It was expected that the midspan of the approach span would experience the largest strains due to the positive moment incurred by loading. Therefore, the strain gages near the loading areas would be able to capture the maximum strains that occurred during Test 1 and Test 2.

Concrete strain gages, referred to as BDIs, were placed on the surface of the specimen to infer the strains that occurred in the concrete during loading in Test 1 and Test 2. The placement of these gages mirrored that of the reinforcing strain gages so that results from both could be directly compared. There were 13 concrete strain gages in total. Figure 4.6 and Figure 4.7 show the locations of these gages. Gages 9, 11, and 13 were placed on the underside of the specimen in the concrete diaphragm section.

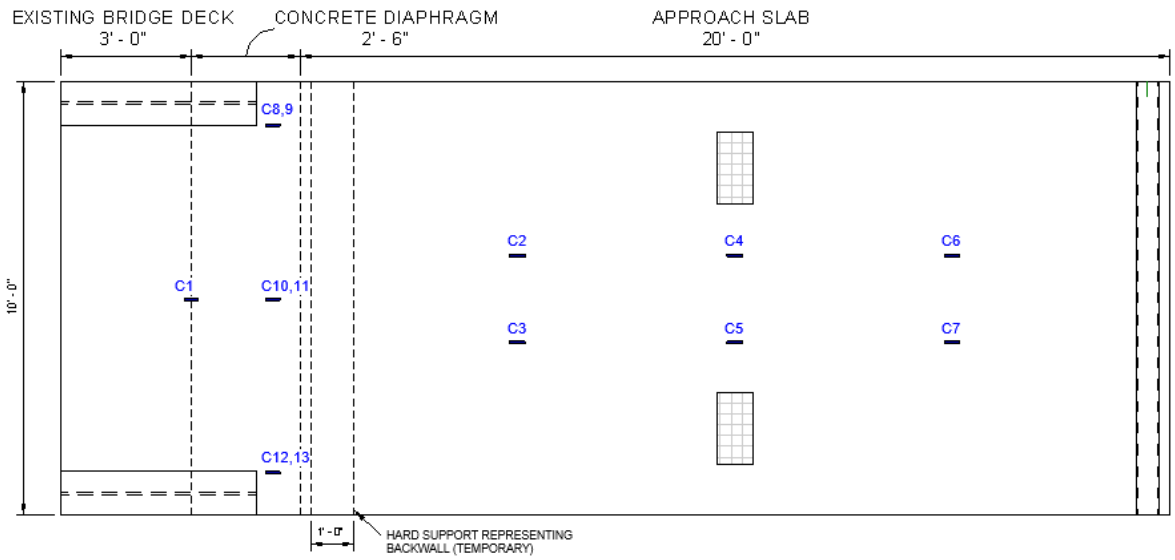

Figure 4.6. Concrete strain gage (BDI) layout

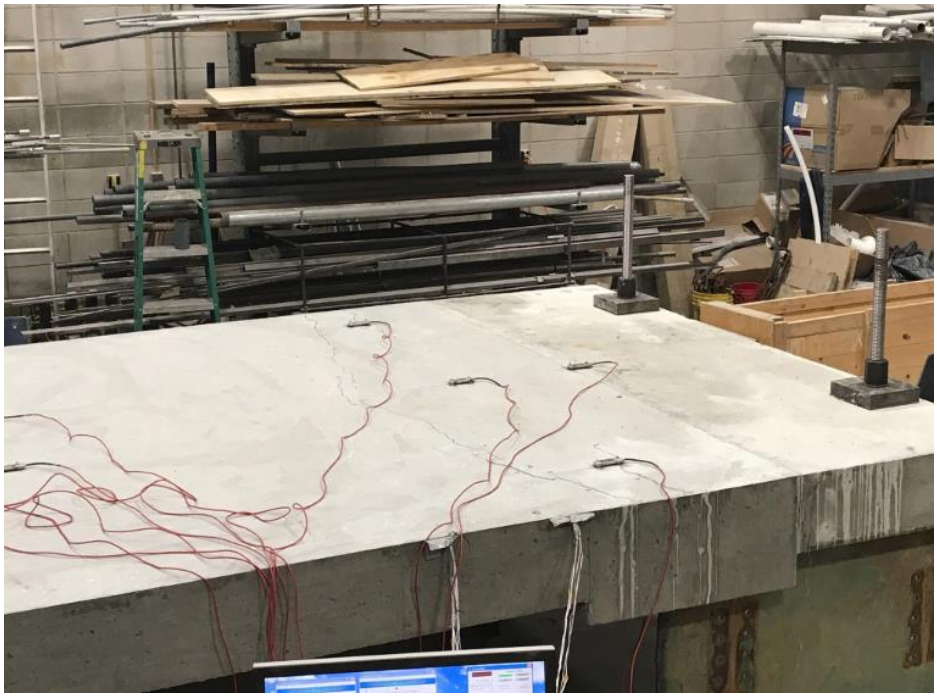

Figure 4.7. BDIs on laboratory specimen

4.2.6.2 String Pots

String pots were placed in several locations on the specimen to record the displacement that would occur during testing. Figure 4.8 shows the locations of these displacement meters.

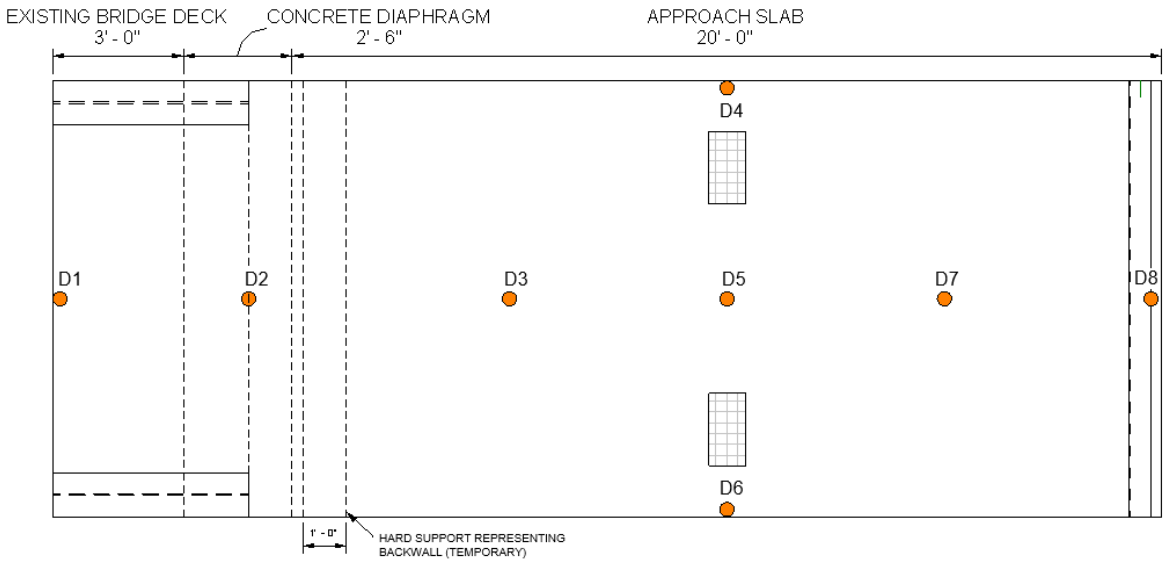

Figure 4.8. String pot (displacement meter) layout

In total, there were eight string pots, with D1 and D8 placed on opposing ends of the specimen. The output from these devices would be used to infer how the specimen deflected at the supports during tests. D3 through D7 were placed on the main body of the approach slab. Three of these string pots were placed perpendicular to the plane of loading. D4 and D6 were placed to capture any unsymmetrical twisting that the approach slab might experience during loading, if loading were not completed symmetrically. Finally, D2 was placed at the end of the steel girders at the diaphragm section.

4.2.6.3 Linear Velocity Displacement Transducers (LVDTs)

Three LVDTs were utilized to measure the horizontal widening of the saw cut that was made through the top of the approach slab and reinforcing during Test 2. These LVDTs were placed along the length of the cut, with one LVDT measuring displacement at the center and two measuring displacement at the outer edges of the width of the specimen.

4.3 Experimental Testing Results

Results were gathered from Test 1 and Test 2. The results for each test will first be presented independently, then comparisons between the two tests will be made.

While the results for Test 2 were altered by the effects that Test 1 had on the specimen, such as cracking, general trends between the two tests can still be compared. Additionally, utilizing a calibrated finite element analysis, the results for Test 2 can be generalized and applied to an untested specimen. The FE modeling and its results are presented in Section 4.4 of this report.

4.3.1 Test 1 Results

During Test 1, both the top and bottom longitudinal reinforcing was continuous through the concrete diaphragm section. The specimen was loaded until there were 16 kips on each loading area, corresponding to the full load of the rear axle of an HS20-44 truck. Figure 4.9 shows the general loading pattern used during Test 1.

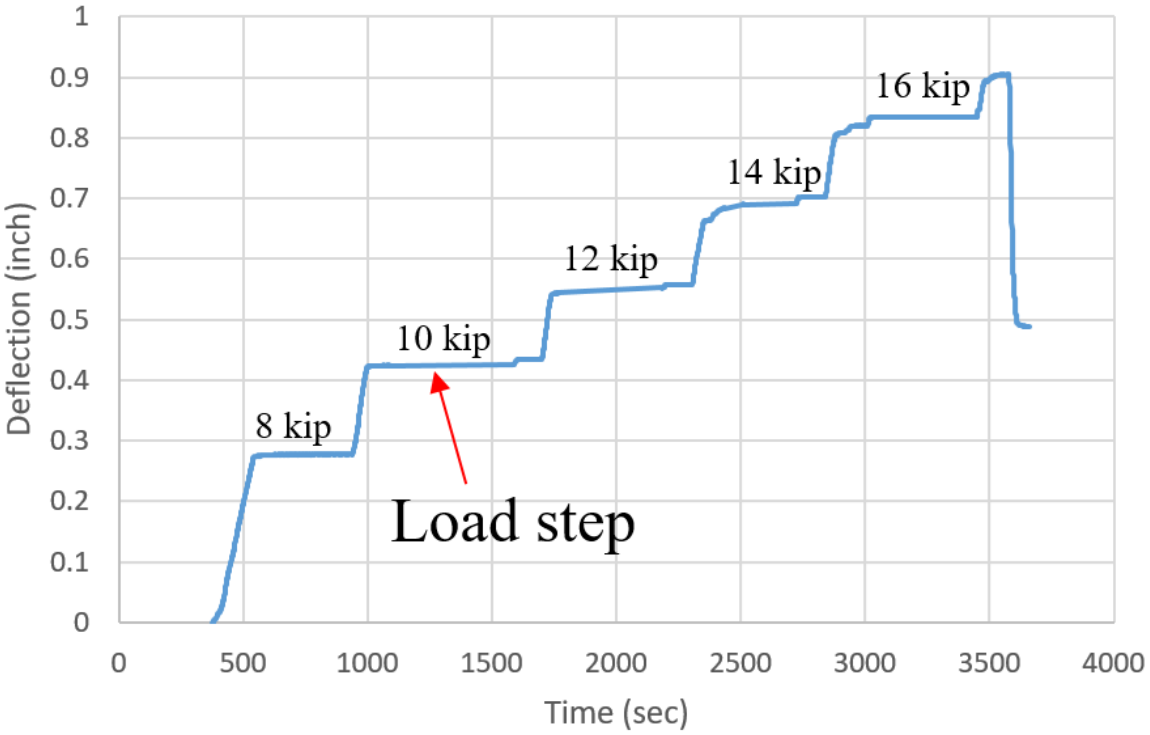

Figure 4.9. General loading with load steps for Test 1

The load was applied incrementally and then halted as the specimen was checked for cracking and strains were monitored. This pattern continued until 16 kips was reached on each loading area.

4.3.1.1 Cracking Patterns

Cracks were monitored on the top, bottom, and sides of the specimen during the entirety of Test 1. Particular attention was paid to two areas: near the concrete diaphragm, where the cut would be made in Test 2, and the bottom of the approach slab, where the largest positive moment (and, therefore, largest strains) would be.

In order to accurately record cracking, a grid was created on all surfaces of the test specimen, subdividing the specimen into 1 ft by 1 ft sections. Figure 4.10 shows the labelling scheme for the grid sections of the specimen.

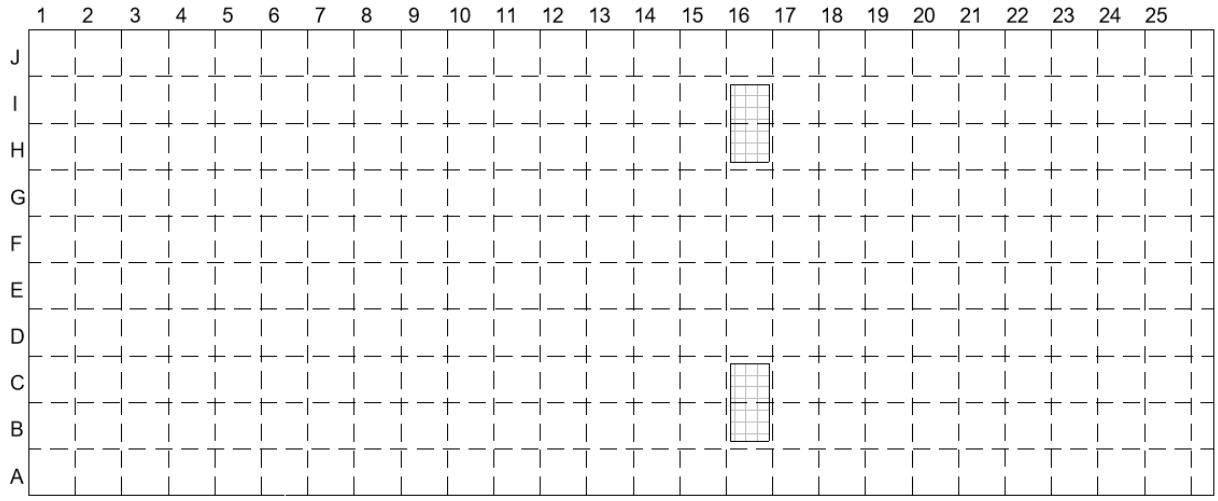

Figure 4.10. Gridded laboratory specimen for cracking documentation

During testing, cracks were marked incrementally, and at the end of testing, photos were taken of each individual grid section in order to create an overall cracking pattern map for the various surfaces of the specimen.

Figure 4.11 shows the cracking that occurred on the top of the slab during Test 1.

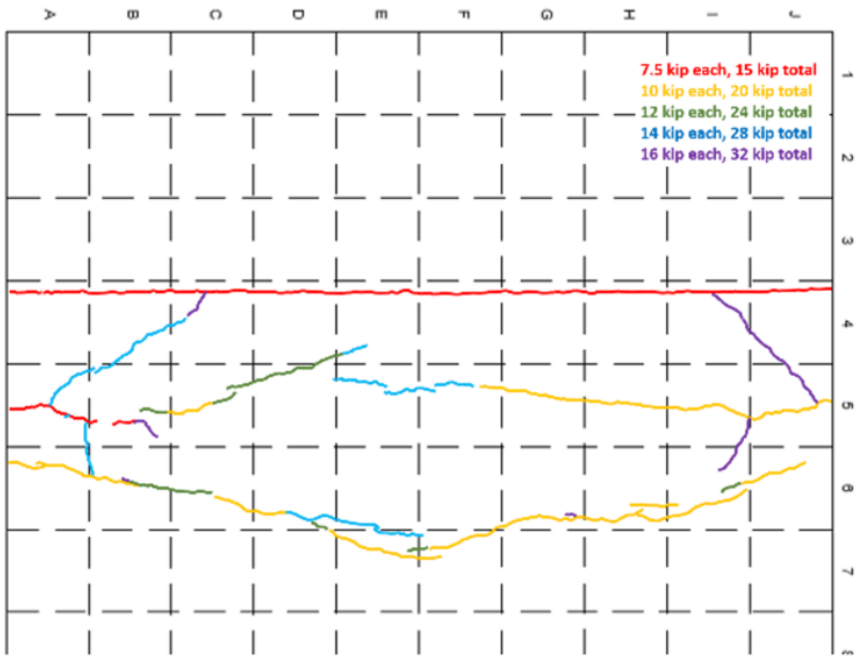

Figure 4.11. Cracking on the top of the slab, Test 1

The cracks are color coded by the load at which they occurred. As the figure shows, the majority of cracking on the top of the specimen occurred near the interface of the concrete diaphragm and the existing bridge deck.

The first crack to appear was at the cold joint between the concrete diaphragm and the existing bridge deck. Even though the surface of this joint was roughened, the concrete bond at this surface was not as strong as the remainder of the specimen. This large, horizontal crack at the joint can be seen in Figure 4.12.

Figure 4.12. Cracking at the construction joint

The crack formed near a loading condition of 7.5 kips on each tire area. Looking at the remainder of the cracks on the top of the specimen, it can be seen that the continuity of the top reinforcing caused stress to be transferred from the approach slab to the concrete diaphragm.

Figure 4.13 shows the cracking that occurred on the bottom of the slab during Test 1.

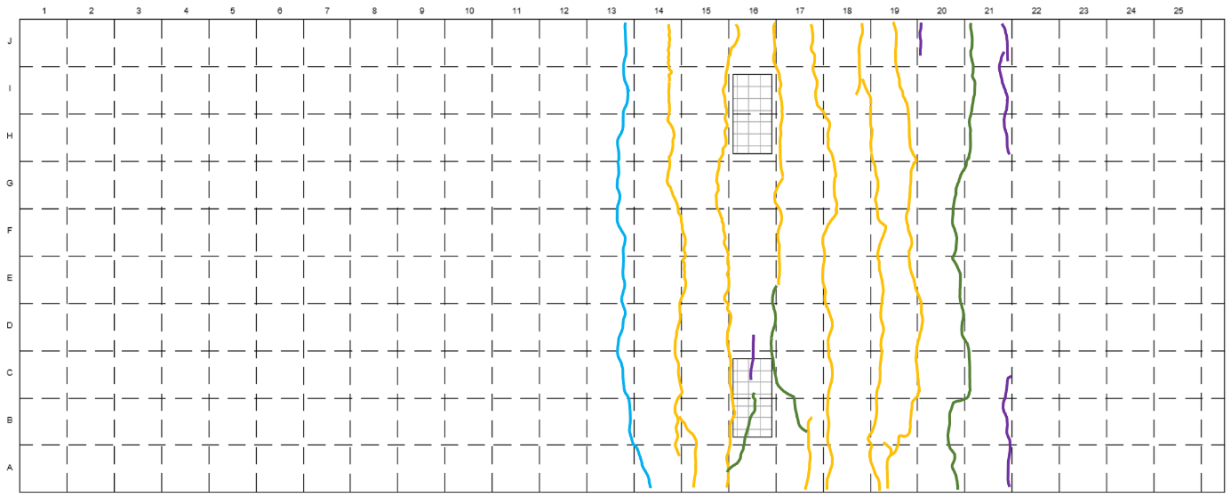

Figure 4.13. Cracking on the bottom of the slab, Test 1

Similar to those in Figure 4.12, the cracks are color coded by the load at which they occurred. All of the cracks that formed on the bottom of the slab extended across the width of the slab and were primarily concentrated under the application area of the load, where the largest tensile stresses existed. As load was applied, transverse cracks formed on either side of the width of the specimen; as the load increased, the cracks propagated until coming together and forming one crack along the full width of the slab. Those cracks were formed earlier in the loading stage (i.e., the cracks shown in yellow in Figure 4.13, corresponding to 10 kips per loading area) began to exhibit hairline cracks that branched off at later loading stages. To summarize, those cracks on the bottom of the slab extended a total length of 10 ft and were located approximately 1 ft apart.

Figure 4.14 and Figure 4.15 show the cracking that occurred on the sides of the slab.

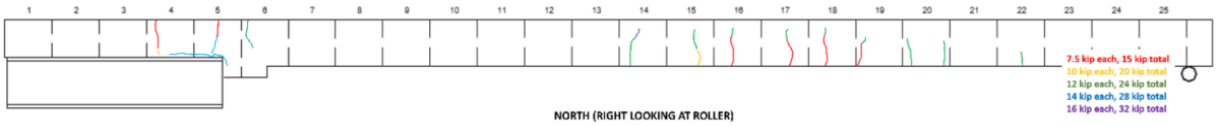

Figure 4.14. Cracking on the north side of the slab, Test 1

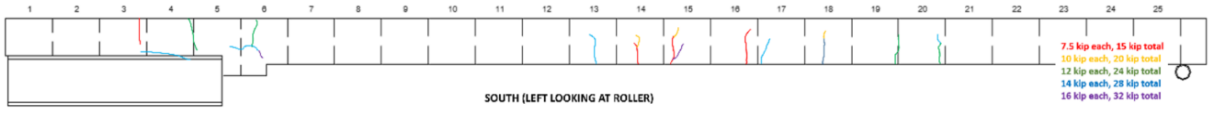

Figure 4.15. Cracking on the south side of the slab, Test 1

The sides of the specimens are labeled “North” (the right side when looking down the length of the slab from the roller) and “South” (the left side when looking down the length of the slab from the roller). As the figures show, the majority of the cracks on both sides were flexural cracks that

propagated from the bottom of the slab and that were concentrated at the middle of the approach slab.

Additional cracks formed in the concrete that surrounded the steel girder. A closeup of this cracking area can be seen in Figure 4.16.

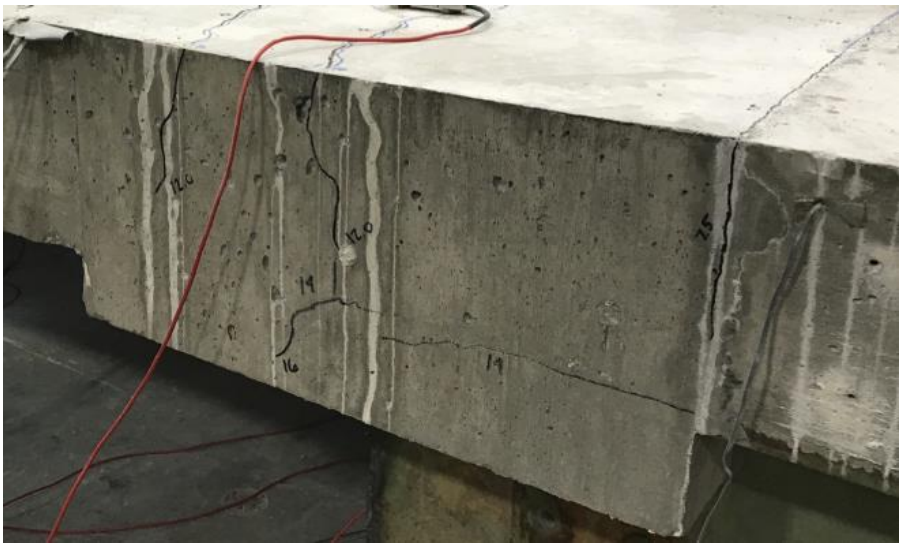

Figure 4.16. Cracking occurring in the concrete diaphragm section at the intersection with the steel girder, Test 1

Cracks from the top of the slab near the concrete diaphragm section also grew toward the side of the specimen.

4.3.1.2 Deflection

The load-displacement curve for the center of the approach slab, where the maximum moment occurred, can be seen in Figure 4.17.

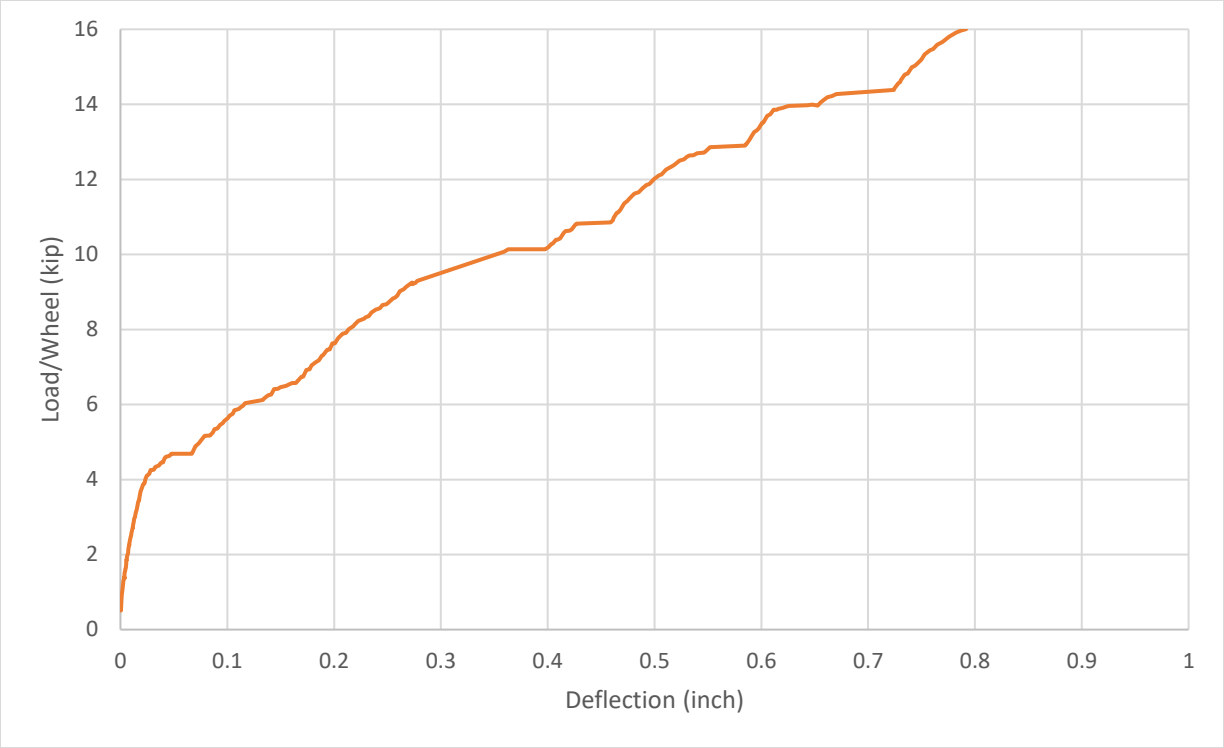

Figure 4.17. Load-deflection curve at midspan of the approach slab, Test 1

As the figure shows, the deflection becomes nonlinear after a loading condition of approximately 4 kips per tire area. However, the first visible crack occurred at the construction joint at 7.5 kips per loading area, after the point where the load-displacement curve becomes nonlinear. This discrepancy could be due to microcracking that was unable to be seen. This theory is supported by the strain data from the BDIs located in the area. At the truck loading condition, the maximum deflection experienced by the slab at midspan was approximately 0.8 in. It should be noted that the load-displacement curve is not smooth due to minor jolting experienced by the loading equipment when cracking occurred underneath in the approach slab.

Table 4.3 presents the deflection occurring along the specimen at the standard truck loading condition.

Table 4.3. Deflection along the length of the specimen at 16 kips per loading area, Test 1

Location, x (ft)	**0**	**4 ft 0 in.**	**10 ft 6 in.**	**15 ft 6 in. L**	**15 ft 6 in. R**	**15 ft 6 in. M**	**20 ft 6 in.**	**25 ft 0 in.**
Meter	D1	D2	D3	D4	D5	D6	D7	D8
Deflection (in.)	0.00	0.06	0.50	0.79	0.81	0.81	0.51	0.04

The locations are specified by distance from the end of the steel girders. As expected, those meters at the ends of the specimen experienced very little deflection compared to the rest of the specimen. However, a small rotation of the approach slab occurred at the roller support. At the

third points of the approach slab, the specimen experienced approximately 0.5 in. of deflection, shown by D3 and D7. Comparing the deflection along the width of the approach slab at midspan, it can be seen that the deflections are reasonably similar, indicating that loading was approximately symmetric.

The two main areas of interest within the specimen were near the concrete diaphragm and the approach slab, where the largest deflection and strains occurred. Therefore, the following two sections present the patterns of strain in these two areas.

4.3.1.4 Strains Near Concrete Diaphragm

Figure 4.18 shows the magnitudes of the strains existing within the reinforcing at standard truck loading.

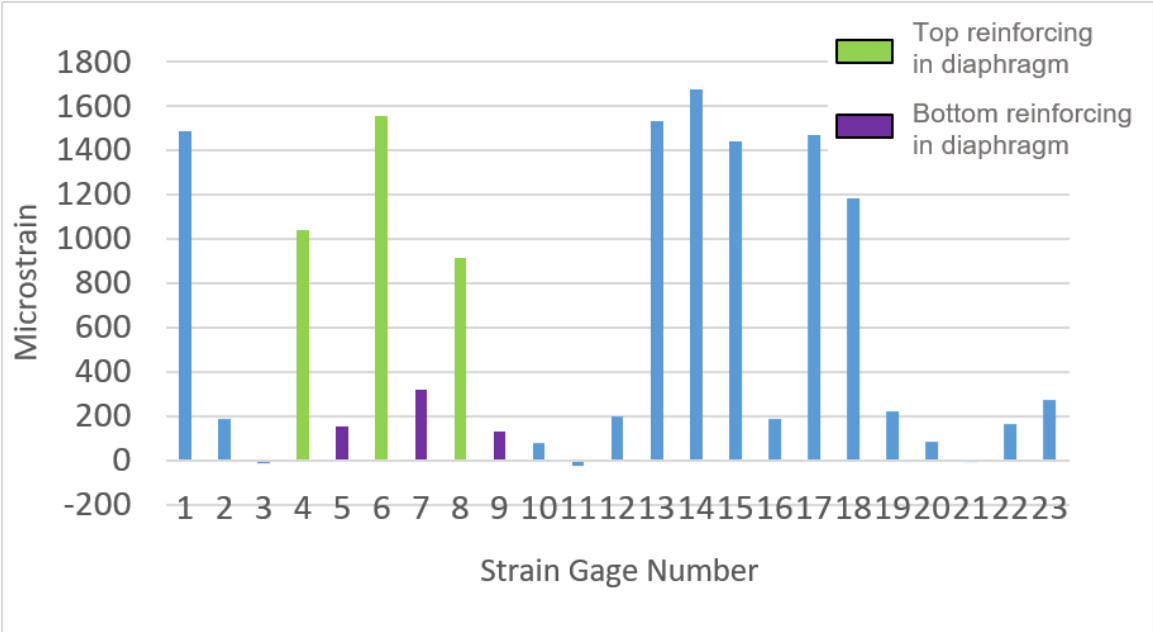

Figure 4.18. Magnitude of strain in the reinforcing at 16 kips per loading area, with a focus on the gages in concrete diaphragm, Test 1

The simple bar chart allows a direct comparison between locations of gages and allows patterns to be detected easily. Strain gages SG4, SG6, and SG8 were located on the top reinforcing in the concrete diaphragm and are highlighted in green in the figure. Strain gages SG5, SG7, and SG9 were in the same location but were placed on the bottom reinforcing. These gages are highlighted in purple. It can clearly be seen that the strain experienced by the top reinforcing in the diaphragm is substantially higher than the strain experienced by the bottom reinforcing. Strain gages SG2 and SG10 were also located in the concrete diaphragm on the top reinforcing but were on the outer longitudinal bars. It can be seen that the strain in these two areas was much smaller in comparison, perhaps due to the stiffness provided by the steel girders.

Figure 4.19 presents the strain experienced by the concrete gages on the top of the concrete diaphragm, and Figure 4.20 presents the strain experienced by the concrete gages on the bottom of the concrete diaphragm.

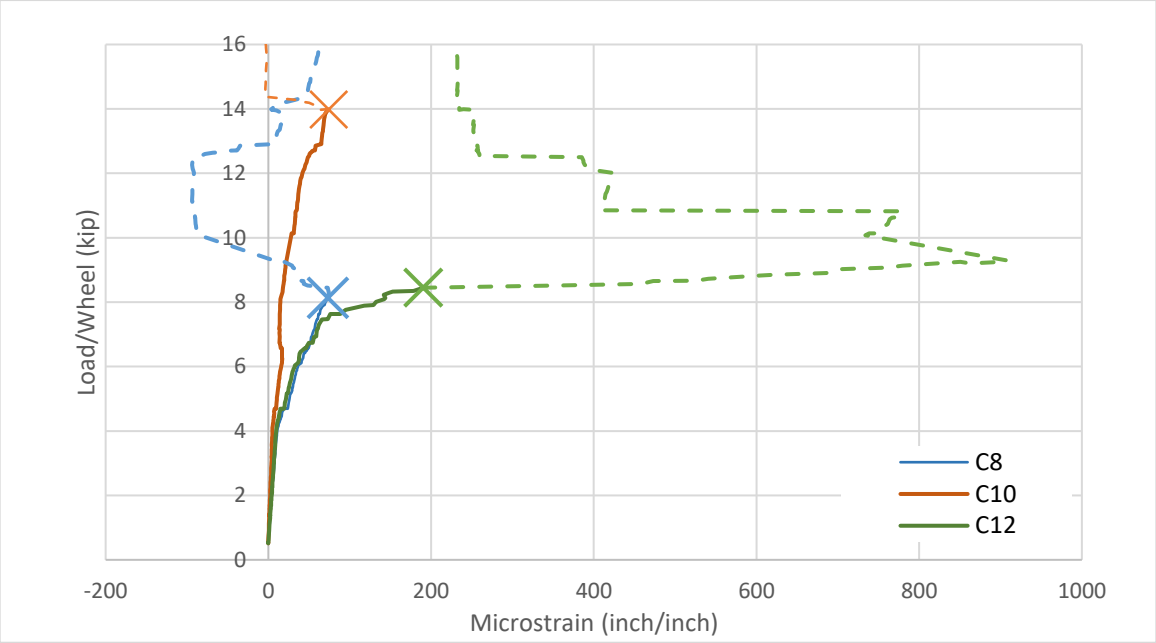

Figure 4.19. Load versus strain curve for BDIs on the top surface of the concrete diaphragm, Test 1

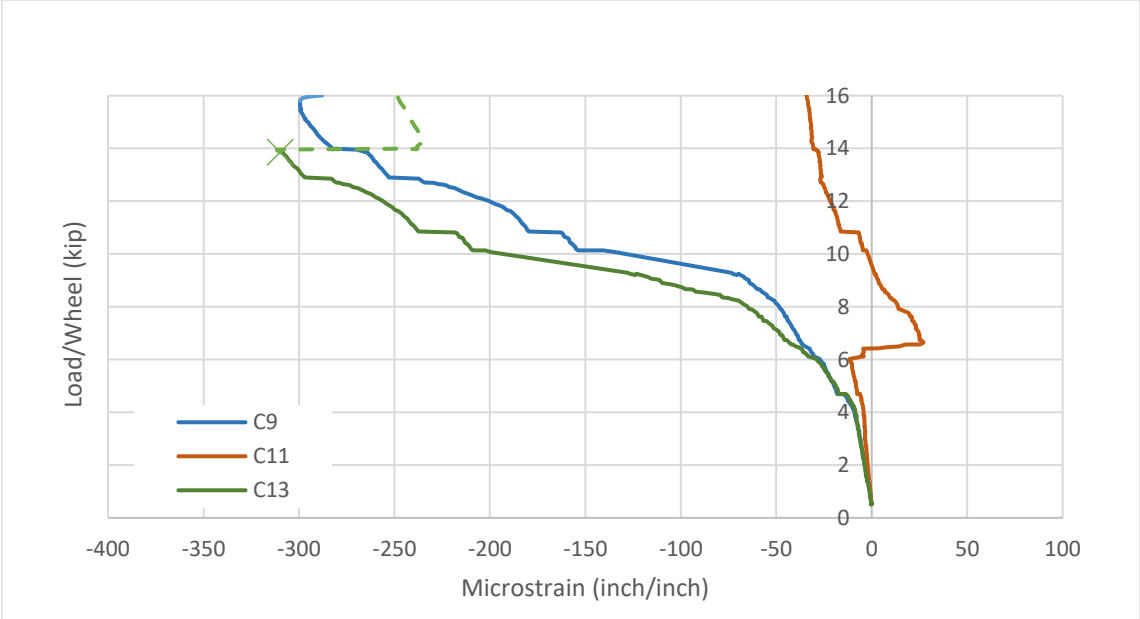

Figure 4.20. Load versus strain curve for BDIs on the bottom surface of the concrete diaphragm, Test 2

The *X* markings in the figures indicate the point at which cracking occurred near or underneath the gages, after which the data from the gages are not accurate. It is evident that cracking was experienced by the gages on the top of the concrete diaphragm, coinciding with the cracking pattern data. The majority of cracks occurred on the top of the deck at around 8 to 10 kips per wheel area. It is also evident that the top concrete gages, similar to the top reinforcing gages, experienced tension, as shown by the positive microstrain values. Conversely, the bottom concrete gages experienced compression, as shown by the negative microstrain values. This indicates that the concrete diaphragm experienced negative moment as the approach slab rotated into the steel girders.

4.3.1.4 Midspan of Approach Slab

Figure 4.21 presents the magnitude of strain in the reinforcing at 16 kips per wheel.

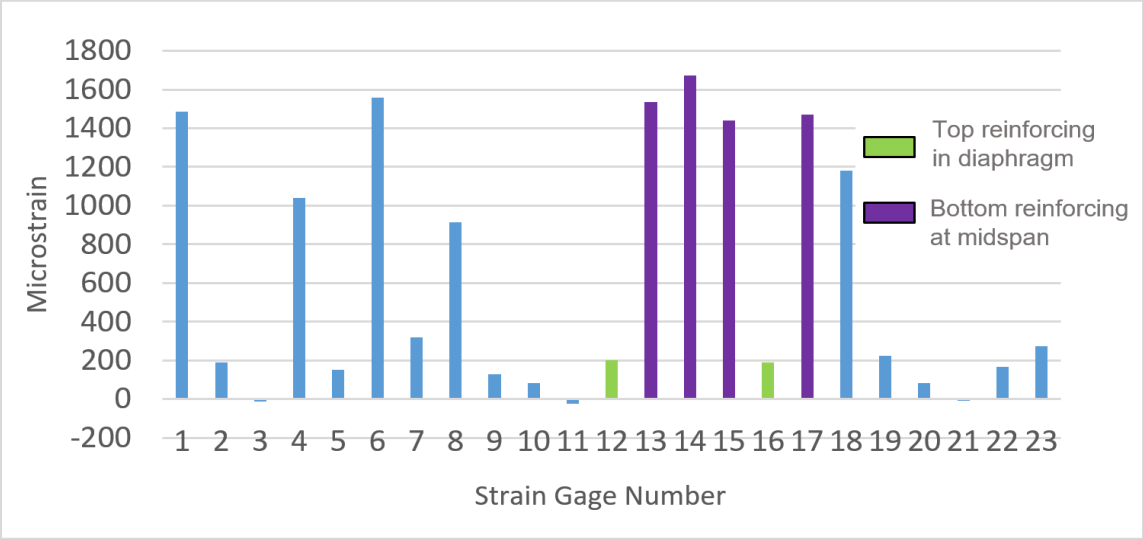

Figure 4.21. Magnitude of strain in reinforcing at 16 kips per loading area, with a focus on the gages at the midspan of the approach slab, Test 1

The bars shown in purple represent the magnitude of strain on the bottom reinforcing, and those shown in green represent the strain on the top reinforcing. It can be seen that with the large positive moment, the top reinforcing was engaged in tension at the midspan. Overall, in comparing the strains at this location to all other locations, it is clear that the midspan of the approach slab experienced the largest strains, as expected.

The concrete gages at the midspan and second third point of the approach slab experienced compression for the duration of loading in Test 1. However, the first third point of the approach slab switched from experiencing compression to experiencing tension on the top, though the amount of tension was very minor. This correlates with a switch from a region of positive moment to a region of negative moment and correlates with previously presented data. Figure 4.22, Figure 4.23, and Figure 4.24 present the data for these strain gages.

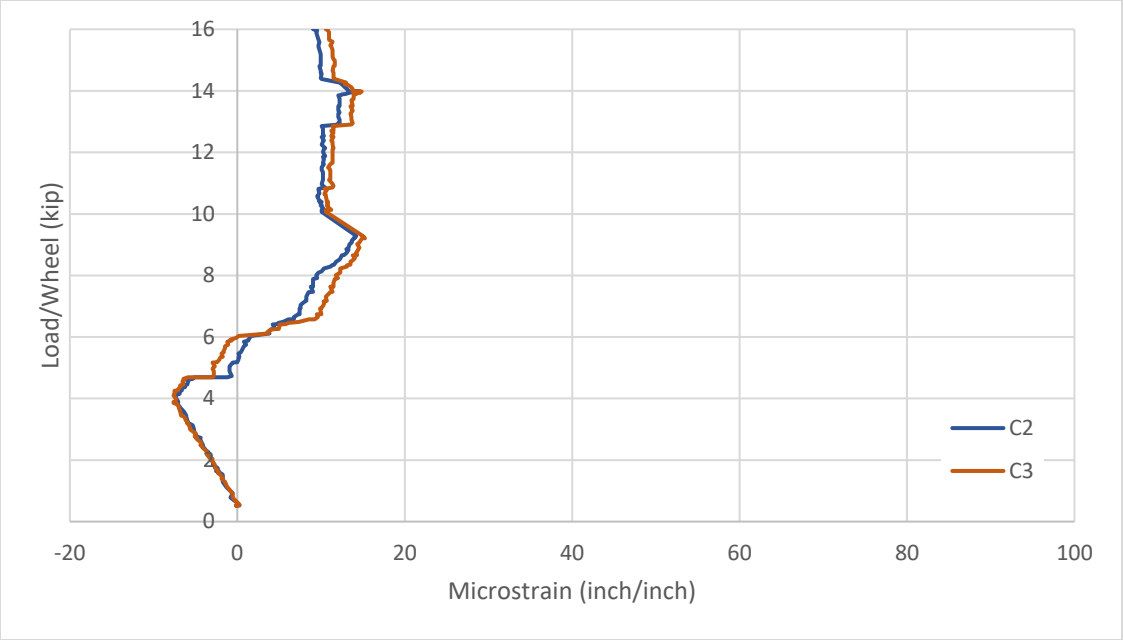

Figure 4.22. Load versus strain for BDIs at the first third point on the approach slab, Test 1

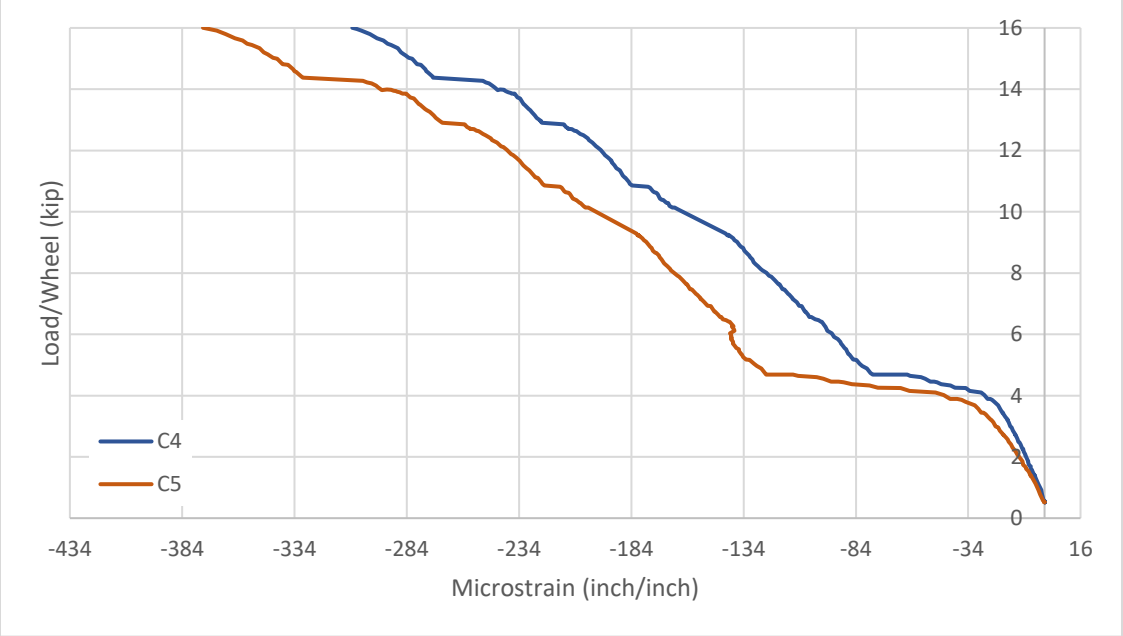

Figure 4.23. Load versus strain for BDIs at the midspan on the approach slab, Test 1

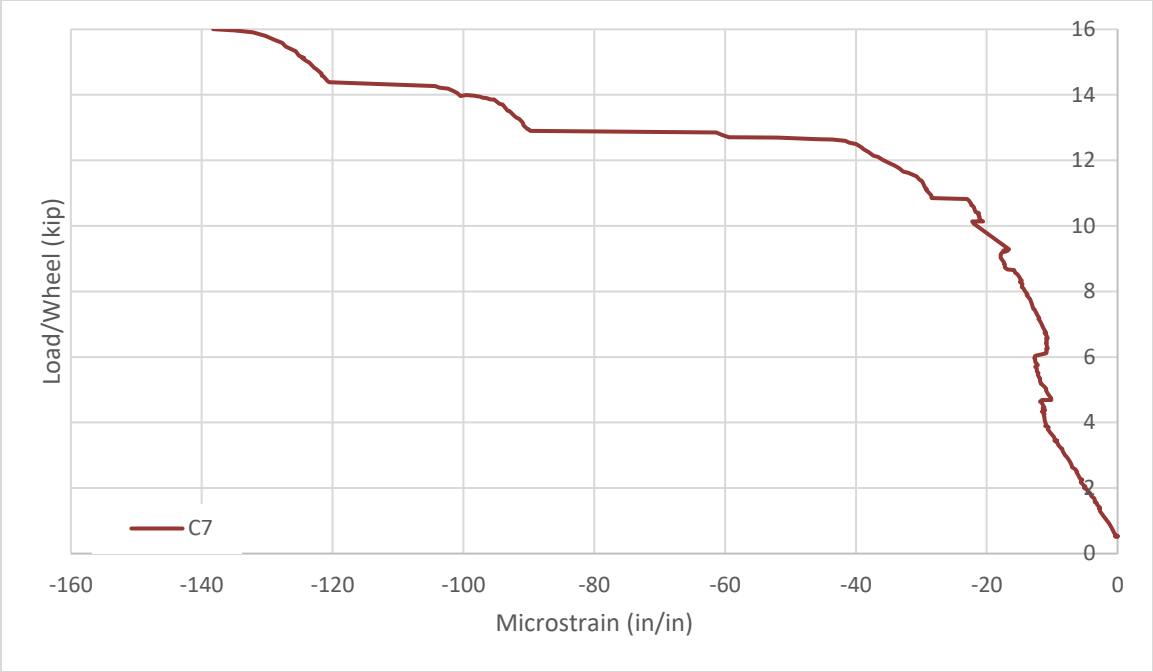

Figure 4.24. Load versus strain for BDIs at the second third point on the approach slab, Test 1

4.3.2 Test 2 Results

In Test 2, a hard support representing the backwall was inserted approximately 3 in. from the end of the diaphragm section. Above the middle of this backwall, the top longitudinal reinforcing was cut. Additionally, during Test 2, the specimen was loaded until failure. The loading pattern was similar in nature to that used in Test 1 and is shown in Figure 4.25.

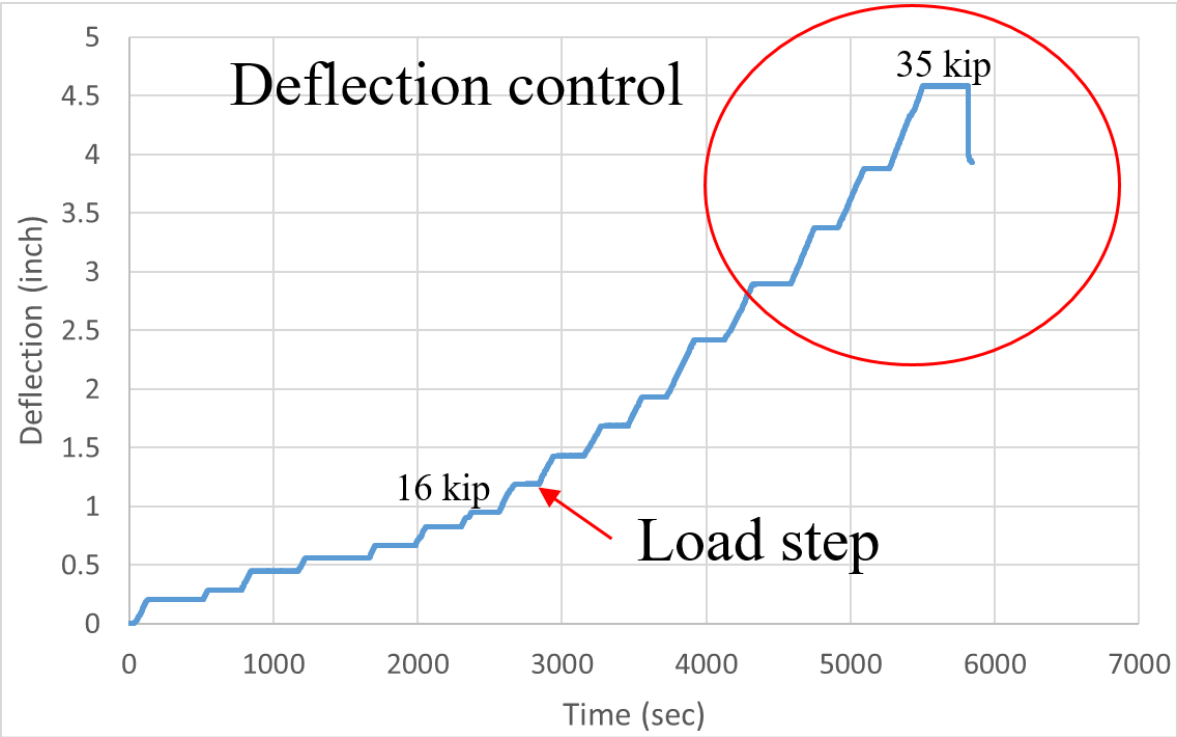

Figure 4.25. General loading with load steps for Test 2

Toward the end of testing, deflection control was utilized, as indicated in the figure. Because Test 2 was completed on an already tested and cracked specimen, it is important to note that the Test 2 values cannot be directly compared to those values obtained from Test 1. It would not make sense to compare strain values directly because residual stress could have been left in the reinforcing bars after Test 1 was complete, even if the bars did not yield. However, the patterns between the two tests can be compared and conclusions can be drawn on that basis.

4.3.2.1 Cracking Patterns

During Test 2, no new cracks formed on the top of the specimen. While cracking was already present in the diaphragm and bridge deck sections from Test 1, it is presumed that the presence of the saw cut created a release for the stress from the negative moment (Figure 4.26).

Figure 4.26. Saw cut at the top of the approach slab through the top reinforcing in preparation for Test 2

Therefore, if Test 2 were completed on a specimen that had not been previously tested, it is assumed that cracking would still not occur on the top of the specimen. This assumption was verified using finite element software, as presented in Section 4.4.

Because the specimen was tested until failure during Test 2 and cracks were already present from Test 1, cracking patterns were not recorded underneath the slab due to the safety risks posed. However, from both visual and audible inspection near the specimen, it was clear that additional cracking occurred on the bottom of the approach slab. Cracks that formed during Test 2 could have formed from either opening, propagation, or branching of the cracks formed during Test 1 or from the development of new stress areas. A better understanding of the cracks that formed on the bottom of the approach slab during Test 2 can be achieved by examining those cracks that occurred on the sides of the specimens, shown in Figure 4.27 and Figure 4.28.

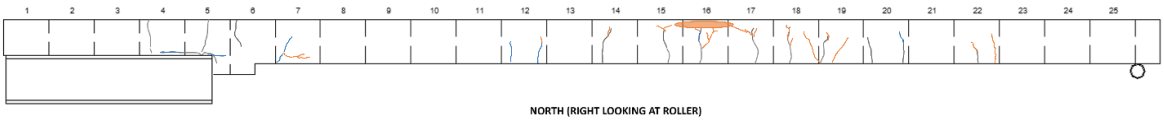

Figure 4.27. Cracking on the north side of the slab, Test 2

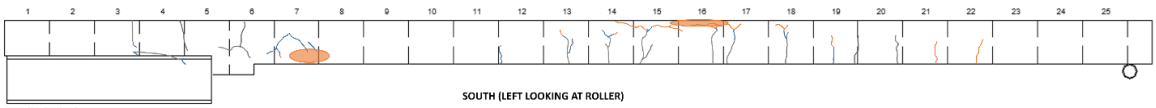

Figure 4.28. Cracking on the south side of the slab, Test 2

Those cracks that were already present from Test 1 are shown in gray. Those cracks that formed before or at 16 kips per loading area are shown in blue, and those cracks that occurred after this loading condition until failure are shown in orange. Shaded, circled orange areas indicate that the area experienced significant crushing or spalling of the concrete.

As the figures show, many of the cracks that formed on the sides of the slab during Test 1 propagated during Test 2, specifically those occurring from grid sections 14 through 20. The cracks that had previously extended approximately half of the thickness of the approach slab grew very close to the top of the slab.

An example of this behavior can be seen in Figure 4.29.

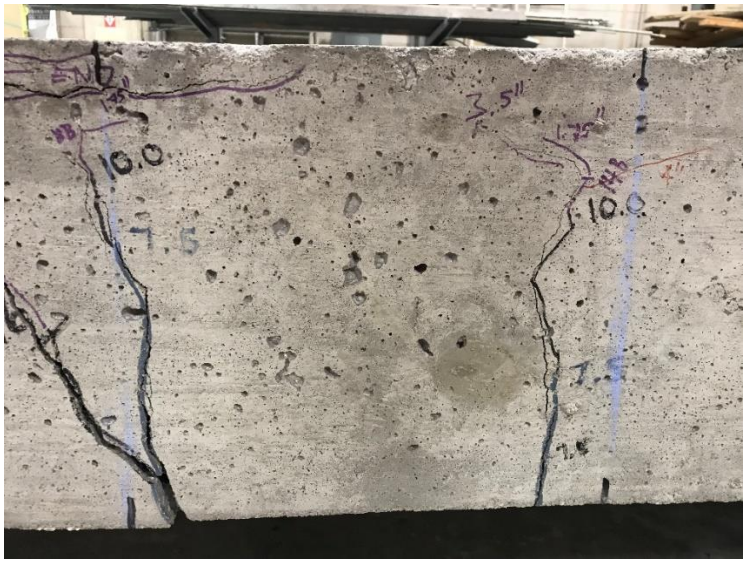

Figure 4.29. Propagation of cracks occurring near midspan of approach slab, Test 2

Additional cracks that formed during Test 2 near this area mainly occurred at higher loads. However, it can be seen that on both sides of the slab, additional cracks formed at or prior to the standard truck load within grid section 12. New cracks also formed on the other side of the loading area, in grid sections 20 through 22. However, these cracks formed after the standard truck load. Similar to those cracks formed during Test 1, it can be assumed that the new cracks that formed during Test 2 on the side of the specimen at midspan of the approach slab also exist on the bottom of the approach slab across the width of the specimen.

From grid sections 15 through 17, it can be seen that the concrete experienced considerable damage. At failure, the entire width of the approach slab experienced crushing. This can be seen in Figure 4.30.

Figure 4.30. Crushing occurring at the midspan of the approach slab at failure, Test 2

Before failure, several cracks grew towards this location as the load increased. However, because failure during Test 2 occurred at approximately 35 kips on each loading area, there is no concern that this type of crushing would occur on real bridge structures.

The most significant cracking, other than the cracking experienced at the midspan of the approach slab, occurred underneath the saw cut made above the hard support. As seen in Figure 4.27 and Figure 4.28, this saw cut occurs approximately in the middle of grid section 7. Cracks started forming underneath this saw cut at 7.5 kips per loading area, less than half of the standard truck load. Figure 4.31 shows the progression of cracks in this area as load was applied.

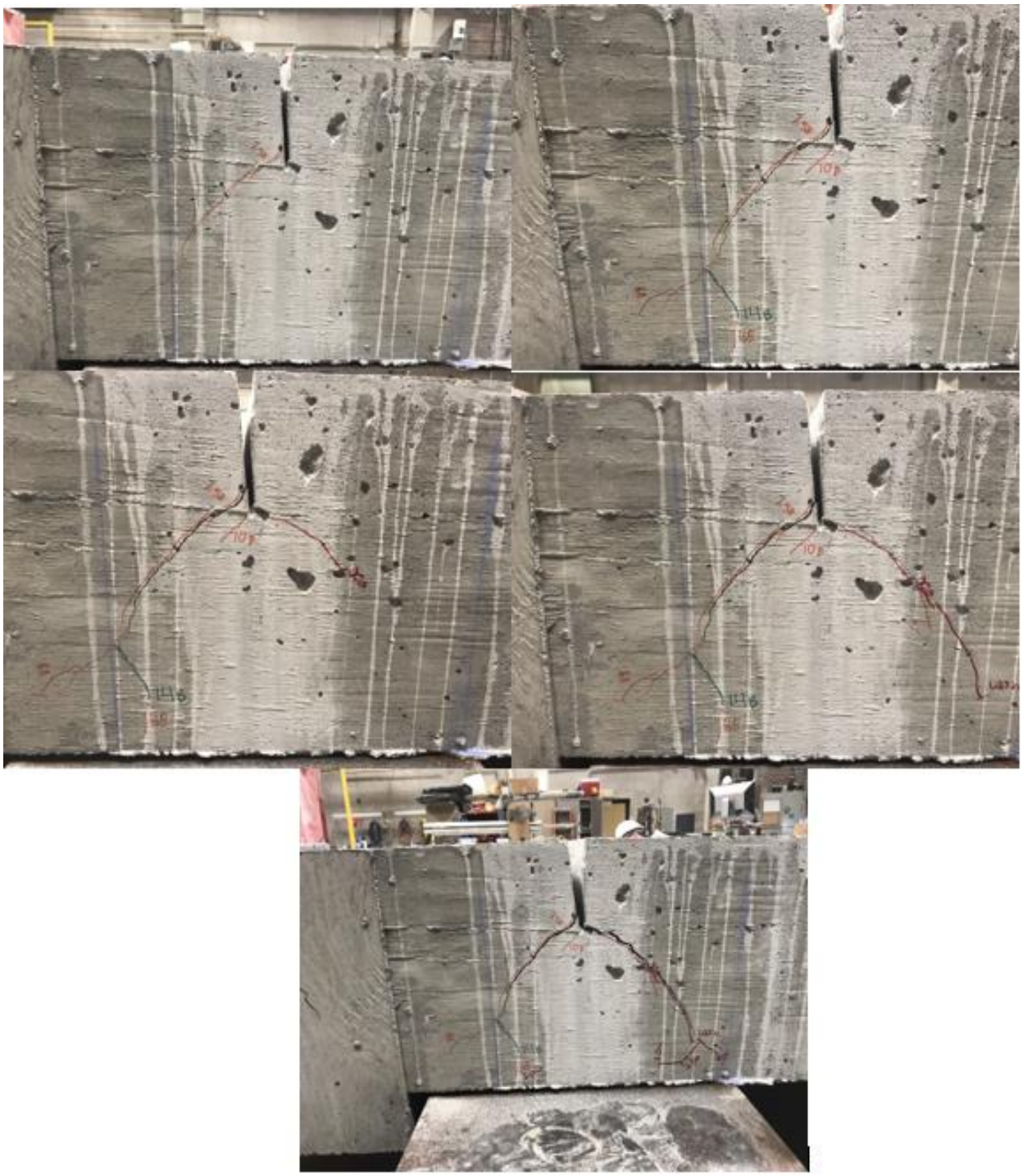

Figure 4.31. Sequence showing the propagation of cracking occurring above the hard support until failure, Test 2

As the figure shows, cracks developed on either side of the joint, progressing toward the bottom of the slab. Both the lengths and widths of these cracks were noticeable. Throughout loading, some cracks opened up more than ¼ in. This area could be a point of concern when using a similar detail in the future.

4.3.2.2 Deflection

Figure 4.32 shows the load-deflection curve for the specimen during Test 2.

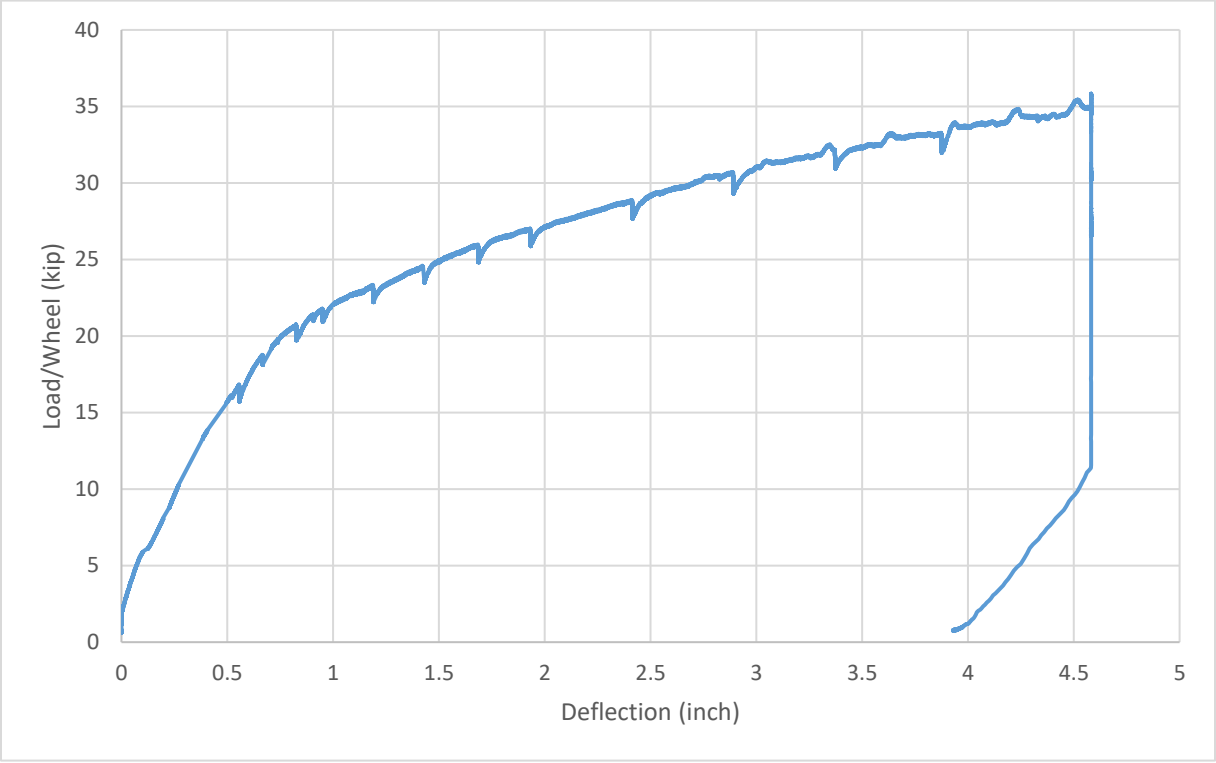

Figure 4.32. Load-deflection curve at the midspan of the approach slab, Test 2

As the figure shows, the deflection until standard truck loading is fairly linear due to the cracking already present from Test 1.

Figure 4.33 shows the deflection along the length of the curve at both the standard truck loading condition and failure.

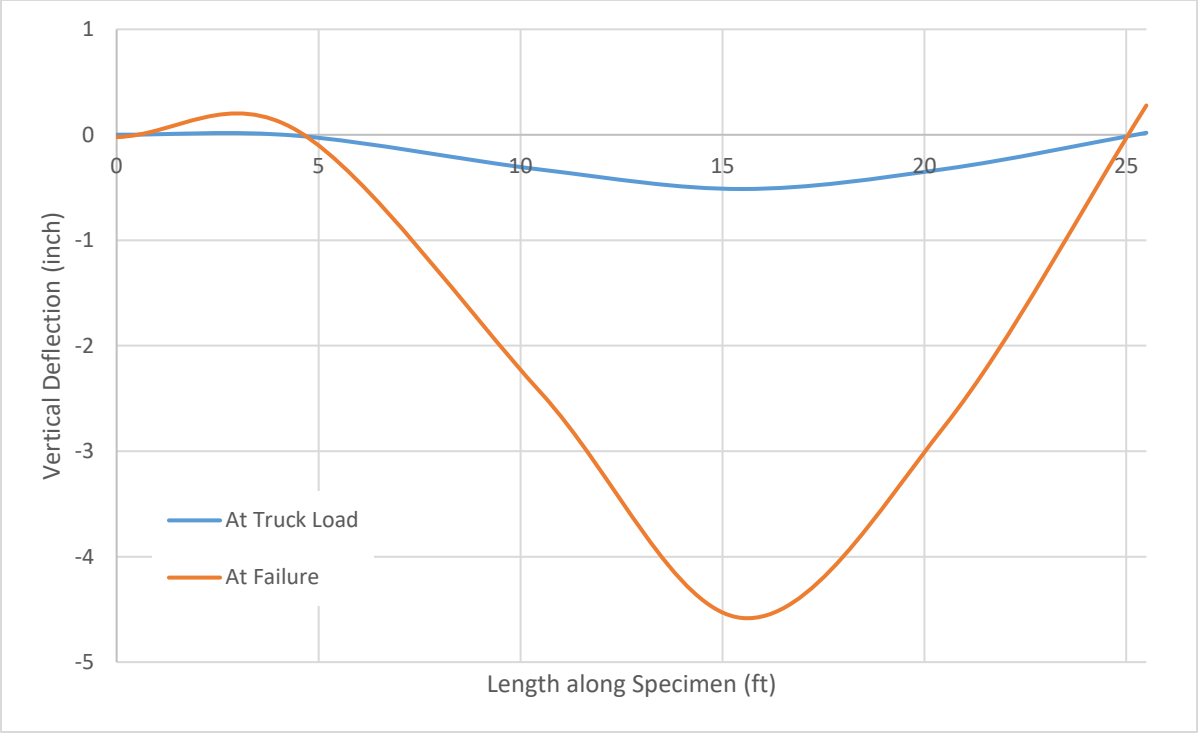

Figure 4.33. Deflection along the length of the specimen at the truck loading condition and failure, Test 2

As expected, in both conditions, the largest deflection occurred at the midspan of the approach slab where the load was being applied. The largest deflection that occurred is approximately ½ in. during standard truck loading. Similar to Test 1, the end of the approach slab resting on the roller support experienced upward displacement due to the curvature of the specimen.

At failure, the deflection encountered at the midspan of the approach slab increased dramatically to more than 4½ in. Due to this large deflection, the approach slab end rotated an additional amount, and the end with the roller experienced a horizontal displacement of more than ¼ in. The horizontal movement associated with the slab deflecting on the roller can be seen in Figure 4.34.

Figure 4.34. Horizontal movement of the slab at the roller support, Test 2

A side view of the deflection of the specimen and the rotation at the beginning of the approach slab can be seen in Figure 4.35.

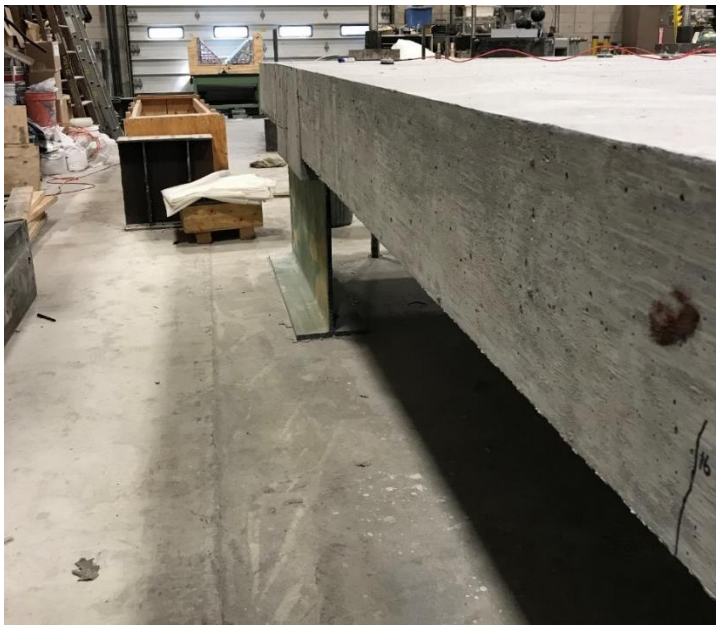

Figure 4.35. Side view of the deflection of the specimen and the rotation at the beginning of the approach slab, Test 2

4.3.2.3 LVDTs

LVDTs were utilized during Test 2 to monitor how far the saw cut opened during loading. Three displacement meters were placed along the width of the crack: two on the outer edges and one at the center. At the standard truck loading of 16 kips per wheel, the saw cut at the center of the width of the specimen had widened by 0.03 in., and the outer edges of the saw cut widened by an average of approximately 0.06 in. When the slab failed at more than 35 kips per loading area, the middle of the cut had widened by approximately 0.28 in., and the two sides had widened by more than 0.64 in.

4.3.2.4 Strains Near Concrete Diaphragm

Because the top reinforcing was cut in Test 2, strain gages SG2, SG4, SG6, SG8, and SG10 were removed because they had been placed at the location of the cut. Figure 4.36 shows the magnitudes of the remaining strain gages on the concrete diaphragm.

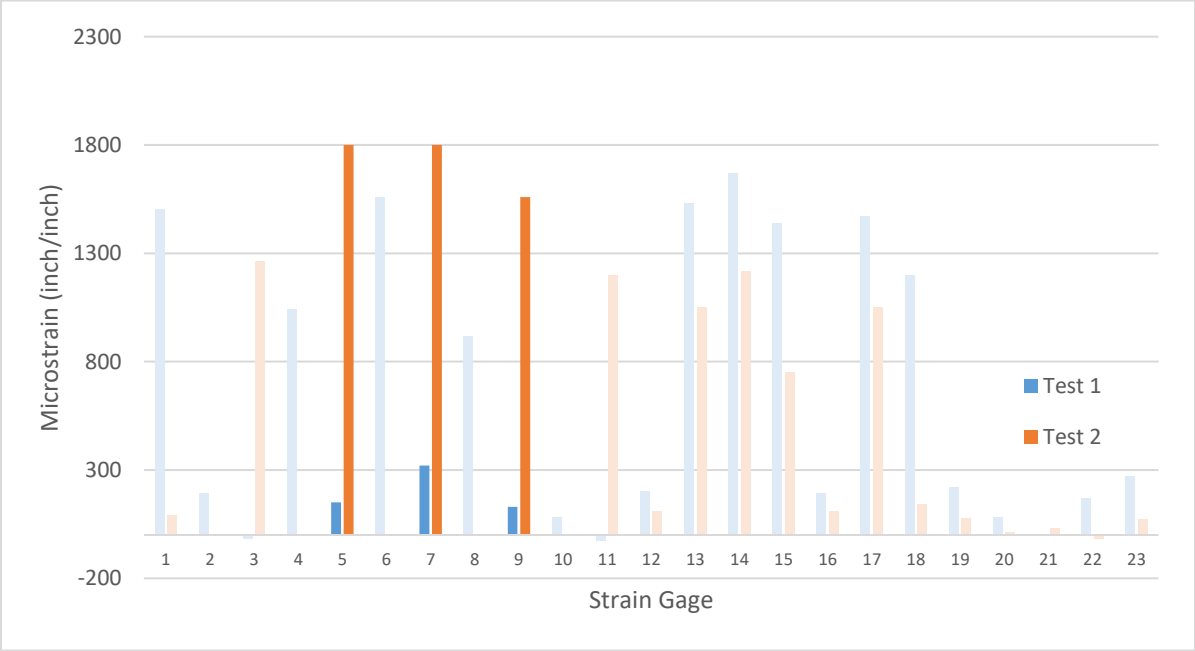

Figure 4.36. Reinforcing strain gage magnitudes at 16 kips per loading area

The bottom reinforcing gages are highlighted. As the figure shows, the bottom reinforcing in the diaphragm experienced the largest tensile strain in the specimen during Test 2. Because the top reinforcing was cut, the bottom reinforcing was forced to take additional stress.

Figure 4.37 and Figure 4.38 show the strain experienced by the concrete in the diaphragm during loading up to 16 kips per loading area.

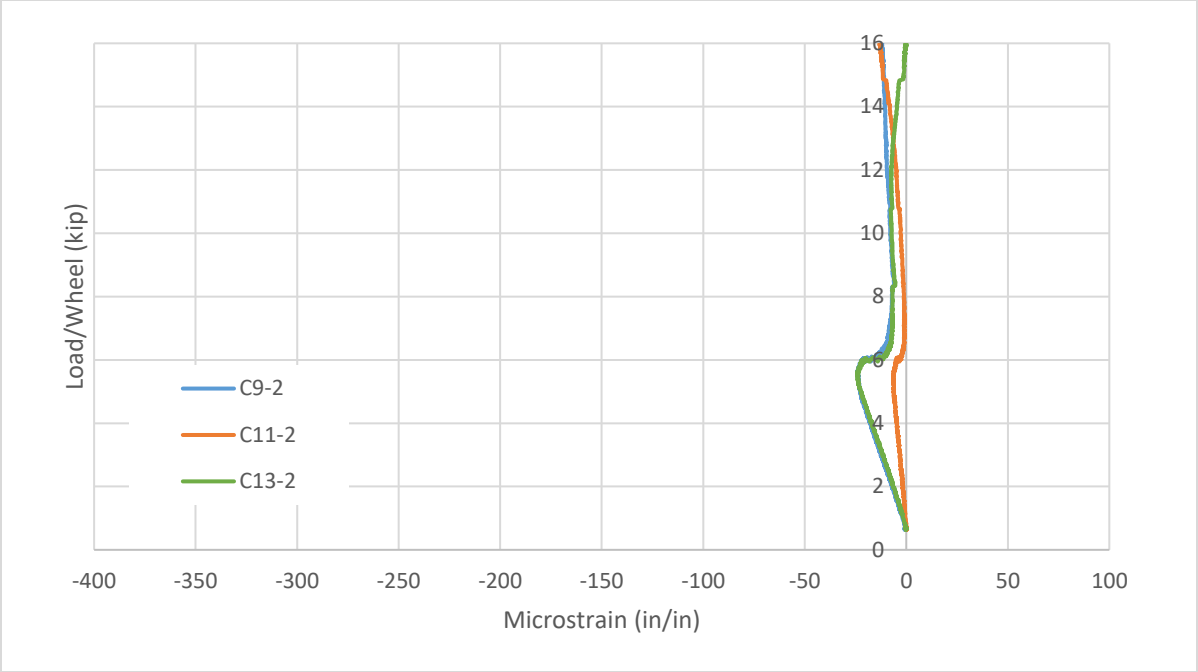

Figure 4.37. Load versus strain curve for BDIs on the bottom surface of the concrete diaphragm, Test 2

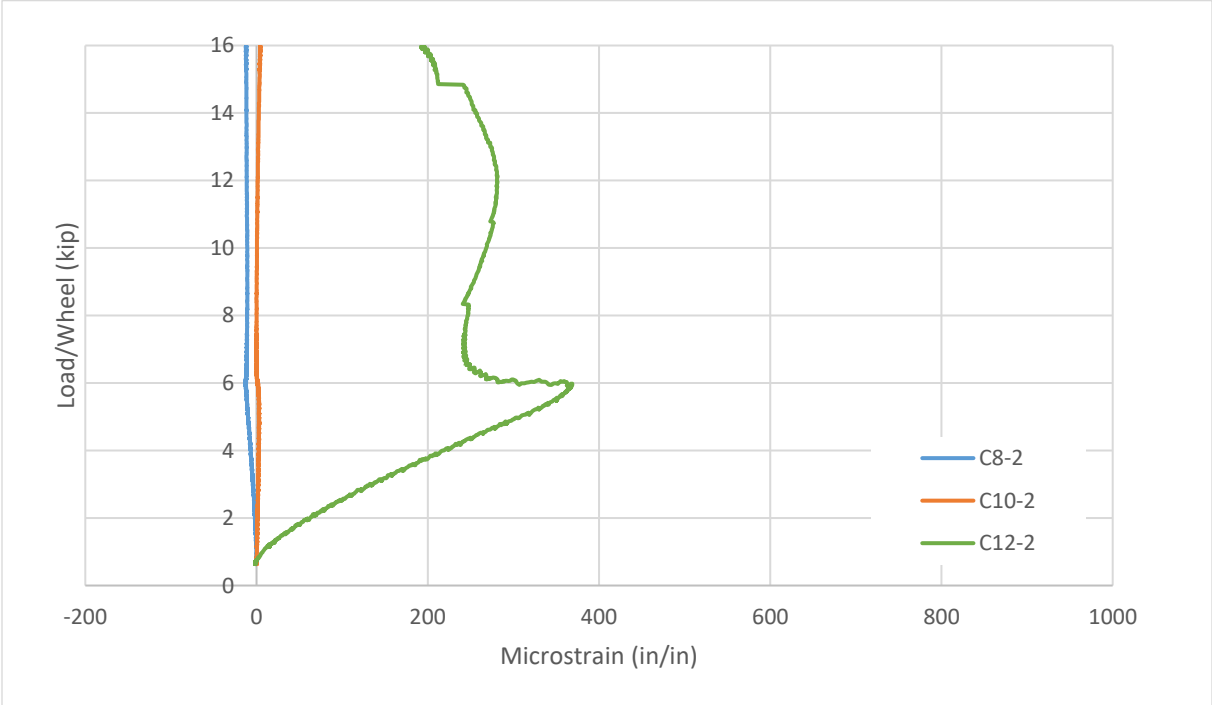

Figure 4.38. Load versus strain curve for BDIs on the top surface of the concrete diaphragm, Test 2

As the figures show, very little strain was experienced by the concrete on either the top or the bottom of the specimen. Unlike in Test 1, due to the presence of the saw cut very little strain was felt in the diaphragm section past the cut in the reinforcing.

The minimal strain experienced by the diaphragm is also shown in Table 4.4, which presents the strain felt by the reinforcing gages at 16 kips per loading area during Test 1 and Test 2.

Table 4.4. Comparison of continuity of strain in the reinforcing in Test 1 and Test 2 in the concrete diaphragm section

Reinforcing Gage	Location	Test 1 Microstrain	Test 2 Microstrain
2	Outer reinforcing, above support	200	-
18	Outer reinforcing, past support	1,560	140
6	Middle reinforcing, above support	1,640	-
20	Middle reinforcing, past support	100	10
10	Outer reinforcing, above support	100	-
22	Outer reinforcing, past support	400	-10

Gages SG2, SG6, and SG22 existed above the hard support during Test 1 and therefore were cut during Test 2. Gages SG18, SG20, and SG22 existed on the same reinforcing bar past the hard support. Therefore, by comparing gages SG2 and SG18, SG6 and SG20, and SG10 and SG22, the continuity of strain in the two tests can be seen. As Table 4.4 shows, the reinforcing past the hard support experienced very little strain in Test 2 compared to Test 1.

4.3.2.4 Midspan of Approach Slab

As expected, the reinforcing strain gages at the midspan of the approach slab experienced less strain during Test 2 than Test 1 due to the shortened effective length of the approach slab with the presence of the hard support. With the shortened length, the positive moment caused by the load at midspan was minimized. At the standard truck loading, gages SG14 and SG15, the gages in the center of the slab, experienced an average of 1,555 microstrain.

The concrete gages on the top of the approach slab at midspan experienced similar compressive strains to those observed during Test 1. However, differences in the concrete strain at the third points are evident when comparing the results for Test 1 and Test 2. Table 4.5 presents these differences.

Table 4.5. Concrete strain along approach slab at standard truck loading, Test 1 and Test 2

Concrete Gage	Location	Test 1 Microstrain	Test 2 Microstrain
2/3	First third point	10	-150
4/5	Midspan	-210	-260
6/7	Second third point	0	0

As the table shows, the first third point of the approach slab is in tension due to the negative moment in Test 1. However, because of the presence of the hard support and the cut in the top reinforcing, the entirety of the approach slab was in positive moment in Test 2, causing the first third point to experience compression.

4.4 Finite Element Modeling

Two finite element models were developed for comparison with the laboratory results, each model corresponding to either the Test 1 or Test 2 conditions. A brief overview pertaining to the characteristics of the finite element models is provided next.

4.4.1 Finite Element Model Characteristics

4.4.1.1 Element Types

To model the geometry of the laboratory specimens, three-dimensional solid shapes were used for the concrete slab and steel girders. The steel reinforcing was modeled using wire shapes, with an associated cross-sectional area that matched that of the #5 or #6 reinforcing steel bars where applicable. Hex elements were utilized for the three-dimensional shapes to ensure accurate results and reduce computational time. A linear 3D truss element was utilized to model the wire elements. A mesh size of 2 in. was utilized to model all parts.

4.4.1.2 Material Properties

4.4.1.2.1 Concrete

The elastic material properties for the concrete included the mass density, Poisson's ratio, and modulus of elasticity. The mass density was based on a typical density of 150 lb/ft^3. The modulus of elasticity was based on an average compressive strength of 5.2 ksi, obtained from cylinder tests completed at the time of testing. The lower of the strengths from the bridge deck and the approach slab was used. Hsu and Hsu (1994) stated that the ACI 318-14 building code overestimates the modulus of elasticity with the typical equation $57{,}000\sqrt{f'_c}$. Therefore, an adjusted modulus of elasticity was used.

$$E_0 = 1.2431 * 10^2 f'_c + 3.28312 * 10^3 \quad \textbf{(1)}$$

Using this equation, the modulus of elasticity utilized in the model was 3,919.1 ksi. The Poisson's ratio was taken as 0.15.

Hsu and Hsu's (1994) model was used to generate the nonlinear stress-strain behavior for the concrete. Unlike other models developed, Hsu and Hsu's (1994) model only relies on the compressive strength of the concrete. As shown in Figure 4.39, concrete follows a linear stress-strain relationship corresponding to its maximum compressive strength, f'_c.

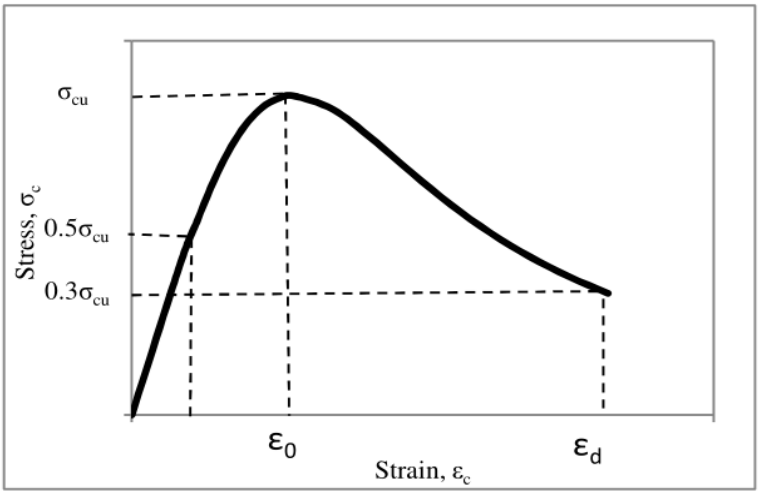

Hsu and Hsu 1994

Figure 4.39. Compression stress-strain curve

Hsu and Hsu's (1994) model begins at $0.5f'_c$ and ends when the stress descends to $0.3f'_c$. Between these points, equation (6) describes the compressive stress values:

$$f_c = \left(\frac{\beta\left(\varepsilon_c/\varepsilon_o\right)}{\beta-1+\left(\varepsilon_c/\varepsilon_o\right)}\right)f'_c \quad \textbf{(6)}$$

where

$$\beta = \frac{1}{1-\left[f'_c/\varepsilon_o E_o\right]} \quad \textbf{(7)}$$

and

$$\varepsilon_o = 8.9 * 10^{-5} f'_c + 2.114 * 10^{-3} \quad \textbf{(8)}$$

The inelastic strain of the concrete, ε_c^{in}, is equivalent to the total strain, ε_c, minus the elastic strain, calculated as follows:

$$\varepsilon_c^{in} = \varepsilon_c - \frac{f'_c}{E_o} \quad \textbf{(9)}$$

A damage factor was be used to represent the degradation of the elastic stiffness of the system and is calculated using the following equation:

$$d = 1 - \frac{f_c}{f'_c} \quad \textbf{(10)}$$

The relationship between the elastic modulus and the compressive damage factor is as follows:

$$E = (1 - d)E_o \quad \textbf{(11)}$$

To capture the tension stiffening in the concrete, the Nayal and Rasheed (2006) model, modified by Wahalathantri et al. (2011), was used. Similar to the concrete compressive parameters, both the nonlinear stress-strain behavior and the tensile damage were defined. Figure 4.40 shows the tensile behavior of the concrete.

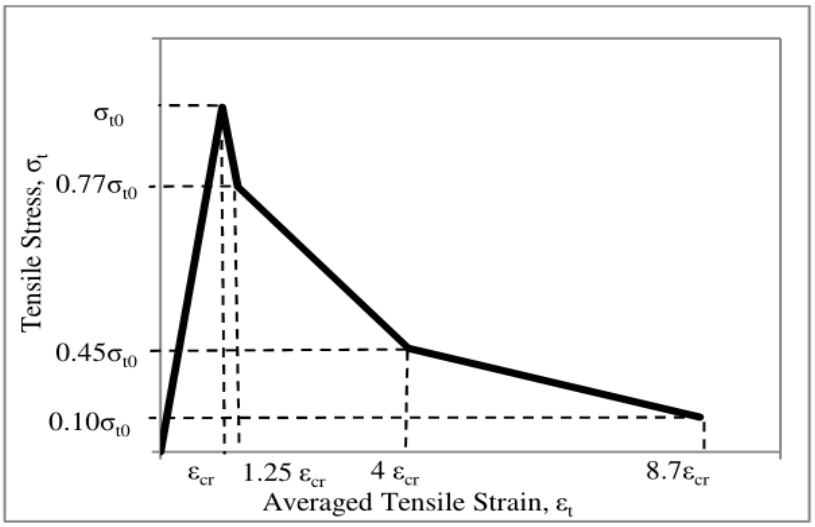

Wahalathantri et al. 2011

Figure 4.40. Tension stress-strain curve

The concrete behavior is linear until reaching the maximum tensile stress, f_{to}, corresponding to the cracking strain, ε_{cr}. Then, the stress decreases until $0.77f_{to}$, corresponding to $1.25\varepsilon_{cr}$. The stress decreases additionally to $0.45f_{to}$, corresponding to $4\varepsilon_{cr}$, until reaching $0.1f_{to}$, corresponding to $8.7\varepsilon_{cr}$. The maximum tensile stress was calculated using $7.5\sqrt{f'c}$ and Hooke's Law. The tension damage parameters were calculated in a fashion similar to that for the compression parameters.

Figure 4.41 describes the relationship between the compressive and tensile stress and the compressive and tensile damage, respectively.

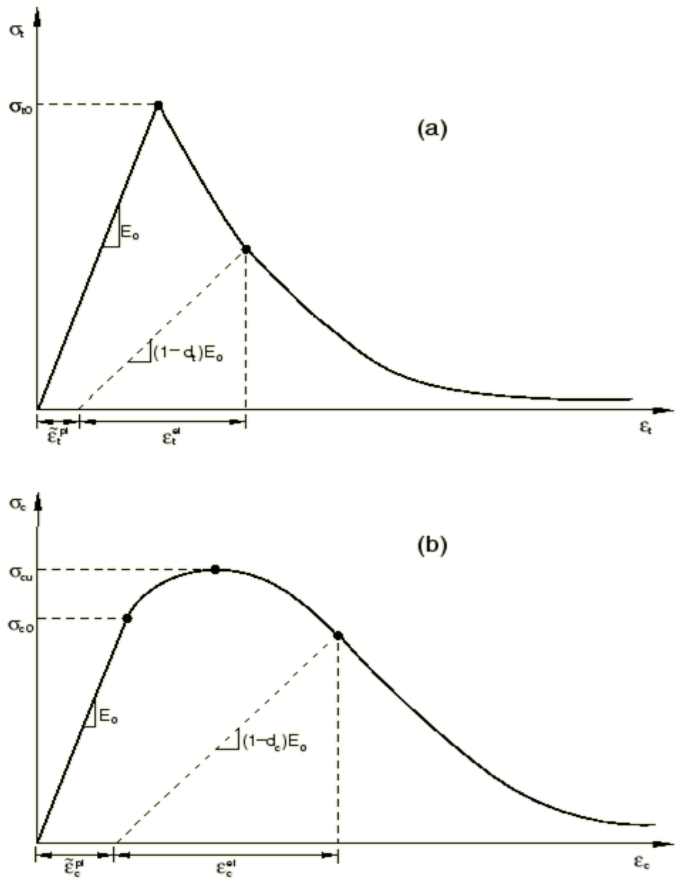

Dassault Systemes SIMULIA Abaqus 2013

Figure 4.41. Relationship between tension (a) and compression (b) stress-strain response and damage

In addition to the stress-strain tension and compression models, the following properties were utilized in the FE model:

- Dilation angle: 31°
- Eccentricity: 0.1
- Ratio of biaxial strength to uniaxial strength, f_{bo}/f_{co}: 1.16
- Ratio of the second stress invariant on tensile meridian, K: 0.667
- Viscosity parameter: 0.0005

4.4.1.2.2 Steel

Only elastic properties were defined for the reinforcing steel and the steel girders because both of these components were expected to stay in their elastic range during testing. A modulus of elasticity of 29,000 ksi and a Poisson's ratio of 0.19 was utilized for both.

4.4.1.3 Boundary Conditions and Constraints

The boundary conditions were the same in both FE models. As shown in Figure 4.42, the bottoms of the steel girders were fixed.

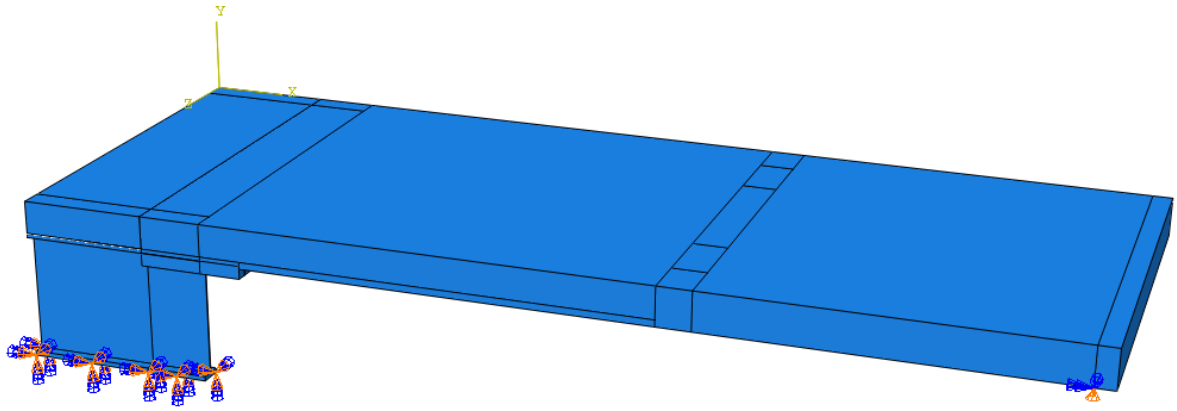

Figure 4.42. Boundary conditions in both the Test 1 and Test 2 FE models

Six inches in from the edge of the approach slab, a boundary condition restrained movement in the y direction, simulating a roller support.

Constraints were added to both models by tying the top of the steel girder to the bottom of the concrete resting against those girders. This is shown in Figure 4.43.

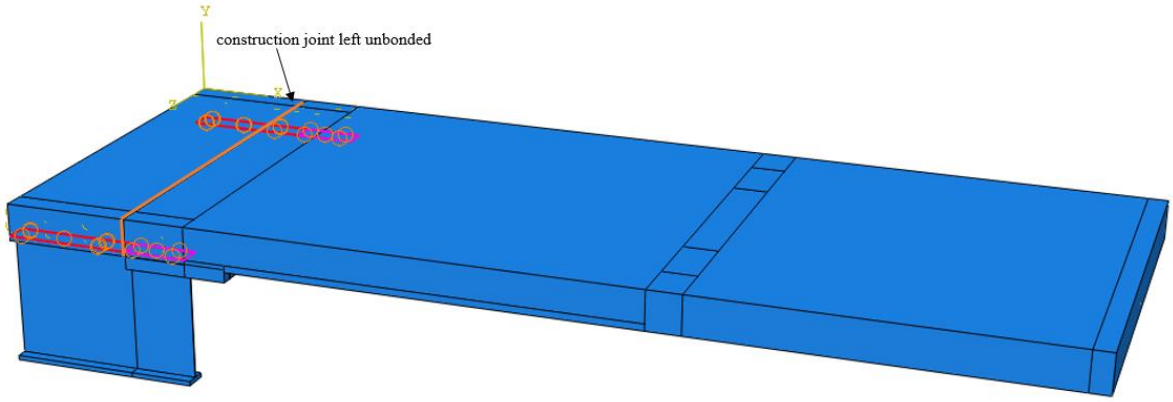

Figure 4.43. Constraints and the unbonded construction joint in the FE model

Additionally, the reinforcing was embedded into the concrete element.

For Test 2, a hard support was inserted under the approach slab, and the top concrete cover and reinforcing steel was cut centered above the support. The edge of the hard support was constrained to the bottom of the approach slab as shown in Figure 4.44.

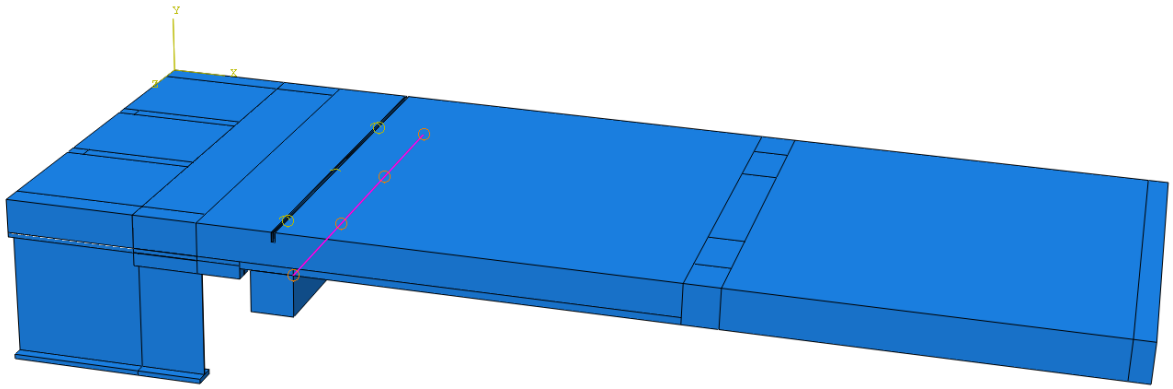

Figure 4.44. Test 2 FE model with added elements

The bottom of the hard support was fixed, preventing it from moving translationally or rotationally. Besides these changes for Test 2, all other constraints and boundary conditions were kept the same as in Test 1.

4.4.2 FE Model versus Experimental Results

Figure 4.45 shows the deflection along the length of the span for the FE model compared to the results for Test 1.

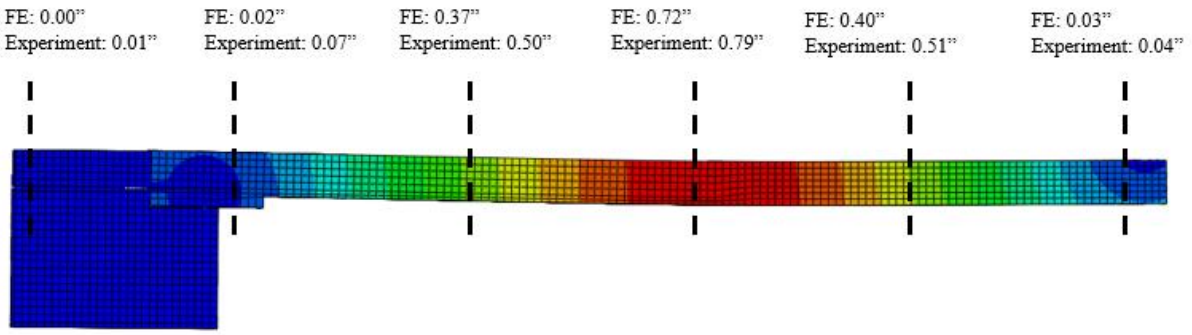

Figure 4.45. Comparison between the FE model and the experimental results for deflection along the length of specimen, Test 1

As the figure shows, the results for Test 1 are fairly consistent with the FE model throughout. With these consistent results, more accurate results can be confidently inferred by simulating Test 2 with further FE analyses. Such FE simulations may produce more credible results in comparison to the laboratory test using the cracked specimen.

Cracking patterns in the finite element model are shown through tensile damage parameters. Cracking patterns for the FE models of the specimen are presented in Figure 4.46 through Figure 4.49.

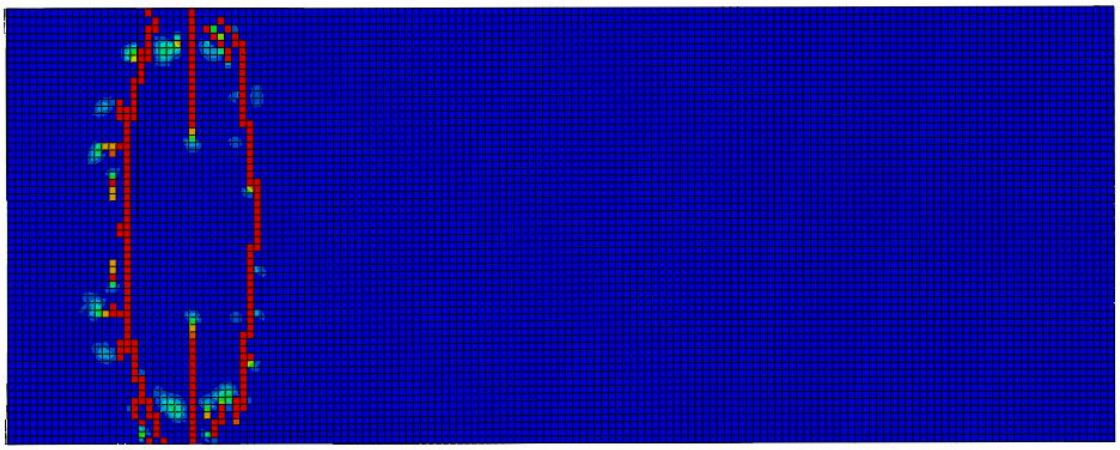

Figure 4.46. Tensile damage on the top of the specimen, Test 1

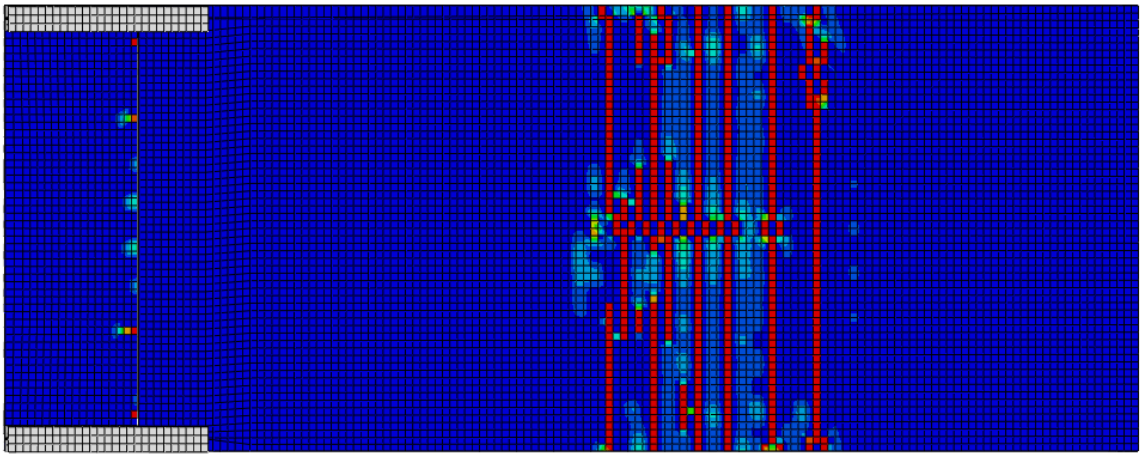

Figure 4.47. Tensile damage on the bottom of the specimen, Test 1

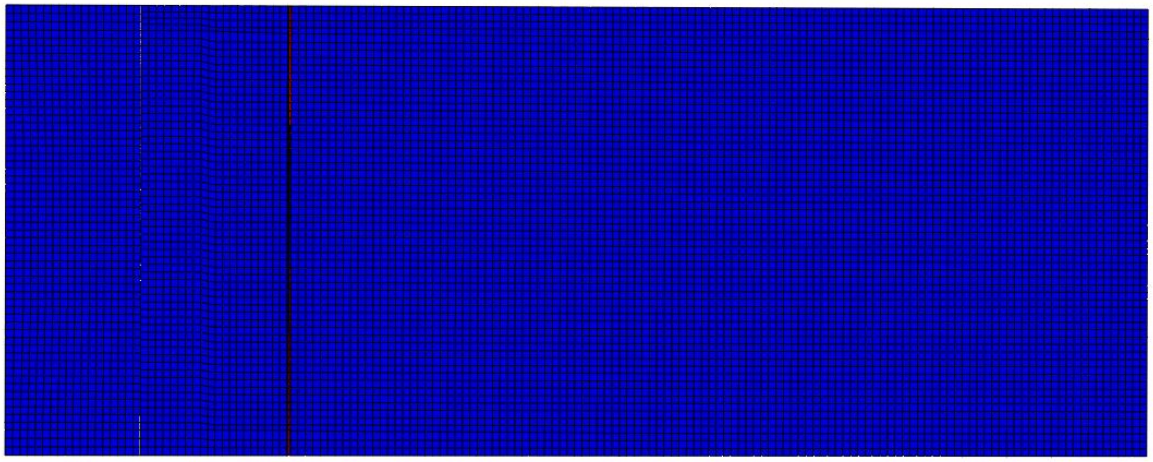

Figure 4.48. Tensile damage on the top of the specimen, Test 2

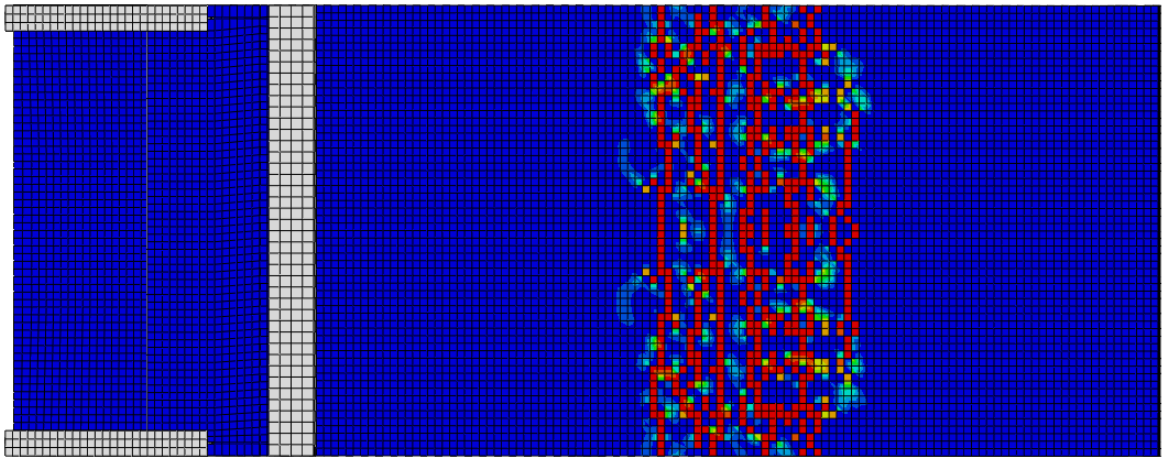

Figure 4.49. Tensile damage on the bottom of the specimen, Test 2

The figures show that the cracking patterns in the FE models for Test 1 closely resemble those experienced by the specimen during the laboratory experiment. Fortunately, through FE modeling, the cracking that would occur during Test 2 can be more accurately predicted. As shown, no cracking is experienced by the top of the specimen in the FE simulation for Test 2, specifically in the existing bridge section, due to the release of stress at the saw cut. Overall, the tensile damage is similar on the bottom of the specimen between the Test 1 and Test 2 FE models. However, the cracks in the Test 1 model do extend slightly further along the length of the specimen, and the cracks in the Test 2 model are spaced more closely together. Both of these observations are due to the presence of the hard support representing the backwall for Test 2 only.

This same pattern can be seen in Figure 4.50, which presents the distribution of E11 strain along the length of the specimen for the Test 1 and Test 2 FE models.

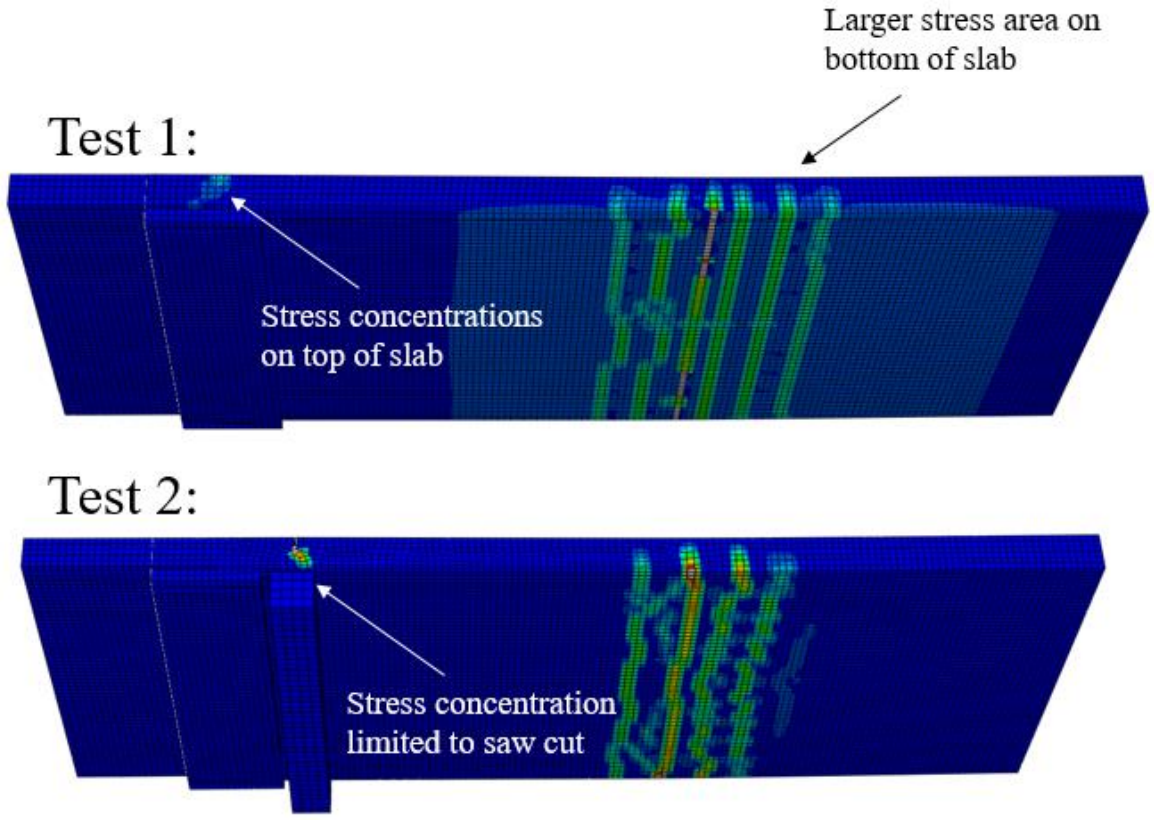

Figure 4.50. Strain (E11) in the concrete along the length of the specimen, Test 1 (top) and Test 2 (bottom)

Similar to the results described above, the figure shows that the stress on the bottom of the slab is more concentrated in Test 2 than in Test 1 Additionally, the stress concentration in the diaphragm and bridge deck sections in Test 2 is in the saw cut area, whereas in Test 1 it is not. Figure 4.51 shows the same strain in the reinforcing along the length of the specimen for Test 1 and Test 2 FE models.

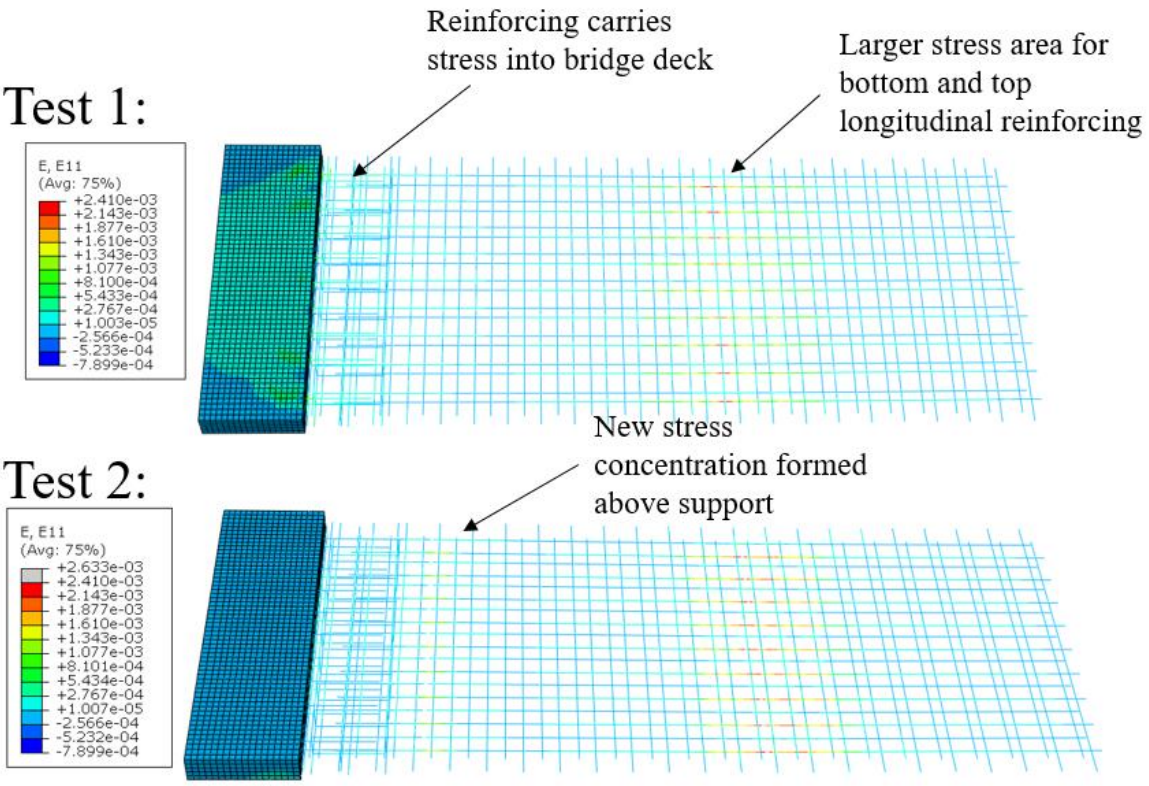

Figure 4.51. Strain (E11) in the reinforcing along the length of the specimen, Test 1 (top) and Test 2 (bottom)

The Test 1 model has a larger stress concentration at the midspan of the approach slab compared to the Test 2 model. However, a new stress concentration formed above the hard support in Test 2 due to the high strain experienced by the bottom reinforcing. Moreover, the reinforcing is carrying stress into the bridge deck in Test 1, whereas in Test 2 the stress is released before this point.

Similar to the observations regarding the cracking experienced by the laboratory specimen during testing, the FE model for Test 2 shows a very large stress concentration near the saw cut and hard support. During laboratory testing, cracks propagated from the bottom of the saw cut to the bottom of the approach slab. Figure 4.52(a) shows similar cracking occurring in the FE model for Test 2. Figure 4.52(b) shows the stress occurring in this area.

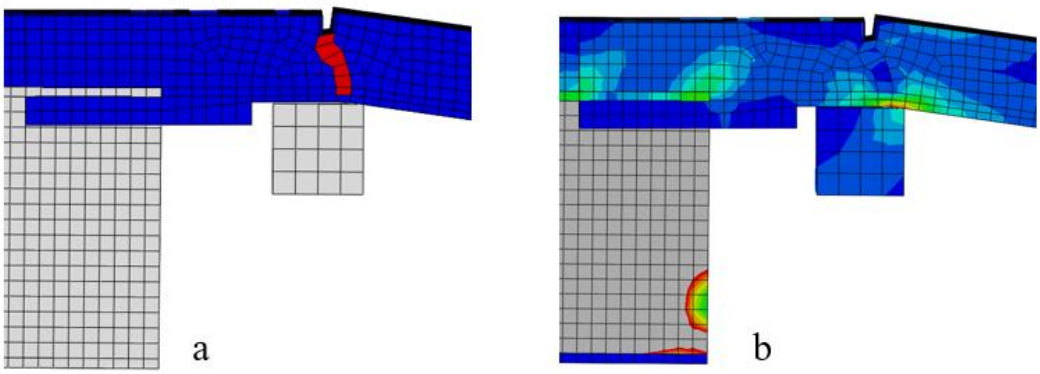

Figure 4.52. Cracking (a) and stress concentration (b) at the saw cut and hard support, Test 2

The figure shows that a large stress concentration occurred where the approach slab was resting on the corner of the hard support. Because the slab had rotated, only a small part of the specimen was resting on this corner, causing a large stress concentration. The weakness of the saw cut, coupled with an increase in stress directly below, naturally caused cracking to occur at this location.

CHAPTER 5. COST ANALYSIS

An estimate of the installation and repair or replacement costs over the service life of a bridge was developed for various types of joints, including the deck over backwall concept. In addition, the construction costs of the Iowa DOT's design for the deck over backwall concept (shown in Figure 1.3 through Figure 1.5) were estimated using the Iowa DOT's Final Bridge Design software. With the cost estimate over the service life of a bridge and the construction cost of the concept, the implementation of the bridge over backwall concept was compared that of other joint types.

5.1 Background

To develop the cost estimate, a service life and a cost associated with each type of joint was needed. As part of a study for the Massachusetts DOT (MassDOT), Civjan and Quinn (2016) researched the best practices for bridge expansion joints and headers in the northeastern states of the US. The authors surveyed MassDOT and several neighboring DOTs on their use of expansion joints and, more particularly for this research, the service life of each type of joint. The nine states surveyed were Connecticut, Maine, Massachusetts, New Hampshire, New Jersey, New York, Pennsylvania, Rhode Island, and Vermont. Table 5.1 shows the responses from the nine states in terms of the service life for the various types of joints.

Table 5.1. Typical service life of joints

Years	SS:D	SS:O	APJ	CS	SS	EM	PS	MJ	SPJ	FJ	OJ	LS
0-4	0	1	6	2	2	1	11	0	0	0	1	0
5-8	1	1	13	2	1	1	0	1	0	0	0	0
9-12	5	1	1	6	5	1	2	3	0	1	1	1
13-16	1	0	1	5	7	0	0	4	3	2	0	2
>16	4	0	0	2	4	1	0	8	3	16	3	4

Civjan and Quinn 2016
SS:D = Saw and Seal Deck over Backwall; SS:O = Saw and Seal over EM-SEAL; APJ = Asphalt Plug Joint; CS = Compression Seal; SS = Strip Seal; EM = EM- SEAL; PS = Pourable Seal; MJ = Modular Joint; SPJ = Sliding Plate Joint; FJ = Finger Joint; OJ = Open Joint; LS = Link Slab

Civjan and Quinn (2016) compiled the service life of the various types of joints from the responses of the nine states and categorized them in ranges from 0 to 4 years, 5 to 8 years, 9 to 12 years, 13 to 16 years, and over 16 years.

Civjan and Quinn (2016) also provided typical costs in cost per linear foot in US dollars ($) for the installation of the various joint types. For the cost estimate developed in the following pages, the installation cost for all joints was assumed to be the same as the repair or replacement cost with the exception of Strip Seal, where the installation cost was taken as $300 to $800 per linear foot while the repair or replacement cost was taken as $75 per linear foot. These costs are listed alongside the different types of joints in Table 5.2.

Table 5.2. Typical cost of joints

Joint Type	Cost per Linear ft.
Finger Joints	$1375-$1750
Pourable Seal	$300 (including header)
Compression Seal	$450
Strip Seal	$300-$800, $75 to replace seal
Saw and Seal Deck over Backwall	$15-$25
Saw and Seal over EM-SEAL	$60
Asphalt Plug Joint	$120-$200
Modular Joint	$1750-$4600
EM-SEAL	$90

Civjan and Quinn 2016

The cost for three types of joints was not provided: Sliding Plate Joints, Open Joints, and Link Slabs. In the service life study and the cost estimate detailed in the following pages, these types of joints were omitted because a direct comparison in terms of cost could not be established.

As the table shows, the cost of Saw and Seal Deck over Backwall is extremely low, $15 to $25 per linear foot, compared to the rest of the joint types. The saw and seal detailing can be seen in the joint developed by the Iowa DOT described in Chapter 4, Figure 4.1. The highest costs listed are for Finger Joints, with costs of $1,375 to $1,750 per linear foot, and Modular Joints, with costs of $1,750 to $4,600 per linear foot.

To develop the cost estimate, three different cost points were determined for each joint: low, average, and high. The lowest cost of each type of joint corresponds to the low cost point, the average cost to the average cost point, and the highest cost to the high cost point. For example, for the Asphalt Plug Joint, the low cost would be $20 per linear foot, the average cost would be $160 per linear foot, and the high cost would be $200 per linear foot. Some of the joint types have the same value for all three cost points, for example, Pourable Seal, Compression Seal, Strip Seal replacement, Saw and Seal over EM-SEAL, and EM-SEAL.

5.2 Service Life of Joints

As seen in Table 5.1, each type of joint listed has various values for its service life. To develop the cost estimate, the service life of each type of joint was studied in relation to the bridge service life. The aim was to find the number of times the joint has to be repaired or replaced in the service life of the bridge. A variable bridge service life of 25 years or 50 years was used.

Three different service life values were determined for each joint: early, average, and late. For the early service life of each joint, the lowest value of the range in Table 5.1 was used to determine the average service life. For example, in the 5 to 8 years range, 5 years of service life was used for the early value. For the average service life of each joint, the average of the range was used to determine the average service life. For the late service life of each joint, the highest value of the range was used to determine the average service life. Some adjustments were made in the process. For the over 16 years range, 16 years was used across all three stages. For

example, if the service life of particular joint was 20 years, the data for that joint would be capped at 16 years. For the 0 to 4 years range, a minimum of 1 year was used for the early service life since it is unrealistic for a joint to have a service life of 0 years.

Using the process detailed above, the number of repairs or replacements for each joint over a bridge service life of 25 years or 50 years was determined. Every joint type starts with an installation, and that was assumed to be equivalent to a repair or replacement in this study with the exception of Strip Seal joints. Table 5.3 and Table 5.4 show the number of times each joint has to be repaired or replaced for a bridge service life of 25 years and 50 years, respectively.

Table 5.3. Repairs or replacements over 25 years

Joint Type	Repair or Replacements		
	Early	Average	Late
Finger Joints	2	2	2
Pourable Seal	14	8	5
Compression Seal	3	3	3
Strip Seal	3	3	2
Saw and Seal Deck over Backwall	3	3	2
Saw and Seal over EM-SEAL	6	4	4
Asphalt Plug Joint	6	5	4
Modular Joint	2	2	2
EM-SEAL	4	3	3

Table 5.4. Repairs or replacements over 50 years

Joint Type	Repair or Replacements		
	Early	Average	Late
Finger Joints	4	4	4
Pourable Seal	28	16	10
Compression Seal	6	5	5
Strip Seal	5	5	4
Saw and Seal Deck over Backwall	5	5	4
Saw and Seal over EM-SEAL	11	8	7
Asphalt Plug Joint	12	9	7
Modular Joint	4	4	4
EM-SEAL	7	6	6

Each table has the three stages, early, average, and late, as described above for each joint type.

From the results presented in these tables, it can be recognized that the number of repairs or replacements for Saw and Seal Deck over Backwall ranks among the lowest of the nine joint types being studied. In contrast, the Pourable Seal joint has the highest number of repairs or replacements. Generally, each type of joint can be ranked in terms of the number of repairs or replacements as follows: Finger Joint and Modular Joint, Strip Seal and Saw and Seal Deck over

Backwall, Compression Seal, EM-SEAL, Saw and Seal over EM-SEAL, Asphalt Plug Joint, and Pourable Seal. These numbers are used in the cost estimate described in the following sections.

5.3 Cost Estimate over Bridge Service Life

A cost estimate of the repair or replacement costs of various types of joints over a design service life of a bridge of 25 years or 50 years was developed. Various factors were taken into account for this analysis. The joint length would change with the bridge in question and therefore influence the cost of each repair or replacement. The analysis was conducted for the two case study bridges, the Story County bridge and the Marshall County bridge. The Story County bridge has a roadway width of 30 ft and is a non-skewed bridge; therefore, the joint is taken as 30 ft. On the other hand, the Marshall County bridge has a roadway width of 44 ft transversely, but the joint is approximately 62 ft diagonally due to the skew of the bridge.

Another factor that was taken into account was the inflation rate. The inflation rate was assumed as 2%, 3%, and 4% during the course of this analysis. Another factor that was considered was the service life of each joint. As previously discussed, three different service life values were determined for each joint: early, average, and late. The last factor that was taken into account was the service life of the bridge itself; 25 years or 50 years was used for this variable.

Throughout the discussion, the indicators LE, LA, LL, AE, AA, AL, HE, HA, and HL are used. The first letter refers to the repair or replacement cost used (low, average, or high) and the second letter refers to the service life used (early, average, or late). For example, the designation AE would mean an average cost with an early service life.

The future cost of repair or replacement of each joint at the end of its service life was determined using equation (12).

$$FV = PV \times (1 + i)^N \quad \textbf{(12)}$$

where FV is the future value, PV is the present value, i is the inflation rate, and N is the number of periods.

To develop the cost estimate, the FV of the repair or replacement of the various types of joints was calculated using PV as the cost of each type of joint shown in Section 5.1, Table 5.2, and N as the service life of each type of joint discussed in Section 5.2, Table 5.3 and Table 5.4.

The results for the Marshall County bridge with an inflation rate of 2% and a bridge service life of 25 years are shown in Figure 5.1 for AE, Figure 5.2 for AA, and Figure 5.3 for AL.

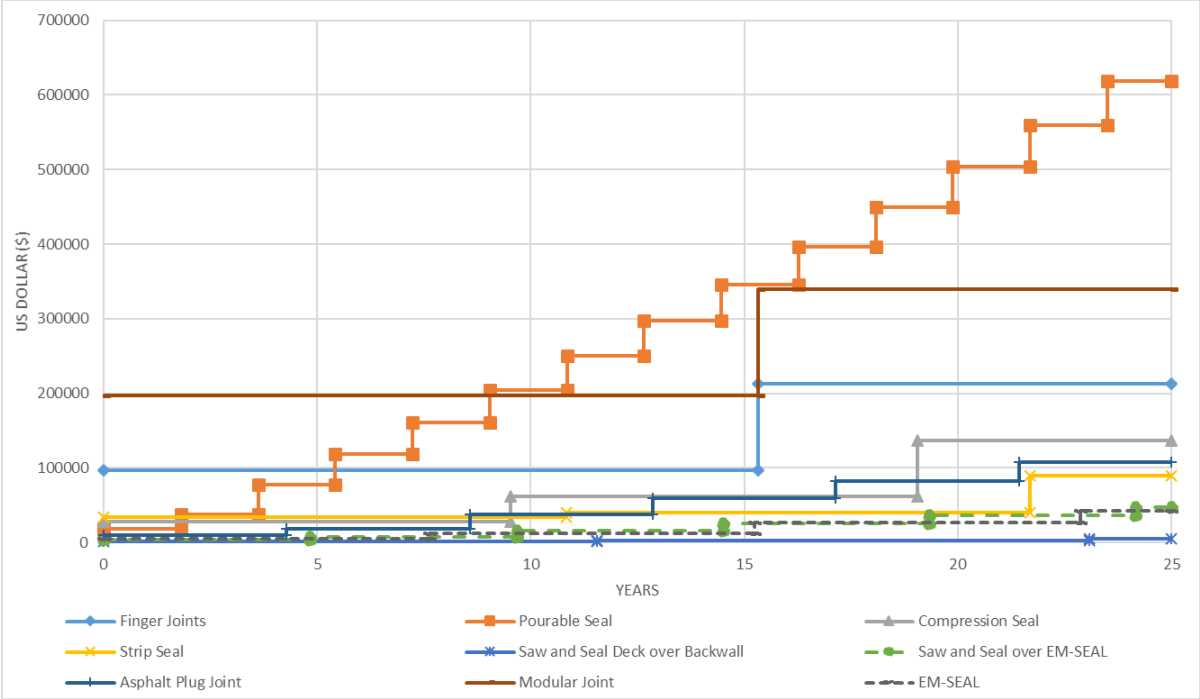

Figure 5.1. Marshall County bridge - 25 year service life, average cost, early service life

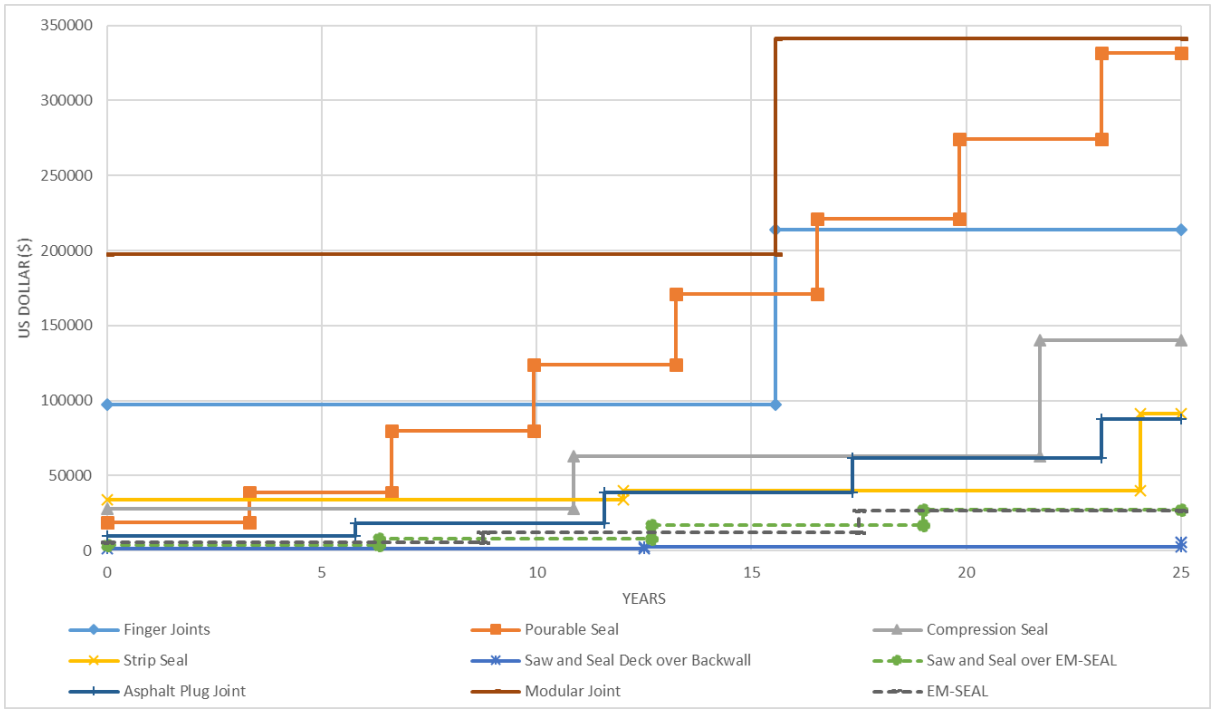

Figure 5.2. Marshall County bridge - 25 year service life, average cost, average service life

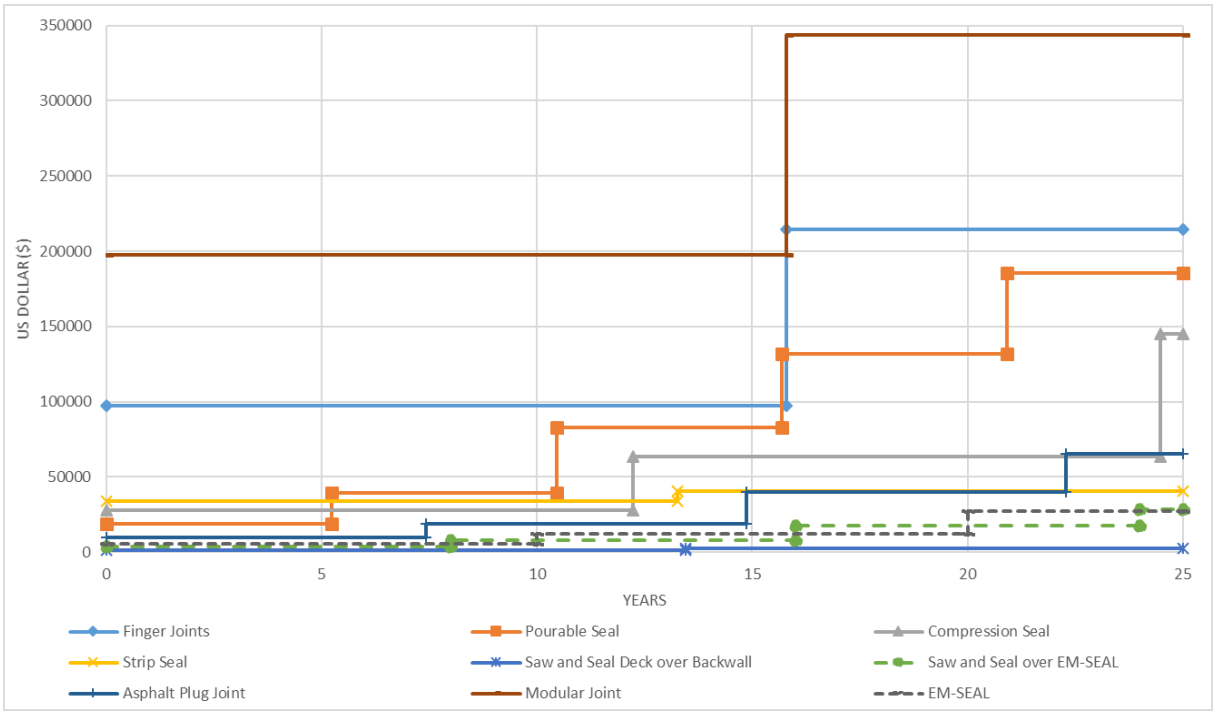

Figure 5.3. Marshall County bridge - 25 year service life, average cost, late service life

The results for a bridge service life of 50 years are shown in Figure 5.4 for AE, Figure 5.5 for AA, and Figure 5.6 for AL.

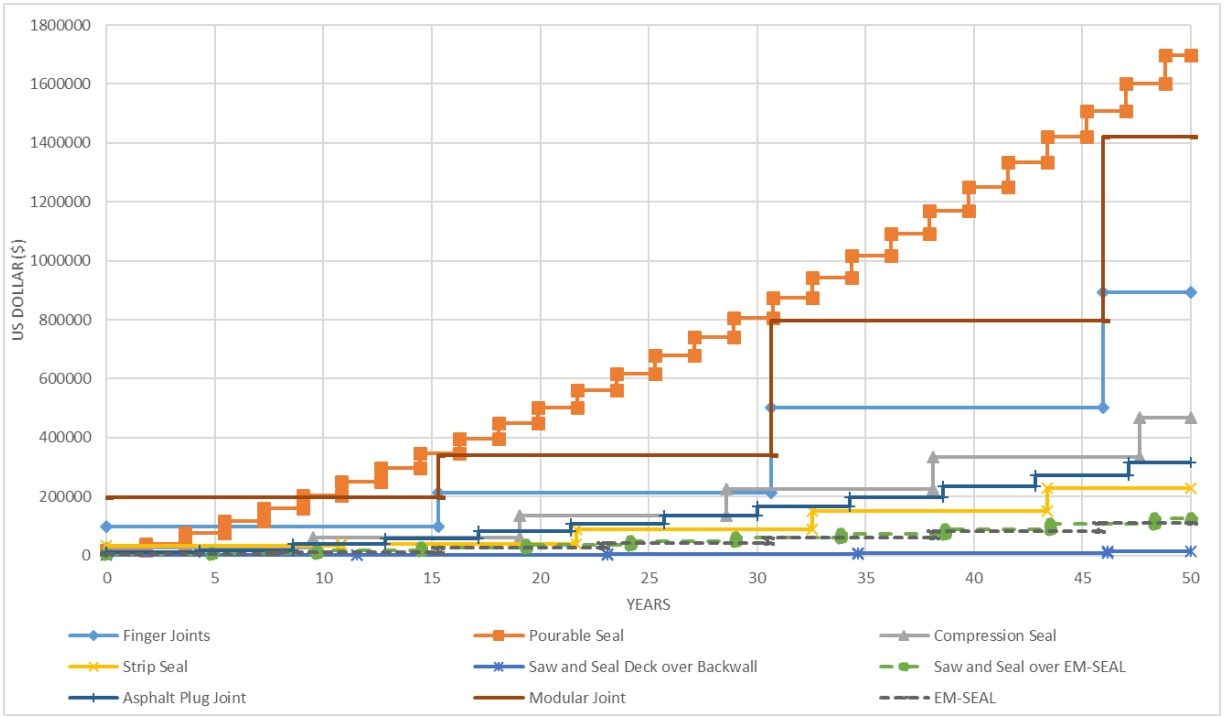

Figure 5.4. Marshall County bridge - 50 year service life, average cost, early service life

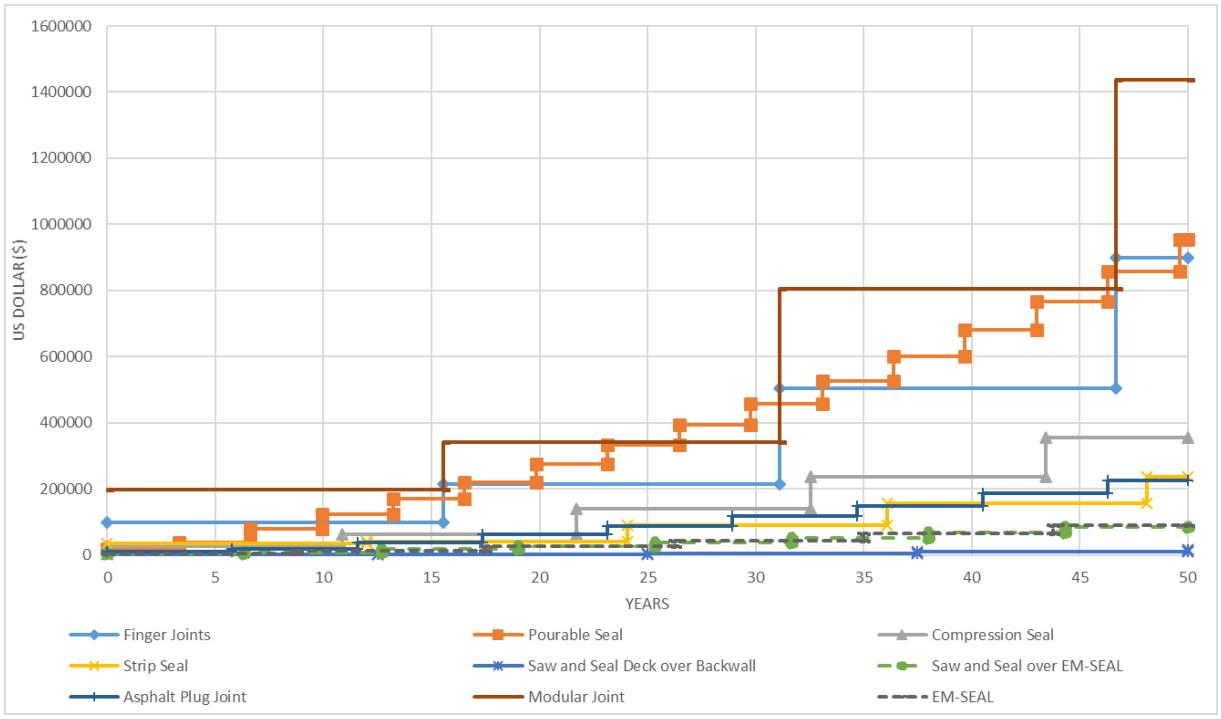

Figure 5.5. Marshall County bridge - 50 year service life, average cost, average service life

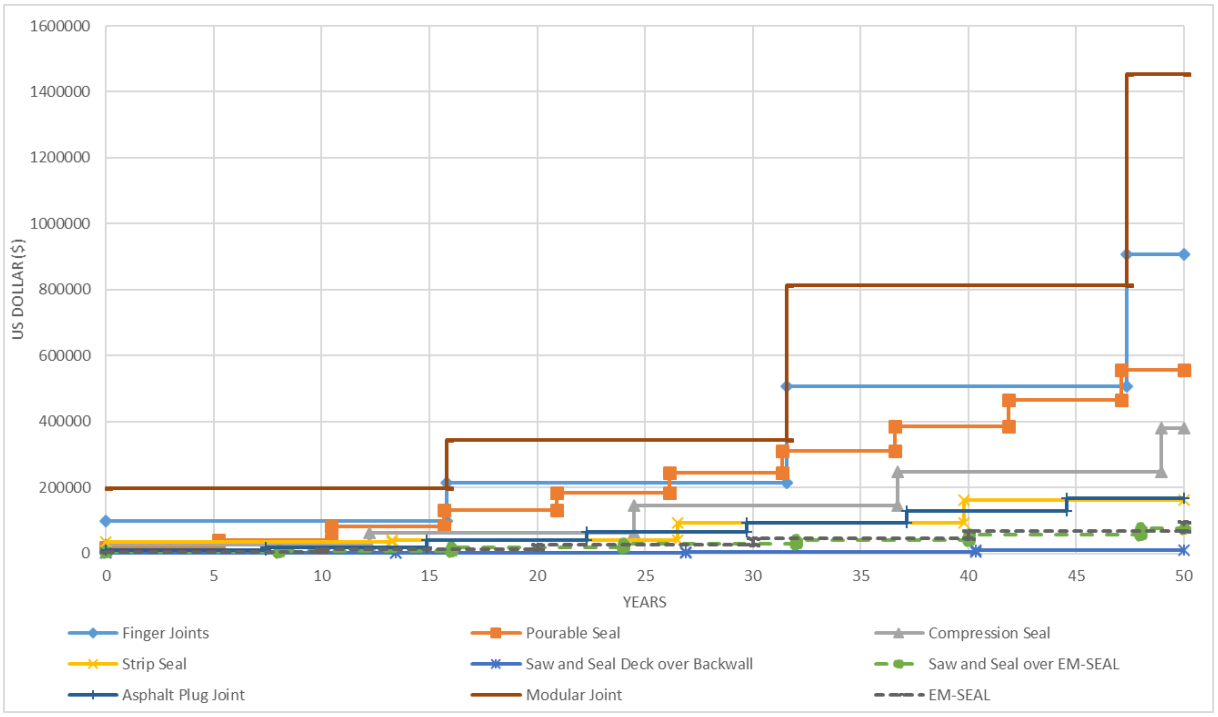

Figure 5.6. Marshall County bridge - 50 year service life, average cost, late service life

Figures are not shown for the rest of the cases (the Story County bridge, other cost and service life combinations, and other inflation rates). Each step in the graph represents a repair or

replacement cost. Each joint type begins with an installation cost in the present, or year 0. This installation cost is assumed to be the same as the repair or replacement cost for all types of joints except Strip Seal.

The costs for the Story County bridge are shown in Table 5.5, Table 5.6, Table 5.7, Table 5.8, Table 5.9, and Table 5.10.

Table 5.5. Story County bridge - 25 year service life, 2% inflation rate

Joint Type	US Dollar ($)								
	LE	LA	LL	AE	AA	AL	HE	HA	HL
Finger Joints	97115	97378	97642	102740	103003	103267	108365	108628	108892
Pourable Seal	298007	159914	89288	298007	159914	89288	298007	159914	89288
Compression Seal	65797	67723	69820	65797	67723	69820	65797	67723	69820
Strip Seal	26401	26898	11926	43197	43915	19426	59993	60931	26926
Saw and Seal Deck over Backwall	2292	2341	1037	2631	2683	1187	2969	3025	1337
Saw and Seal over EM-SEAL	23103	13130	13855	23103	13130	13855	23103	13130	13855
Asphalt Plug Joint	44871	36574	27201	52032	42321	31402	59193	48068	35602
Modular Joint	120751	121773	122809	163501	164523	165559	206251	207273	208309
EM-SEAL	20531	12940	13295	20531	12940	13295	20531	12940	13295

Table 5.6. Story County bridge - 50 year service life, 2% inflation rate

Joint Type	US Dollar ($)								
	LE	LA	LL	AE	AA	AL	HE	HA	HL
Finger Joints	406765	410168	413608	430325	433861	437435	453885	457554	461262
Pourable Seal	819095	459409	267887	819095	459409	267887	819095	459409	267887
Compression Seal	225164	171813	183172	225164	171813	183172	225164	171813	183172
Strip Seal	66962	70207	47600	109563	114622	77535	152164	159038	107469
Saw and Seal Deck over Backwall	5913	6182	4159	6786	7085	4760	7660	7989	5362
Saw and Seal over EM-SEAL	60384	40408	36140	60384	40408	36140	60384	40408	36140
Asphalt Plug Joint	131027	94412	69492	151939	109247	80223	172851	124082	90955
Modular Joint	505764	512921	520216	684821	692989	701303	863878	873058	882391
EM-SEAL	52826	43060	46279	52826	43060	46279	52826	43060	46279

Table 5.7. Story County bridge - 25 year service life, 3% inflation rate

Joint Type	US Dollar ($)								
	LE	LA	LL	AE	AA	AL	HE	HA	HL
Finger Joints	106119	106575	107033	111744	112200	112658	117369	117825	118283
Pourable Seal	337950	181040	99860	337950	181040	99860	337950	181040	99860
Compression Seal	72998	76356	80091	72998	76356	80091	72998	76356	80091
Strip Seal	28771	29633	12330	46605	47835	19830	64438	66036	27330
Saw and Seal Deck over Backwall	2607	2694	1120	2968	3062	1270	3329	3429	1420
Saw and Seal over EM-SEAL	26322	14532	15796	26322	14532	15796	26322	14532	15796
Asphalt Plug Joint	50311	41441	30695	58165	47759	35251	66020	54076	39807
Modular Joint	130170	131911	133691	172920	174661	176441	215670	217411	219191
EM-SEAL	23250	14223	14834	23250	14223	14834	23250	14223	14834

Table 5.8. Story County bridge - 50 year service life, 3% inflation rate

Joint Type	US Dollar ($)								
	LE	LA	LL	AE	AA	AL	HE	HA	HL
Finger Joints	535431	542624	549936	563813	571264	578838	592194	599904	607739
Pourable Seal	1089052	614352	352402	1089052	614352	352402	1089052	614352	352402
Compression Seal	298084	221395	245181	298084	221395	245181	298084	221395	245181
Strip Seal	83388	89965	57586	135074	145224	92614	186761	200483	127642
Saw and Seal Deck over Backwall	7765	8336	5267	8840	9472	5973	9916	10607	6678
Saw and Seal over EM-SEAL	80094	52224	47907	80094	52224	47907	80094	52224	47907
Asphalt Plug Joint	172379	123574	90007	199291	142413	103368	226204	161252	116729
Modular Joint	656782	671624	686903	872481	889286	906551	1088180	1106947	1126200
EM-SEAL	68965	55519	62269	68965	55519	62269	68965	55519	62269

Table 5.9. Story County bridge - 25 year service life, 4% inflation rate

Joint Type	US Dollar ($)								
	LE	LA	LL	AE	AA	AL	HE	HA	HL
Finger Joints	116465	117167	117875	122090	122792	123500	127715	128417	129125
Pourable Seal	337950	181040	99860	337950	181040	99860	337950	181040	99860
Compression Seal	72998	76356	80091	72998	76356	80091	72998	76356	80091
Strip Seal	28771	29633	12330	46605	47835	19830	64438	66036	27330
Saw and Seal Deck over Backwall	2607	2694	1120	2968	3062	1270	3329	3429	1420
Saw and Seal over EM-SEAL	26322	14532	15796	26322	14532	15796	26322	14532	15796
Asphalt Plug Joint	50311	41441	30695	58165	47759	35251	66020	54076	39807
Modular Joint	130170	131911	133691	172920	174661	176441	215670	217411	219191
EM-SEAL	23250	14223	14834	23250	14223	14834	23250	14223	14834

Table 5.10. Story County bridge - 50 year service life, 4% inflation rate

Joint Type	US Dollar ($)								
	LE	LA	LL	AE	AA	AL	HE	HA	HL
Finger Joints	716040	729655	743578	750624	764684	779062	785207	799714	814545
Pourable Seal	1468563	833705	469895	1468563	833705	469895	1468563	833705	469895
Compression Seal	400492	288990	333581	400492	288990	333581	400492	288990	333581
Strip Seal	105162	117084	70481	168552	186744	111826	231941	256403	153170
Saw and Seal Deck over Backwall	10346	11434	6753	11687	12882	7588	13027	14329	8423
Saw and Seal over EM-SEAL	107752	68327	64437	107752	68327	64437	107752	68327	64437
Asphalt Plug Joint	229846	163892	118058	264942	188122	134888	300038	212351	151718
Modular Joint	865520	893103	921796	1128352	1159329	1191470	1391185	1425554	1461145
EM-SEAL	91238	72482	85153	91238	72482	85153	91238	72482	85153

These tables vary in terms of the bridge service life (25 or 50 years) and the inflation rate (2%, 3%, or 4%). The tables are color coded, with red cells representing the higher cost values and green cells representing the lower cost values. Each table shows all of the different cost and service life combinations (LE, LA, LL, etc.).

The costs for the Marshall County bridge are shown in Table 5.11, Table 5.12, Table 5.13, Table 5.14, Table 5.15, and Table 5.16, varying the same factors.

Table 5.11. Marshall County bridge - 25 year service life, 2% inflation rate

Joint Type	US Dollar ($)								
	LE	LA	LL	AE	AA	AL	HE	HA	HL
Finger Joints	201435	201979	202527	213102	213647	214194	224769	225314	225861
Pourable Seal	618119	331691	185200	618119	331691	185200	618119	331691	185200
Compression Seal	136476	140470	144819	136476	140470	144819	136476	140470	144819
Strip Seal	54761	55791	24736	89599	91087	40293	124437	126383	55849
Saw and Seal Deck over Backwall	4754	4856	2152	5456	5565	2463	6159	6275	2774
Saw and Seal over EM-SEAL	47919	27233	28738	47919	27233	28738	47919	27233	28738
Asphalt Plug Joint	93070	75862	56420	107923	87782	65133	122777	99702	73846
Modular Joint	250460	252578	254728	339131	341250	343399	427803	429921	432071
EM-SEAL	42585	26840	27575	42585	26840	27575	42585	26840	27575

Table 5.12. Marshall County bridge - 50 year service life, 2% inflation rate

Joint Type	US Dollar ($)								
	LE	LA	LL	AE	AA	AL	HE	HA	HL
Finger Joints	843703	850762	857896	892571	899906	907319	941439	949050	956741
Pourable Seal	1698951	952897	555646	1698951	952897	555646	1698951	952897	555646
Compression Seal	467030	356372	379931	467030	356372	379931	467030	356372	379931
Strip Seal	138891	145621	98730	227253	237747	160821	315615	329874	222911
Saw and Seal Deck over Backwall	12265	12822	8627	14076	14696	9874	15887	16570	11121
Saw and Seal over EM-SEAL	125248	83813	74962	125248	83813	74962	125248	83813	74962
Asphalt Plug Joint	271774	195827	144139	315149	226598	166398	358524	257368	188657
Modular Joint	1049045	1063891	1079021	1420441	1437385	1454629	1791838	1810879	1830237
EM-SEAL	109571	89315	95990	109571	89315	95990	109571	89315	95990

Table 5.13. Marshall County bridge - 25 year service life, 3% inflation rate

Joint Type	US Dollar ($)								
	LE	LA	LL	AE	AA	AL	HE	HA	HL
Finger Joints	220110	221055	222007	231777	232722	233674	243444	244389	245341
Pourable Seal	700970	375510	207128	700970	375510	207128	700970	375510	207128
Compression Seal	151411	158375	166124	151411	158375	166124	151411	158375	166124
Strip Seal	59677	61465	25575	96667	99218	41131	133656	136971	56687
Saw and Seal Deck over Backwall	5406	5589	2323	6155	6350	2634	6904	7112	2945
Saw and Seal over EM-SEAL	54597	30143	32764	54597	30143	32764	54597	30143	32764
Asphalt Plug Joint	104353	85956	63666	120645	99060	73117	136938	112164	82567
Modular Joint	269996	273607	277299	358667	362278	365971	447338	450949	454642
EM-SEAL	48224	29501	30768	48224	29501	30768	48224	29501	30768

Table 5.14. Marshall County bridge - 50 year service life, 3% inflation rate

Joint Type	US Dollar ($)								
	LE	LA	LL	AE	AA	AL	HE	HA	HL
Finger Joints	1110581	1125500	1140667	1169449	1184904	1200613	1228317	1244308	1260559
Pourable Seal	2258889	1274277	730946	2258889	1274277	730946	2258889	1274277	730946
Compression Seal	618280	459212	508550	618280	459212	508550	618280	459212	508550
Strip Seal	172961	186604	119444	280169	301221	192098	387376	415839	264753
Saw and Seal Deck over Backwall	16105	17291	10925	18336	19646	12388	20567	22001	13852
Saw and Seal over EM-SEAL	166129	108321	99368	166129	108321	99368	166129	108321	99368
Asphalt Plug Joint	357544	256315	186691	413366	295390	214404	469187	334466	242117
Modular Joint	1362285	1393070	1424760	1809683	1844539	1880351	2257080	2296008	2335942
EM-SEAL	143047	115156	129157	143047	115156	129157	143047	115156	129157

Table 5.15. Marshall County bridge - 25 year service life, 4% inflation rate

Joint Type	US Dollar ($)								
	LE	LA	LL	AE	AA	AL	HE	HA	HL
Finger Joints	241569	243025	244494	253236	254692	256162	264903	266359	267829
Pourable Seal	797353	426423	232280	797353	426423	232280	797353	426423	232280
Compression Seal	168514	179319	191608	168514	179319	191608	168514	179319	191608
Strip Seal	65292	68053	26519	104649	108541	42075	144006	149030	57632
Saw and Seal Deck over Backwall	6178	6470	2515	6979	7289	2827	7779	8108	3138
Saw and Seal over EM-SEAL	62427	33444	37508	62427	33444	37508	62427	33444	37508
Asphalt Plug Joint	117321	97725	72093	135235	112172	82371	153149	126620	92648
Modular Joint	291998	297464	303094	380669	386136	391765	469341	474807	480436
EM-SEAL	54811	32511	34451	54811	32511	34451	54811	32511	34451

Table 5.16. Marshall County bridge - 50 year service life, 4% inflation rate

Joint Type	US Dollar ($)								
	LE	LA	LL	AE	AA	AL	HE	HA	HL
Finger Joints	1485197	1513435	1542315	1556929	1586093	1615914	1628660	1658751	1689513
Pourable Seal	3046065	1729253	974646	3046065	1729253	974646	3046065	1729253	974646
Compression Seal	830692	599418	691908	830692	599418	691908	830692	599418	691908
Strip Seal	218125	242854	146190	349606	387340	231946	481087	531827	317703
Saw and Seal Deck over Backwall	21460	23716	14007	24240	26719	15739	27020	29722	17471
Saw and Seal over EM-SEAL	223496	141722	133654	223496	141722	133654	223496	141722	133654
Asphalt Plug Joint	476742	339942	244874	549537	390198	279783	622332	440454	314691
Modular Joint	1795244	1852457	1911970	2340406	2404656	2471324	2885568	2956856	3030678
EM-SEAL	189245	150341	176623	189245	150341	176623	189245	150341	176623

The results of the cost analysis clearly show that Saw and Seal Deck over Backwall has the lowest cost compared to all other types of joints and across all combinations of cost and service life (LE, LA, LL, etc.). It also has the lowest cost whether the bridge service life is 25 years or 50 years. This can easily be recognized in the color-coded tables; the greenest cells in each table correspond to Saw and Seal Deck over Backwall. From the other types of joints, Modular Joint, Finger Joint, and Pourable Seal were identified as having the highest costs by a wide margin for all of the cases shown. Saw and seal over EM-SEAL, Asphalt Plug Joint, Strip Seal, and EM-SEAL ranked the lowest in terms of costs among the remaining types of joints.

5.4 Construction Cost of Deck over Backwall Concept

Various items were taken into consideration to develop an estimate of the construction cost of the deck over backwall concept. The Iowa DOT's Final Bridge Design software (Iowa DOT Office of Bridges and Structures 2018b) was used to identify items that would pertain to the construction cost of the Iowa DOT's design for the deck over backwall concept. Specifically, a spreadsheet titled Prepare Cost Estimate, last updated on April 25, 2017 (Iowa DOT Office of Bridges and Structures 2018b), was used. This spreadsheet stores historical cost data for bid items in state job estimates. Most items have cost data from May 2016 through April 2017, while some items have cost data within the past 10 years

Figure 5.17 shows the items that were chosen in the software with the long bid and short bid descriptions, measuring unit, unit price for each item, and date of the cost data.

Table 5.17. Deck over backwall concept construction items

Item Code	Long Bid Item Description	Unit	Unit Price ($)			Date of Cost Data	Short Bid Item Description
			Low	High	Average		
2102-2710070	EXCAVATION, CLASS 10, ROADWAY AND BORROW	CY	2	89.5	3.07	5-2016 thru 4-2017	EXCAVATION, CL 10, RDWY+BORROW
2115-0100000	MODIFIED SUBBASE	CY	17	135	40.36	5-2016 thru 4-2017	MODIFIED SUBBASE
2301-0690205	BRIDGE APPROACH, BR-205	SY	150	190	174.06	5-2016 thru 4-2017	BRIDGE APPROACH, BR-205
2401-7207020	REMOVAL OF CONCRETE	CY	267	267	267	12-2014 thru 10-2015	RMVL OF CONC

Iowa DOT Office of Bridges and Structures 2018

The first item shown in the table is the excavation of Class 10 soil. According to the Iowa DOT (2018), Class 10 soils include normal earth materials such as loam, silt, gumbo, peat, clay, soft shale, sand, and gravel. It was determined that this class applies for most cases; therefore, it was used in the estimate. The excavation extends 24 in. below the approach slab according to the Iowa DOT Office of Design (2016). Placement of a new modified subbase was also considered in the cost estimate. The design for the deck over backwall concept calls for the modified subbase to be placed in the same volume that was excavated to support the new approach slab. Using the bridge design standards from the Iowa DOT Office of Design (2016), the bridge approach for the deck over backwall concept was estimated as having a cost similar to that of the BR-205 approach slab, as shown in Table 5.17. Finally, concrete removal for the current approach slab and the abutment interface was assumed for the length of the deck over backwall concept and a 12 in. thickness.

Even though the Marshall County bridge was chosen as the test bridge where the deck over backwall concept would be implemented, calculations were performed for both the Story County bridge and the Marshall County bridge. A substantial difference in the estimate can be seen by comparing a non-skewed bridge to a skewed bridge because different units of area and volume lead to different cost estimates. The skew of the Marshall County bridge results in one end of the approach slab being a 20 ft section and the other being a 64 ft section. This increases the cost compared to non-skewed counterparts like the Story County bridge. A summary of the costs associated with the deck over backwall concept is presented in Table 5.18 and Table 5.19 for the Story County bridge and the Marshall County bridge, respectively.

Table 5.18. Story County bridge - construction cost of deck over backwall concept

Short Bid Item Description	Total Quantity	Unit	Total Cost ($)	Unit Price ($)		
				Low	High	Average
EXCAVATION, CL 10, RDWY+BORROW	44.44	CY	136.44	2	89.5	3.07
MODIFIED SUBBASE	44.44	CY	1,793.78	17	135	40.36
BRIDGE APPROACH, BR-205	66.67	SY	11,603.88	150	190	174.06
RMVL OF CONC	22.22	CY	5,933.33	267	267	267
	Total Cost ($)		19,467.44			

Table 5.19. Marshall County bridge - construction cost of deck over backwall concept

Short Bid Item Description	Total Quantity	Unit	Total Cost ($)	Unit Price ($)		
				Low	High	Average
EXCAVATION, CL 10, RDWY+BORROW	136.89	CY	420.25	2	89.5	3.07
MODIFIED SUBBASE	136.89	CY	5,524.84	17	135	40.36
BRIDGE APPROACH, BR-205	205.33	SY	35,739.96	150	190	174.06
RMVL OF CONC	68.44	CY	18,274.67	267	267	267
	Total Cost ($)		59,959.71			

The average unit price from the Iowa DOT's Final Bridge Design software was used for both estimates.

The total construction cost of the deck over backwall concept was found to be approximately $20,000 for the Story County bridge and $60,000 for the Marshall County bridge. The approach slab itself, the cost of which was assumed to be equivalent to that of the BR-205 approach slab from the Iowa DOT bridge design standards, accounts for more than half of the total construction cost of the deck over backwall concept. Meanwhile, the concrete removal accounts for almost a third of the cost, and the excavation and the modified subbase account for the other portions of the construction cost.

From these total cost numbers, the impact of the skew on the approach slab costs can be recognized. An almost 50% increase in roadway length, 44 ft for the Marshall County bridge compared to 30 ft for the Story County bridge, with a 45° skew triples the construction cost of the approach slab. This major difference is due to the larger area and volume requirements of an approach slab with a skewed end in comparison to one with a non-skewed end. In comparison, for other types of joints, the differences in the skew and the roadway length would more than double the construction costs due to the relatively high cost of the expansion joint hardware and materials, which are calculated per foot (62 ft for Marshall County and 30 ft for Story County).

Combining the repair or replacement costs of Saw and Seal Deck over Backwall and the construction cost of the deck over backwall concept allows for a better comparison to be made to other types of joints. The results for the Marshall County bridge are shown in Table 5.20 and Table 5.21 for an inflation rate of 2% and in Table 5.22 and Table 5.23 for an inflation rate of 3%.

Table 5.20. Deck over backwall comparison, 25 year service life, 2% inflation rate

Joint Type	US Dollar ($)								
	LE	LA	LL	AE	AA	AL	HE	HA	HL
Strip Seal	54761	55791	24736	89599	91087	40293	124437	126383	55849
Saw and Seal Deck over Backwall	64714	64815	62111	65416	65525	62423	66118	66235	62734
Saw and Seal over EM-SEAL	47919	27233	28738	47919	27233	28738	47919	27233	28738
Asphalt Plug Joint	93070	75862	56420	107923	87782	65133	122777	99702	73846
EM-SEAL	42585	26840	27575	42585	26840	27575	42585	26840	27575

Table 5.21. Deck over backwall comparison, 50 year service life, 2% inflation rate

Joint Type	US Dollar ($)								
	LE	LA	LL	AE	AA	AL	HE	HA	HL
Strip Seal	138891	145621	98730	227253	237747	160821	315615	329874	222911
Saw and Seal Deck over Backwall	72224	72782	68586	74036	74656	69834	75847	76530	71081
Saw and Seal over EM-SEAL	125248	83813	74962	125248	83813	74962	125248	83813	74962
Asphalt Plug Joint	271774	195827	144139	315149	226598	166398	358524	257368	188657
EM-SEAL	109571	89315	95990	109571	89315	95990	109571	89315	95990

Table 5.22. Deck over backwall comparison, 25 year service life, 3% inflation rate

Joint Type	US Dollar ($)								
	LE	LA	LL	AE	AA	AL	HE	HA	HL
Strip Seal	59677	61465	25575	96667	99218	41131	133656	136971	56687
Saw and Seal Deck over Backwall	65366	65549	62282	66115	66310	62593	66864	67071	62905
Saw and Seal over EM-SEAL	54597	30143	32764	54597	30143	32764	54597	30143	32764
Asphalt Plug Joint	104353	85956	63666	120645	99060	73117	136938	112164	82567
EM-SEAL	48224	29501	30768	48224	29501	30768	48224	29501	30768

Table 5.23. Deck over backwall comparison, 50 year service life, 3% inflation rate

Joint Type	US Dollar ($)								
	LE	LA	LL	AE	AA	AL	HE	HA	HL
Strip Seal	172961	186604	119444	280169	301221	192098	387376	415839	264753
Saw and Seal Deck over Backwall	76065	77250	70885	78296	79606	72348	80526	81961	73812
Saw and Seal over EM-SEAL	166129	108321	99368	166129	108321	99368	166129	108321	99368
Asphalt Plug Joint	357544	256315	186691	413366	295390	214404	469187	334466	242117
EM-SEAL	143047	115156	129157	143047	115156	129157	143047	115156	129157

For each inflation rate, tables are presented for a bridge service life of 25 years and 50 years, respectively. Only the comparable types of joints in terms of costs are shown. Four types of joints (Finger Joint, Pourable Seal, Compression Seal, and Modular Joint) were omitted because their costs were extremely high compared to the ones shown in the tables. The tables are color coded in the same manner as those shown above.

The tables show that for a bridge service life of 25 years, the deck over backwall concept has a higher cost than other comparable types of joints. The high initial cost accounts for most of the costs, since the repair or replacement cost of Saw and Seal Deck over Backwall was found to be the lowest among all types of joints by a wide margin. While the deck over backwall concept might not be the best option in terms of cost for a bridge service life of 25 years, for a bridge service life of 50 years, the deck over backwall concept has the lowest costs when compared to all other types of joints across all combinations of cost point and service life (LE, LA, LL, etc.).

It should be noted that much of the cost of the saw and seal over backwall alternative is associated with the removal and construction of the bridge approach. If the bridge approach requires replacement in any case, an analysis would be much more likely to favor the saw and seal over backwall alternative.

5.5 Break-Even Point Analysis

As demonstrated above for the Marshall County bridge, the deck over backwall concept produced the lowest costs for a bridge service life of 50 years. In contrast, it did not rank as the best alternative for a bridge service life of 25 years. Because of this, a break-even point (BEP) between a bridge service life of 25 years and 50 years was identified. Beyond that point, the deck over backwall concept would produce the lowest costs among all other types of joints across all combinations of cost point and service life. Figure 5.7, Figure 5.8, and Figure 5.9 show the cost estimate graphs presented above for the Marshall County bridge with an interest rate of 2% but with the vertical axis limited to $100,000 so that the BEP can more easily be identified.

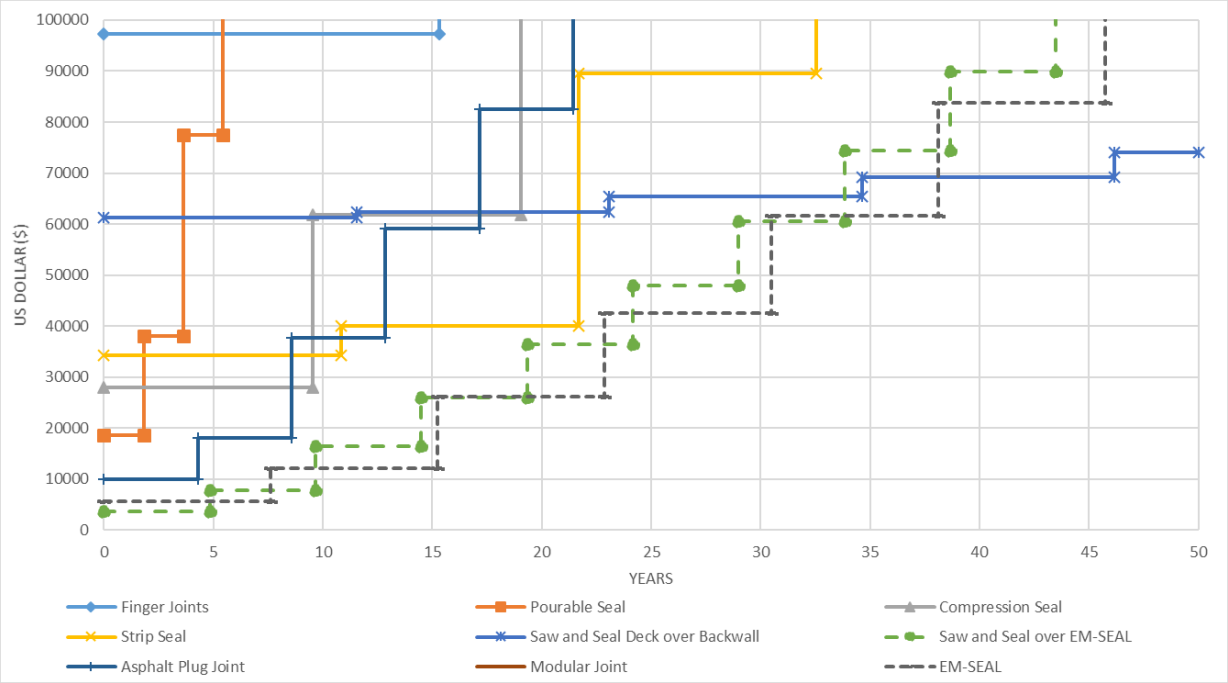

Figure 5.7. Break-even point - average cost, early service life

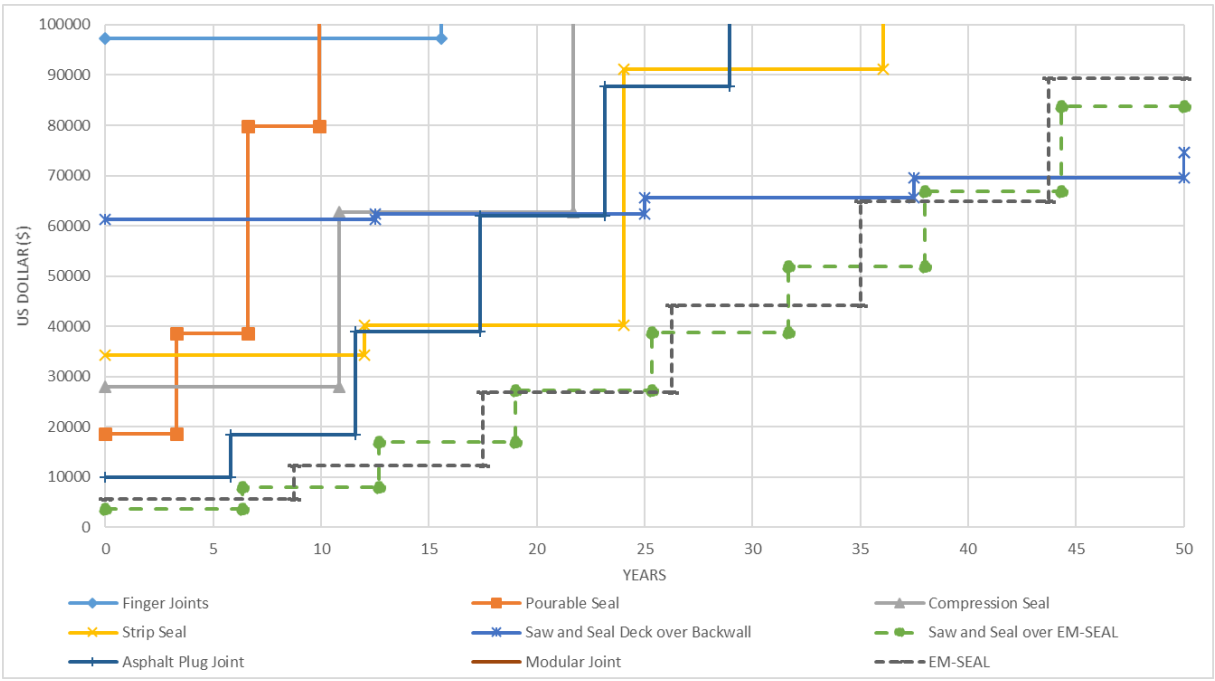

Figure 5.8. Break-even point - average cost, average service life

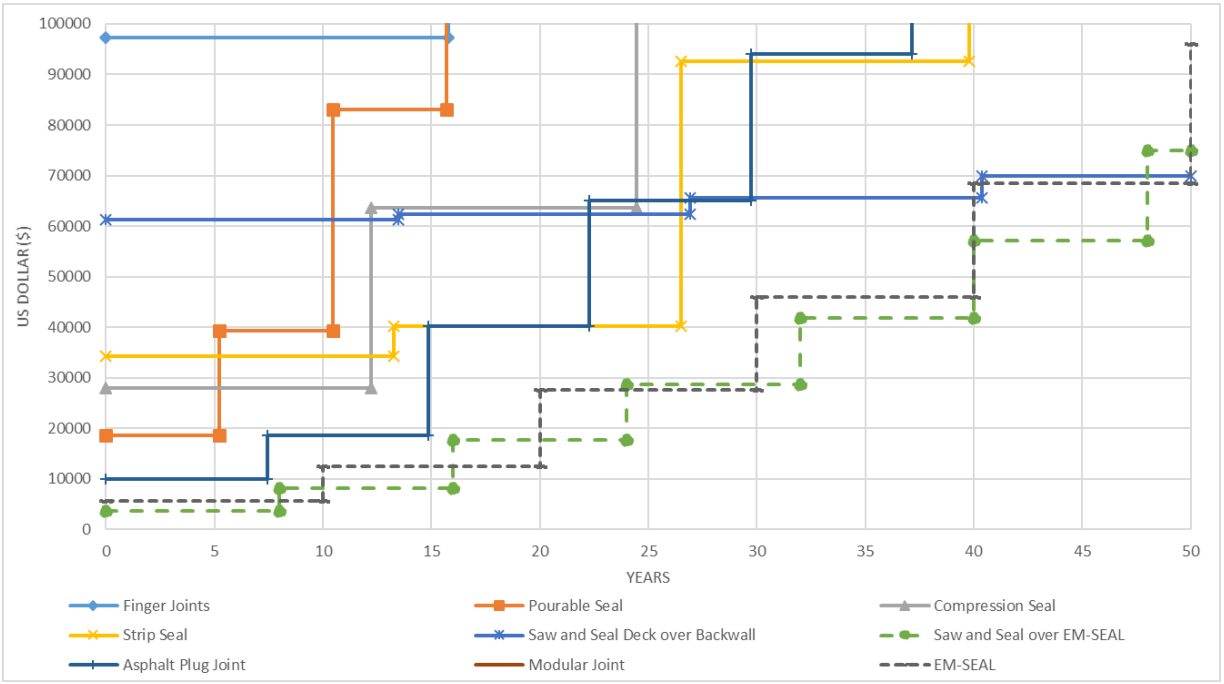

Figure 5.9. Break-even point - average cost, late service life

Table 5.24 presents the BEP for the Marshall County bridge across all different combinations of cost point and service life for interest rates of 2%, 3%, and 4%. The average BEP for each interest rate is also shown.

Table 5.24. Break-even point of deck over backwall concept

Break-Even Point (Years)										
Interest Rate	LE	LA	LL	AE	AA	AL	HE	HA	HL	Average
2%	38	44	50	38	44	50	38	44	50	44
3%	33	38	40	31	38	48	31	38	48	38
4%	33	35	40	31	38	40	31	38	40	36

As the table shows, the BEP for the deck over backwall concept ranges from 31 years to 50 years. Some BEPs are calculated at exactly 50 years because the particular type of joint that would be comparable to the deck over backwall concept would need a repair or replacement in that same year. The lowest BEP that was obtained in the study was 31 years for 4 of the 27 different cases considered. The average BEP is shown for all three interest rates used in the analysis. The average BEPs were 44 years, 38 years, and 36 years for interest rates of 2%, 3%, and 4%, respectively. From these results, it can be concluded that as the interest rate increases, the BEP decreases. In this analysis, the interest rate does not affect the initial construction cost of the deck over backwall concept. Since the repair or replacement costs of Saw and Seal Deck over Backwall were the lowest among the various types of joints, as the interest rate increases, all repair or replacement costs for the other types of joints would increase more than the costs of Saw and Seal Deck over Backwall.

5.6 Summary and Discussion

To develop a cost analysis comparing the deck over backwall concept and various types of joints, pertinent information was used from Civjan and Quinn (2016) regarding the service life and installation costs of several types of joints. Both variables, service life and installation costs, were varied throughout the development of the cost estimates. Using the information from Civjan and Quinn (2016), three service life values were determined for each type of joint: early, average, and late. The installation and repair or replacement costs of each joint were also varied throughout the study, with three different cost points determined for each type of joint: low, average, and high. Other factors were also varied during the cost analysis. The interest rates used were 2%, 3%, and 4%, though results are only presented for 2% and 3%. In addition, cost analyses were conducted for both the Story County bridge and the Marshall County bridge, even though the majority of the results presented correspond to the Marshall County bridge.

Cost estimates for nine different types of joints were developed based on the number of times each type of joint must be repaired or replaced during the service life of the bridge. The installation costs were assumed to be the same as the repair or replacement costs for each type of joint except Strip Seals. Two different service lives, 25 years and 50 years, were used throughout the study. The results from this estimate show that Saw and Seal Deck over Backwall produced the lowest repair or replacement costs among all nine joints for all different interest rates (2%, 3%, and 4%), for both bridges under investigation (Story County bridge and Marshall County bridge), and for all combinations of cost point and service life (LE, LA, LL, etc.).

The initial construction cost of the Iowa DOT's design for the deck over backwall concept was estimated. The Iowa DOT's Final Bridge Design software was used to estimate the construction

cost using comparable bid items. The total construction cost of the deck over backwall concept was found to be approximately $20,000 for the Story County bridge and $60,000 for the Marshall County bridge. Skew was found to have a significant impact on cost, in that an approach slab with a skewed end has a much greater length and area than an approach slab with a non-skewed end.

The construction cost was incorporated into the repair or replacement cost estimates previously discussed. The results show that for a bridge service life of 25 years, the deck over backwall concept has a higher cost than other comparable types of joints. The high initial cost accounts for most of the cost, since the repair or replacement cost of Saw and Seal Deck over Backwall was found to be the lowest among all types of joints. For a bridge service life of 50 years, the Saw and Seal Deck over Backwall concept has the lowest costs when compared to all other types of joints across all combinations of cost point and service life. Because of this, a BEP between a bridge service life of 25 years and 50 years was identified. Beyond that point, the deck over backwall concept would produce the lowest costs among all other types of joints across all combinations of cost point and service life. The results show that as the interest rate increases, the BEP decreases. The average BEPs were 44 years, 38 years, and 36 years for interest rates of 2%, 3%, and 4%, respectively. The BEP for the deck over backwall concept ranges from 31 years to 50 years.

Many assumptions and simplifications were made to estimate the costs of the various types of joints. Numerous factors could have been incorporated to improve the accuracy of this analysis. The costs of maintenance for the interaction between the abutment/bridge deck and the approach slab were not taken into account, nor was the costs of maintenance for the steel girders, bearings, reinforcement, etc. These factors, among many others, could affect the cost of the various types of joints compared in this study. Ideally, all of these factors would increase the costs of all types of joints uniformly. However, since the deck over backwall concept would not be composed of an expansion joint in the abutment interface, some of the costs associated with these factors could be greatly reduced, and, quite possibly, eliminated in their entirety.

In conclusion, if these factors are all taken into account, the type of joint whose costs would increase the least would likely be Saw and Seal Deck over Backwall, which would further increase the cost difference between this joint and the joint with the next lowest cost for any particular combination of cost point and service life (LE, LA, LL, etc.). Moreover, most of the cost of the Saw and Seal Deck over Backwall concept is associated with the removal and replacement of the bridge approach panel. If this approach panel would need to be replaced in any case, the analysis would be much more favorable for the Saw and Seal Deck over Backwall concept.

While this cost analysis covered the critical elements of the construction process, many other components could be factored into the analysis. Some of these components could be formwork costs, labor costs, work zone costs, lane closure costs, mobilization costs, etc. These can all be added to the construction costs of the deck over backwall concept. At the same time, these components and many others could also be added to the installation and repair or replacement costs of all types of joints investigated.

CHAPTER 6. CONSTRUCTION OBSERVATION AND POST-CONSTRUCTION TESTING PLAN

In this chapter, a construction observation and post-construction testing plan was developed for the deck over backwall joint developed by the Iowa DOT. An instrumentation plan was developed with various types of sensors and equipment. A post-construction plan with various truck loading cases was developed as well. The correlations between the results from future field testing based on this plan and the predictions of the FE models described in Chapter 3 will serve to calibrate and improve the accuracy of the FE models. The test results will also provide vital information on the behavior of expansion joints and allow for their efficient design.

6.1 Joint Detailing

The joint developed by the Iowa DOT, detailed in Chapter 1 was designated as the deck over backwall concept and was selected by Iowa DOT staff members for implementation in a future Iowa DOT construction season. This joint design was used for the development of the instrumentation and post-construction testing plans discussed in this chapter.

6.2 Instrumentation

The instrumentation plan developed for the deck over backwall concept consists of various types of sensors and equipment. The instrumentation includes strain gages with temperature sensors, monitoring plates for surveying data, surveying equipment, and gapmeters. Each sensor and piece of equipment serves a purpose in obtaining real-world data to correlate with the FE results discussed in Chapter 3.

Thiagarajan et al. (2013) detailed the Missouri DOT's (MoDOT) experience with the field performance of various types of bridge approach slab designs. Monitoring plates were incorporated into MoDOT's approach slabs to provide a smooth and flat surface to collect accurate readings. The deflections of the approach slab can be monitored over time using surveying equipment over these monitoring plates. The equipment is shown in Figure 6.1.

Thiagarajan et al. 2013

Figure 6.1. Surveying prism (left), total station (right)

Detailed information on how to embed the monitoring plates is provided in Figure 6.2.

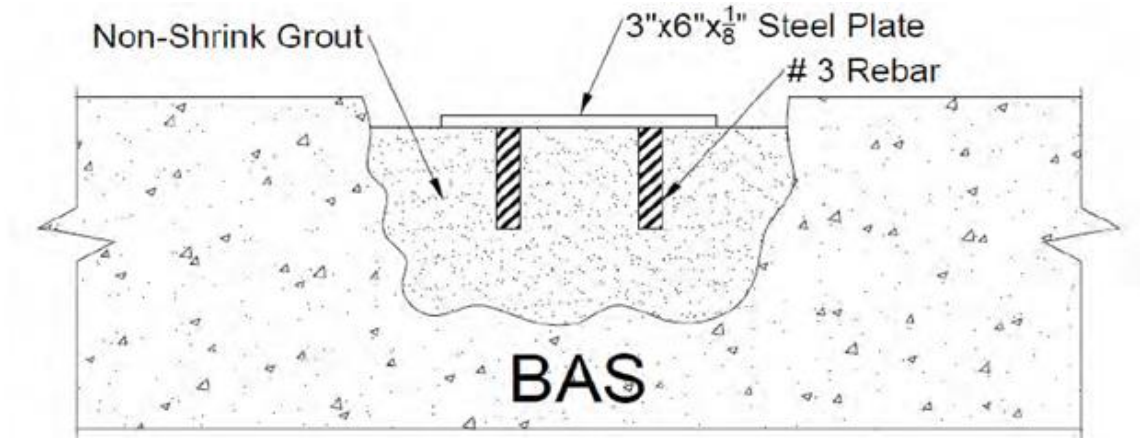

Thiagarajan et al. 2013

Figure 6.2. Monitoring plate details

In discussions between the research team for the present project and the Iowa DOT, the option of using vertical reinforcement bars embedded into the concrete was brought up as an alternative to using monitoring plates. The main advantage in using monitoring plates is that the plates would not be chipped away by snowplow strikes or traffic loads. However, the rebar option could be implemented as well because surveying data can be collected at the same points. It is recommended that monitoring plates or vertical rebars be placed at nine points of interest on an approach slab, as shown in Figure 6.3.

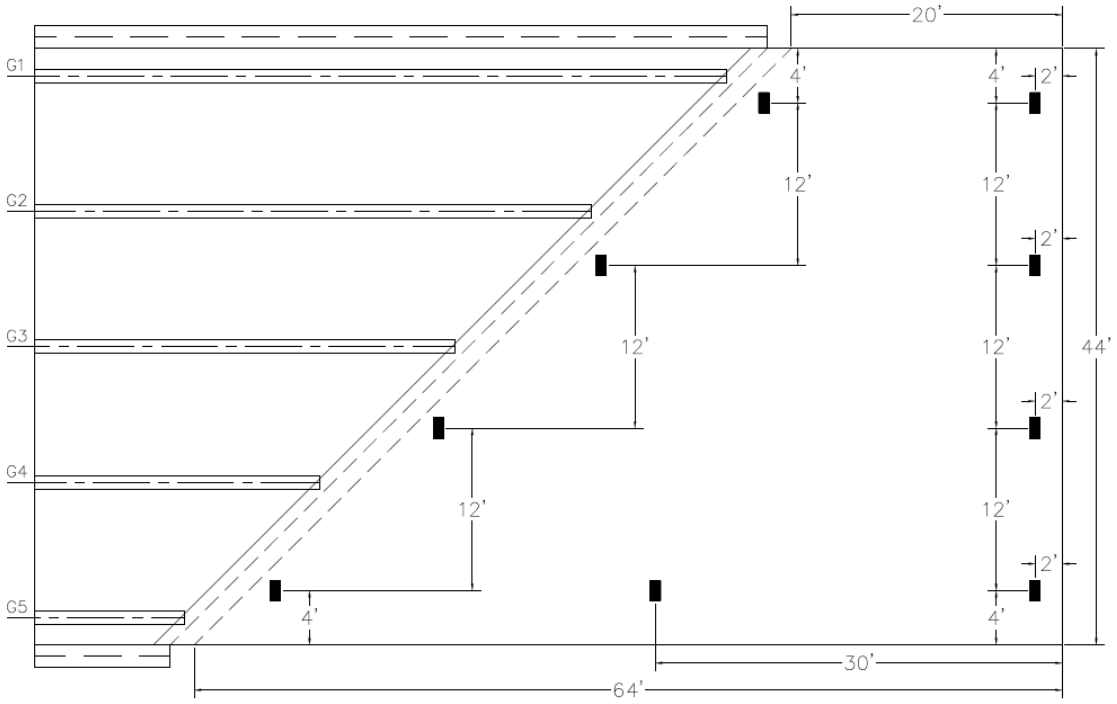

Figure 6.3. Monitoring plate distribution

It is also recommended that gapmeters be incorporated between the girders and the abutment stud wall. These sensors would monitor the displacement of the girders at a certain height in the longitudinal direction. With these data, the rotation of the girders can also be monitored.

A total of 13 strain gage locations are recommended. Nine of these strain gage locations are recommended across the abutment interface, four at the midspan of the transverse spans and five across each girder support. Four additional strain gage locations are recommended at the midspan of the approach slab. This arrangement can be viewed in more detail on the instrumentation plan shown in Figure 6.4.

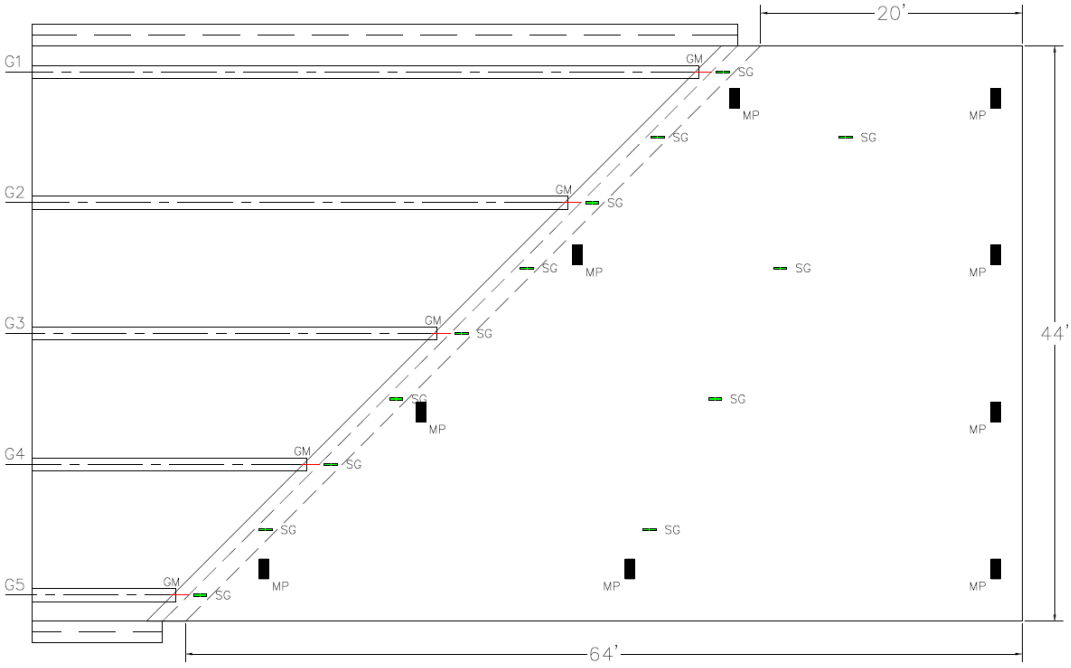

SG: strain gage (13 locations); MP: monitoring plate (8 locations); GM: gapmeter (5 girders)

Figure 6.4. Instrumentation plan

Both top and bottom reinforcement bars can be fitted with strain gages. Multiple strain gages should be used at each location because of the possibility that a certain number of strain gages may malfunction due to improper installation or construction damage. The strain gages can be used to monitor stress levels at the desired locations of the joint and approach slab over time.

6.3 Truck Loading Cases

Various truck loading allocations were considered for the post-construction testing of the deck over backwall concept. For the purposes of this research and for continuity's sake, HS20-44 truck loading conditions are recommended for this plan. These truck loads are shown in Chapter 3, Figure 3.56, Figure 3.57, Figure 3.58, and Figure 3.59, for the FE model of the Marshall County bridge with the approach slab. During the discussion that follows, the middle and rear axles of the trucks are used for allocation purposes. Therefore, even if a different truck with different dimensions and tire spacing is used in the real-world simulations, these same axles can be used for the truck allocations.

The various recommended truck cases can be seen in Figure 6.5, Figure 6.6, Figure 6.7, and Figure 6.8 as Case 1, Case 2, Case 3, and Case 4, respectively.

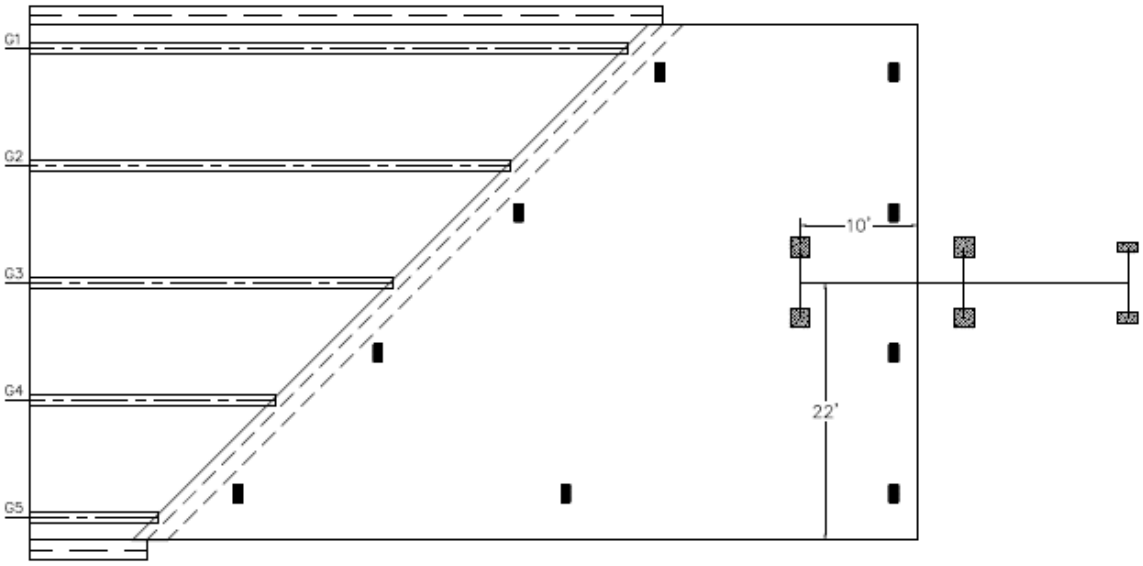

Figure 6.5. Truck loading Case 1

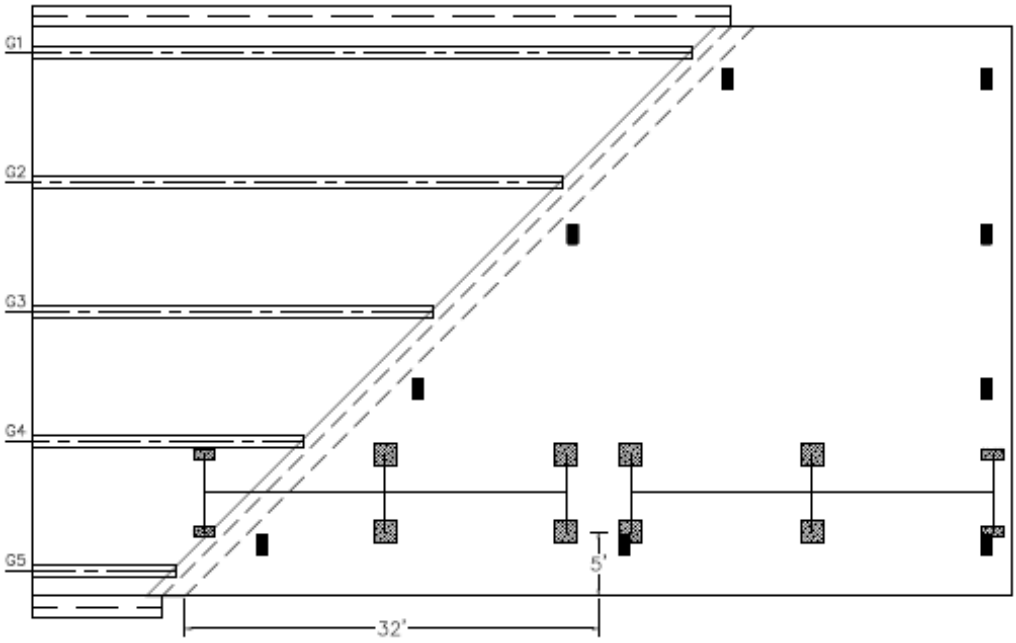

Figure 6.6. Truck loading Case 2

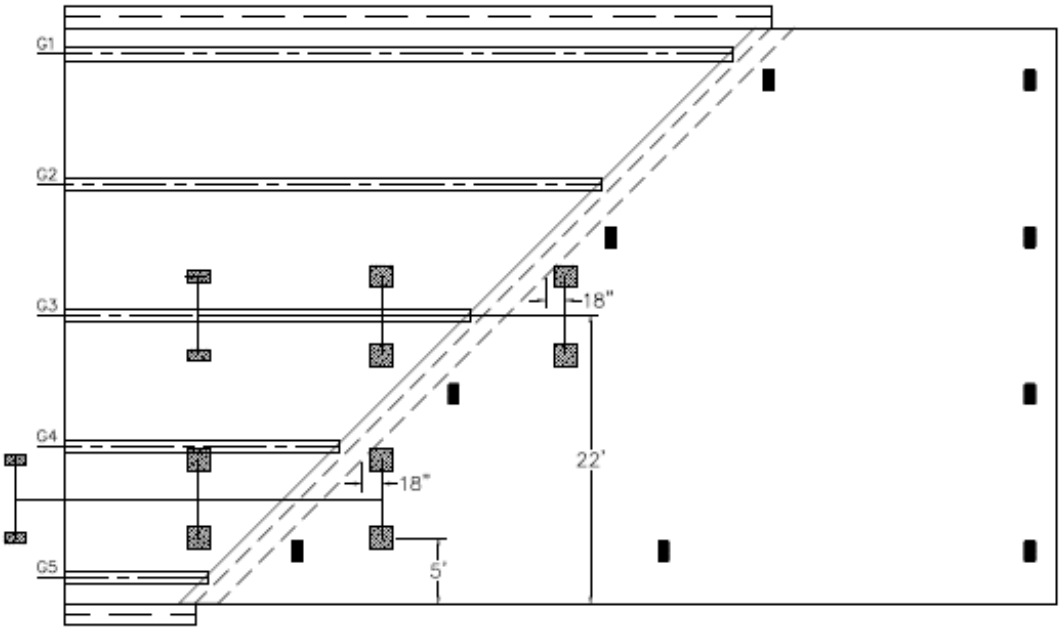

Figure 6.7. Truck loading Case 3

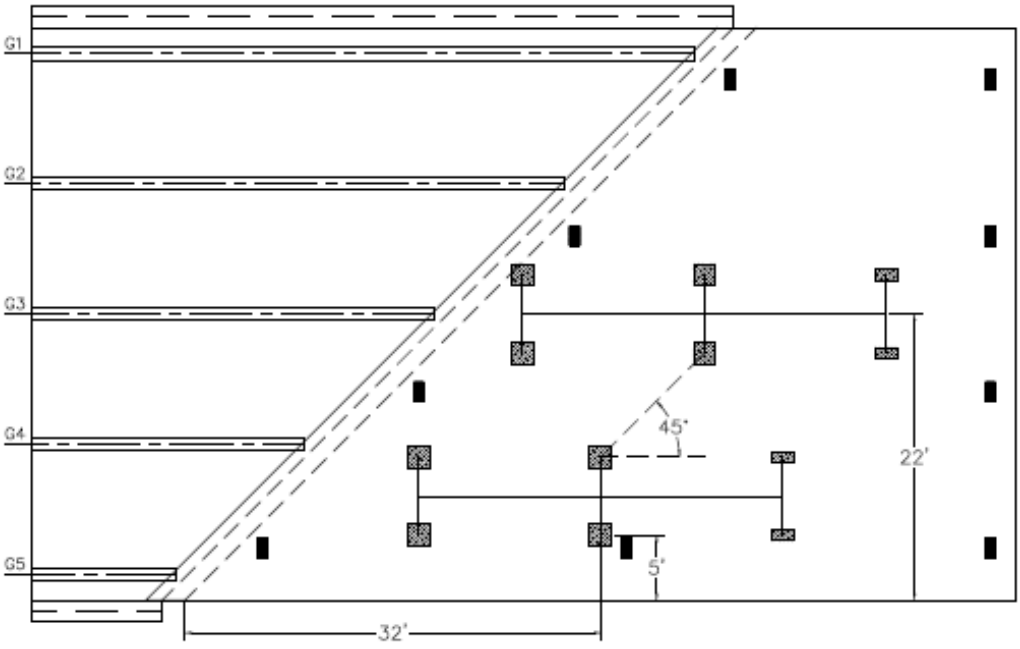

Figure 6.8. Truck loading Case 4

Case 1 would have a larger maximum effect on the abutment and bearings of a non-skewed bridge in comparison to a skewed bridge. That is because both wheels of the rear axle are closer to the abutment on a non-skewed bridge in comparison to a skewed bridge when the load is placed near the middle of the approach slab. For this case, the rear axle of the truck would be located at the midspan of the 20 ft edge of the new approach slab. Case 2 corresponds to two trucks back to back at the midspan of the 64 ft edge of the approach panel. This would maximize

deflection values and stress levels in the approach slab. Case 3 corresponds to two trucks side by side with the rear axles close to the abutment interface. This would maximize the live load abutment reactions while causing deflection at the abutment interface. Case 4 corresponds to two trucks side by side at the midspan of the 64 ft edge and at the center of the approach slab. This would provide high midspan deflection values and stress levels while adding to the live load abutment reactions of both the exterior and interior supports, thereby adding live loads to the bearing loads.

CHAPTER 7. CONCLUSIONS AND FUTURE WORK

The objectives of the research set out in Chapter 1 were accomplished. Conclusions were drawn from each chapter, and possible avenues of future work were recommended. These conclusions and recommendations are discussed in detail in this chapter.

7.1 Joint Detailing

Further development of the deck over backwall concept was accomplished in Chapter 3. The research team proposed various options, with many alternatives considered by the research team and the Iowa DOT. The Iowa DOT developed a joint taking into account the options presented by the research team and various other factors.

While the Iowa DOT might move forward with the joint it developed, further detailing should be developed regarding the deck over backwall concept. Various options remain for several of the joints in the Iowa DOT joint and bridge approach panel detailing, such as selecting exactly where a joint or saw cut might be placed in relation to the abutment backwall and the possibility of moving the joint 15 ft from the abutment backwall. Possible options to include with this concept are sleeper slabs, subdrains, EF joints, CF joints, CD joints, or any combination of these. Consideration could also be given to whether to replace the fill under the approaches and correct possible underdrain deficiencies.

Prior to selecting the aforementioned details, it would be desirable to contact the Michigan Department of Transportation and New York State Department of Transportation to ascertain whether further information is available regarding the performance of their deck over backwall concept approach panels and how such information might improve Iowa DOT designs.

7.2 Finite Element Modeling and Analysis

Full-scale FE models of two different bridges, one non-skewed bridge in Story County and one skewed bridge in Marshall County, were developed and detailed in Chapter 3. These models were analyzed with various loading conditions from dead loads, temperature loading, and live loads corresponding to various truck loading cases. Both models were validated using the original drawing plans. The same process of modeling was used for both models in terms of material properties, boundary conditions, constraints, loading conditions, and other factors.

The impact of the deck over backwall concept was studied with the Marshall County bridge model, which showed an increase in bearing loads due to the additional dead load of the approach slab and in live loads with the truck loading conditions. Relevant deflection values and stress levels at various points of interest across the abutment interface and the midspan of the approach slab were also determined. These FE results provide the Iowa DOT with a case study example that will aid in the further development of the deck over backwall concept and possibly a detailed design for a test installation.

A parametric study of various bridge skew angles (no skew, 30°, 45°, and 60°) was also conducted with the Marshall County bridge. The results for models without soil support show that generally the increase in the bridge skew angle leads to increased loads at the points of interest under this study: the dead load abutment reactions and temperature deformation of the bridges with and without the approach slab, the live load abutment reactions, and the deflection values and stress levels at the abutment interface and in the midspan of the approach slab. The results for models with soil support show more variance and do not follow a general trend due to several factors. With these models, future correlations between the models and possible future laboratory and field measurements can be accomplished.

While these models served the purpose of this research to study and develop the deck over backwall concept, further analysis might also be desirable. Incorporating the steel bar reinforcement and studying its behavior at the abutment interface and at the midspan of the approach slab could be beneficial and provide more information for future designs of the deck over backwall concept. In addition, a plastic analysis could also be performed under certain truck loading conditions. The FE models were verified with loading conditions used at the time of the original bridge design. While those loads are not entirely different from the loads used at the time of writing, the FE models can be calibrated with current design loads. Further calibration of the FE models would also be possible with the post-construction field testing. It should be noted that further FE modeling would be desirable before selecting the concrete thickness and the reinforcing configuration in the end diaphragm area and the longitudinal reinforcing for the approach panels. Clarification of the exact removal limits for the abutment backwall location would also be desirable; members of this project's technical advisory committee noted that such areas are often heavily deteriorated and require replacement under any circumstance.

Given the high loads that are predicted when the abutment is skewed but the sleeper slab that supports the approach panel is not skewed, it would be desirable to consider designing the sleeper slab so that it is parallel with the abutment. In doing so, the length that the approach panel would have to bridge would be limited to 20 ft.

7.3 Experimental Investigation

An experimental laboratory investigation was completed, as discussed in Chapter 4. It was discovered that cutting the top longitudinal reinforcing minimizes the stress that the bridge deck experiences from the negative moment caused by loading. If not cut, cracks will form on the surface of the bridge deck, possibly leading to harmful chemicals penetrating the interior of the slab.

If the decision is made to cut the top longitudinal reinforcing, special care must be taken with the filler material in the saw cut. The material should be able to withstand considerable stretching and deformation. Additionally, the material should serve as a protective layer against the cracking that could occur underneath the saw cut due to the increased stresses that form there. Due to cracking and deformation, this saw cut could create a bump on the driving surface. Cracking could be mitigated underneath the saw cut by moving the cut to the edge of the

backwall. When the saw cut is in the middle of the backwall, the rotation of the approach slab causes stress to traverse from the contact point to the bottom of the saw cut, creating cracking.

The far end of the approach slab, independent of whether the top longitudinal reinforcing is cut, will experience upward rotation. When designing the connection between the roadway and approach slab, the engineer should take this rotation into account. The presence of a backwall increases the moment capacity of the approach slab section due to a decrease in the effective length. This, in turn, reduces the stresses in the midspan of the slab. If soil support is effective underneath the approach slab, the stresses will be reduced, depending on the soil support properties.

Additional testing can be performed for the deck over backwall concept. Various truck loading cases can be tested for the approach slab. Variations in soil support could be incorporated into the field testing plan for the approach slab. Soil compaction could be controlled to simulate the three compositions (loose, moderately stiff, and stiff) considered in the FE model.

7.4 Cost Analysis

A comparison between the various types of joints and the deck over backwall concept in terms of cost was performed and is documented in Chapter 5. When combining the repair or replacement costs and the construction cost of the deck over backwall concept, the concept is the best alternative among nine types of joints considered for a bridge service life of 50 years. For a bridge service life of 25 years, the deck over backwall concept has a higher cost than other comparable types of joints. For most cost point and service life scenarios considered, the concept generally ranked between the third and fourth lowest cost out of the nine types of joints. The high initial cost accounts for most of the concept's life cycle costs, since the repair or replacement costs were found to be the lowest among all types of joints by a considerable margin. A BEP between 25 years and 50 years was identified to determine the point at which the deck over backwall concept would produce the lowest costs among all other types of joints across all combinations of cost point and service life. The results show that the BEP is 44 years for a 2% interest rate and lowers as the interest rate increases.

Many assumptions and simplifications were made as part of the cost comparison. Numerous factors could have been incorporated into the cost of installation, repair, replacement, and construction of not only the deck over back wall concept but also the other types of joints considered. A more in-depth cost analysis could be performed by taking into account additional factors, such as the maintenance costs of the abutment interface, approach slab, steel girders, bearings, and the steel reinforcement bars in the bridge deck and the abutment and the costs of formwork, labor, work zones, lane closures, mobilization, and other aspects of the work. Other methods of performing a cost analysis could also be used to corroborate the analysis of the research team. One such method could be to develop a probabilistic approach with a Monte Carlo simulation that takes into account fluctuations in the costs of the various project items across the life cycle of a particular project.

7.5 Construction Observation and Post-construction Testing

A plan for construction observation and post-construction testing was developed and is described in Chapter 6. The deck over backwall concept and this observation and testing plan are expected to be implemented in a future Iowa DOT construction season.

The FE models would also need further modification after the post-construction testing. The truck loads used in real-world simulations are expected to be different than those of the HS20-44 truck loading conditions that were used for the purpose of this investigation. The Iowa DOT would likely use various trucks with various loads and tire spacings in the post-construction testing. The results of these field tests can be compared with those of the FE models, and correlations between both sets of results will serve to calibrate and improve the accuracy of the FE models

REFERENCES

AASHTO. 2014. *AASHTO Load and Resistance Factor Design (LRFD) Bridge Design Specifications*. American Association of State Highway and Transportation Officials, Washington, DC.

Abdulrahman, K. and F. Portus. 2015. Numerical Analysis and Model Updating of a Steel-Concrete Composite Bridge. MS thesis. KTH Royal Institute of Technology, Stockholm, Sweden.

ACI Committee 239 – Ultra-High Performance Concrete. 2012. *Minutes of Committee Meeting October 2012*, ACI Annual Conference 2012, Toronto, ON.

Aktan, H., U. Attanayake, and E. Ulku. 2008. *Combining Link Slab, Deck Sliding over Backwall, and Revising Bearings*. Western Michigan University, Department of Civil and Construction Engineering, College of Engineering and Applied Sciences, Lansing, MI.

Alampalli, S. and A. P. Yannotti. 1998. In-Service Performance of Integral Bridges and Jointless Decks. *Transportation Research Record: Journal of the Transportation Research Board,* No. 1624, pp. 1–7.

Baker Engineering. 2006. *Evaluation of Various Types of Bridge Deck Joints.* For the Arizona Department of Transportation, Phoenix, AZ.

Bengtsson, R. and M. Widén. 2010. *FE-Analysis of Vårby Bridge: Investigation of Fatigue Damage in a Composite Bridge*. MS thesis. Chalmers University of Technology, Göteborg, Sweden.

Bierwagen, D., B. Moore, and V. Perry. 2006. Revolutionary Concrete Solutions. *Concrete Specifier*.

Biggs, R. M., F. W. Barton, J. P. Gomez, P. J. Massarelli, and W. T. McKeel. 2000. *Finite Element Modeling and Analysis of Reinforced-Concrete Bridge Decks*. Virginia Transportation Research Council, Charlottesville, VA.

Civjan, S. A. and B. Quinn. 2016. *Better Bridge Joint Technology*. Department of Civil and Environmental Engineering, University of Massachusetts–Amherst, MA.

Cosgrove, E. F. and B. Lehane. 2003. Cyclic Loading of Loose Backfill Placed Adjacent to Integral Bridge Abutments. *International Journal of Physical Modelling in Geotechnics*, Vol. 3, No. 3, pp. 9–16.

Dassault Systemes SIMULIA Abaqus. 2013. 23.6.3 Concrete Damaged Plasticity in Abaqus Analysis User's Guide. http://ivt-abaqusdoc.ivt.ntnu.no:2080/v6.13/books/usb/default.htm?startat=pt05ch23s06abm39.html.

Dunker, K. F. and A. Abu-Hawash. 2005. Expanding the Use of Integral Abutments in Iowa. 2005 Mid-Continent Transportation Research Symposium, Ames, IA.

Fehling, E., M. Schmidt, J. Walraven, T. Leutbecher, and S. Fröhlich. 2015. *Ultra-High Performance Concrete UHPC: Fundamentals, Design, Examples*.

Ghosn, M. and G. Fiorillo. 2013. Appendix B.1: Nonlinear Redundancy Analysis of Truss Bridges. In *NCHRP Report: 776: Bridge System Safety and Redundancy*. National Cooperative Highway Research Program, Washington, DC.

Graybeal, B. 2004. Fabrication of an Optimized UHPC Bridge, PCI National Bridge Conference, Atlanta, GA.

——. 2008. UHPC in the US Highway Transportation System, HiPerMat, 2nd International Symposium on UHPC, Kassel, Germany.

——. 2014. *Design and Construction of Field-Cast UHPC Connections*. Federal Highway Administration, Washington, DC, pp. 1–36.
Helwany, S. 2007. *Applied Soil Mechanics: With ABAQUS Applications*. *Applied Soil Mechanics: With ABAQUS Applications*, John Wiley & Sons, Inc., Hoboken, NJ.
Hsu, L. S. and C.-T. T. Hsu. July–August 1994. Stress-Strain Behavior of Steel-Fiber High-Strength Concrete. *ACI Structural Journal*, Vol. 91, No. 4, pp. 448–457.
Hsu, L. S. and C.-T. T. Hsu. 1994. Complete Stress-Strain Behavior of High-Strength Concrete under Compression. *Magazine of Concrete Research*, Vol. 46, No. 169, pp. 301–312.
Iowa DOT. 2018. Standard Specifications with GS-15006 Revisions, Section 2102 - April 17, 2018. https://www.iowadot.gov/erl/current/GS/Navigation/nav21.htm.
Iowa DOT Office of Bridges and Structures. 2018a. *LRFD Bridge Design Manual*. Iowa Department of Transportation, Ames, IA.
——. 2018b. Prepare Cost Estimate 4/25/17. Iowa Department of Transportation, Ames, IA.
Iowa DOT Office of Design. 2016. *Standard Road Plans - BR Series*, *Double Reinforced 12" Approach (Slab Bridge)*. Iowa Department of Transportation, Ames, IA.
Klein, L. E. 2006. Finite Element Analysis of a Composite Bridge Deck. Bachelors dissertation. University of Southern Queensland, Toowoomba, Australia.
Lam, C., D. Lai, J. Au, L. Lim, W. Young, and B. Tharmabala. 2008. Development of Concrete Link Slabs to Eliminate Bridge Expansion Joints over Piers. 2008 Annual Conference of the Transportation Association of Canada, September 21–24, Toronto, ON.
Liu, D. and J. Schiff. 2016. Design and Construction of Illinois's First Precast Deck Panel Bridge with UHPC Joints. First International Interactive Symposium on UHPC, July 18–20, Des Moines, IA.
Maruri, R. F. and S. H. Petro. 2005. Integral Abutment and Jointless Bridges (IAJB) 2004 Service Summary. *Proceedings of the Integral Abutment and Jointless Bridges (IAJB 2005)*, pp. 12–29. March 16–18, Baltimore, MD.
McDonagh, M. D. and A. J. Foden. 2016. Benefits of Ultra-High Performance Concrete for the Rehabilitation of the Pulaski Skyway. First International Interactive Symposium on UHPC, July 18–20, Des Moines, IA.
Miller, A. M. and C. T. Jahren. 2014. *Rapid Replacement of Bridge Deck Expansion Joints Study – Phase I.* Construction Management and Technology Program, Institute for Transportation, Iowa State University, Ames, IA. https://intrans.iastate.edu/app/uploads/2018/03/bridge_deck_expansion_joint_repair_phase_I_w_cvr.pdf.
——. 2017. *Rapid Bridge Deck Expansion Joints– Phase II.* Construction Management and Technology Program, Institute for Transportation, Iowa State University, Ames, IA.
MnDOT. 2012. Chapter 5: Bridge Mechanics. In *Bridge Inspectors Reference Manual*. Minnesota Department of Transportation, St. Paul, MN.
Nayal, R. and H. A. Rasheed. 2006. Tension Stiffening Model for Concrete Beams Reinforced with Steel and FRP Bars. *Journal of Materials in Civil Engineering,* Vol. 18, No. 6.
Palle, S., T. Hopwood II, and B. W. Meade. 2012. *Improved Bridge Expansion Joints*. Kentucky Transportation Center, University of Kentucky College of Engineering, Lexington, KY.
Perry, V. H. and D. Corvez. 2016. An Innovative Technology for Accelerated Bridge Construction – The Owner Designer Dilemma. First International Interactive Symposium on UHPC, July 18–20, Des Moines, IA.

Perry, V. H. and M. Royce. 2010. Innovative Field-Cast UHPC Joints for Precast Bridge Decks (Side-by-Side Deck Bulb-Tees), Village of Lyons, New York: Design, Prototyping, Testing and Construction. Third FIB International Congress, Washington, DC.

Perry, V. H. and P. J. Seibert. 2013. Fifteen Years of UHPC Construction Experience in Precast Bridges in North America. *Proceedings of the RILEM-FIB-AFGC International Symposium on Ultra-High Performance Fibre-Reinforced Concrete*, Marseille, France, pp. 229–238.

Phares, B. and M. Cronin. 2015. *Synthesis on the Use of Accelerated Bridge Construction Approaches for Bridge Rehabilitation*. Accelerated Bridge Construction University Transportation Center, Florida International University, Miami, FL. http://utcdb.fiu.edu/files/2016-12-19_21-48-12.pdf.

Rajek, G. S. 2010. Numerical Modeling of the Performance of Highway Approach Slabs. MS thesis. University of Wisconsin – Madison, WI.

Ronanki, V. S., D. B. Valentim, and S. Aaleti. 2016. Development Length of Reinforcing Bars in UHPC: An Experimental and Analytical Investigation. First International Interactive Symposium on UHPC, July 18–20, Des Moines, IA.

Royce, M. 2016. Utilization of Ultra-High Performance Concrete (UHPC) in New York. First International Interactive Symposium on UHPC, July 18–20, Des Moines, IA.

Russell, H. G. and B. A. Graybeal. 2013. *Ultra-High Performance Concrete: A State-of-the-Art Report for the Bridge Community*. Federal Highway Administration, Turner-Fairbank Highway Research Center, McLean, VA.

Ryan, T. W., J. Mann, Z. M. Chill, and B. T. Ott. 2012. *Bridge Inspector's Reference Manual (BIRM)*. FHWA NHI 12-049. Federal Highway Administration, National Highway Institute, Arlington, VA.

Schuettpelz, C. C., D. Fratta, and T. B. Edil. 2010. Mechanistic Corrections for Determining the Resilient Modulus of Base Course Materials Based on Elastic Wave Measurements. *Journal of Geotechnical and Geoenvironmental Engineering*, Vol. 136, No. 8, pp. 1086–1094.

Thiagarajan, G., J. Myers, C. Halmen, J. Nalagotla, and N. Muncy. 2013. *Bridge Approach Slabs for Missouri DOT Field Evaluation of Alternative and Cost Efficient Bridge Approach Slabs*. Missouri Department of Transportation, Jefferson City, MO.

Wahalathantri, B., D. Thambiratnam, T. Chan, and S. Fawzia. 2011. A Material Model for Flexural Crack Simulation in Reinforced Concrete Elements using ABAQUS. *Proceedings of the First International Conference on Engineering, Designing and Developing the Built Environment for Sustainable Wellbeing*, pp. 260–264. April, Queensland University of Technology, Brisbane, Australia.

Wing, K. M. and M. J. Kowalsky. 2005. Behavior, Analysis, and Design of an Instrumented Link Slab Bridge. *Journal of Bridge Engineering*, Vol. 10, No. 3, pp. 331–334.

Yannotti, A. P., S. Alampalli, and H. L. White II. 2005. New York State Department of Transportation's Experience with Integral Abutment Bridges. *Proceedings of the Integral Abutment and Jointless Bridges (IAJB 2005)*, pp. 44–49. March 16–18, Baltimore, MD.

THE INSTITUTE FOR TRANSPORTATION IS THE FOCAL POINT FOR TRANSPORTATION AT IOWA STATE UNIVERSITY.

InTrans centers and programs perform transportation research and provide technology transfer services for government agencies and private companies;

InTrans contributes to Iowa State University and the College of Engineering's educational programs for transportation students and provides K–12 outreach; and

InTrans conducts local, regional, and national transportation services and continuing education programs.

IOWA STATE UNIVERSITY

Visit **InTrans.iastate.edu** for color pdfs of this and other research reports.